UNIVERSITY OF CALIFORNIA
SANTA CRUZ

Advancing Assays, Exploring Environments, and Mapping Pathways: a Journey Through Hematopoietic Dynamics

A dissertation submitted in partial satisfaction
of the requirements for the degree of

DOCTOR OF PHILOSOPHY

in

MOLECULAR, CELL, AND DEVELOPMENTAL BIOLOGY

by

Alessandra Rodriguez y Baena

December 2023

The Dissertation of Alessandra Rodriguez y Baena
is approved by:

Camilla Forsberg, Ph.D.

Lindsay Hinck, Ph.D.

Susan Carpenter, Ph.D.

Peter Biehl
Vice Provost and Dean of Graduate Studies

Table of Contents

List of Figures

List of Tables

Abstract

Advancing Assays, Exploring Environments, and Mapping Pathways:

a Journey Through Hematopoietic Dynamics

Alessandra Rodriguez y Baena

Hematopoiesis is the process through which hematopoietic stem cells (HSCs) produce all mature and immune cells in the blood. This thesis focuses on three aspects of hematopoiesis research: methods for studying hematopoiesis, the effects of environmental exposures of fetal hematopoiesis, and epigenetic changes influencing hematopoiesis during aging.

The first part of this thesis delves into the historical and ongoing significance of the spleen colony-forming unit assay, a pioneering in vivo functional assay to elucidate bone marrow cell functions. Then, the focus shifts to overcoming the limitations of traditional host conditioning methods, introducing innovative mouse models for selective ablations of all hematopoietic cells or HSCs specifically. These models offer non-irradiation alternative for studying HSC function, engraftment ability, and differentiation pathways. Together, these chapters contribute to advancing our understanding of HSC identity and functions.

The second part of this thesis investigates the impact of environmental toxic compounds on hematopoiesis and immune function. We specifically reviewed the effects of nicotine on HSCs and other blood cells. Then, we investigated the effects of in utero nicotine exposure on the establishment of the hematopoietic system and we

determined its long-term consequences. These chapters collectively offer insights into the perturbations of normal hematopoiesis by environmental exposures during development.

The last part of this thesis focuses on unraveling the dynamics of HSC differentiation and lineage fate decisions, with an emphasis on platelet differentiation. First, we reviewed evidence suggesting the existence of a non-canonical platelet differentiation pathway from HSCs, predominantly primarily observed during inflammation. Then, we investigated how epigenetic lineage priming drives differentiation of HSCs into the five mature lineages by maintaining chromatin accessibility at lineage-specific regulatory regions. Finally, we investigated how epigenetic priming of the Nuclear Protein 1 (Nupr1) gene in aged HSCs drives non-canonical platelet differentiation, offering a comprehensive understanding of the intricate processes governing aging hematopoiesis.

Ultimately, the studies presented here promise advance in our comprehension of hematopoiesis and open avenues for innovative approaches in regenerative medicine and therapeutic interventions.

Dedication

My accomplishments so far couldn't have happened without the love and support of the incredible community that surrounds me.

My sincere appreciation to my PI, Dr. Camilla Forsberg, for her guidance, mentorship, and belief in me throughout my doctoral research. Thank you for always pushing me to excel, for giving me the space to grow as a scientist, and providing me with the opportunity to figure out where I fit in.

I am indebted to my fellow lab members for their friendship and collaborative spirit. The intellectually stimulating environment of our lab has significantly enriched my research experience and contributed to my personal and professional growth. Thank you for spending long nights with me on the Aria, for offering suggestions and solutions when experiments didn't work, for always being willing to collaborate on projects, and for celebrating all the wins while also preventing me from getting discouraged by failures. And thank you to my collaborators, who were willing to mentor me, teach me, and answer all my questions when working on projects outside of my expertise.

Special thanks go to my friends, who provided me with a safe space to escape from the demands of academia. Your understanding, encouragement, and shared laughter have made this journey memorable.

One person I couldn't have done this without is my husband who has been through it all with me. Thank you for being my pillar of strength, for celebrating the highs and comforting me during the lows, for your constant belief in me, for helping

me fight my self-doubt, for your patience during challenging times, and for believing in my dreams. This accomplishment is as much yours as it is mine, and I am grateful to have you by my side.

Finally, I want to acknowledge the unwavering support, love, and encouragement of my parents. Their influence has been the foundation of my academic journey, and I am profoundly thankful for the sacrifices they made to pave the way for my success. Their belief in me has not only been my greatest motivation but has also instilled in me the resilience to overcome challenges. I extend heartfelt thanks to my sister, who stands as a example of dedication, drive, and exemplifies the delicate art of maintaining a work-life balance. Your inspiration has been a guiding force, showing me the importance of passion, perseverance, and equilibrium in navigating the academic and personal spheres. And, as a tribute to my Italian heritage, I want to express my gratitude in my mother tongue – Grazie di tutto. This is for you. The sentiment transcends words and encapsulates the depth of my appreciation for the invaluable role my family has played in shaping my academic journey.

Acknowledgements

The text of this dissertation includes reprints of the following previously published materials. Alessandra Rodriguez y Baena's contributions to collaborative chapters are listed below the citations.

Rodriguez Y Baena A, Manso BA, Forsberg EC. CFU-S assay: a historical single-cell assay that offers modern insight into clonal hematopoiesis. Exp Hematol. 2021 Dec;104:1-8. doi: 10.1016/j.exphem.2021.10.003. Epub 2021 Oct 22. PMID: 34688837; PMCID: PMC9045698.

Rodriguez y Baena A, Rajendiran S, Manso BA, Krietsch J, Boyer SW, Kirschmann J, Forsberg EC. New transgenic mouse models enabling pan-hematopoietic or selective hematopoietic stem cell depletion in vivo. Sci Rep. 2022 Feb 24;12(1):3156. doi: 10.1038/s41598-022-07041-6. PMID: 35210475; PMCID: PMC8873235.

Cool T, **Rodriguez y Baena A**, Forsberg EC. Clearing the Haze: How Does Nicotine Affect Hematopoiesis before and after Birth? Cancers (Basel). 2021 Dec 30;14(1):184. doi: 10.3390/cancers14010184. PMID: 35008347; PMCID: PMC8750289.

- Rodriguez y Baena A generated the figures, edited the text, did a literature search to ensure all the latest publications on the topic were cited properly, and addressed all the submission revisions for this review.

Martin EW, **Rodriguez Y Baena A**, Reggiardo RE, Worthington AK, Mattingly CS, Poscablo DM, Krietsch J, McManus MT, Carpenter S, Kim DH, Forsberg EC. Dynamics of Chromatin Accessibility During Hematopoietic Stem Cell Differentiation Into Progressively Lineage-Committed Progeny. Stem Cells. 2023 May 15;41(5):520-539. doi: 10.1093/stmcls/sxad022. PMID: 36945732; PMCID: PMC10183972.

- Rodriguez y Baena A wrote the introduction, generated Figure 3 and associated Supplementary Figure 1, generated Figure 5, helped generate Figure 6, contributed to data collection for Figure 7 and helped generate Figure 7, wrote sections (results, methods, and discussion) related to figures above mentioned, reviewed the manuscript, and helped with revisions.

Dr. Camilla Forsberg directed and supervised the research which forms the basis of this dissertation work.

PART I

Chapter 1.

CFU-S assay: a historical single-cell assay that offers modern insight into clonal hematopoiesis.

The text of this chapter includes a reprint of the following previously published paper: Rodriguez Y Baena A, Manso BA, Forsberg EC. CFU-S assay: a historical single-cell assay that offers modern insight into clonal hematopoiesis. Exp Hematol. 2021 Dec;104:1-8. PMID: 34688837.

Abstract

Hematopoietic stem cells (HSCs) have been studied extensively since their initial functional description in 1961 when Drs. James Till and Ernest McCulloch developed the first *in vivo* clonal strategy, termed the "spleen colony-forming unit" (CFU-S) assay, to assess the functional capacity of bone marrow-derived hematopoietic progenitors at the single-cell level. By transplanting bone marrow cells and analyzing the resulting cellular nodules in the spleen, the CFU-S assay revealed both the self-renewal and clonal differentiation capacity of hematopoietic progenitors. Further development and use of this assay have identified highly proliferative, self-renewing, and differentiating HSCs that possess clonal, multilineage differentiation. The CFU-S strategy has also been adapted to interrogating single purified hematopoietic stem and progenitor cell populations, advancing our knowledge of the hematopoietic hierarchy. In this review, we explore the major discoveries made with the CFU-S assay, consider

its modern use and recent improvements, and compare it to commonly used long-term transplantation assays to demonstrate the continued value of the CFU-S assay for understanding HSC biology and hematopoiesis.

Introduction: A blast from the past

Hematopoietic stem cells (HSCs) are the only cells within the hematopoietic system that possess the combined ability to differentiate into all lineages of functional blood cells and self-renew indefinitely to sustain hematopoiesis throughout life. HSCs were originally hypothesized to exist after the discovery that transplantation of healthy bone marrow (BM) cells could rescue irradiated recipient animals and replenish their hematopoietic cells through a tremendously dynamic process[1]. The hypothesis for the existence of HSCs was reinforced when cells with multilineage capacity were discovered in 1961 by Drs. James Till and Ernest McCulloch, who developed the first *in vivo* functional assay for the quantification of the clonal and differentiation potential of hematopoietic progenitor cells[2]. Since then, HSCs have remained one of the best-characterized tissue-specific stem cells, both from a basic biology perspective and for their use in regenerative medicine, with particular emphasis on clonal function[3-13].

In their seminal studies, Till and McCulloch developed the first *in vivo* assay to assess the proliferative and differentiation capacity of primitive hematopoietic cells in mouse BM[2, 14, 15]. In these early experiments, the identity of cells capable of forming multilineage spleen colonies was still uncertain and were appropriately and carefully termed “colony forming units” (CFU) based on their functional capacity. This initial

demonstration of a BM cell population capable of multilineage blood cell reconstitution resulted in a paradigm shift in the field of hematopoiesis and opened several questions that this elegant assay is uniquely positioned to answer. Here, we explore the major utilities of the spleen colony forming unit (CFU-S) assay, consider its modern use and recent improvements, and discuss its utility in current hematopoiesis research.

One from all or all from one: Are spleen colonies clonal?

Spleen colony formation is rare, with transplantation of approximately 10,000 BM cells into conditioned recipients required to yield one spleen colony[2]. Initially, the linear relationship between the number of hematopoietic nucleated BM cells transplanted and the number of spleen colonies formed indicated that single cells may be able to give rise to individual spleen colonies[2]. The CFU-S assay utilized by Till, McCulloch, and their colleagues consisted of intravenously injecting BM cells from the femora of healthy donor mice into recipients conditioned through lethal irradiation for host cell ablation. In a subsequent version of this assay, the donor cells were irradiated prior to transplantation to induce unique, random chromosomal breaks that distinguish them from host cells and distinguish single donor cells from one another. After 10-11 days, recipient mice presented macroscopic nodules of cellular expansion in the spleen that are formed by rapidly proliferating hematopoietic cells and composed of undifferentiated (stem and progenitor) cells along with erythroblasts, granulocytes, and megakaryocytes (Figure 1A)[14, 16, 17]. If more than one differentiated cell type within a spleen colony, as readily scored by cell morphology under a microscope,

contained the same unique chromosome aberration, these cells must have a shared cellular origin. As this was indeed the outcome, these studies definitively demonstrated that individual cells with multilineage capacity exist within mouse BM. Additionally, the vast majority of scored cells from a single colony harbored the same unique chromosomal aberration, indicating a single, shared progenitor cell. Inducing chromosomal breaks via irradiation to establish clonality was a particularly clever strategy when more modern tools, such as flow cytometry (late 1960s[18]), PCR (1983[19]), monoclonal antibodies (1975[20]), and others had not yet been established. Thus, this CFU-S strategy provided direct cytological evidence demonstrating that most, if not all, cells within a single colony arose from a single, highly proliferative, multipotent CFU-S cell.

One caveat of the early CFU-S strategy was that radiation-induced chromosomal aberration was only obvious in a small fraction of the colonies obtained and that only intact cells in metaphase could be scored based on their karyotype, leaving the possibility that the unscored cells were derived from one or more additional cells. More recent data from our group and others support the evidence that each colony consists of progeny from a single cell. In one of our studies, transplantation of as few as 10 HSCs directly into the spleen resulted in several colonies, with some mice approaching a 1:1 ratio of HSC:colony[21]. In a second study using fluorescent microscopy and flow cytometry, we observed only single-color splenic colonies when an equal mixture of GFP and Tomato fluorescent cells were transplanted into the same recipient[22]. Similarly, the Fehse group assessed clonality using a red-green-blue cell

tracking methodology that resulted in mostly homogenously colored spleen colonies upon transplantation[23]. In their study, the very few CFU-S colonies that contained more than one color was potentially due to two colonies initiating in close proximity and fusing together upon growth. Definitive evidence for clonality could be obtained via the relatively recent clonal tracking strategies, such as single-cell barcoding[24-27]. Though not entirely unequivocal, the collective evidence uniformly supports the original conclusion by Till and McCulloch that spleen colonies are clonal.

Persistence matters: Do CFU-S self-renew?

One hallmark of a true HSC is the ability to self-renew, often demonstrated by the cell's ability to maintain multilineage reconstitution upon secondary transplantation. In one of the first direct demonstrations of *in vivo* self-renewal, injection of day-10 spleen colony content into secondary irradiated recipient mice revealed that colony forming cells include cells with the regenerative capacity expected of stem cells (Figure 1A)[15]. Self-renewal can also be considered as the ability of a multipotent cell to give rise to multilineage-capable progeny. Supporting this definition, it was observed that the number of colony forming cells rapidly increased between days 10 and 14 post-transplantation, thus revealing that CFU-S cells had self-renewal capacity (i.e. they can give rise to more cells with both self-renewal and multilineage capacity)[15]. Additional studies from Schofield et al. (1980) calculated the probability of CFU-S self-renewal and estimated that, on average, 68.3% of cells will produce more CFU-S while 31.7% will differentiate[28]. Thus, CFU-S cells were

defined as colony forming hematopoietic progenitor cells that are highly proliferative, and capable of differentiation and self-renewal.

CFU-S kinetics: What do early and late spleen colony formation tell us?

Upon transplantation of BM cells, a fraction of CFU-S cells (containing both stem and progenitor populations) will home to the spleen of the recipient mouse and give rise to colonies of heterogeneous composition. Given that transplanted, heterogeneous BM contains various hematopoietic progenitor populations along all stages of differentiation, the cellular output kinetics could inform relative contributions by unique CFU-S subpopulations. Indeed, an initial study showed that colonies present at day 7-8 post-BM transplantation consisted primarily of erythroblasts and were formed by unilineage, non-self-renewing mature erythroid precursors[29]. Importantly, cell purification technology progressed in parallel with CFU-S assays, allowing more purified populations, rather than whole BM, to be transplanted. Thus, although a small proportion of megakaryocyte/erythrocyte progenitor (MEP)-derived erythroid colonies persisted through day 12[29-32], transplantation of MEPs purified via fluorescent activated cell sorting (FACS) confirmed that day-8 erythroid-only colonies originated primarily from the MEP, and not the HSC, population[22, 31, 33].

Conversely, cells higher in the hematopoietic hierarchy form colonies with slower kinetics. Upon transplantation of purified HSCs or multipotent progenitors (MPPs), no spleen colonies formed at day 8, potentially due to their differentiation kinetics causing a delay in the production of effector cells[22, 31, 33]. Instead, HSCs

and MPPs primarily formed colonies at day 12 when transplanted together[17] or at day 11-12 (MPPs) or 12-14 (HSCs) when transplanted separately, with HSCs showing a much higher CFU-S frequency than MPPs[33, 35, 22]. Moreover, purified long term (LT)-HSCs and short term (ST)-HSCs showed similar day 11-12 CFU-S activity and frequency, but ST-HSCs were able to form visible spleen colonies at day 8 which is consistent with their increased radioprotective capacity compared to LT-HSCs[22, 33-38]. The composition of both HSC- and MPP-derived spleen colonies was heterogeneous and multilineage, with most colonies containing erythrocytes, granulocytes, and some megakaryocytes[22]. Previously, all day-12 colonies had been shown to contain CFU-S cells of varying self-renewal and differentiation potential[15, 17, 30, 39]. Thus, the splenic colonies appearing at this time point contain self-renewing primitive stem cells that are multipotent at the single-cell level[30, 39, 40]. HSC-derived colonies arise between days 12-14 and only colonies with this timing contain multipotent HSCs. Of note, beyond 14 days, satellite colonies start forming, confounding identification and analysis of primary colonies. Taken together, multiple progenitor cells can form spleen colonies with different kinetics and cell output, and the CFU-S assay can resolve these temporal and cellular features.

Technology boosts the resolution and throughput of CFU-S assays

Historically, the determination of the composition of splenic colonies relied solely on histological analysis of dissected spleens. New technologies, most importantly the development of monoclonal antibodies and flow cytometry, have

enabled strategies with increased resolution and higher throughput. To improve the measurement of CFU-S cell output, we recently published an updated, flow cytometry-based version of the original CFU-S assay (Figure 1B) [22, 41]. This consists of transplanting specific FACS-purified hematopoietic populations, scoring colony frequency, then dissecting and individually analyzing the resulting splenic colonies qualitatively and quantitatively by flow cytometry for erythroid, megakaryocyte, granulocyte, and B cell lineages (Figure 1B). The detection of B cells ($Mac1^-$, $Gr1^-$, $B220^+$) is an important addition as previous histology-based analyses were unable to assess B cell production, and lymphoid output would reinforce both the identity and multilineage potential of the input cells. Importantly, by first excluding myeloid (Mac1/CD11b) and granulocytic (Gr1, Ly6C/Ly6G) cells, B220 expression will only assess B-lineage cells. We note that T cell output cannot be assessed as more time and thymic involvement is required to produce these cells. The enhanced sensitivity flow cytometry provides also allows for the quantitative determination of rare stem and progenitor populations among individual colonies. Using this updated method, we found that day-13.5 colonies formed by purified HSCs, and day-11.5 colonies from Flk2-positive MPPs, contained cells from the erythroid, myeloid, megakaryocytic, and B cell lineages, with erythroid cells comprising most cells within a colony. Collectively, these data demonstrate that this updated CFU-S assay can determine the multilineage potential of HSCs beyond what histological analyses provide, coupled with magnitudes higher throughput and sensitivity. Additionally, as indicated earlier,

combining this improvement with cellular barcoding and intrasplenic transplantation may provide even more robust experimental CFU-S determination.

The CFU-S assay can also be used to determine the clonal differentiation capacity of many hematopoietic progenitors, similar to what was initially done to determine that MEPs were the cells responsible for producing most day-8 splenic colonies[22, 31]. Transplantation of FACS-purified common myeloid progenitors (CMPs), which are classically placed upstream of both myeloid and erythroid/megakaryocytic lineages, gave rise to colonies primarily containing erythroid cells at day 9.5; the scarcity of non-erythroid cells is possibly due to their low burst size [22, 31]. Transplantation of megakaryocyte progenitors (MkPs) did not produce colonies visible to the eye between days 8-12, however, histological analysis showed microscopic foci of megakaryocytes in recipient mice[42]. Finally, common lymphoid progenitors (CLPs)[43] and granulocyte/monocyte progenitors (GMPs)[31, 33] do not possess day 8-12 CFU-S capacity. This could be due either to inefficient homing to the spleen, their low burst size, and/or differentiation kinetics outside the optimal 8-14 day window. Lack of CLP or GMP-derived CFU-S colonies also reinforce the notion that erythroid potential is a hallmark of CFU-S. Further research into the dynamics of specific progenitor populations in the CFU-S assay may reveal additional and/or differential functional capacity, further informing hematopoietic progenitor biology.

Combining CFU-S assays with modern genetics

Although not currently as common as other *in vivo* analyses, CFU-S assays remain valuable as a qualitative and quantitative method to assess the properties and function of various stem and progenitor cell populations. Genetic manipulation of hematopoietic cells and/or their environment is increasingly common, and the CFU-S assay is uniquely positioned to, quickly and accurately, provide functional insights into subsequent effects on hematopoietic stem and progenitor cell (HSPC) differentiation, expansion, and homing. For example, Kruse et al. (2009) observed that transplantation of whole BM from double heterozygous mutants for Fli-1 and Erg, two Ets proteins known to play roles in hematopoiesis and leukemia, respectively, formed significantly fewer and smaller day-11 spleen colonies compared to wild type or single heterozygous mice for either gene[44]. This suggested that the genetic interaction between Fli-1 and Erg is critical for normal HSC and progenitor function. Similarly, Summers et al. (2013) observed that loss of histone deacetylase 3 (HDAC3) yielded no colonies at either day-8 or -12 following BM transplantation, confirming HDAC3's role in supporting the proliferation of HSC and progenitor cells[45].

The CFU-S assay is also used to study extramedullary hematopoiesis in the splenic environment. For example, Mehatre et al. (2021) investigated the role of periostin (POSTN)-integrin-αv signaling in splenic HSC function by transplanting healthy BM cells into wild type or Postn knockout (KO) mice and compared the number of spleen colonies at day 12[46]. They observed a significant decrease in the number of spleen colonies in Postn KO mice, suggesting that the POSTN-deficient

splenic microenvironment may not be able to support either the homing and/or growth of hematopoietic progenitors. In another study by our group, Rajendiran et al. (2020) transplanted wild type HSCs into control and CXCL12-overexpressing mice, which showed no differences in size, number, or composition of splenic colonies[41]. This suggested that overexpression of CXCL12, which is essential for HSC trafficking, does not affect homing of HSCs to the spleen. Relevantly, a modified CFU-S assay can be used to study homing itself. Upon transplantation of BM cells or more purified populations, only a fraction of the colony forming cells will home to the spleen while the rest will migrate elsewhere. To address this homing issue, we previously altered the CFU-S assay protocol to inject donor cells directly into the spleen (intrasplenic, IS). By comparison, the CFU-S frequency of MPPs injected IS was comparable to the CFU-S frequency of HSCs injected retro-orbitally, suggesting that homing efficiency affects, but does not entirely account for, differential efficiency of colony formation[21]. Given the importance of homing, the traditional application of this assay underestimated the CFU-S frequency potential of the cell population of interest. Collectively, the historical importance combined with recent advancements underscore the power of the CFU-S assay and support its continued use for assessing the functional capacity of hematopoietic stem and progenitor cells.

The heavy weight championship: CFU-S versus long-term reconstitution assays

The most widely accepted methods for investigating *in vivo* HSPC self-renewal, differentiation, and expansion capacity are CFU-S and the more recently developed long-term repopulation assay (LTRA)[47]. Similar to CFU-S assays, LTRA requires

transplantation of donor BM or purified hematopoietic stem/progenitor cells into (usually) pre-conditioned hosts. Blood is then monitored at different time points to assess long-term reconstitution of hematopoietic lineages [21, 22, 41, 48-51]. A transplanted cell population is considered to have long-term multilineage reconstitution (LTMR) potential, a key HSC property, if it continues to self-renew and differentiate in primary recipients beyond 16 weeks post-transplantation and upon secondary transplantation[52, 53]. LTRAs are performed to verify that one or more *bona fide* HSCs are present among the transplanted population of interest; persistence and secondary reconstitution distinguish HSCs from hematopoietic progenitors, as the latter will not support hematopoiesis beyond a few weeks post-transplantation.

CFU-S and LTRA assays readily complement each other (Table 1). For example, Forsberg et al. (2006) transplanted HSCs, short-term (ST)-HSCs, MPPs, and CMP/MEPs for both CFU-S and LTRA analysis[33]. The CFU-S assay demonstrated the short-term kinetics of erythropoietic output potential and revealed that erythroid cell generation is a clonal feature of all these populations (but not of GMPs); whereas LTRA allowed the investigation of their long-term kinetics of peripheral blood reconstitution. Transplantation of bulk cell populations in a recipient can be used to determine self-renewal and LTMR at the population level, however, it cannot determine whether the donor cells are homogeneous or heterogeneous. To determine the clonal capacity of each transplanted cell, single cell *in vivo* clonal analyses are required. These include CFU-S assays and single-cell transplantation[36]. It is important to note that CFU-S assays cannot, alone, be used to assess *long term*

multilineage reconstitution and self-renewal because spleen colonies get resorbed before LTMR can be determined. Importantly, however, relative to the resource-intensive and technically challenging single-cell transplantation, CFU-S assays are fast and straightforward, and can be used to answer similar questions. For example, CFU-S assays, like single-cell transplantation[22, 54], demonstrated that a substantial fraction of HSCs and MPPs are multipotent at the single-cell level and can differentiate into both erythromyeloid and lymphoid lineages[22].

Conclusion: CFU-S strategies standing strong

The CFU-S assay revolutionized hematopoiesis and stem cell biology at a time when rare hematopoietic cells had not yet been identified based on immunophenotypic markers. It provided the first direct *in vivo* evidence of stem cells and led to both transformational strategies and pioneering discoveries that we continue to build upon today. This includes the first "draft" of the hematopoietic hierarchy that places the multipotent CFU-S at the top, followed by more committed progenitors that give rise to mature myeloid and lymphoid effector cells[15, 55-57]. To this day, CFU-S are an important complement to *in vivo* assays and *in vitro* clonal assays with the advantage of being able to address questions of stem cell clonality under a spectrum of physiological, disease, and experimental conditions.

Acknowledgements

We thank Connor Mattingly for pre-reviewing the manuscript. This work was supported by NIH NIDDK and NIA awards (R01DK100917 and R01 AG062879) to ECF; by a Tobacco-Related Disease Research Program (TRDRP) Predoctoral Fellowship (T31DT1690) to ARyB and by NIGMS IRACDA Postdoctoral Training Grant (K12GM139185) to BAM. Figure 1 was created with BioRender.com, agreement numbers YL22WB7VLT and NV22WB7PTB. ECF is the 2021 recipient of the McCulloch & Till Award, bestowed by the International Society for Experimental Hematology.

Figures

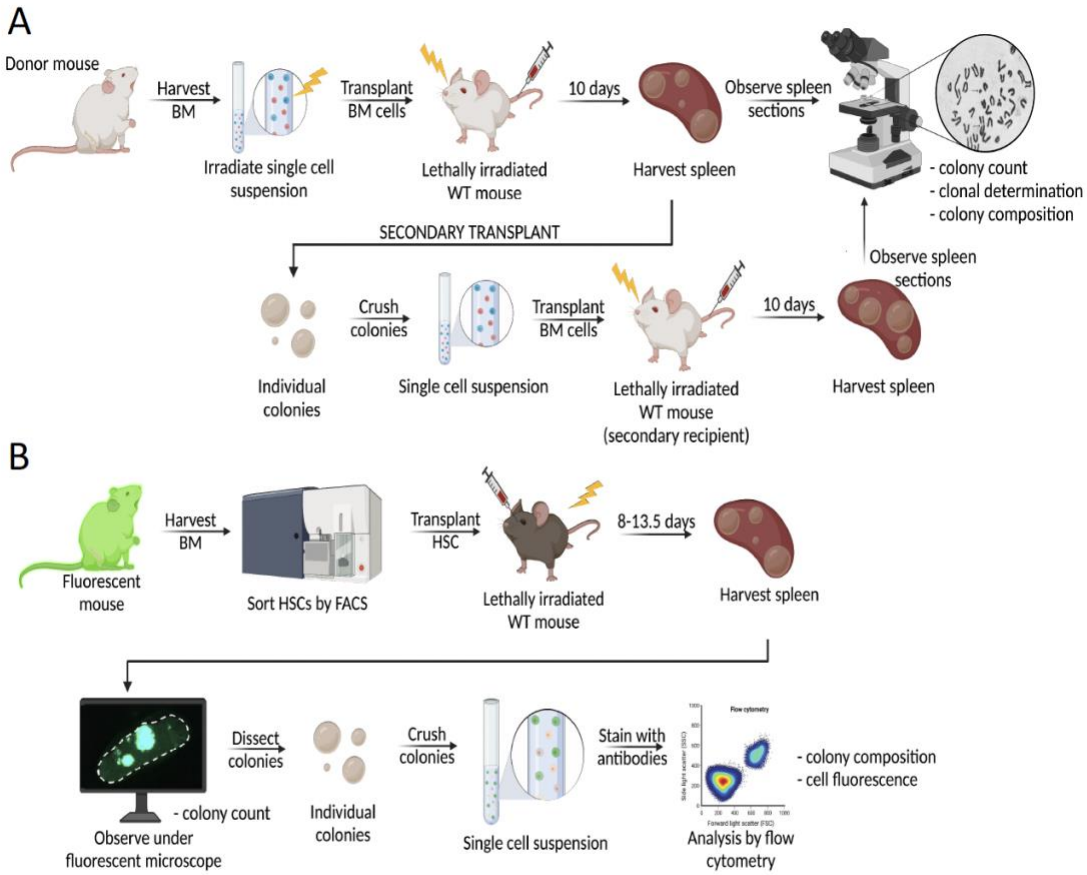

Lineage	Markers
Erythroid	FSC^{mid-hi},$TER119^{+}$,$CD41^{-}$,$Mac1^{-}$,$Gr1^{-}$, $B220^{-}$
Megakaryocytic	FSC^{mid-hi},$TER119^{-}$,$CD41^{+}$,$Mac1^{-}$,$Gr1^{-}$, $B220^{-}$
Granulocytic	FSC^{mid-hi},$TER119^{-}$,$CD41^{-}$,$Mac+^{-}$,$Gr1^{+}$, $B220^{-}$
B cell	FSC^{mid-hi},$TER119^{-}$,$CD41^{-}$,$Mac1^{-}$,$Gr1^{-}$, $B220^{+}$

Figure 1.1 Schematic of CFU-S assay.

A) In the original CFU-S assay developed by Till and McCulloch in 1961[2], bone marrow cells were harvested from donor mice and irradiated prior to intravenous injection into irradiated recipient mice. 10 days post-transplantation, spleens were counted, harvested, and sectioned for histological analysis. For serial transplantations to determine self-renewal of CFU-S cells within spleen colonies[15], individual colonies were dissected and transplanted into secondary recipients as single-cell suspensions. Spleen colonies formed after secondary transplantation were analyzed similarly to those from primary transplantations[15].
B) In the updated CFU-S assay with high throughput, quantitative analysis, HSCs (or other hematopoietic progenitors) were FACS-purified and transplanted into irradiated

recipient mice. 13.5 days post-transplantation, individual spleen colonies were counted, harvested, and dissected under a fluorescent microscope[22]. Single cell suspensions from each colony were then analyzed by flow cytometry to assess colony composition and cell fluorescence. Four lineages (erythroid, megakaryocytic, granulocytic, and B cell) were identified using the markers shown in the table[22, 41].

	CFU-S assay	LTRA
Assay details and considerations		
Input cell population	Heterogeneous or sorted populations	Heterogeneous or sorted populations
Cell purification	Bulk	Bulk or single cell
Assay speed	Fast (8-14 days)	Slow (16+ weeks)
Assay type	Terminal	Allows serial sampling from same recipient
Assessment of progeny	Cells that home to the spleen, then expand and differentiate within 8-14 days	Cells that may take longer to be generated across all tissues; in spleen: T cells, tissue resident cells
Technical requirements	Low, requires little special equipment/expertise	High, requires more specialized equipment
Relative assay cost	$	$$$
Questions that can be addressed		
Evaluate stem cell clonality?	Yes, inferred	Yes, if single-cell transplant
Determine stem cell self-renewal and LTMR?	Only if secondary transplants are performed	Yes
Evaluate blood cell reconstitution capacity?	Yes	Yes
Reconstitution kinetics?	Yes, only between 8-14 days	Yes, between 6 days to >16 weeks
Evaluate extramedullary hematopoiesis and the splenic microenvironment?	Optimal	Suboptimal
Can perform secondary transplantation?	Yes	Yes

Table 1.1. Comparison of similarities and differences between CFU-S and LTRA.

References

[1] Ford CE, Hamerton JL, Barnes DW, Loutit JF. Cytological identification of radiation-chimaeras. Nature. 1956;177:452-454.

[2] Till JE, McCulloch EA. A direct measurement of the radiation sensitivity of normal mouse bone marrow cells. 1961. Radiat Res. 1961;178:Av3-7.

[3] Ayachi S, Buscarlet M, Busque L. 60 Years of clonal hematopoiesis research: From X-chromosome inactivation studies to the identification of driver mutations. Exp Hematol. 2020;83:2-11.

[4] Fujino T, Kitamura T. ASXL1 mutation in clonal hematopoiesis. Exp Hematol. 2020;83:74-84.

[5] Cook EK, Luo M, Rauh MJ. Clonal hematopoiesis and inflammation: Partners in leukemogenesis and comorbidity. Exp Hematol. 2020;83:85-94.

[6] Steensma DP, Ebert BL. Clonal hematopoiesis as a model for premalignant changes during aging. Exp Hematol. 2020;83:48-56.

[7] Park SJ, Bejar R. Clonal hematopoiesis in cancer. Exp Hematol. 2020;83:105-112.

[8] Swierczek S, Prchal JT. Clonal hematopoiesis in hematological disorders: Three different scenarios. Exp Hematol. 2020;83:57-65.

[9] Pardali E, Dimmeler S, Zeiher AM, Rieger MA. Clonal hematopoiesis, aging, and cardiovascular diseases. Exp Hematol. 2020;83:95-104.

[10] Wang K, Yan Z, Zhang S, Bartholdy B, Eaves CJ, Bouhassira EE. Clonal origin in normal adults of all blood lineages and circulating hematopoietic stem cells. Exp Hematol. 2020;83:25-34 e22.

[11] Ganuza M, Hall T, Obeng EA, McKinney-Freeman S. Clones assemble! The clonal complexity of blood during ontogeny and disease. Exp Hematol. 2020;83:35-47.

[12] King KY, Huang Y, Nakada D, Goodell MA. Environmental influences on clonal hematopoiesis. Exp Hematol. 2020;83:66-73.

[13] Lee-Six H, Kent DG. Tracking hematopoietic stem cells and their progeny using whole-genome sequencing. Exp Hematol. 2020;83:12-24.

[14] Becker AJ, Mc CE, Till JE. Cytological demonstration of the clonal nature of spleen colonies derived from transplanted mouse marrow cells. Nature. 1963;197:452-454.

[15] Siminovitch L, McCulloch EA, Till JE. The distribution of colony-forming cells among spleen colonies. J Cell Comp Physiol. 1963;62:327-336.

[16] Wu AM, Till JE, Siminovitch L, McCulloch EA. A cytological study of the capacity for differentiation of normal hemopoietic colony-forming cells. J Cell Physiol. 1967;69:177-184.

[17] Fowler JH, Wu AM, Till JE, McCulloch EA, Siminovitch L. The cellular composition of hemopoietic spleen colonies. Journal of Cellular Physiology. 1967;69:65-71.

[18] Herzenberg LA, Parks D, Sahaf B, Perez O, Roederer M, Herzenberg LA. The history and future of the fluorescence activated cell sorter and flow cytometry: a view from Stanford. Clin Chem. 2002;48:1819-1827.

[19] Mullis K, Faloona F, Scharf S, Saiki R, Horn G, Erlich H. Specific enzymatic amplification of DNA in vitro: the polymerase chain reaction. Cold Spring Harb Symp Quant Biol. 1986;51 Pt 1:263-273.

[20] Kohler G, Milstein C. Continuous cultures of fused cells secreting antibody of predefined specificity. Nature. 1975;256:495-497.

[21] Beaudin AE, Boyer SW, Forsberg EC. Flk2/Flt3 promotes both myeloid and lymphoid development by expanding non-self-renewing multipotent hematopoietic progenitor cells. Exp Hematol. 2014;42:218-229.e214.

[22] Boyer SW, Rajendiran S, Beaudin AE, et al. Clonal and Quantitative In Vivo Assessment of Hematopoietic Stem Cell Differentiation Reveals Strong Erythroid Potential of Multipotent Cells. Stem Cell Reports. 2019;12:801-815.

[23] Weber K, Thomaschewski M, Warlich M, et al. RGB marking facilitates multicolor clonal cell tracking. Nat Med. 2011;17:504-509.

[24] Lu R, Neff NF, Quake SR, Weissman IL. Tracking single hematopoietic stem cells in vivo using high-throughput sequencing in conjunction with viral genetic barcoding. Nat Biotechnol. 2011;29:928-933.

[25] Naik SH, Perié L, Swart E, et al. Diverse and heritable lineage imprinting of early haematopoietic progenitors. Nature. 2013;496:229-232.

[26] Verovskaya E, Broekhuis MJ, Zwart E, et al. Heterogeneity of young and aged murine hematopoietic stem cells revealed by quantitative clonal analysis using cellular barcoding. Blood. 2013;122:523-532.

[27] Grosselin J, Sii-Felice K, Payen E, Chretien S, Tronik-Le Roux D, Leboulch P. Arrayed lentiviral barcoding for quantification analysis of hematopoietic dynamics. Stem Cells. 2013;31:2162-2171.

[28] Schofield R, Lord BI, Kyffin S, Gilbert CW. Self-maintenance capacity of CFU-S. J Cell Physiol. 1980;103:355-362.

[29] Magli MC, Iscove NN, Odartchenko N. Transient nature of early haematopoietic spleen colonies. Nature. 1982;295:527-529.

[30] Spangrude GJ, Heimfeld S, Weissman IL. Purification and characterization of mouse hematopoietic stem cells. Science. 1988;241:58-62.

[31] Na Nakorn T, Traver D, Weissman IL, Akashi K. Myeloerythroid-restricted progenitors are sufficient to confer radioprotection and provide the majority of day 8 CFU-S. J Clin Invest. 2002;109:1579-1585.

[32] Wolf NS, Priestley GV. Kinetics of early and late spleen colony development. Exp Hematol. 1986;14:676-682.

[33] Forsberg EC, Serwold T, Kogan S, Weissman IL, Passegué E. New evidence supporting megakaryocyte-erythrocyte potential of flk2/flt3+ multipotent hematopoietic progenitors. Cell. 2006;126:415-426.

[34] Yang L, Bryder D, Adolfsson J, et al. Identification of Lin(-)Sca1(+)kit(+)CD34(+)Flt3- short-term hematopoietic stem cells capable of rapidly

reconstituting and rescuing myeloablated transplant recipients. Blood. 2005;105:2717-2723.

[35] Pietras EM, Reynaud D, Kang YA, et al. Functionally Distinct Subsets of Lineage-Biased Multipotent Progenitors Control Blood Production in Normal and Regenerative Conditions. Cell Stem Cell. 2015;17:35-46.

[36] Osawa M, Hanada K, Hamada H, Nakauchi H. Long-term lymphohematopoietic reconstitution by a single CD34-low/negative hematopoietic stem cell. Science. 1996;273:242-245.

[37] Nakauchi H, Takano H, Ema H, Osawa M. Further characterization of CD34-low/negative mouse hematopoietic stem cells. Ann N Y Acad Sci. 1999;872:57-66; discussion 66-70.

[38] Zhao Y, Lin Y, Zhan Y, et al. Murine hematopoietic stem cell characterization and its regulation in BM transplantation. Blood. 2000;96:3016-3022.

[39] Harris RA, Hogarth PM, Wadeson LJ, Collins P, McKenzie IF, Penington DG. An antigenic difference between cells forming early and late haematopoietic spleen colonies (CFU-S). Nature. 1984;307:638-641.

[40] Morrison SJ, Weissman IL. The long-term repopulating subset of hematopoietic stem cells is deterministic and isolatable by phenotype. Immunity. 1994;1:661-673.

[41] Rajendiran S, Smith-Berdan S, Kunz L, et al. Ubiquitous overexpression of CXCL12 confers radiation protection and enhances mobilization of hematopoietic stem and progenitor cells. Stem Cells. 2020;38:1159-1174.

[42] Nakorn TN, Miyamoto T, Weissman IL. Characterization of mouse clonogenic megakaryocyte progenitors. Proc Natl Acad Sci U S A. 2003;100:205-210.

[43] Kondo M, Weissman IL, Akashi K. Identification of clonogenic common lymphoid progenitors in mouse bone marrow. Cell. 1997;91:661-672.

[44] Kruse EA, Loughran SJ, Baldwin TM, et al. Dual requirement for the ETS transcription factors Fli-1 and Erg in hematopoietic stem cells and the megakaryocyte lineage. Proc Natl Acad Sci U S A. 2009;106:13814-13819.

[45] Summers AR, Fischer MA, Stengel KR, et al. HDAC3 is essential for DNA replication in hematopoietic progenitor cells. J Clin Invest. 2013;123:3112-3123.

[46] Mehatre SH, Roy IM, Biswas A, et al. Niche-Mediated Integrin Signaling Supports Steady-State Hematopoiesis in the Spleen. J Immunol. 2021;206:1549-1560.

[47] Perry JM, Li L. Functional assays for hematopoietic stem cell self-renewal. Methods Mol Biol. 2010;636:45-54.

[48] Cool T, Worthington A, Poscablo D, Hussaini A, Forsberg EC. Interleukin 7 receptor is required for myeloid cell homeostasis and reconstitution by hematopoietic stem cells. Exp Hematol. 2020;90:39-45.e33.

[49] Leung GA, Cool T, Valencia CH, Worthington A, Beaudin AE, Forsberg EC. The lymphoid-associated interleukin 7 receptor (IL7R) regulates tissue-resident macrophage development. Development. 2019;146.

[50] Poscablo DM, Worthington AK, Smith-Berdan S, Forsberg EC. Megakaryocyte progenitor cell function is enhanced upon aging despite the functional decline of aged hematopoietic stem cells. Stem Cell Reports. 2021;16:1598-1613.

[51] Smith-Berdan S, Bercasio A, Kramer L, Petkus B, Hinck L, Forsberg EC. Acute and endothelial-specific Robo4 deletion affect hematopoietic stem cell trafficking independent of VCAM1. PLoS One. 2021;16:e0255606.

[52] Szilvassy SJ, Humphries RK, Lansdorp PM, Eaves AC, Eaves CJ. Quantitative assay for totipotent reconstituting hematopoietic stem cells by a competitive repopulation strategy. Proc Natl Acad Sci U S A. 1990;87:8736-8740.

[53] Domen J, Weissman IL. Self-renewal, differentiation or death: regulation and manipulation of hematopoietic stem cell fate. Mol Med Today. 1999;5:201-208.

[54] Yamamoto R, Morita Y, Ooehara J, et al. Clonal analysis unveils self-renewing lineage-restricted progenitors generated directly from hematopoietic stem cells. Cell. 2013;154:1112-1126.

[55] Till JE, McCulloch EA, Siminovitch L. A stochastic model of stem cell proliferation, based on the growth of spleen colony-forming cells. Proc Natl Acad Sci U S A. 1964;51:29-36.

[56] Worton RG, McCulloch EA, Till JE. Physical separation of hemopoietic stem cells differing in their capacity for self-renewal. J Exp Med. 1969;130:91-103.

[57] Iscove NN, Till JE, McCulloch EA. The proliferative states of mouse granulopoietic progenitor cells. Proc Soc Exp Biol Med. 1970;134:33-36.

Chapter 2.

New transgenic mouse models enabling pan-hematopoietic or selective hematopoietic stem cell depletion *in vivo*

The text of this chapter includes a reprint of the following previously published paper: Rodriguez Y Baena A, Rajendiran S, Manso BA, Krietsch J, Boyer SW, Kirschmann J, Forsberg EC. New transgenic mouse models enabling pan-hematopoietic or selective hematopoietic stem cell depletion in vivo. Sci Rep. 2022 Feb 24;12(1):3156. doi: 10.1038/s41598-022-07041-6. PMID: 35210475; PMCID: PMC8873235.

Abstract

Hematopoietic stem cell (HSC) multipotency and self-renewal are typically defined through serial transplantation experiments. Host conditioning is necessary for robust HSC engraftment, likely by reducing immune-mediated rejection and by clearing limited HSC niche space. Because irradiation of the recipient mouse is non-specific and broadly damaging, there is a need to develop alternative models to study HSC performance at steady-state and in the absence of radiation-induced stress. We have generated and characterized two new mouse models where either all hematopoietic cells or only HSCs can be specifically induced to die *in vivo* or *in vitro*. Hematopoietic-specific Vav1-mediated expression of a loxP-flanked diphtheria-toxin receptor (DTR) renders all hematopoietic cells sensitive to diphtheria toxin (DT) in "Vav-DTR" mice. Crossing these mice to Flk2-Cre mice results in "HSC-DTR" mice which exhibit HSC-

selective DT sensitivity. We demonstrate robust, rapid, and highly selective cell ablation in these models. These new mouse models provide a platform to test whether HSCs are required for long-term hematopoiesis *in vivo*, for understanding the mechanisms regulating HSC engraftment, and interrogating *in vivo* hematopoietic differentiation pathways and mechanisms regulating hematopoietic homeostasis.

Introduction

Permanent or conditional ablation of targeted cell populations has been widely used as a strategy to investigate cell function *in vivo*. This has been accomplished in a variety of ways, ranging from broadly acting, non-specific targeting to tissue- and cell type-specific approaches[1-5]. Whole body exposure to radiation followed by transplantation has long served as the "gold standard" for understanding the hematopoietic system[6]. Because radiation is non-specific, broadly damaging, and induces a multitude of potentially confounding responses[7-10], there is a clear need for complementary and more targeted approaches to specifically and efficiently eliminate specific cell types.

One powerful conditioning approach for specific cell ablation is to employ the cytotoxic diphtheria toxin (DT) system where mice are engineered to express either the active A subunit of DT (DT-A) or the human diphtheria toxin receptor (DTR) in a cell type-specific and/or inducible manner. The human DTR (also known as epithelial growth factor receptor, EGFR) is particularly useful in the murine system as DT specifically binds to the human, but not murine, homolog. Therefore, when

extracellular DT is administered, only the cells expressing human DTR will be killed, vastly improving specificity[11-13]. Upon induced expression or receptor-mediated endocytic entry into the cytoplasm, DT-A catalyzes the inactivation of elongation factor-2, halting protein synthesis and inducing apoptosis. Therefore, only the cells containing DT-A will be ablated[12,14-16]. Importantly, DT-A toxicity is exceedingly efficient as one molecule in the cytosol is sufficient to induce cell death[16]. The substantial toxicity of DT-A and human DTR specificity results in a combinatorial ablation system that is highly sensitive and efficient.

Here, we generated and characterized two mouse strains with either pan-hematopoietic or hematopoietic stem cell (HSC)-selective DT sensitivity. These two new mouse models enable hematopoietic cell ablation that is magnitudes more specific than currently used strategies such as irradiation and chemotherapy. Thus, they provide a new radiation-independent system that opens new avenues for understanding the mechanisms regulating HSC biology.

Results

A novel mouse model for pan-hematopoietic expression of DTR

We sought to generate a novel transgenic mouse line with pan-hematopoietic expression of the human DTR for targeted depletion of all hematopoietic cells. We used the murine regulatory elements of the *Vav1* gene, which is highly and exclusively expressed throughout the hematopoietic system[17-22] to drive expression of DTR in the "Vav-DTR" mice. Pronuclear injection of the Vav-DTR construct (Figure 1a) into

C57BL/6 zygotes resulted in several Vav-DTR founders with confirmed germline transmission. In this model, DTR would be expressed in all hematopoietic cells, except for red blood cells (RBC, Figure 1b), similar to our previously published Vav-GFP mouse model[20]. The GFP in the construct would not be expressed unless the Vav-DTR mice contained active Cre-recombinase (Figure 1a). Presence of the DTR transgene was confirmed to be specific to various hematopoietic cells from Vav-DTR mice and absent in cells from wild type (WT) mice (Figure 1c-d), as expected.

<u>In vitro and in vivo depletion of hematopoietic cells is highly specific in Vav-DTR mice</u>

To investigate the functional expression of DTR and specificity of DT sensitivity of hematopoietic cells *in vitro*, hematopoietic stem and progenitor cell (HSPC) populations were isolated from the bone marrow (BM) of Vav-DTR mice and treated with DT in culture. Independent of the dose, DT did not affect WT cells (Figure 1e), but very efficiently and significantly depleted HSCs, multipotent progenitors (MPPs), and myeloid progenitors (MyPros) from Vav-DTR mice (Figure 1f).

We then determined the ability of DT to exclusively deplete hematopoietic cells *in vivo*, and if the degree of ablation was comparable to irradiation, the most commonly used regimen for ablation of HSPCs from the BM[3,23-25]. To achieve this, we compared cell numbers in the BM and peripheral blood (PB) of WT and Vav-DTR mice 24 hours post-treatment with a high dose of DT or saline, or 9 days post sub-lethal irradiation (Figure 2a)[23]. As expected, DT did not alter cell numbers in WT mice, but significantly

depleted HSPCs (KLS**,** Figure 2b; and MyPro, Figure 2c; Supplementary Figure 1a) and mature (GM, B, and T) cells (Figure 2d) in the BM of Vav-DTR mice, similar to levels of ablation achieved with irradiation. Thus, DT very rapidly depleted the vast majority of all hematopoietic cells in the BM of Vav-DTR mice.

In PB, not all mature cells were ablated equally. As expected, B cells (Figure 3a) and T cells (Figure 3b) were significantly depleted from Vav-DTR mice 24 hours post-DT treatment to levels similar to 9 days post-irradiation. DT-induced depletion of platelets was also observed in Vav-DTR mice (Supplementary Figure 1b), while RBCs (Supplementary Figure 1c) remained unaffected at this timepoint, likely due to the lack of Vav1-driven DTR expression by RBCs themselves and consistent with the Vav-GFP mice we previously described[20]. Surprisingly, GM cell counts significantly increased 24 hours after DT treatment which contrasts the significant depletion observed 9 days post-sublethal irradiation (Figure 3c). A time course tail bleed analysis revealed that this increase in GMs was temporary until 37 hours post DT treatment, followed by a subsequent steep decrease 42 hours post DT in Vav-DTR mice (Figure 3d). Due to poor overall health after 42 hours, mice were sacrificed, and no further time points were recorded. Of note, DT-mediated depletion of mature blood cells was remarkably robust in both BM (Figure 2) and PB (Figure 3).

To test the specificity of DT sensitivity to the hematopoietic compartment, we investigated the effects of DT on non-hematopoietic cells of the spleen and BM 24 hours post-DT treatment. DT-dependent cell number decrease was found to be specific to cells labeled by the pan-hematopoietic marker CD45, but did not affect CD45- spleen

cells 24 hours after treatment (Figure 3e). Additionally, bones were evaluated for endothelial cell (EC) or non-EC stromal populations. Despite contradicting reports of off-target *vav*-driven labeling of ECs[19,20,26], ECs from our Vav-DTR mice showed no sensitivity to DT (Figure 3f). Taken together, our *in vitro* and *in vivo* data demonstrate that the Vav-DTR mice are exclusively and specifically sensitive to very rapid and robust hematopoietic cell ablation upon administration of DT.

DT-mediated hematopoietic ablation increased donor chimerism in transplanted recipients

Having demonstrated the efficiency and specificity of DT in depleting hematopoietic cells in the Vav-DTR mouse model, we hypothesized that this system could be exploited to increase donor chimerism upon transplantation. Thus, we transplanted WBM cells from UBC-GFP mice (where all cells express GFP) into sub-lethally irradiated (non-fluorescent) Vav-DTR mice (GFP→VavDTR; Figure 4a) or WT (GFP→WT; Supplementary Figure 2a) mice. After chimeras were established (>16-weeks post-transplant), we treated them with increasing sequential doses of DT. Since we previously observed how specific, effective, and quick DT-induced cell death occurs (Figures 2-3), we reasoned that multiple increasing doses of DT would avoid abrupt and overwhelming cell death in these chimeras. We analyzed the peripheral blood composition 1 week after each DT injection to determine any changes in donor chimerism (Figure 4b, Supplementary Figure 2b). As shown in Figure 4b, we observed a gradual increase in donor chimerism upon DT treatment of the GFP→VavDTR

chimeras, which became significant after a second 50ng DT dose. Meanwhile, donor chimerism in the respective control chimeras (GFP→VavDTR untx) remained stable (Figure 4b, Supplementary Figure 2b). When comparing GM donor chimerism at chimera establishment with endpoint analysis, we observed that donor chimerism increased to over 90% in DT-treated GFP→VavDTR chimeras where the host was DT-sensitive (Figure 4c). Similar to GFP→Vav-DTR untreated chimeras (Figure 4b,c), GM donor chimerism remained unaltered in GFP→WT chimeras untreated or DT-treated (Supplementary Figure 2c). Consistent with GM donor chimerism, total donor chimerism in GFP→VavDTR chimeras increased significantly after DT treatment as well, while no significant differences were observed in all other chimera groups (Supplementary Figure 2d). DT treatment also led to a significant increase in bone marrow donor chimerism in the GFP→VavDTR chimeras compared to the untreated controls (Figure 4d). We also isolated KLS and MyPro cells from control GFP→VavDTR chimeras (GFP→VavDTR untx) and treated them *in vitro* (as in Figure 1e) to confirm that the results observed *in vivo* was due to differential DT sensitivity. Similar to the *in vivo* data, GFP+ and WT cells from GFP→WT chimeras were not affected by DT *in vitro* (Supplementary Figure 2e). In contrast, and as expected, only GFP+ donor cells from VavDTR recipient mice survived DT treatment while Vav-DTR cells were depleted **(**Figure 4e, Supplementary Figure 2f**)**. Overall, these data demonstrate the specificity of DT in a transplant setting, which allow selective increase of donor chimerism *in situ*.

Generation and characterization of an HSC-specific DT-sensitive mouse model

We next crossed our Vav-DTR mouse to the well-characterized Flk2-driven Cre mouse line[27-29,42-43,50] to generate "HSC-DTR" mice where DTR would be expressed only by HSCs. In this model, Flk2-driven expression of Cre recombinase catalyzes the excision of loxP-flanked transgenes in all hematopoietic cells except HSCs[28,29] (Figure 5a). Flk2 is expressed at the MPP stage, thus all cells expressing Flk2 or with a history of Flk2 expression will have undergone loxP recombination. When crossed to the Vav-DTR mice, Flk2-Cre should excise the DTR gene and STOP codon and induce irreversible excision of the DTR transgene and subsequent expression of GFP in all hematopoietic cells except HSCs (Figures 1a and 5a-b). Treatment of these mice with DT should then lead to HSC-specific cell death.

To evaluate floxing efficiency and the ability of the reporter construct to label hematopoietic cells with GFP fluorescence, HSPCs and mature cell populations were isolated from the BM and PB of HSC-DTR mice. Flow cytometry analysis revealed GFP reporter expression in a fraction of all hematopoietic cells of HSC-DTR, but not WT, mice except for HSCs and circulating red blood cells and platelets (Figure 5c). We noted that the overall proportion of cells expressing GFP was far from complete, even in the lymphoid lineage that expresses robust levels of the Flk2-Cre transgene at multiple stages of differentiation[28-31,42-43,50]. Although both the frequency of GFP+ cells and GFP expression levels were low, we detected significantly reduced levels of the DTR transgene in (GFP+) MPPs and compared to (GFP-) HSCs from HSC-DTR mice (Figure 5d). Thus, it appeared that the DTR transgene was deleted as intended, and that

GFP expression was insufficiently strong to be a reliable indication of Flk2-Cre recombination (floxing) efficiency in this model.

In vitro and in vivo DT sensitivity is specific to HSCs in HSC-DTR mice

We then tested whether DT sensitivity was indeed limited to the HSC population. We sorted HSCs, MPPs, and MyPros and treated them with DT *in vitro*. Consistent with the weak GFP expression in this model (Figure 5c), the MPP and MyPro populations included both GFP+ and GFP- cells. As expected, HSCs, but not MPPs and MyPros, were efficiently depleted by two different doses of DT (Figure 6a, Supplemental Figure 3a). We additionally treated HSC-DTR mice with DT *in vivo* and observed a significant reduction of HSCs in HSC-DTR mice, while MPPs remained unaffected (Figure 6b). These data indicated that the DTR gene had been successfully excised in HSC progeny to make these cells DT-resistant. In contrast, HSCs remained highly DT sensitive, consistent with the floxing pattern of previous Flk2-Cre models[20,28-30].

We next transplanted WBM cells from HSC-DTR mice into sub-lethally irradiated fluorescent WT mice (HSCDTR→WT) to establish chimeras (Figure 6c). Importantly, the mTmG or KuO fluorescent hosts uniformly and robustly express their respective transgene, allowing identification of both GFP+ and GFP- donor cells. After recovery and verification of chimerism (Supplementary Figure 3b), we treated these chimeras with a single dose of DT 24 hours prior to analysis of BM donor chimerism (Figure 6c-f). This analysis revealed that DT significantly reduced HSC donor

chimerism by specifically killing donor GFP- HSCs (Figure 6d, green patterned bars). Importantly, the percentage of donor MPPs (whether GFP+ or GFP-) (Figure 6e) and MyPros (GFP+ and GFP-; Figure 6f) were unaffected by DT treatment *in vivo*. Overall, these *in vitro* and *in vivo* data demonstrate that DT selectively targets HSCs in HSC-DTR mice and suggests that the HSC-DTR mouse line is a suitable model for *in vivo* targeted ablation of HSCs.

Discussion

We have developed two new mouse models where cell death of either nucleated hematopoietic cells, or only HSCs, can be induced *in vivo* by administration of DT. The "Vav-DTR" mice show Vav1-driven expression of DTR in all hematopoietic cells (Figure 1). This Vav-dependent model is consistent with the previously reported hematopoietic specificity of Vav1 activity[19-21]. Our *in vitro* (Figure 1) and *in vivo* (Figure 2 and 3) data show that DT selectively and efficiently ablates hematopoietic cells from Vav-DTR mice. Interestingly, we also observed a transient increase in PB GMs suggesting a neutrophilic influx to possibly remove cellular debris accumulated from extensive cell death upon systemic DT treatment[32-34]. Similarly, lower levels of splenic mature cell depletion after DT treatment compared to BM and PB may be due to transient neutrophil influx into the spleen as well. More importantly, non-hematopoietic cells from the spleen and BM stromal cells of Vav-DTR mice remained unaffected by DT (Figure 3e-f). We speculate that the trend towards an increase in ECs in the Vav-DTR BM upon DT treatment, which was previously observed by others in

a similar context[33], is more likely due to increased recovery, rather than an increase in actual cell numbers, of ECs due to decreased adherens to BM stroma upon the quick and overwhelming DT-induced death of hematopoietic BM cells. We also demonstrated that the selectivity of DT sensitivity could be exploited in a transplant setting to increase donor chimerism (Figure 4).

Given how quickly, efficiently, and specifically DT leads to death of DTR-expressing cells, DT pre-conditioning in the Vav-DTR model must be more carefully optimized before use as an alternative to irradiation. The massive death of DTR-expressing cells withing 24 hours of in vivo administration of 50 μg/kg DT may cause death due to vaso-occlusion and/or inability of rescue by transplanted cells that cannot immediately replenish host cells. Two straightforward options that we have not yet been able to fully explore is to reduce the DT dose and/or utilize HSC-DTR mice as recipients. A third alternative was uncovered by a recent publication that employed an inducible Gata2 knockout model for the depletion of HSCs. The study demonstrated that HSPCs transplanted into unconditioned recipients persist in the BM for at least 4 weeks, allowing for post-transplant niche clearance and subsequent reconstitution of the pre-transplanted HSPCs[35]. This intriguing result suggests that a post-transplant conditioning approach may address the timing discrepancy between DT-induced host cell death and rescue by donor cells, thus making our Vav-DTR and/or HSC-DTR models potentially suitable for HSC engraftment in a non-irradiated, more selectively perturbed environment.

We then crossed the Vav-DTR mice to our well-characterized Flk2-Cre transgenic mice to achieve HSC-specific DTR expression (Figure 5). We previously demonstrated efficient Flk2-Cre-mediated excision of a floxed transgene in all hematopoietic cells except for HSCs[28-29,42-43,50]. In the new "HSC-DTR" model, HSCs express the DTR while all cells downstream of HSCs, via differentiation through Flk2+ MPPs, do not express the DTR (Figure 5d) and were therefore unaffected by DT (Figure 6). Although GFP expression in this model is relatively low and underestimates floxing efficiency, our *in vitro* and *in vivo* data demonstrated that DT-sensitivity was indeed highly restricted to the HSC compartment of HSC-DTR mice (Figure 6).

These two new mouse models are suited to investigate the cellular mechanisms of hematopoietic homeostasis, *in situ* HSC differentiation cascades, the ability of progenitor cells to sustain hematopoiesis in the absence of HSCs, and to manipulate post-transplant engraftment and chimerism similar to a recently published study[35]. Experimental use of these mice has the potential to uncouple self-renewal capability *in situ* from the ability to provide long-term hematopoietic reconstitution upon transplantation and may therefore impact our understanding of the mechanisms regulating self-renewal. For example, these mice could be utilized to ask such questions as: are multipotent progenitors capable of self-renewal *in situ*, despite their inability to self-renew upon transplantation? Is differentiation re-routed to cells necessary for survival, at the expense of other cell types, when endogenous HSCs are ablated? Certainly, transplantation assays have demonstrated the ability of HSCs to self-renew and differentiate into all the hematopoietic lineages[23,24,30,36-38]. However, the extent to

which this reflects *in situ* hematopoiesis is unclear as transplantation is conducted under broadly damaging conditioning regimens that force HSCs to proliferate to replenish the entire hematopoietic system of a recipient mouse[39-41]. Importantly, recent studies have also argued that the *in situ* contribution of HSCs to steady-state hematopoiesis is less than what is observed upon transplantation[33,39-41]. The use of our new HSC-DTR mice, where a large proportion of HSCs can be depleted due to expression of DTR, could therefore complement these studies, including a recent functional report suggesting that hematopoiesis may proceed normally despite a reduction of HSCs to less than 10% of normal numbers[33].

Here, we generated two new mouse models, Vav-DTR and HSC-DTR, which respectively achieve efficient and selective depletion of all hematopoietic cells or only HSCs in response to DT treatment. Both mouse models were extensively characterized and showed restricted DTR expression in selected tissues or cells of interest, along with specific DT sensitivity *in vitro, in vivo*, and in transplantation settings. These two new mouse models will be useful tools to advance our understanding of hematopoietic homeostasis, HSC engraftment, and properties of HSCs under steady-state and varying physiological conditions.

Methods

Mice

Vav-DTR and HSC-DTR mice were generated in house as described below. WT C57BL/6 (cat# 000664), WT UBC-GFP (cat# 004353), WT mT/mG (cat# 007576)

were purchased from Jackson Laboratories. Mice were maintained and bred in the UCSC AAALAC-approved vivarium according to IACUC approved protocols, under which all experiments were conducted. In addition to this, we confirm that the experimental protocols, Forsc1906, were approved by the UCSC IACUC (Institutional Animal Care and Use Committee), which is a named institutional and/or licensing committee. Mice were sacrificed by CO2 (carbon dioxide) inhalation, as per our IACUC-approved protocols, Forsc1906. The study was carried out in compliance with the ARRIVE guidelines.

Generation of Vav-DTR and HSC-DTR transgenic mice

The Vav-DTR plasmid was generated by inserting the DTR sequence followed by a STOP codon between loxP sites, flanked at the two ends by Vav regulatory elements and a GFP sequence respectively. The vector was linearized and injected into pronuclei of C57BL/6 mice at the University of California Santa Cruz (UCSC) transgenic facility. Multiple founders were used to establish a colony, but founder lines were not analyzed separately. Characterization of the founders revealed nothing of concern and consistent normal phenotypes. Vav-DTR litters were genotyped using the following primers: 5'-AGCTGCTCCAGGCTCTCG-3' (binds to DTR sequence) and 5'-GTGTTGTAGTTGTCCCCACTGG-3' (binds to Vav1 regulatory elements sequence). HSC-DTR mice were generated by breeding Vav-DTR mice and Flk2-Cre mice. The PB from male HSC-DTR mice was analyzed by flow cytometry to confirm Flk2-Cre recombinase activity and determine Cre-driven DTR excision, referred to as "floxing",

efficiency. Floxing efficiencies ranged depending on the cell type. Only male HSC-DTR mice were analyzed as Flk2-Cre recombination is inefficient in females[28,30,42].

qPCR analysis

DNA was isolated from BM cells sorted from WT and Vav-DTR mice using QIAamp® DNA Blood Mini Kit (Qiagen) according to manufacturer's protocol (Figure 1d). qPCR was run on a QuantStudio 6 Flex PCR thermal cycler (Thermo Fisher Scientific) using SensiMix™ SYBR® No-ROX Kit (Bioline) according to the manufacturer's protocol. Messenger RNA was extracted from the various tissues using Trizol (Invitrogen). RNA was used to obtain cDNA using High Capacity cDNA Reverse Transcriptase Kit (Applied Biosystems) according to the manufacturer's protocol (Figure 5d). Quantitative real-time PCR was run on a ViiA 7 or QuantStudio 6 Flex PCR thermal cycler (Thermo Fisher Scientific) using SensiMix SYBR No-ROX Kit (Bioline) according to the manufacturer's protocol. β-actin was used to normalize expression levels. qPCR was conducted using the following primers: 5'-AGGCAAGGGACTAGGGAAGA-3' and 5'-CCACCACAGCCAGGATAGTT-3' for DTR; 5'-CCACAGCTGAGAGGGAAATC-3' and 5'-CTTCTCCAGGGAGGAAGAGG-3' for β-actin.

Flow cytometry

BM and spleen cells were obtained by crushing the tibia and femur or spleen in 1X PBS supplemented with 5mM EDTA with 2% serum. PB was collected directly into

1X PBS supplemented with 5mM EDTA with 2% serum from the tail vein or femoral artery. Single cell suspensions were passed through 70-micron filters, and RBCs were lysed (spleen and PB only). Cells were then stained with monoclonal antibodies on ice in the dark for 20 minutes and analyzed using a FACSAria or an LSRII flow cytometer (BD Biosciences, San Jose, CA) as described previously[23,43,44]. FlowJo Software 10.7.1 (Ashland, OR) was used for data analysis and display. Live cells were determined by staining with propidium iodide. Following pre-gating on single, live cells, hematopoietic cell populations were defined by the following cell surface phenotypes: KLS ($Lin^{-}Sca1^{+}c\text{-}kit^{+}$), HSCs ($Lin^{-}Sca1^{+}c\text{-}kit^{+}Slam^{+}Flk2^{-}$), MPPs ($Lin^{-}Sca1^{+}c\text{-}kit^{+}Slam^{-}Flk2^{+}$), MyPros ($Lin^{-}Sca1^{-}c\text{-}kit^{+}$), GMs ($Ter119^{-}CD3^{-}B220^{-}Mac1^{+}Gr1^{+}$), T cells ($Ter119^{-}Mac1^{-}Gr1^{-}B220^{-}CD3^{+}$), B cells ($Ter119^{-}Mac1^{-}Gr1^{-}CD3^{-}B220^{+}$), platelets ($FSC^{lo}Ter119^{-}CD61^{+}$), and RBCs ($Ter119^{+}$). The lineage (Lin) mixture consisted of antibodies recognizing CD3, CD4, CD5, CD8, B220, Gr1, Mac1, and Ter119 cell surface proteins. Bone endothelial cells (ECs; $CD45^{-}Ter119^{-}CD31^{+}Sca^{+}$) and non-EC stroma cells ($CD45^{-}Ter119^{-}CD31^{-}$) were prepared as described previously[45]. Briefly, tibia and femur were dissected and homogenized with PBS using a mortar and pestle. Bone fragments were digested in a 3 mg/mL collagenase I solution for 1 hour at 37°C with intermittent vortexing and finally neutralized by adding serum containing EDTA/PBS media. Samples were then washed with PBS, filtered, and stained prior to analysis by flow cytometry.

Cell sorting

Hematopoietic cells were isolated and prepared from the BM of mice in accordance with UCSC guideline as described above and previously using a BD FACSAria[23,24,28,30,42,45-49].

Absolute cell number quantification

A known volume of PB was mixed with an antibody solution in 1X PBS supplemented with 5mM EDTA with 2% serum containing a known quantity of Calibrite APC beads prior to flow cytometry analysis. For tissues, such as BM and spleen, a known quantity of beads was added to each tissue prior to homogenization. The ratio of number of beads added to the sample to the number of beads collected by flow cytometry was used to calculate the absolute number of mature cells per microliter of blood or within each tissue[23,48].

Irradiation assays

Mice were irradiated using an X-ray tube irradiator (Faxitron CP-160). For the experiments described in Figure 2-3, PB and BM cells were analyzed by flow cytometry 9 days after sub-lethal (~750 rads) irradiation as this time point represents the lowest detectable cell numbers post-irradiation, prior to recovery[23]. Sublethal irradiation is often used as the preferred conditioning regimen of host mice prior to transplant.

Transplantation assays

Transplantation assays were performed as previously described[23-25,28,30,42,46]. For the Vav-DTR chimeras, 3.75 million or 7.5 million whole bone marrow (WBM) cells from donor UBC-GFP mice were retro-orbitally transplanted into ¾ (~750 rads) or ½ (~500 rads) lethally irradiated Vav-DTR and WT hosts. These two chimera set ups, as expected, led to similar donor chimerism to allow comparison of experiments. For the HSC-DTR chimeras, 1 million WBM from donor HSC-DTR mice were retro-orbitally transplanted into sub-lethally irradiated (~500 rads) mTmG or KuO hosts. Recipient mice were bled at 4-, 12-, and 16-weeks post-transplantation via the tail vein for analysis of donor/host contribution in the peripheral blood (data not shown), detectable by GFP or Tomato/KuO expression, to confirm long term multilineage reconstitution.

Diphtheria toxin treatment

DT (50 µg/kg; Sigma) was administered to WT and Vav-DTR mice via intraperitoneal (i.p.) injection 24 hours prior to take-down to determine depletion of hematopoietic or non-hematopoietic cells as shown in Figures 2-3. BM chimeras generated with GFP donor cells into Vav-DTR (GFP→Vav-DTR) or control WT (GFP→WT) were administered 6 DT doses ranging between 5-50ng/mouse and bled 1 week after each DT treatment as shown in Figure 4b. HSC-DTR mice were administered 100ng (~5 µg/kg) of DT 24 hours prior to BM analysis as shown in Figure 6b. BM chimeras, with HSC-DTR donor cells into WT recipients (HSCDTR→WT) were administered 100ng/mouse (~5 µg/kg) of DT 24 hours prior to takedown for BM analysis. 0.1 ng/µl

or 1.0 ng/µl DT was added once to the cell culture media for 7 (Figure 1e-f, Figure 6a, and Supplementary Figure 3a) or 3 (Figure 4e, and Supplementary Figure 2e-f) days prior to analysis by flow cytometry to determine *in vitro* DT sensitivity of Vav-DTR and HSC-DTR cells.

In vitro culture

Using anti-CD117/cKit microbeads (Miltenyi Biotec), BM cells from WT, HSC-DTR, VAV-DTR, and chimeric mice were enriched for c-Kit positive cells and sorted via flow cytometry into 5mM EDTA in 1X PBS with 2% serum and then spun down. 100 HSCs, 200 MPPs, and 500 MyPros were plated in triplicates in IMDM media supplemented with 20% FBS, TPO (50ng/ml), SCF (50 ng/ml), IL-6 (20ng/ml), IL-3 (10ng), IL-11 (20ng/ml), 1X Primocin, and 1X Non-Essential Amino Acids. Live and nucleated cells were harvested and analyzed by flow cytometry after 7 days for Figure 1e-f, Figure 6a, and Supplementary Figure 3a. HSCs, MPPs, and MyPros were analyzed after 3 days in culture for Figure 4e and Supplementary Figure 2e-f.

Statistics

Unpaired two-tailed Student's t-tests and one-way ANOVAs adjusted for multiple comparisons with Tukey or Dunnett's post-hoc tests were used to assess statistical significance for comparisons of different groups, as appropriate. The sample size, number of independent experiments, and p-values are provided for each experiment in the respective figure legend.

Author Contributions

A.R.y.B., S.R., J. Krietsch, S.W.B., B.A.M., and J. Kirschmann performed experiments; A.R.y.B. and S.R. analyzed results and made the figures; A.R.y.B., B.A.M. and E.C.F. wrote the paper.

Acknowledgments

We thank Drs. Bleul and Boehm for providing the Flk2-Cre mice, Dr. Waisman for providing the iDTR plasmid, Drs. Graf and Stadfelt for the Vav vector, Armen Shamamian at the UCSC vivarium for generation of transgenic mice, and Bari Nazario and the UCSC Institute for the Biology of Stem Cells for flow cytometry support. This work was supported by an NIH R21 award (R21AI103656) to E.C.F, a Tobacco-Related Disease Research Program (TRDRP) Predoctoral Fellowship (T31DT1690) to A.R.y.B.; a California Institute for Regenerative Medicine (CIRM) training grant (TG2-01157) to S.W.B. and J.Krietsch; a NIGMS IRACDA Postdoctoral Training Grant (K12GM139185) to B.A.M. and a CIRM Facilities awards CL1-00506 and FA1-00617-1 (RRIDs SCR_021149, SCR_021353 and SCR_021135) to University of California Santa Cruz (UCSC).

Figures

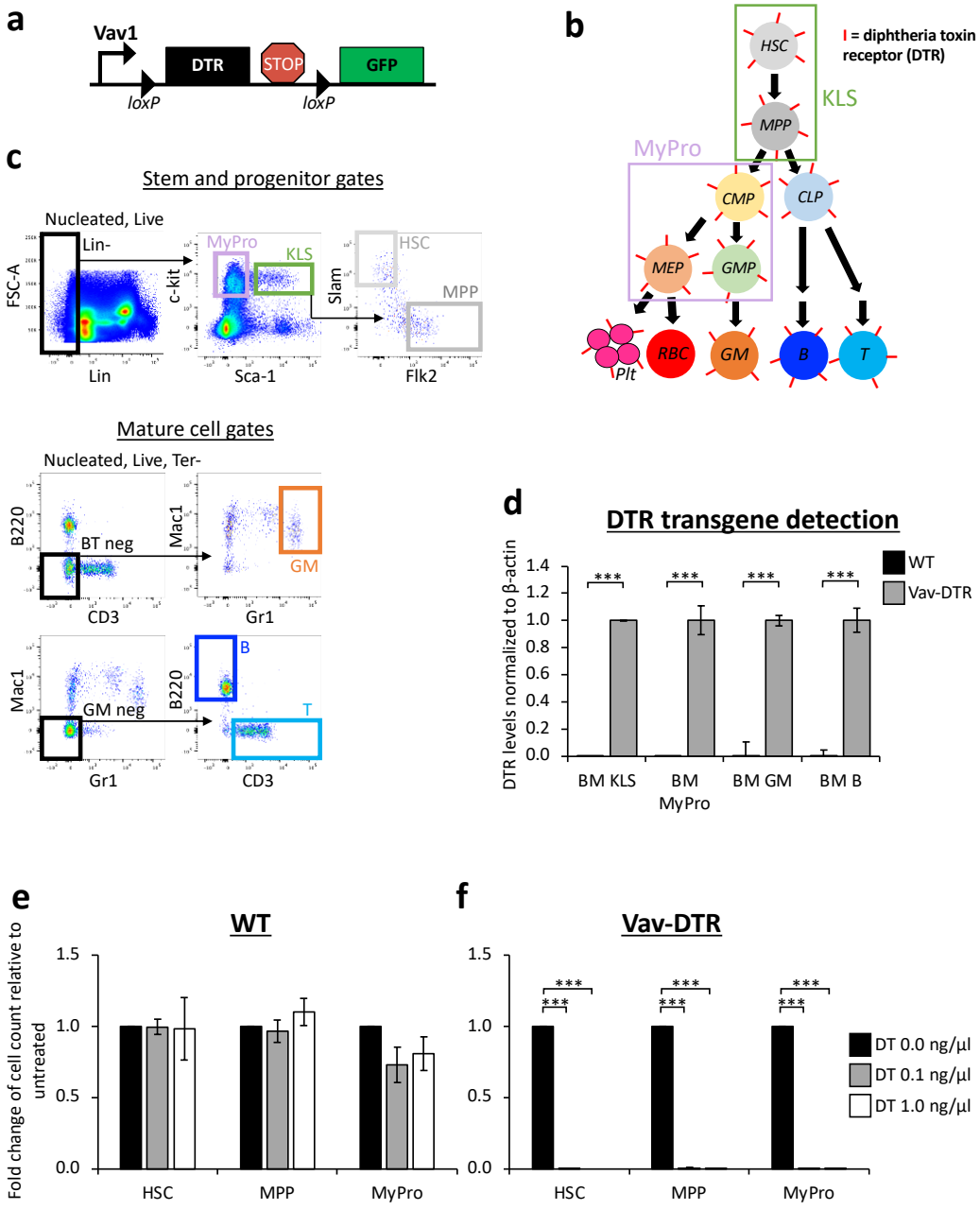

Figure 2.1. Hematopoietic cells from Vav-DTR mice were sensitive to DT in vitro.

(a) Schematic diagram of the Vav-DTR transgene construct.
(b) Simplified model of the hematopoietic tree. All hematopoietic cells that express Vav1 should express DTR (shown as a "I"-shaped surface receptor).

(c) Representative flow cytometry plots of the main populations analyzed: myeloid progenitors (MyPro), ckit+Lineage-Sca1+ (KLS), hematopoietic stem cells (HSC), multipotent progenitor cells (MPP), granulocyte-myelomonocytic (GM), B, and T cells. Pre-gates are shown above the plots.
(d) Quantitative PCR analysis of BM KLS, MyPro, GM, and B cell populations sorted from WT and Vav-DTR mice detected the DTR transgene only in Vav-DTR mice. Bar graph indicates the relative levels of DTR transgene in cells isolated from WT (black bar) or Vav-DTR mice (gray bar). β-actin was used to normalize expression levels. N=3 mice. Error bars indicate SEM, ***$p<0.001$ (Student's t-test).
(e) HSCs, MPPs, and MyPros sorted from WT mice remained unaffected *in vitro* 7 days after diphtheria toxin (DT) exposure,
(f) while Vav-DTR cells were drastically depleted. Bar graphs indicate the fold change in cell number relative to untreated (black bar, DT 0.0 ng/µl) after a 7-day 0.1 ng/µl (gray bar) and 1.0 ng/µl (white bar) DT treatment. N=2 (Vav-DTR) and N=3 (WT) independent experiments. Error bars indicate SEM, ***$p<0.001$ (One-way ANOVA with Dunnett's post-hoc test).

BM, bone marrow; HSC, hematopoietic stem cell; MPP, multipotent progenitor; CMP, common myeloid progenitor; CLP, common lymphoid progenitor; MEP, megakaryocyte-erythroid progenitor; GMP, granulocyte-macrophage progenitor; plt, platelet; RBC, red blood cell; GM, granulocyte/macrophage; B, B cell; T, T cell; KLS, $ckit^{+}Lin^{-}Sca1^{+}$ cells include HSCs and MPPs; MyPro, myeloid progenitors are c-$kit^{+}Lin^{-}Sca1^{-}$ cells include CMPs, MEPs, and GMPs; BM, bone marrow.

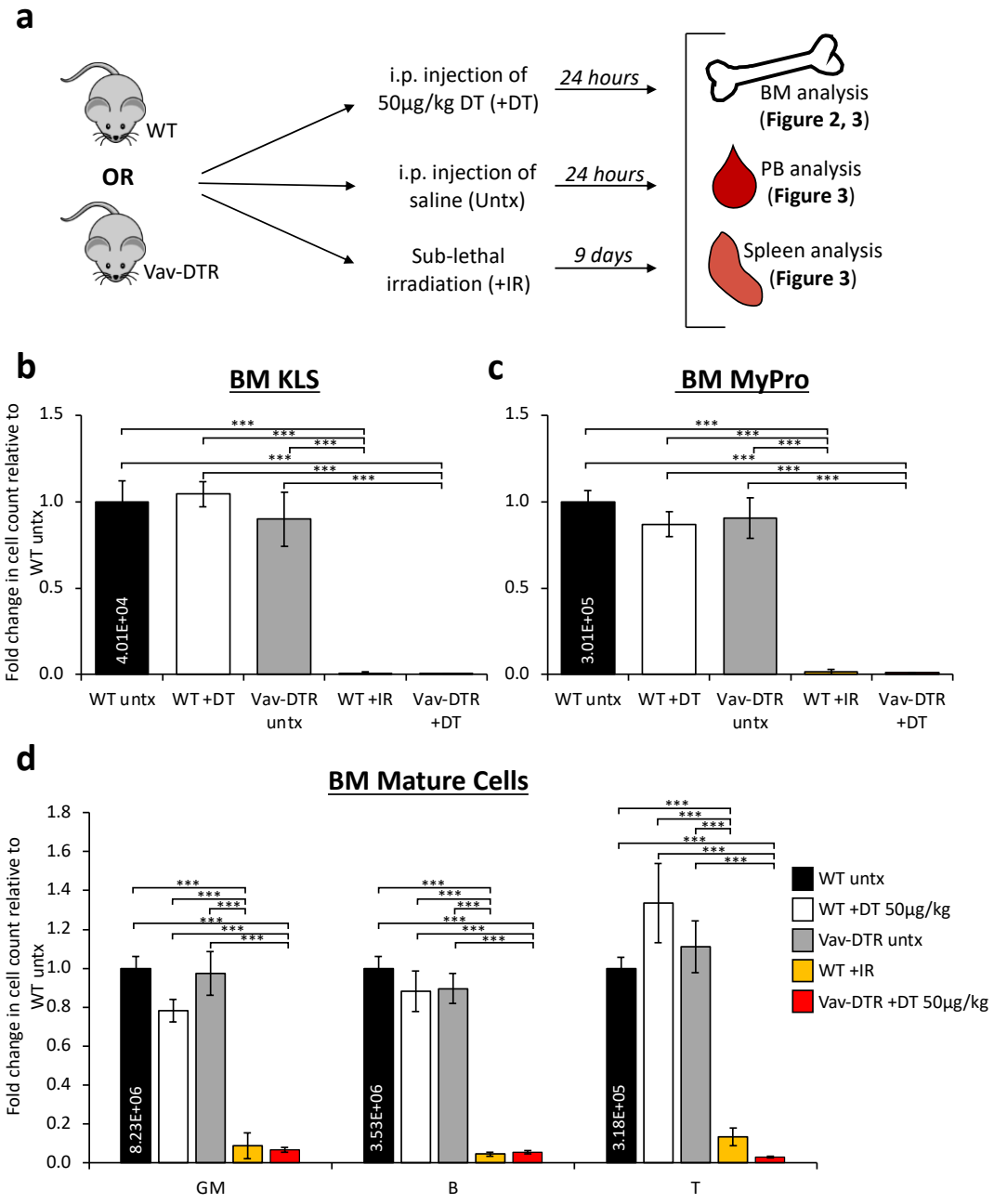

Figure 2.2. HSPCs and mature cells from the BM of Vav-DTR mice are depleted by DT in vivo.

(a) Schematic of experimental design. WT and Vav-DTR mice received an i.p. injection of 50 µg/kg of DT 24 hours prior to takedown for BM, PB, and spleen analysis. These data were compared to WT and Vav-DTR mice treated with a control saline injection (untreated), and WT mice that were sub-lethally irradiated 9 days prior to takedown. DT depleted KLS **(b)**, MyPro **(c)** and mature blood cells **(d)** in the BM of

Vav-DTR mice (red bar), similar to 9-days post sublethal (750 rads) irradiation (IR, yellow bar; positive control). WT mice were unaffected by DT treatment (white bars), harboring similar cell numbers to untreated WT mice (black bar; negative control), and untreated Vav-DTR mice (gray bars). The numbers in the black bar represent absolute cell count in the BM. Bar graphs indicate the fold change in cell number relative to untreated WT mice. N=4-9 mice in at least three independent experiments. Error bars indicate SEM, ***$p<0.001$ (One-way ANOVA with Tukey post-hoc test).

HSPCs, hematopoietic stem and progenitor cells; i.p., intraperitoneal; PB, peripheral blood; Untx, untreated; IR, irradiated.

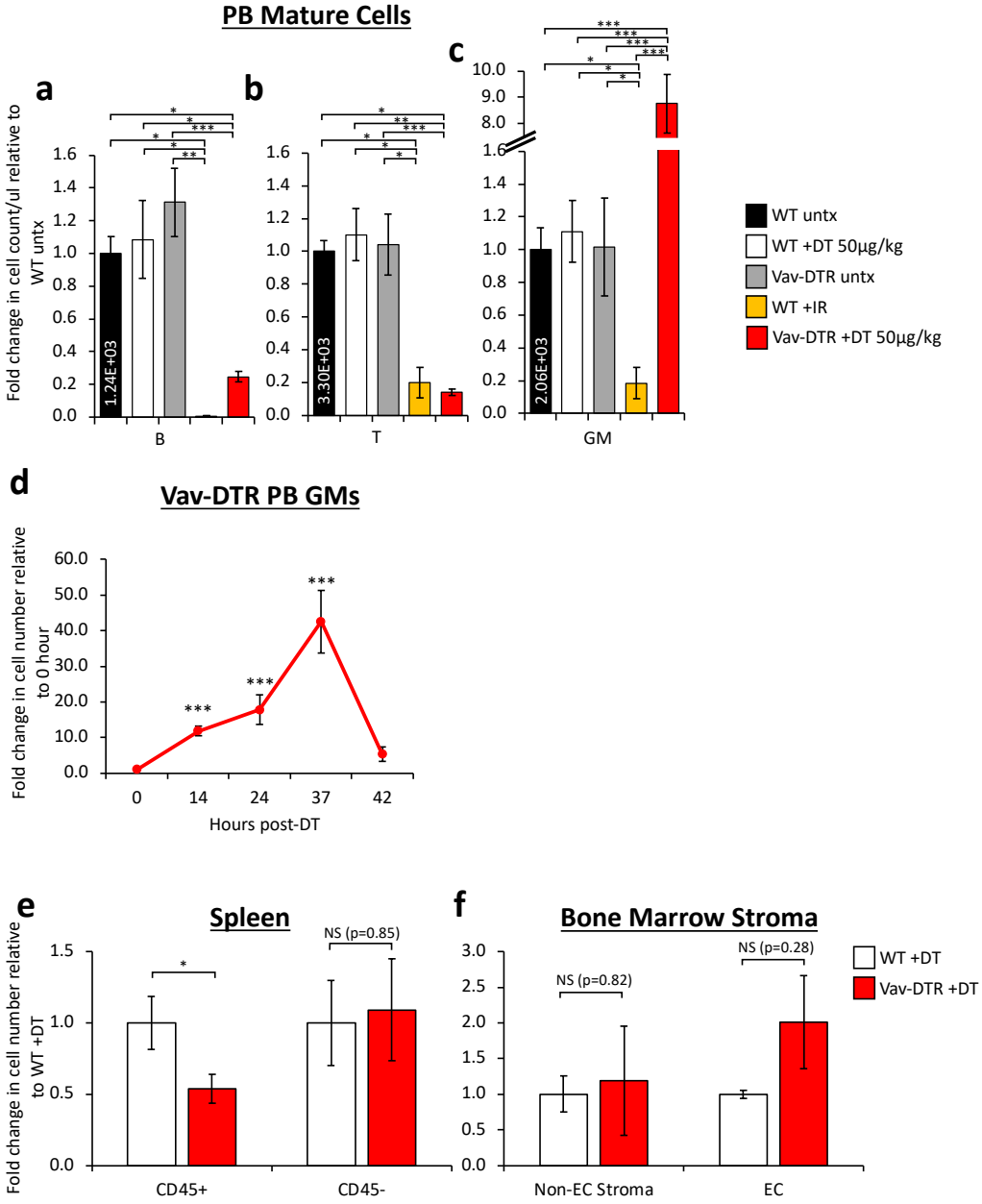

Figure 2.3. Cells in the PB and spleen of Vav-DTR mice are differentially affected by DT in vivo.

Treatment groups are indicated in Figure 2A. DT (50 µg/kg) depleted B **(a)** and T **(b)** in the peripheral blood of Vav-DTR mice (red bar) at 24 hours post-treatment, similar to 9-days post-sublethal (750 rads) irradiation (IR, yellow bar). **(c)** GMs increased in the peripheral blood of Vav-DTR mice at 24 hours post-DT treatment, but were depleted by irradiation. **(a-c)** WT mice were unaffected by DT treatment (white bars), with cell numbers similar to untreated WT mice (black bar) and untreated Vav-DTR

mice (gray bars). The numbers in the black bar represent absolute cell count per microliter of PB. Bar graphs indicate the fold change in cell number relative to WT untreated. N=6-14 mice in at least three independent experiments. Error bars indicate SEM, *p<0.05, **p<0.01, ***p<0.001 (One-way ANOVA with Tukey post-hoc test).
(d) Time course of DT effects on PB GMs of Vav-DTR mice. Line graph indicates the fold change in cell number relative to pre-DT time point (0 hour), showing an initial increase in GMs until 37 hours post-DT followed by quick depletion by 42 hours. Later time points could not be collected due to poor mouse health. N=2 mice. Error bars indicate SEM, ***p<0.001 (One-way ANOVA with Dunnett's post-hoc test).
(e) Reduction in the number of hematopoietic cells ($CD45^+$), but not non-hematopoietic ($CD45^-$), cells in the spleen of Vav-DTR mice 24 hours after DT (50 μg/kg) treatment (red bars).
(f) Stromal cells (non-EC stroma; $Ter119^-CD45^-Sca1^+CD31^-$) and endothelial cells (EC; $Ter^-CD45^-Sca1^+CD31^+$) from the BM of Vav-DTR mice (red bars) were not depleted by DT. Bar graphs indicate the fold change in cell number in Vav-DTR+DT (red bars) relative to WT+DT (white bars) mice. For Figure 3e-f, N=6-8 mice in at least three independent experiments. Error bars indicate SEM, *p<0.05 (Student's t-test). NS, not significant.

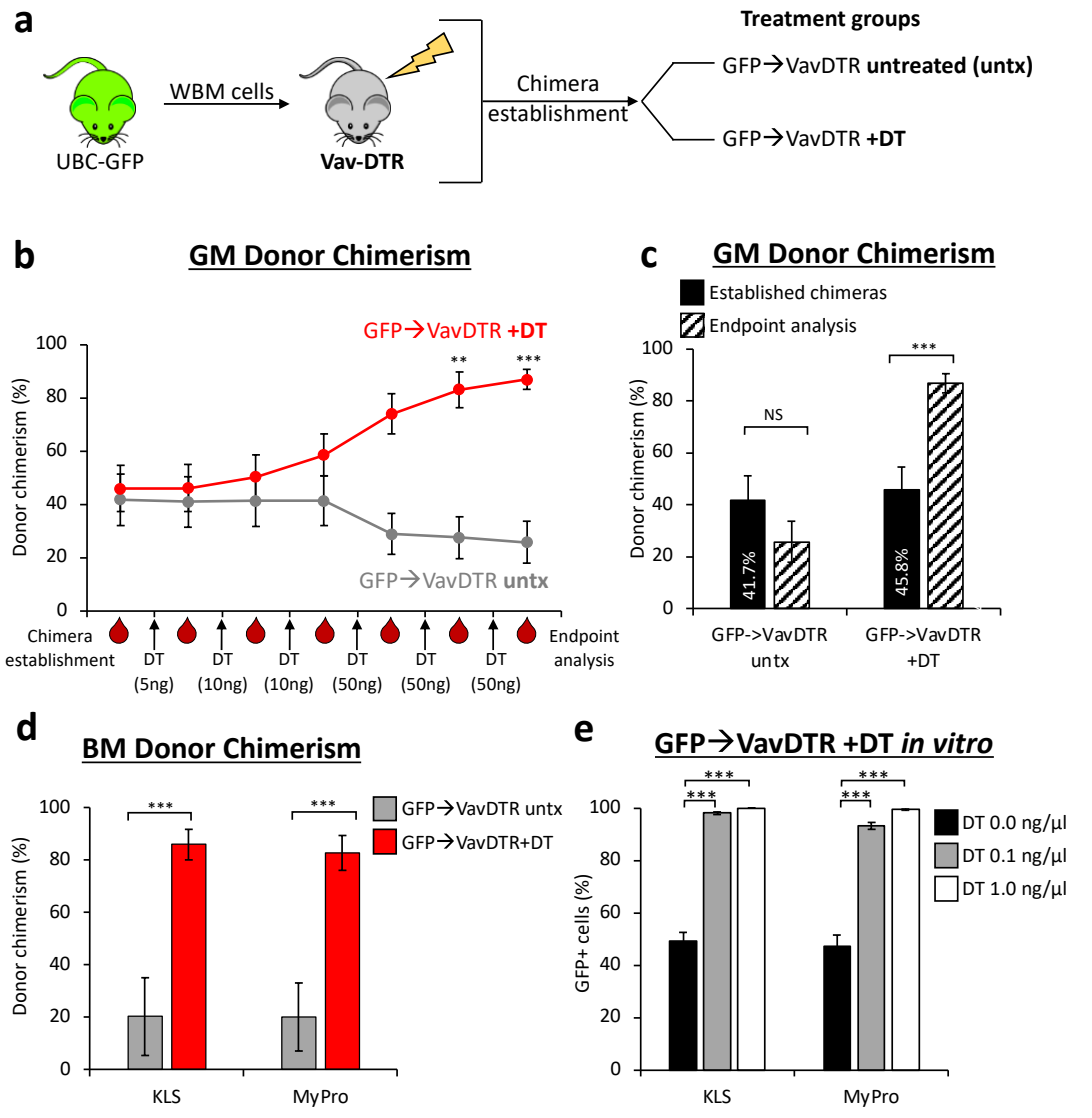

Figure 2.4. DT treatments selectively increased chimerism of donor-derived WT cells in Vav-DTR recipients.

(a) Schematic of experimental design. Chimeras were established: UBC-GFP donor BM cells were transplanted into sublethally irradiated Vav-DTR (GFP→Vav-DTR) recipients. 16 weeks after transplant, these chimeras were split into two groups, a DT treatment (+DT), and a control untreated (untx). Chimeras in the DT group received multiple (6) doses of DT (5-50ng), each one week apart and bled intermittently to monitor chimerism levels.
(b) GM donor chimerism increased over time in GFP→VavDTR chimeras treated with DT but not in the untreated control chimeras. In the graph, the arrows represent DT treatments, and the blood drops represent the tail bleeds performed 1 week after each DT treatment. N=2-3 mice per group in four independent experiments. Error bars

indicate SEM, **p<0.01, ***p<0.001 (one-way ANOVA with Dunnett's post-hoc test).

(c) Tail bleeds at chimera establishments (prior to DT) and endpoint (following last DT treatment) demonstrated a significantly increase in GM donor chimerism in GFP→VavDTR chimeras treated with DT but not in untreated Vav-DTR controls. Bar graphs indicate GM donor chimerism upon chimera establishment (black filled bars) and after DT treatment (endpoint analysis; patterned black bars). The percentages shown in the black bars represent the average donor chimerism at establishment of the chimeras, prior to initiation of the DT regimen. N=2-3 mice per group in four independent experiments. Error bars indicate SEM, ***p<0.001 (Student's t-test). NS, not significant.

(d) BM KLS and MyPro donor chimerism also significantly increased in GFP→VavDTR +DT chimeras (red bars) compared to untreated GFP→VavDTR controls. N=2-3 mice per group in four independent experiments. Error bars indicate SEM, ***p<0.001 (Student's t-test).

(e) KLS and MyPro cells sorted from untreated GFP→VavDTR chimeras were treated with DT *in vitro*. Bar graphs represent the percent of GFP+ donor (UBC-GFP) cells. The increase in the proportion of GFP+ cells to nearly 100% indicated that host cells (GFP-) were significantly depleted after a 3-day 0.1 ng/µl (gray bar) and 1.0 ng/µl (white bar) DT treatment, while untreated cells maintained the ratio observed *in vivo* (black bar, DT 0.0 ng/µl). N=3 in 3 independent experiments. Error bars indicate SEM, ***p<0.001 (One-way ANOVA with Dunnett's post-hoc test).

WBM, whole bone marrow; KLS, $ckit^{+}Lin^{-}Sca1^{+}$ cells include HSCs and MPPs; MyPro, myeloid progenitors are $c\text{-}kit^{+}Lin^{-}Sca1^{-}$ cells include CMPs, MEPs, and GMPs; untx, untreated; DT, diphtheria toxin.

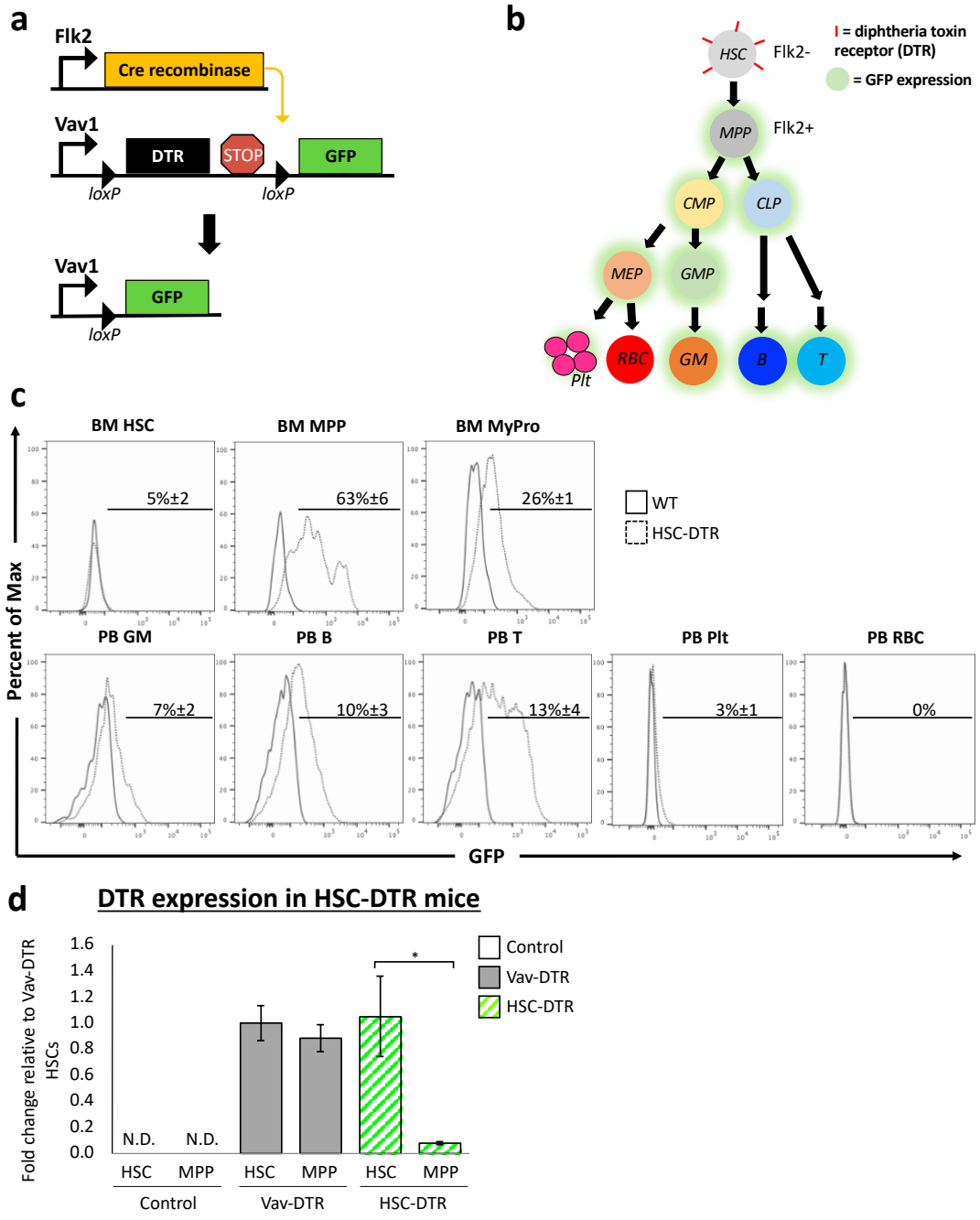

Figure 2.5. DTR expression is restricted to HSCs in HSC-DTR mice.

(a) Flk2-Cre mice were crossed to Vav-DTR mice to generate "HSC-DTR" mice. **(b)** Simplified model of hematopoietic tree in HSC-DTR mice. Cell types that are Flk2+ or derived from Flk2+ progenitor cells should express GFP but not DTR, while

Flk2- cells that have no history of Flk2 expression should express DTR and remain GFP-.
(c) Representative histograms of flow cytometry data indicating GFP expression levels in BM and PB cells in WT mice (black line) and HSC-DTR mice (dotted black line). Percentages represent the frequency of cells labeled by GFP.
(d) RT-qPCR analysis of DTR HSCs and MPPs sorted from control (white bars), Vav-DTR (gray bars), and HSC-DTR (white and green pattern bars) mice revealed that the DTR transgene is efficiently and significantly deleted in MPPs from HSC-DTR mice. Bar graph indicates the relative expression of DTR, normalized to β-actin. N=6 mice. Error bars indicate SEM. *$p<0.05$ (Student's t-test). N.D, not detected.

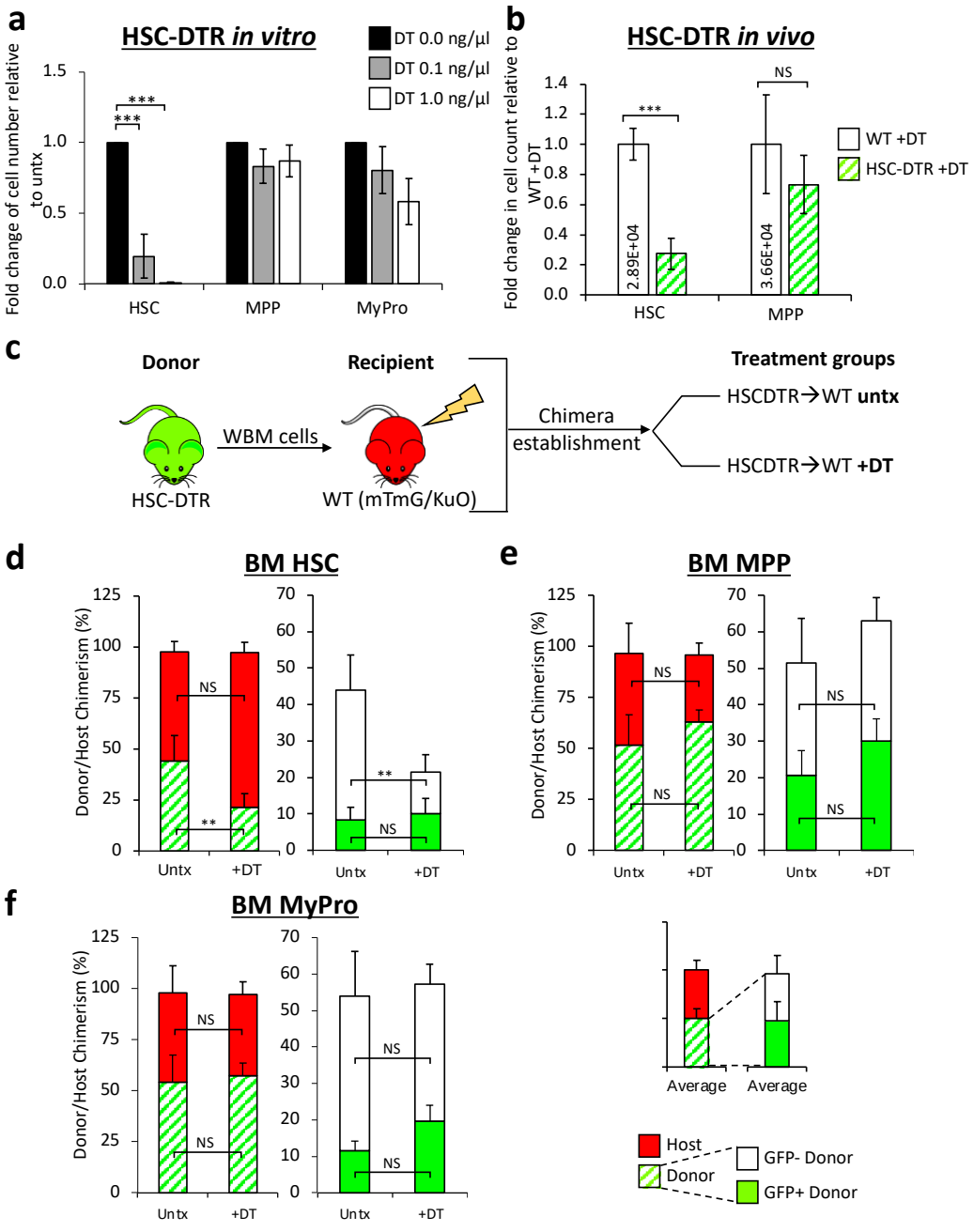

Figure 2.6. DT selectively depleted HSCs in the HSC-DTR mouse model.

(a) HSCs isolated from HSC-DTR mice were significantly depleted by DT treatment *in vitro*, while MPPs and MyPros from the same mice were unaffected. Bar graphs indicate the fold change in cell number relative to untreated (black bar, DT 0.0 ng/µl) upon a 7-day 0.1 ng/µl (gray bar) and 1.0 ng/µl (white bar) DT treatment. N=3 independent experiments. Error bars indicate SEM, ***p<0.001 (One-way ANOVA with Dunnett's post-hoc test).

(b) HSCs in HSC-DTR mice were significantly depleted by DT (100ng/mouse) treatment *in vivo*, while MPPs remained unaffected. Bar graphs indicate the fold change in cell number relative to DT-treated WT mice (white bars). The numbers in the white bars represent absolute cell count in the BM. N=2-5 mice in three independent experiments. Error bars indicate SEM, ***$p<0.001$ (Student's t-test).
(c) Schematic of chimera experimental design. WBM cells from HSC-DTR donor mice were transplanted into sublethally irradiated (500 rads) WT recipients (HSC-DTR→WT). Upon chimera establishment, chimeras were split into two groups: one was treated with DT and the control group was untreated. Chimeras in the DT group received one dose of 100ng DT, 24 hours prior to takedown for BM analysis.
(d) HSC donor chimerism significantly decreased upon DT treatment, while **(e)** MPP and **(f)** MyPro donor chimerism remained unaffected. The first set of bar graphs for each cell type represents donor (white and green pattern) and host (red) chimerism, while the second set of bar graphs shows the breakdown of GFP- (white) and GFP+ (green) donor chimerism. N=1-3 mice in 4 independent experiments. Error bars indicate SEM, **$p<0.01$ (Student's t-test).

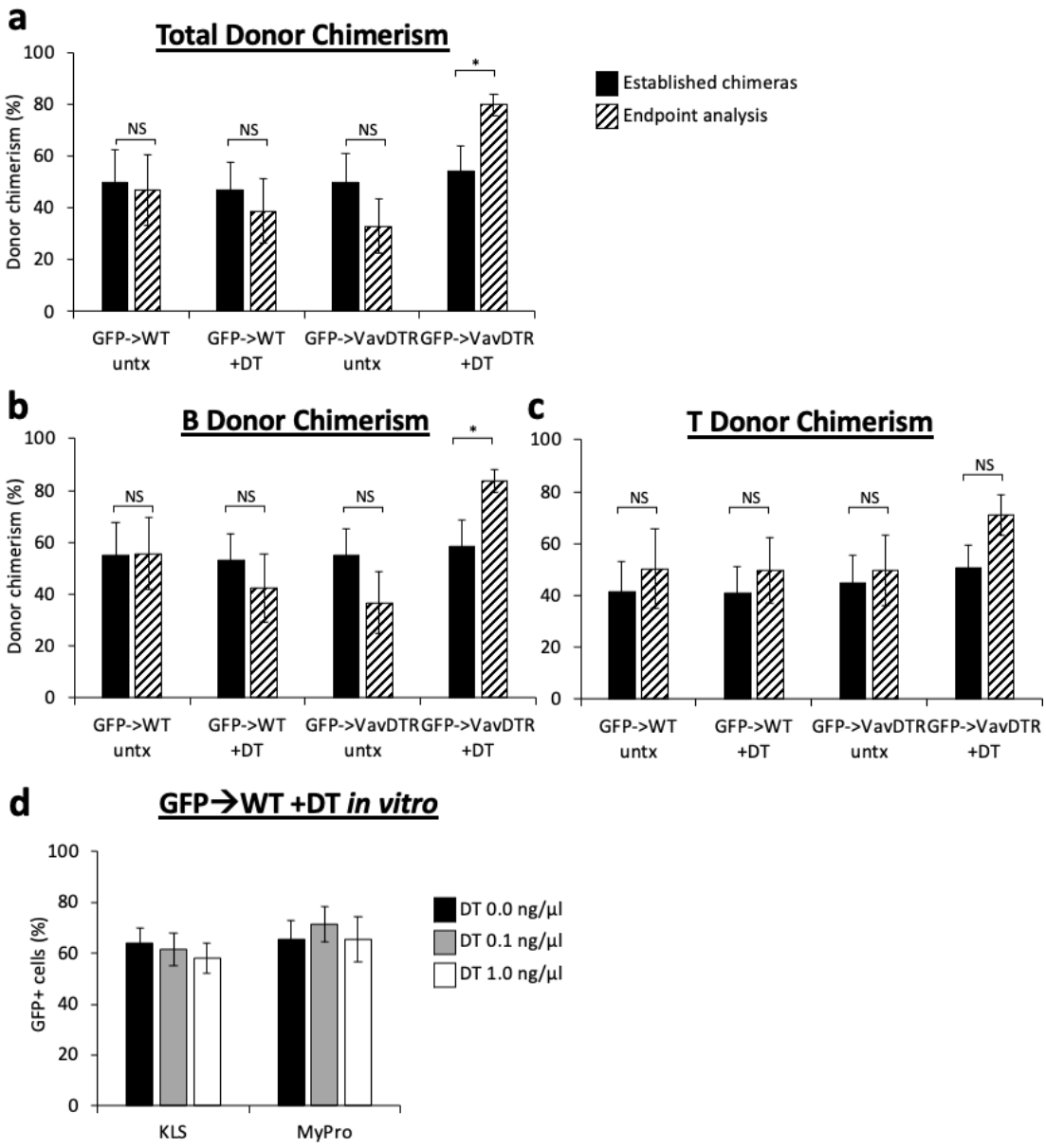

Figure 2.7. Supplementary Figure 1.

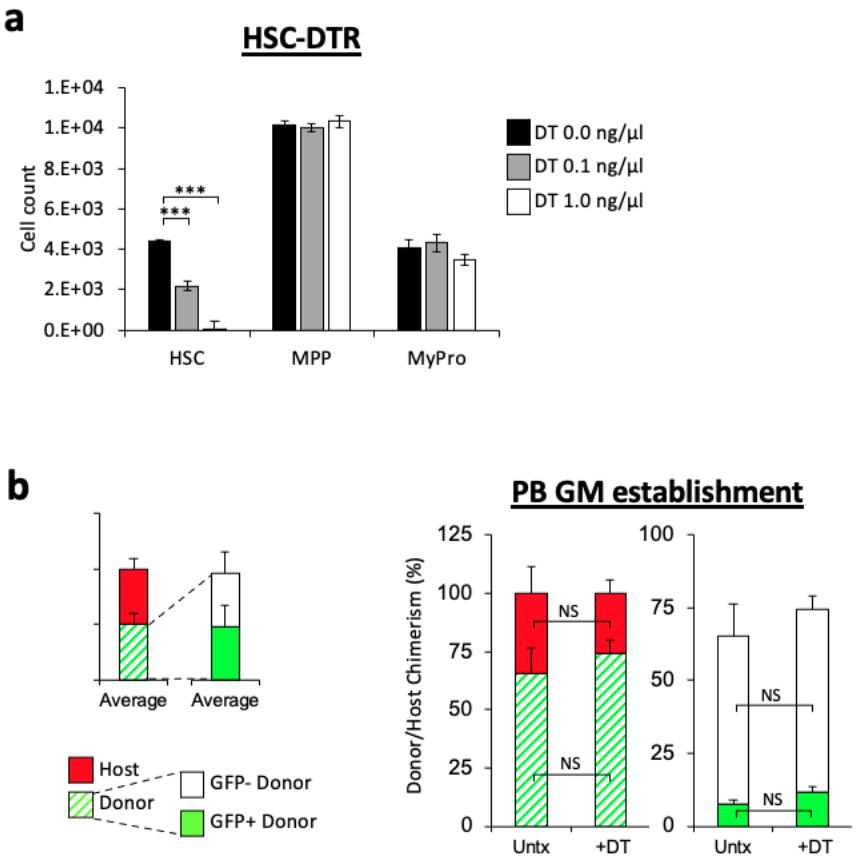

Figure 2.8. Supplementary Figure 2.

References

1 Czechowicz, A., Kraft, D., Weissman, I. L. & Bhattacharya, D. Efficient transplantation via antibody-based clearance of hematopoietic stem cell niches. *Science* **318**, 1296-1299, doi:10.1126/science.1149726 (2007).

2 Migliaccio, A. R., Carta, C. & Migliaccio, G. In vivo expansion of purified hematopoietic stem cells transplanted in nonablated W/Wv mice. *Exp Hematol* **27**, 1655-1666, doi:10.1016/s0301-472x(99)00110-1 (1999).

3 Till, J. E. & Mc, C. E. A direct measurement of the radiation sensitivity of normal mouse bone marrow cells. *Radiat Res* **14**, 213-222 (1961).

4 Wang, Z., Li, G., Tse, W. & Bunting, K. D. Conditional deletion of STAT5 in adult mouse hematopoietic stem cells causes loss of quiescence and permits efficient nonablative stem cell replacement. *Blood* **113**, 4856-4865, doi:10.1182/blood-2008-09-181107 (2009).

5 Waskow, C. *et al.* Hematopoietic stem cell transplantation without irradiation. *Nature Methods* **6**, 267-269, doi:10.1038/nmeth.1309 (2009).

6 Rodriguez, Y. B. A., Manso, B. A. & Forsberg, E. C. CFU-S assay: a historical single-cell assay that offers modern insight into clonal hematopoiesis. *Exp Hematol* **104**, 1-8, doi:10.1016/j.exphem.2021.10.003 (2021).

7 Cao, X. *et al.* Irradiation induces bone injury by damaging bone marrow microenvironment for stem cells. *Proc Natl Acad Sci U S A* **108**, 1609-1614, doi:10.1073/pnas.1015350108 (2011).

8 Domen, J., Gandy, K. L. & Weissman, I. L. Systemic overexpression of BCL-2 in the hematopoietic system protects transgenic mice from the consequences of lethal irradiation. *Blood* **91**, 2272-2282 (1998).

9 Dominici, M. *et al.* Restoration and reversible expansion of the osteoblastic hematopoietic stem cell niche after marrow radioablation. *Blood* **114**, 2333-2343, doi:10.1182/blood-2008-10-183459 (2009).

10 Zhang, M. *et al.* Response patterns of cytokines/chemokines in two murine strains after irradiation. *Cytokine* **58**, 169-177, doi:10.1016/j.cyto.2011.12.023 (2012).

11 Nakamura, J. *et al.* Myofibroblasts acquire retinoic acid-producing ability during fibroblast-to-myofibroblast transition following kidney injury. *Kidney Int* **95**, 526-539, doi:10.1016/j.kint.2018.10.017 (2019).

12 Saito, M. *et al.* Diphtheria toxin receptor-mediated conditional and targeted cell ablation in transgenic mice. *Nat Biotechnol* **19**, 746-750, doi:10.1038/90795 (2001).

13 van Blijswijk, J. *et al.* Altered lymph node composition in diphtheria toxin receptor-based mouse models to ablate dendritic cells. *J Immunol* **194**, 307-315, doi:10.4049/jimmunol.1401999 (2015).

14 Buch, T. *et al.* A Cre-inducible diphtheria toxin receptor mediates cell lineage ablation after toxin administration. *Nat Methods* **2**, 419-426, doi:10.1038/nmeth762 (2005).

15 Gillet, D. & Barbier, J. in *The Comprehensive Sourcebook of Bacterial Protein Toxins (Fourth Edition)* (eds Joseph Alouf, Daniel Ladant, & Michel R. Popoff) 111-132 (Academic Press, 2015).

16 Yamaizumi, M., Mekada, E., Uchida, T. & Okada, Y. One molecule of diphtheria toxin fragment A introduced into a cell can kill the cell. *Cell* **15**, 245-250, doi:10.1016/0092-8674(78)90099-5 (1978).

17 Almarza, E. *et al.* Characteristics of lentiviral vectors harboring the proximal promoter of the vav proto-oncogene: a weak and efficient promoter for gene therapy. *Mol Ther* **15**, 1487-1494, doi:10.1038/sj.mt.6300213 (2007).

18 Bustelo, X. R. & Barbacid, M. Tyrosine phosphorylation of the vav proto-oncogene product in activated B cells. *Science* **256**, 1196-1199, doi:10.1126/science.256.5060.1196 (1992).

19 Ogilvy, S. *et al.* Promoter elements of vav drive transgene expression in vivo throughout the hematopoietic compartment. *Blood* **94**, 1855-1863 (1999).

20 Perez-Cunningham, J., Boyer, S. W., Landon, M. & Forsberg, E. C. Hematopoietic stem cell-specific GFP-expressing transgenic mice generated by genetic excision of a pan-hematopoietic reporter gene. *Exp Hematol* **44**, 755-764 e751, doi:10.1016/j.exphem.2016.05.002 (2016).

21 Stadtfeld, M. & Graf, T. Assessing the role of hematopoietic plasticity for endothelial and hepatocyte development by non-invasive lineage tracing. *Development* **132**, 203-213, doi:10.1242/dev.01558 (2005).

22 Zmuidzinas, A. *et al.* The vav proto-oncogene is required early in embryogenesis but not for hematopoietic development in vitro. *EMBO J* **14**, 1-11 (1995).

23 Boyer, S. W. *et al.* Clonal and Quantitative In Vivo Assessment of Hematopoietic Stem Cell Differentiation Reveals Strong Erythroid Potential of Multipotent Cells. *Stem Cell Reports* **12**, 801-815, doi:10.1016/j.stemcr.2019.02.007 (2019).

24 Poscablo, D. M., Worthington, A. K., Smith-Berdan, S. & Forsberg, E. C. Megakaryocyte progenitor cell function is enhanced upon aging despite the functional decline of aged hematopoietic stem cells. *Stem Cell Reports* **16**, 1598-1613, doi:10.1016/j.stemcr.2021.04.016 (2021).

25 Smith-Berdan, S. *et al.* Acute and endothelial-specific Robo4 deletion affect hematopoietic stem cell trafficking independent of VCAM1. *PLoS One* **16**, e0255606, doi:10.1371/journal.pone.0255606 (2021).

26 Georgiades, P. *et al.* VavCre transgenic mice: a tool for mutagenesis in hematopoietic and endothelial lineages. *Genesis* **34**, 251-256, doi:10.1002/gene.10161 (2002).

27 Benz, C., Martins, V. C., Radtke, F. & Bleul, C. C. The stream of precursors that colonizes the thymus proceeds selectively through the early T lineage precursor stage of T cell development. *J Exp Med* **205**, 1187-1199, doi:10.1084/jem.20072168 (2008).

28 Boyer, S. W., Schroeder, A. V., Smith-Berdan, S. & Forsberg, E. C. All hematopoietic cells develop from hematopoietic stem cells through Flk2/Flt3-positive progenitor cells. *Cell Stem Cell* **9**, 64-73, doi:10.1016/j.stem.2011.04.021 (2011).

29 Boyer, S. W., Beaudin, A. E. & Forsberg, E. C. Mapping differentiation pathways from hematopoietic stem cells using Flk2/Flt3 lineage tracing. *Cell Cycle* **11**, 3180-3188, doi:10.4161/cc.21279 (2012).

30 Beaudin, A. E. *et al.* A Transient Developmental Hematopoietic Stem Cell Gives Rise to Innate-like B and T Cells. *Cell Stem Cell* **19**, 768-783, doi:10.1016/j.stem.2016.08.013 (2016).

31 Vooijs, M., Jonkers, J. & Berns, A. A highly efficient ligand-regulated Cre recombinase mouse line shows that LoxP recombination is position dependent. *EMBO Rep* **2**, 292-297, doi:10.1093/embo-reports/kve064 (2001).

32 Roberts, L. M. *et al.* Depletion of alveolar macrophages in CD11c diphtheria toxin receptor mice produces an inflammatory response. *Immun Inflamm Dis* **3**, 71-81, doi:10.1002/iid3.51 (2015).

33 Schoedel, K. B. *et al.* The bulk of the hematopoietic stem cell population is dispensable for murine steady-state and stress hematopoiesis. *Blood* **128**, 2285-2296, doi:10.1182/blood-2016-03-706010 (2016).

34 Tittel, A. P. *et al.* Functionally relevant neutrophilia in CD11c diphtheria toxin receptor transgenic mice. *Nat Methods* **9**, 385-390, doi:10.1038/nmeth.1905 (2012).

35 Miharada, N., Rydstrom, A., Rak, J. & Larsson, J. Uncoupling key determinants of hematopoietic stem cell engraftment through cell-specific and temporally controlled recipient conditioning. *Stem Cell Reports* **16**, 1705-1717, doi:10.1016/j.stemcr.2021.05.019 (2021).

36 Biasco, L. *et al.* In Vivo Tracking of Human Hematopoiesis Reveals Patterns of Clonal Dynamics during Early and Steady-State Reconstitution Phases. *Cell Stem Cell* **19**, 107-119, doi:10.1016/j.stem.2016.04.016 (2016).

37 Dykstra, B. *et al.* Long-term propagation of distinct hematopoietic differentiation programs in vivo. *Cell Stem Cell* **1**, 218-229, doi:10.1016/j.stem.2007.05.015 (2007).

38 Lu, R., Neff, N. F., Quake, S. R. & Weissman, I. L. Tracking single hematopoietic stem cells in vivo using high-throughput sequencing in conjunction with viral genetic barcoding. *Nat Biotechnol* **29**, 928-933, doi:10.1038/nbt.1977 (2011).

39 Busch, K. *et al.* Fundamental properties of unperturbed haematopoiesis from stem cells in vivo. *Nature* **518**, 542-546, doi:10.1038/nature14242 (2015).

40 Busch, K. & Rodewald, H. R. Unperturbed vs. post-transplantation hematopoiesis: both in vivo but different. *Curr Opin Hematol* **23**, 295-303, doi:10.1097/MOH.0000000000000250 (2016).

41 Sun, J. *et al.* Clonal dynamics of native haematopoiesis. *Nature* **514**, 322-327, doi:10.1038/nature13824 (2014).

42 Cool, T., Worthington, A., Poscablo, D., Hussaini, A. & Forsberg, E. C. Interleukin 7 receptor is required for myeloid cell homeostasis and reconstitution by hematopoietic stem cells. *Exp Hematol* **90**, 39-45 e33, doi:10.1016/j.exphem.2020.09.001 (2020).

43 Leung, G. A. *et al.* The lymphoid-associated interleukin 7 receptor (IL7R) regulates tissue-resident macrophage development. *Development* **146**, doi:10.1242/dev.176180 (2019).

44 Smith-Berdan, S., Bercasio, A., Rajendiran, S. & Forsberg, E. C. Viagra Enables Efficient, Single-Day Hematopoietic Stem Cell Mobilization. *Stem Cell Reports* **13**, 787-792, doi:10.1016/j.stemcr.2019.09.004 (2019).

45 Smith-Berdan, S., Nguyen, A., Hong, M. A. & Forsberg, E. C. ROBO4-mediated vascular integrity regulates the directionality of hematopoietic stem cell trafficking. *Stem Cell Reports* **4**, 255-268, doi:10.1016/j.stemcr.2014.12.013 (2015).

46 Beaudin, A. E., Boyer, S. W. & Forsberg, E. C. Flk2/Flt3 promotes both myeloid and lymphoid development by expanding non-self-renewing multipotent hematopoietic progenitor cells. *Exp Hematol* **42**, 218-229 e214, doi:10.1016/j.exphem.2013.11.013 (2014).

47 Martin, E. W. *et al.* Chromatin accessibility maps provide evidence of multilineage gene priming in hematopoietic stem cells. *Epigenetics Chromatin* **14**, 2, doi:10.1186/s13072-020-00377-1 (2021).

48 Rajendiran, S., Boyer, S. W. & Forsberg, E. C. A quantitative hematopoietic stem cell reconstitution protocol: Accounting for recipient variability, tissue distribution and cell half-lives. *Stem Cell Res* **50**, 102145, doi:10.1016/j.scr.2020.102145 (2020).

49 Ugarte, F. *et al.* Progressive Chromatin Condensation and H3K9 Methylation Regulate the Differentiation of Embryonic and Hematopoietic Stem Cells. *Stem Cell Reports* **5**, 728-740, doi:10.1016/j.stemcr.2015.09.009 (2015).

50 Worthington, A., Cool, T., Poscablo, D., Hussaini, A., Beaudin, A.E. & Forsberg, E. C. IL7Rα, but not Flk2/Flt3, is required for hematopoietic stem cell reconstitution of tissue-resident lymphoid cells. *In press.*

PART II

Chapter 3.

Clearing the Haze: How Does Nicotine Affect Hematopoiesis before and after Birth?

The text of this chapter includes a reprint of the following previously published paper: Cool T, Rodriguez y Baena A, Forsberg EC. Clearing the Haze: How Does Nicotine Affect Hematopoiesis before and after Birth? Cancers (Basel). 2021 Dec 30;14(1):184. doi: 10.3390/cancers14010184. PMID: 35008347; PMCID: PMC8750289.

Simple Summary

E-cigarettes have gained popularity as alternatives to traditional tobacco products over the past several decades. Despite being marketed as safer, they still contain several highly toxic compounds, which pose as dangers to human health. Nicotine is one of those toxic compounds and is known to have many deleterious effects on human health and disease susceptibility. Hematopoietic stem cells (HSCs) are the stem cells that give rise to the entire immune system and therefore serve as a compelling point of interrogation for the source of altered health and disease susceptibility in exposed individuals. Here we discuss how nicotine influences HSCs and the immune cells they make, as well as highlight potential mechanisms of altered immunity for life.

Abstract

Hematopoiesis is a tightly regulated process orchestrated by cell-intrinsic and cell-extrinsic cues. Over the past several decades, much effort has been focused on understanding how these cues regulate hematopoietic stem cell (HSC) function. Many endogenous key regulators of hematopoiesis have been identified and extensively characterized. Less is known about the mechanisms of long-term effects of environmental toxic compounds on hematopoietic stem and progenitor cells (HSPCs) and their mature immune cell progeny. Research over the past several decades has demonstrated that tobacco products are extremely toxic and pose huge risks to human health by causing diseases like cancer, respiratory illnesses, strokes, and more. Recently, electronic cigarettes have been promoted as a safer alternative to traditional tobacco products and have become increasingly popular among younger generations. Nicotine, the highly toxic compound found in many traditional tobacco products, is also found in most electronic cigarettes, calling into question their purported “safety”. Although it is known that nicotine is toxic, the pathophysiology of disease in exposed people remains under investigation. One plausible contributor to altered disease susceptibility is altered hematopoiesis and associated immune dysfunction. In this review, we focus on research that has addressed how HSCs and mature blood cells respond to nicotine, as well as identify remaining questions.

Keywords

Hematopoiesis; hematopoietic stem cells; nicotine; immunity; immune dysfunction; white blood cells

Introduction

An environmental exposure that has become increasingly important in the research field is exposure to tobacco products. According to the National Institute of Health (NIH), one-fourth of the U.S. population uses tobacco products [1]. An abundance of evidence has demonstrated that smoking is highly toxic to human health. Societal use of e-cigarettes has emerged recently and been marketed as a "safer alternative" to traditional tobacco products. Currently, 10 million adults and over 5 million middle and high school students use e-cigarettes in the U.S. [2]. Over the last several decades, researchers have demonstrated that tobacco exposure is not only dangerous to the person using the products, but also to people who are exposed second- or even third-hand [3,4]. Tobacco products are highly complex and made up of several extremely toxic compounds, including hydrogen cyanide, formaldehyde, benzene, nicotine, and more [5]. One of the toxic compounds found in almost all present-day tobacco products is nicotine, a stimulant known for its addictive properties. The oral lethal dose (LD50) of nicotine in humans is ~0.8–1 mg/kg [6–9]. Nicotine is still highly prevalent in these so-called safer alternatives, presumably to promote addiction to the products. Nicotine has been associated with many deleterious health consequences, including cancer, pulmonary disease, and increased risk of infections [10]. How nicotine influences immunity in first, second, or third-hand exposed people remains an open area of

investigation. Interestingly, nicotine has been shown to increase inflammation, as well as white blood cell (WBC) counts [11–16]. WBCs are mature, terminally differentiated cells that come from hematopoietic stem cells (HSCs), in a process known as hematopoiesis. WBCs are immune cells with specialized functions, fighting infections and recognizing tumor and diseased cells. Thus, nicotine-induced systemic inflammation and increased WBC count increases the risk for and exacerbates a wide number of clinical conditions, including cancer, cardiovascular disorders, atherosclerosis, autoimmune syndromes, allergy, asthma, and pulmonary disease. The effects that nicotine has on the number and activity of each of these WBC types remains under investigation. This review focuses on the question: what lasting impacts does nicotine have on hematopoiesis and life-long immunity?

The Hematopoietic Hierarchy

The hematopoietic compartment consists of hematopoietic stem and progenitor cells (HSPCs) and their mature, terminally differentiated progeny (Figure 1a) [17,18]. Hematopoietic stem cells (HSCs) are fascinating because they possess the ability to self-renew as well as differentiate into all mature blood and immune cells (Figure 1a). The hematopoietic process occurs in spatially and temporally distinct waves throughout development, and ultimately gives rise to the complex immune system that patrols all tissues. During fetal development, these distinct waves of HSPCs differentially contribute to mature blood and immune cells across tissues [19–22]. This complex orchestra of immune layering consists of (1) early developmental, non-self-renewing progenitors that give rise to self-renewing progeny that persist throughout life with little

to no contribution from adult HSCs, and (2) subsequently developed self-renewing progenitors (HSCs) that give rise to non-self-renewing progeny that are stably replenished throughout life (Figure 1b). At the interphase of these two well-established paradigms of hematopoietic development exist at least one population of developmentally restricted HSCs (drHSCs) that do not normally self-renew, but can be induced to do so upon transplantation into irradiated hosts [23]. Based on their ability to give rise to robust numbers of traditional as well as atypical lymphoid cells, the physiological role of the drHSCs may be to boost production of lymphoid-mediated immunity that is needed after birth. It is also possible that drHSCs—or other normally transient progenitor cells—are induced to persist for longer time periods upon inflammatory stimulus like nicotine exposure, similar to their induced persistence in an irradiated environment [23,24]. This critical window of perinatal hematopoietic development, with distinct non-persisting stem and progenitor populations contributing alongside "true", life-long HSCs to a rapidly developing and dynamic immune system, poses as a vulnerable point of interrogation for long-term effects of altered hematopoiesis and immunity in nicotine-exposed individuals. Persisting alterations in cell function can occur in the absence of genetic mutations [25]; the likelihood of lasting physiological responses, however, is greater if cellular changes occur in cells with long half-lives or with self-renewal capacity than in cells with high turnover rates. Potentially, nicotine alters HSCs (or other fetal progenitors) at the epigenetic level, leading to altered HSC function and/or lineage output for life. Alternatively, nicotine alters the numbers and/or epigenetics of mature blood cells, leading to permanently

altered immune function (Figure 1b). Whether and how nicotine exposure alters HSCs or their progeny, or both, to cause long-term changes in disease susceptibility remains to be determined.

Regulation of Hematopoietic Homeostasis

The development of this complex immune system relies on intrinsic and extrinsic cues [26]. Several key regulators of hematopoiesis have been identified and characterized in detail. Transcription factors such as Runx1, SCL, Gata-2, and C-myb play key roles in the intrinsic regulation of HSC potential during development [20,27,28]. Additionally, inflammatory regulators like interferons, interleukin (IL)-1, IL-6, and TNFα provide HSC-extrinsic cues to regulate HSC fate choice and function [27–30]. Although we have relatively clear and convincing research describing how specific intrinsic and extrinsic regulators influence cell fate choice, many environmental factors that can also significantly impact HSC function and potential have not been thoroughly investigated. Importantly, the timing and duration of these exposures can impact hematopoietic development and function either transiently or for life. While acute exposures can have a transient effect on hematopoiesis, in this review, we focus on the potential mechanisms of altered hematopoiesis and HSC function after chronic challenge. As alluded to above, nicotine may alter long-term immunity via two potential mechanisms: (1) persistent changes in HSCs that then have lasting impacts on hematopoiesis (and immunity) for life, and/or (2) persistent changes in mature immune cells (Figure 1b). In this review, we focus on several studies that have investigated the effects of nicotine

on HSCs and WBCs, as well as how nicotine alters inflammatory mediators. We highlight potential mechanisms of altered hematopoiesis and immunity and identify experiments that could help untangle whether these effects are due to changes in HSCs or changes in their mature progeny.

Does Nicotine Alter Hematopoiesis by Direct Action on HSCs?

Tobacco product use is associated with increased WBC counts in peripheral blood which is a sign of increased systemic inflammation [12–16,31–33]. Specifically, it is known that nicotine in tobacco products can alter WBC counts in the long-term [11]. However, the mechanism underlying these changes remains unclear. Additionally, whether tobacco product use alters counts of non-traditional immune cells in different tissues has not been investigated. Potentially, there are two plausible mechanisms of altered WBC counts: (1) nicotine directly affects hematopoietic cells by direct binding to nicotinic receptors expressed by HSCs and/or their progeny (Figure 2a), or (2) nicotine indirectly affects the hematopoietic compartment by triggering release of inflammatory-mediating cytokines from non-hematopoietic cells that then act on HSCs and/or their progeny (Figure 2b). It is important to note that these potential mechanisms are not mutually exclusive, and that the effects of nicotine could be a combination of both mechanisms (Figure 2a,b). In this section, we discuss the evidence for nicotine acting as a nicotinic cholinergic receptor agonist and directly affecting hematopoiesis via binding to nicotinic acetylcholine receptor (nAChRs) on hematopoietic cell types.

Do HSCs Express Nicotinic Acetylcholine Receptors (nAChRs)?

One potential mechanism of altered WBCs after nicotine exposure is that nicotine directly affects HSCs via nAChRs expressed on their cell membrane. nAChRs are a family of ligand-gated ion channels. There are 16 homologous subunits identified in mammals, and these subunits combine to form many different nAChR subtypes. Interestingly, these subtypes have various expression patterns across tissues, diverse functional properties and pharmacological characteristics [34,35]. A few groups have provided evidence that HSCs, and some of their mature immune cell progeny, express several subunits of the nAChRs at steady state, and that the expression of other subunits can be induced after exposure to nicotine [11,36]. Chang et al. reported an increase in both HSC and WBC numbers in nicotine-exposed mice, and expression of the nAChR alpha 7 subunit (nAChRα7) in total bone marrow, as well as on isolated HSCs [11]. They used a combination of flow cytometry and immunofluorescence imaging to assess nAChRα7 expression on whole bone marrow (WBM) cells which contain HSPCs and mature cells, as well as on purified HSCs. In this experiment they used the nAChRα7 ligand Alpha Bungarotoxin (abgt) conjugated to a FITC fluorophore to determine whether WBM cells or HSCs expressed the receptor on the cell membrane. Abgt is known to bind with high affinity to the nAChRα7 subunit. Using this method, they determined that some cells within the WBM fraction and purified HSCs both displayed the receptor for abgt ligand. Although they demonstrated that WBM and HSCs had positive staining for the abgt ligand (presumably binding to the nAChRα7 subunit), it should be noted that this assay did not directly determine the levels of nAChRα7 in

these cells nor did they include a strong positive control (such as brain homogenate [36]) or negative control (tissue known to not express nAChRα7) to rigorously decipher the relative expression of nAChRα7. An interesting experiment that would have strengthened their findings would be to perform the same experiment with HSCs from wild type (WT) mice and mice lacking nAChRα7. If they had observed that WT HSCs had positive staining for the FITC-abgt, but the mutant HSCs did not, this would more unequivocally have supported their conclusion that HSCs express nAChRα7.

Do Other Hematopoietic Cells Express nAChRs?

In a separate study, St-Pierre et al. took a different approach to address this same question: Do hematopoietic cells express nAChRs [36]? They used freshly isolated murine WBM cells and brain tissue (as a positive control) to perform RT-PCR for the several different subunits of nAChRs. Using this method, they determined that nAChRα9 and nAChRβ2 mRNAs were expressed by nearly all bone marrow cells, while nAChRα7 was expressed only in CD34+ progenitors, monocytes, and B cells. They concluded that long-term HSCs do not actually express the α7 or α9 nAChR subunits, but progenitors and some mature blood cells do. However, one important thing to note about these findings is that they were unable to detect these subunits using qRT-PCR as the detection levels were below threshold at 35 cycles. For this reason, they performed nested RT-PCR instead and observed that nAChR mRNA expression was highly variable across hematopoietic populations. Since mRNA expression does not always result in protein expression, they also investigated whether nicotine could

modulate bone marrow-derived myeloid cell numbers via nAChRα7 and nAChRα9 by performing *in vitro* and *in vivo* experiments using WT, nAChRα7 knockout (KO), and nAChRα9 KO mice. Interestingly, their *in vitro* and *in vivo* experiments provided contradictory results. *In vitro*, nicotine reduced total numbers of bone marrow-derived monocytes (BMDMs) in WT mice, but not in the two mutant mice. However, in their *in vivo* model, nicotine had a protective effect on BMDMs. It is important to note that these *in vitro* and *in vivo* experiments lacked a nicotine-only control group. A more convincing and straightforward experiment would have been to do a systematic side-by-side comparison of the effects on nicotine on BMDMs *in vitro* and *in vivo* in all 3 models (WT, nAChRα7 KO, and nAChRα9 KO) with nicotine only versus control.

Overall, the evidence for robust and functional cell surface expression of nAChR subunits on HSCs and other hematopoietic subsets is not unequivocally convincing. A more direct and definitive approach to determine this would be to purify various hematopoietic cell populations from the murine bone marrow, and test expression by flow cytometry or immunohistochemistry using antibodies specific to each nAChR subunit, with the corresponding cells from gene deletion models serving as controls. If HSCs and mature immune cells do in fact express nAChR subunits on the membrane, it could be assumed that they would directly respond to nicotine, at least in part, via binding of the nAChRs expressed. Additionally, *in vitro* exposure of HSCs and/or their mature immune cell progeny to nicotine-containing media may provide more concrete evidence as to whether nicotine can directly affect these cells, and specifically which

ones. At present, a more thorough investigation of the direct effects of nicotine on hematopoietic cell types is needed.

Does Nicotine Affect Hematopoiesis via an Altered Inflammatory State?

As an alternative to nicotine affecting hematopoiesis through binding nAChRs on hematopoietic cells and/or their progeny, nicotine may potentially affect hematopoiesis indirectly via inflammatory cues (Figure 2). Nicotine is known to induce the release of several inflammatory-mediating cytokines including TNFα, IL-6, IL-1, and others which are also known to play important roles in hematopoietic cell development and homeostasis [30,37–41]. While hematopoietic cells are known to be the source for some of these inflammatory mediators, other cell types may also contribute to altered inflammation, including epithelial cells [42]. In this scenario, one might hypothesize that nicotine acts on non-hematopoietic cells that do express nAChRs, and once the nAChR signaling cascade is initiated in these cell types, the cells undergo molecular changes to respond to the stimulus and can send informative cues (cytokines) to neighboring cell types or into circulation to reach distant tissues and elicit cellular responses [43]. There are several cell types that are known to respond directly to nicotine, including muscle cells and neurons. The vagus nerve is a complex network of neurons that connects the brain with the rest of the organs in the body. It has been recently demonstrated that the vagus nerve, in addition to controlling heart rate, stress, and hormone secretion [44], also acts as an immunomodulator [45]. Coincidentally, acetylcholine is the main neurotransmitter of the vagus nerve, and controls immune cell function via the nAChRα7 subunit. Nicotine, which has a similar structure to

acetylcholine, potentially binds to nAChRs to activate the release of inflammatory-mediating cytokines as a form of communication with surrounding organs (Figure 2). Hematopoietic cells (both HSCs and mature immune cells) are known to express receptors for many cytokines [46] and, although they may not be able to directly respond to nicotine, they can therefore undoubtedly respond to many inflammatory cues.

Nicotine leading to an altered inflammatory state has been supported by several studies [40,47–51]. In rodents, it has been demonstrated that nicotine exposure increases the release of pro-inflammatory cytokines. Since ~10% of pregnant women continue smoking during gestation [52], many studies have focused on understanding the effects of *in utero* nicotine exposure. Similar to data from adults, nicotine is also able to induce inflammation in a developing rodent fetus. Mohsenzadeh et al. exposed pregnant rats to nicotine and measured the serum of their pups after birth to determine concentrations of several inflammatory-mediating cytokines [53]. They found that hs-CRP, IL-6, and TNFα were all elevated in the nicotine-exposed pups compared to their control counterparts. They concluded that *in utero* nicotine exposure induces a dose-dependent increase in inflammatory-mediating cytokines. Similarly, Orellana et al. observed significantly elevated serum levels of IL-1β and TNFα in the offspring of nicotine-exposed mice [54]. Additionally, day 8.5 mouse embryos exposed to nicotine developed abnormalities and showed increased inflammation by elevated expression of TNFα, IL-1β, and caspase 3 [55]. Another study aimed to determine the effects of *in utero* nicotine exposure found an increased risk for intrauterine infection and altered

inflammatory profile of fetal tissues in rodents [39]. In this study, they measured cytokines from placental tissue and amniotic fluid from nicotine-exposed pregnant dams. Interestingly, they observed that nicotine exposure did not significantly increase TNFα in either tissue. IFNγ was significantly elevated in placental tissue, but significantly decreased in the amniotic fluid of nicotine-exposed fetuses. IL-6, which was unchanged in the nicotine-exposed placental tissues, was significantly increased in amniotic fluid. They concluded that these altered inflammatory mediators were the cause of increased infection susceptibility of the fetus of nicotine-exposed dams. It should be noted that the different outcomes of these studies could be attributed to several factors, including the mode and amount of exposure to nicotine, analysis of different tissues (fetal blood versus placenta/amniotic fluid), and time of tissue collection (newborn rats versus gestational day 18). These studies also only probed a few cytokines and did not investigate the underlying mechanism of altered inflammation.

Overall, these studies indicate that the exposure of pregnant females to nicotine can lead to an altered inflammatory environment during gestation, which may have important consequences on fetal hematopoiesis [27,56,57]. Moreover, it is yet unknown whether this is caused directly by nicotine in the fetal environment or by passage of maternal nicotine-induced inflammatory cytokines to the fetus during development. To understand the mechanism of altered inflammation in nicotine-exposed pups, it would be necessary to identify the cells to which nicotine is binding and initiating signaling, and then determining if those cells are the sole source of

cytokines or if they work in concert with other cells to elicit an immune response. Although we know that nicotine can cross the placenta and accumulates in the fetal blood and in the breast milk [58–62], it remains unclear whether these significant fetal and neonatal exposures lead to direct changes in the fetal hematopoietic compartment. It is also unknown whether nicotine leads to transient or persisting alterations in developmental hematopoiesis.

Conclusions

Persisting alterations to hematopoiesis as a mechanism of disease susceptibility

Although it is widely agreed that nicotine is extremely toxic, the mechanism of altered immunity of nicotine-exposed individuals remains a topic of intense investigation. The emergence of e-cigarettes as alternatives to traditional tobacco products has prompted a new wave of health concerns and a need for scientific research into the effects of their toxic components on human health. Nicotine is highly addictive and found in almost all present-day tobacco products, new and old, and therefore serves as a logical starting point of investigation of the toxic effects of tobacco product use on human health. Decades of research have demonstrated that children of smoking mothers have diminished health [63–65], yet the mechanism of altered disease susceptibility remains unclear. As the hematopoietic system is the focal point of immunity and health, the effects of nicotine on hematopoietic cell types warrant further investigation. Nicotine potentially *directly* affects hematopoietic cells, including HSCs, via binding their nAChRs. Direct action on HSCs is consistent with the increase in HSC numbers and detection of nAChRα7 expression on the surface of HSCs [11]. Alternatively, nicotine

may *indirectly* affect hematopoietic cell types, by binding nAChRs on other cell types (likely epithelial, neuronal, muscular cells) that then secrete cytokines to induce inflammation. A third possibility is that nicotine affects hematopoiesis both directly and indirectly, leading to feedback loops that perpetuate inflammation. In order to advance our understanding of the effects of nicotine on hematopoietic cell types and immunity, thorough investigation into these possible mechanisms is needed. Experiments with genetic deletion or gain-of-function models, possibly facilitated by the many rapidly emerging CRISPR technologies [66,67], should enable unequivocal new results. Exciting approaches to move the field forward are increasingly feasible. For example, the effect of nicotine on mature immune cell subsets could be assessed at high resolution by single-cell RNA sequencing, possibly revealing alterations of activation genes in T cells. Analogously, ATAC-seq, of bulk or single cells [68,69], could be implemented to test the hypothesis that fetal and/or adult HSCs have altered functional output in response to nicotine due to lasting epigenetic changes. The discovery of drHSCs [23] and improved characterization of non-traditional immune cells [72–75] opens new and intriguing avenues of exploration. Together with a systematic investigation of the direct and indirect effects of nicotine on hematopoiesis, these strategies will provide insights needed to understand and mitigate damage to its exposure.

Author Contributions

Writing—original draft preparation, T.C.; writing—review and editing, T.C., A.R.y.B., and E.C.F.; visualization, T.C. and E.C.F.; funding acquisition, T.C., A.R.y.B., and E.C.F. All authors have read and agreed to the published version of the manuscript.

Funding

T.C. and A.R.y.B. are both supported by predoctoral fellowships from the Tobacco-Related Disease Research Program (TRDRP). E.C.F. is supported by NIDDK and NIA awards (R01DK100917 and R01AG062879).

Acknowledgments

The authors thank Atesh Worthington for insightful comments on the manuscript. Figures were partially generated using BioRender, license agreement numbers YL22WB7VLT and NV22WB7PTB.

Figures

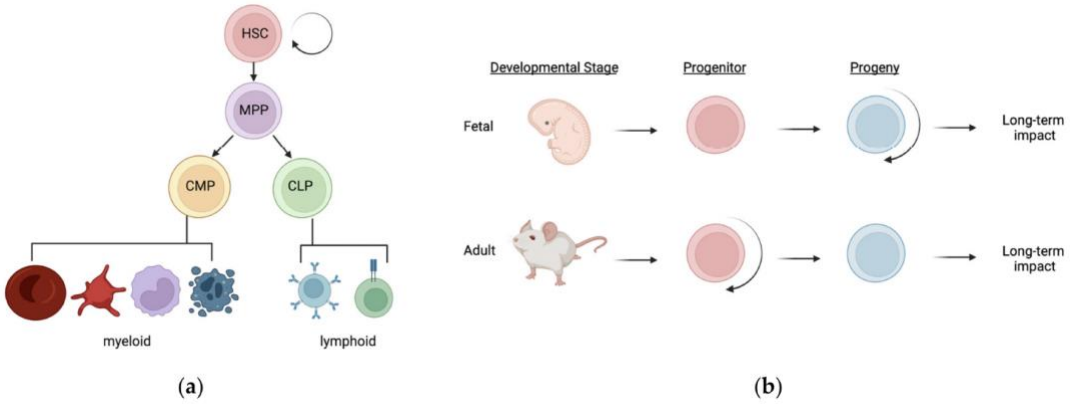

Figure 3.1

The hematopoietic hierarchy and sources of potential long-term impacts following nicotine exposure: (a) Hematopoiesis is the process of generating all mature blood and immune cells from hematopoietic stem cells (HSCs). This process occurs in a well-defined hierarchy during adult steadystate hematopoiesis, as depicted in this simplified tree structure. HSCs differentiate into multipotent progenitors, and then either common myeloid progenitors (CMPs) or common lymphoid progenitors (CLPs), before terminally differentiating into mature blood and immune cells of either myeloid or lymphoid classification. HSCs are unique in their ability to both self-renew as well as differentiate into all of these progenitors and mature cells; (b) During fetal hematopoiesis, distinct waves of hematopoietic stem and progenitors (HSPCs) exist throughout development and adulthood. Many of the progenitors that exist during early fetal development are non-self-renewing but can give rise to self-renewing progeny such as “non-traditional” tissue-resident immune cells. Subsequently and during adult steady-state, hematopoiesis is sustained by self-renewing progenitors (HSCs) that give rise to non-self-renewing, short-lived progeny such as “traditional” circulating RBCs and WBCs. Nicotine exposure may influence life-long immunity by two potential mechanisms: (1) nicotine causes changes or persistence in HSPCs which results in altered hematopoietic output for life, or (2) nicotine causes a change in the long-lived immune cells during their establishment which alters immunity later in life. These mechanisms are not mutually exclusive and a combination of both could lead to altered hematopoiesis and altered immunity for life. Adapted from Cool and Forsberg, 2019 [20].

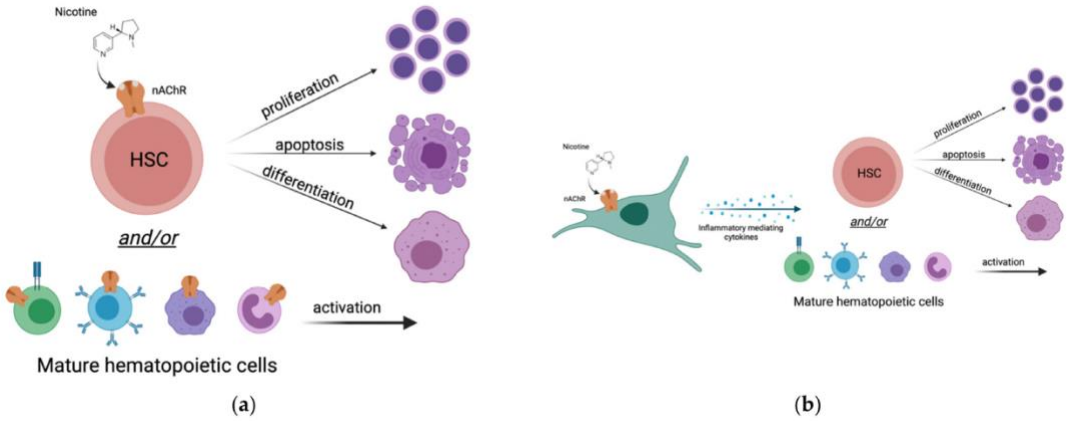

Figure 3.2

Potential mechanisms of altered hematopoiesis and immunity for life following nicotine exposure: (a) Nicotine directly influences the hematopoietic compartment. Nicotine binds to nicotinic acetyl choline receptors (nAChRs) expressed by hematopoietic stem cells or other mature hematopoietic cell types. These cells then undergo molecular changes which lead to proliferation, apoptosis, differentiation, and/or activation; (b) Nicotine indirectly influences the hematopoietic compartment. Nicotine binds to nicotinic-acetyl choline receptors (nAChRs) expressed by non-hematopoietic cells. These cells undergo molecular changes that then lead to release of inflammatory-mediating cytokines. Cytokines released by the non-hematopoietic cells bind to receptors on hematopoietic cell types. Hematopoietic cells then undergo molecular changes in response to the cytokines (directly) and nicotine (indirectly) which leads to proliferation, apoptosis, differentiation, and/or activation.

References

1. National Institute on Drug Abuse. What is the Scope of Tobacco, Nicotine, and E-Cigarette Use in the United States? Available online: www.drugabuse.gov/publications/research-reports/tobacco-nicotine-e-cigarettes/what-scope-tobacco-use-its-costto-society (accessed on 1 December 2021).

2. Ramanathan, G.; Craver-Hoover, B.; Arechavala, R.J.; Herman, D.A.; Chen, J.H.; Lai, H.Y.; Renusch, S.R.; Kleinman, M.T.; Fleischman, A.G. E-Cigarette Exposure Decreases Bone Marrow Hematopoietic Progenitor Cells. Cancers 2020, 12, 2292. [CrossRef][PubMed]

3. Flouris, A.D.; Vardavas, C.I.; Metsios, G.S.; Tsatsakis, A.M.; Koutedakis, Y. Biological Evidence for the Acute Health Effects of Secondhand Smoke Exposure. Am. J. Physiol. Lung Cell. Mol. Physiol. 2010, 298, L3–L12. [CrossRef]

4. Ferrante, G.; Simoni, M.; Cibella, F.; Ferrara, F.; Liotta, G.; Malizia, V.; Corsello, G.; Viegi, G.; La Grutta, S. Third-Hand Smoke Exposure and Health Hazards in Children. Monaldi Arch. Chest Dis. 2015, 79, 38–43. [CrossRef] [PubMed]

5. Harmful and Potentially Harmful Constituents in Tobacco Products and Tobacco Smoke: Established List. Available online: https://www.fda.gov/tobacco-products/rules-regulations-and-guidance/harmful-and-potentially-harmful-constituentstobacco-products-and-tobacco-smoke-established-list (accessed on 1 December 2021).

6. Mayer, B. How Much Nicotine Kills a Human? Tracing Back the Generally Accepted Lethal Dose to Dubious Self-Experiments in the Nineteenth Century. Arch. Toxicol. 2014, 88, 5–7. [CrossRef] [PubMed]

7. Thornton, S.L.; Oller, L.; Sawyer, T. Fatal Intravenous Injection of Electronic Nicotine Delivery System Refilling Solution. J. Med. Toxicol. 2014, 10, 202–204. [CrossRef]

8. Sommerfeld, K.; Łukasik-Gł˛ebocka, M.; Kulza, M.; Dru˙zd˙z, A.; Panie´nski, P.; Florek, E.; Zieli´nska-Psuja, B. Intravenous and Oral Suicidal E-Liquid Poisonings with Confirmed Nicotine and Cotinine Concentrations. Forensic Sci. Int. 2016, 262, e15–e20.[CrossRef] [PubMed]

9. Belkoniene, M.; Socquet, J.; Njemba-Freiburghaus, D.; Pellaton, C. Near Fatal Intoxication by Nicotine and Propylene Glycol Injection: A Case Report of an e-Liquid Poisoning. BMC Pharmacol. Toxicol. 2019, 20, 28. [CrossRef]

10. Mishra, A.; Chaturvedi, P.; Datta, S.; Sinukumar, S.; Joshi, P.; Garg, A. Harmful Effects of Nicotine. Indian J. Med. Paediatr. Oncol. 2015, 36, 24–31. [CrossRef]

11. Chang, E.; Forsberg, E.C.; Wu, J.; Bingyin Wang, B.; Prohaska, S.S.; Allsopp, R.; Weissman, I.L.; Cooke, J.P. Cholinergic Activation of Hematopoietic Stem Cells: Role in Tobacco-Related Disease? Vasc. Med. 2010, 15, 375–385. [CrossRef]

12. Zalokar, J.B.; Richard, J.L.; Claude, J.R. Leukocyte Count, Smoking, and Myocardial Infarction. N. Engl. J. Med. 1981, 304, 465–468. [CrossRef]

13. Smith, M.R.; Kinmonth, A.-L.; Luben, R.N.; Bingham, S.; Day, N.E.;Wareham, N.J.;Welch, A.; Khaw, K.-T. Smoking Status and Differential White Cell Count in Men

and Women in the EPIC-Norfolk Population. Atherosclerosis 2003, 169, 331–337. [CrossRef]

14. Friedman, G.D.; Siegelaub, A.B.; Seltzer, C.C.; Feldman, R.; Collen, M.F. Smoking Habits and the Leukocyte Count. Arch. Environ. Health Int. J. 1973, 26, 137–143. [CrossRef]

15. Roethig, H.J.; Koval, T.; Muhammad-Kah, R.; Jin, Y.; Mendes, P.; Unverdorben, M. Short Term Effects of Reduced Exposure to Cigarette Smoke on White Blood Cells, Platelets and Red Blood Cells in Adult Cigarette Smokers. Regul. Toxicol. Pharmacol. 2010, 57, 333–337. [CrossRef] [PubMed]

16. Fernández, J.A.; Prats, J.; Artero, J.V.; Mora, A.; Fariñas, A.; Espinal, A.; Méndez, J.A. Systemic Inflammation in 222.841 Healthy Employed Smokers and Nonsmokers: White Blood Cell Count and Relationship to Spirometry. Tob. Induc. Dis. 2012, 10, 7. [CrossRef]

17. Rodriguez y Baena, A.; Manso, B.A.; Forsberg, E.C. CFU-S Assay: A Single-Cell Historical Assay Offers Modern Insight to Clonal Hematopoiesis. Exp. Hematol. 2021, 104, 1–8. [CrossRef]

18. Till, J.E.; Mcculloch, E.A. A Direct Measurement of the Radiation Sensitivity of Normal Mouse Bone Marrow Cells. Radiat. Res.1961, 14, 213–222. [CrossRef] [PubMed]

19. Dzierzak, E.; Bigas, A. Blood Development: Hematopoietic Stem Cell Dependence and Independence. Cell Stem Cell 2018, 22, 639–651. [CrossRef] [PubMed]

20. Cool, T.; Forsberg, E.C. Chasing Mavericks: The Quest for Defining Developmental Waves of Hematopoiesis. In Current Topics in Developmental Biology; Elsevier: Amsterdam, The Netherlands, 2019; Volume 132, pp. 1–2. ISBN 978-0-12-810489-7.

21. Klaus, A.; Robin, C. Embryonic Hematopoiesis under Microscopic Observation. Dev. Biol. 2017, 428, 318–327. [CrossRef]

22. Wittamer, V.; Bertrand, J.Y. Yolk Sac Hematopoiesis: Does It Contribute to the Adult Hematopoietic System? Cell. Mol. Life Sci. 2020, 77, 4081–4091. [CrossRef] Cancers 2022, 14, 184 9 of 10

23. Beaudin, A.E.; Boyer, S.W.; Perez-Cunningham, J.; Hernandez, G.E.; Derderian, S.C.; Jujjavarapu, C.; Aaserude, E.; MacKenzie, T.; Forsberg, E.C. A Transient Developmental Hematopoietic Stem Cell Gives Rise to Innate-like B and T Cells. Cell Stem Cell 2016, 19, 768–783. [CrossRef]

24. Beaudin, A.E.; Forsberg, E.C. To B1a or Not to B1a: Do Hematopoietic Stem Cells Contribute to Tissue-Resident Immune Cells? Blood 2016, 128, 2765–2769. [CrossRef]

25. De Laval, B.; Maurizio, J.; Kandalla, P.K.; Brisou, G.; Simonnet, L.; Huber, C.; Gimenez, G.; Matcovitch-Natan, O.; Reinhardt, S.; David, E.; et al. C/EBP - Dependent Epigenetic Memory Induces Trained Immunity in Hematopoietic Stem Cells. Cell Stem Cell 2020, 26, 657–674.e8. [CrossRef]

26. Rodrigues, C.P.; Shvedunova, M.; Akhtar, A. Epigenetic Regulators as the Gatekeepers of Hematopoiesis. Trends Genet. 2021, 37, 125–142. [CrossRef]

27. Wang, Z.; Wang, P.; Li, Y.; Peng, H.; Zhu, Y.; Mohandas, N.; Liu, J. Interplay between Cofactors and Transcription Factors in Hematopoiesis and Hematological Malignancies. Sig. Transduct. Target. Ther. 2021, 6, 24. [CrossRef] [PubMed]

28. Gao, P.; Chen, C.; Howell, E.D.; Li, Y.; Tober, J.; Uzun, Y.; He, B.; Gao, L.; Zhu, Q.; Siekmann, A.F.; et al. Transcriptional Regulatory Network Controlling the Ontogeny of Hematopoietic Stem Cells. Genes Dev. 2020, 34, 950–964. [CrossRef]

29. Pietras, E.M. Inflammation: A Key Regulator of Hematopoietic Stem Cell Fate in Health and Disease. Blood 2017, 130, 1693–1698.[CrossRef]

30. Schuettpelz, L.G.; Link, D.C. Regulation of Hematopoietic Stem Cell Activity by Inflammation. Front. Immunol. 2013, 4, 204.[CrossRef] [PubMed]

31. Baldridge, M.T.; King, K.Y.; Goodell, M.A. Inflammatory Signals Regulate Hematopoietic Stem Cells. Trends Immunol. 2011, 32, 57–65. [CrossRef] [PubMed]

32. Collins, A.; Mitchell, C.A.; Passague, E. Inflammatory Signaling Regulates Hematopoietic Stem and Progenitor Cell Development and Homeostasis. J. Exp. Med. 2021, 218, e20201545. [CrossRef] [PubMed]

33. Flouris, A.D.; Poulianiti, K.P.; Chorti, M.S.; Jamurtas, A.Z.; Kouretas, D.; Owolabi, E.O.; Tzatzarakis, M.N.; Tsatsakis, A.M.; Koutedakis, Y. Acute Effects of Electronic and Tobacco Cigarette Smoking on Complete Blood Count. Food Chem. Toxicol. 2012, 50, 3600–3603. [CrossRef] [PubMed]

34. Pedersen, K.M.; Çolak, Y.; Ellervik, C.; Hasselbalch, H.C.; Bojesen, S.E.; Nordestgaard, B.G. Smoking and Increased White and Red Blood Cells: A Mendelian

Randomization Approach in the Copenhagen General Population Study. Arterioscler. Thromb. Vasc. Biol. 2019, 39, 965–977. [CrossRef]

35. Chmielewski, P.P.; Strzelec, B. Elevated Leukocyte Count as a Harbinger. Folia Morphol. 2018, 77, 171–178. [CrossRef] [PubMed]

36. Dani, J.A. Neuronal Nicotinic Acetylcholine Receptor Structure and Function and Response to Nicotine. In International Review of Neurobiology; Elsevier: Amsterdam, The Netherlands, 2015; Volume 124, pp. 3–19. ISBN 978-0-12-801583-4.

37. Wu, J.; Lukas, R.J. Naturally-Expressed Nicotinic Acetylcholine Receptor Subtypes. Biochem. Pharmacol. 2011, 82, 800–807. [CrossRef]

38. St-Pierre, S.; Jiang,W.; Roy, P.; Champigny, C.; LeBlanc, É.; Morley, B.J.; Hao, J.; Simard, A.R. Nicotinic Acetylcholine Receptors Modulate Bone Marrow-Derived pro-Inflammatory Monocyte Production and Survival. PLoS ONE 2016, 11, e0150230. [CrossRef][PubMed]

39. Osgoei, L.T.; Parivar, K.; Ebrahimi, M.; Mortaz, E. Nicotine Modulates the Release of Inflammatory Cytokines and Expression of TLR2, TLR4 of Cord Blood Mononuclear Cells. Iran. J. Allergy Asthma Immunol. 2018, 17, 372–378.

40. Mohsenzadeh, Y.; Rahmani, A.; Cheraghi, J.; Pyrani, M.; Asadollahi, K. Prenatal Exposure to Nicotine in Pregnant Rat Increased Inflammatory Marker in Newborn Rat. Mediat. Inflamm. 2014, 2014, 274048. [CrossRef]

41. Von Chamier, M.; Reyes, L.; Hayward, L.F.; Brown, M.B. Impact of Gestational Nicotine Exposure on Intrauterine and Fetal Infection in a Rodent Model. Biol. Reprod. 2017, 96, 1071–1084. [CrossRef]

42. Chen, H.; Li, G.; Chan, Y.L.; Chapman, D.G.; Sukjamnong, S.; Nguyen, T.; Annissa, T.; McGrath, K.C.; Sharma, P.; Oliver, B.G. Maternal E-Cigarette Exposure in Mice Alters DNA Methylation and Lung Cytokine Expression in Offspring. Am. J. Respir. Cell Mol. Biol. 2018, 58, 366–377. [CrossRef]

43. Hosseinzadeh, A.; Thompson, P.R.; Segal, B.H.; Urban, C.F. Nicotine Induces Neutrophil Extracellular Traps. J. Leukoc. Biol. 2016, 100, 1105–1112. [CrossRef]

44. Strzelak, A.; Ratajczak, A.; Adamiec, A.; Feleszko, W. Tobacco Smoke Induces and Alters Immune Responses in the Lung Triggering Inflammation, Allergy, Asthma and Other Lung Diseases: A Mechanistic Review. Int. J. Environ. Res. Public Health 2018, 15, 1033. [CrossRef] [PubMed]

45. Hajiasgharzadeh, K.; Sadigh-Eteghad, S.; Mansoori, B.; Mokhtarzadeh, A.; Shanehbandi, D.; Doustvandi, M.A.; Asadzadeh, Z.; Baradaran, B. Alpha7 Nicotinic Acetylcholine Receptors in Lung Inflammation and Carcinogenesis: Friends or Foes? J. Cell. Physiol. 2019, 234, 14666–14679. [CrossRef]

46. Breit, S.; Kupferberg, A.; Rogler, G.; Hasler, G. Vagus Nerve as Modulator of the Brain-Gut Axis in Psychiatric and Inflammatory Disorders. Front. Psychiatry 2018, 9, 44. [CrossRef]

47. Johnston, G.R.; Webster, N.R. Cytokines and the Immunomodulatory Function of the Vagus Nerve. Br. J. Anaesth. 2009, 102, 453–462. [CrossRef] [PubMed]

48. Wong, M.K.; Barra, N.G.; Alfaidy, N.; Hardy, D.B.; Holloway, A.C. Adverse Effects of Perinatal Nicotine Exposure on Reproductive Outcomes. Reproduction 2015, 150, R185–R193. [CrossRef] Cancers 2022, 14, 184 10 of 10

49. Gracia, M.C. Exposure to Nicotine Is Probably a Major Cause of Inflammatory Diseases among Non-Smokers. Med. Hypotheses 2005, 65, 253–258. [CrossRef] [PubMed]

50. Azagba, S.; Manzione, L.; Shan, L.; King, J. Trends in Smoking during Pregnancy by Socioeconomic Characteristics in the United States, 2010–2017. BMC Pregnancy Childbirth 2020, 20, 52. [CrossRef]

51. Orellana, J.A.; Busso, D.; RamÃ rez, G.; Campos, M.; Rigotti, A.; EugenÃ n, J.; von Bernhardi, R. Prenatal Nicotine Exposure Enhances Cx43 and Panx1 Unopposed Channel Activity in Brain Cells of Adult Offspring Mice Fed a High-Fat/Cholesterol Diet. Front. Cell. Neurosci. 2014, 8, 403. [CrossRef]

52. Lin, C.; Yon, J.-M.; Hong, J.T.; Lee, J.K.; Jeong, J.; Baek, I.-J.; Lee, B.J.; Yun, Y.W.; Nam, S.-Y. 4-O-Methylhonokiol Inhibits Serious Embryo Anomalies Caused by Nicotine via Modulations of Oxidative Stress, Apoptosis, and Inflammation: 4-omethylhonokiol prevents nicotine-induced embryotoxicity. Birth Defects Res. B 2014, 101, 125–134. [CrossRef]

53. Apostol, A.C.; Jensen, K.D.C.; Beaudin, A.E. Training the Fetal Immune System through Maternal Inflammation—A Layered Hygiene Hypothesis. Front. Immunol. 2020, 11, 123. [CrossRef]

54. Hayashi, Y.; Sezaki, M.; Takizawa, H. Development of the Hematopoietic System: Role of Inflammatory Factors. WIREs Dev. Biol 2019, 8, e341. [CrossRef] [PubMed]

55. Qu, W.; Liu, H.; Yan, H.; Hou, L.; Ping, J.; Zhao, W.; Wen, X. Prenatal Nicotine Exposure Induces Thymic Hypoplasia in Mice Offspring from Neonatal to Adulthood. Toxicol. Lett. 2018, 304, 30–38. [CrossRef]

56. Kang, N. Effects of in Utero Nicotine Exposure in Immune Cell Disposition after P. Aeruginosa Lung Infection. Master's Thesis, University of Kentucky, Lexington, KY, USA, 2017.

57. Luck, W.; Nau, H. Nicotine and Cotinine Concentrations in Serum and Milk of Nursing Smokers. Br. J. Clin. Pharmacol. 1984, 18, 9–15. [CrossRef] [PubMed]

58. Dahlström, A.; Lundell, B.; Curvall, M.; Thapper, L. Nicotine and Cotinine Concentrations in the Nursing Mother and Her Infant. Acta Paediatr. 1990, 79, 142–147. [CrossRef]

59. Bruin, J.E.; Gerstein, H.C.; Holloway, A.C. Long-Term Consequences of Fetal and Neonatal Nicotine Exposure: A Critical Review. Toxicol. Sci. 2010, 116, 364–374. [CrossRef] [PubMed]

60. Hofhuis, W.; de Jongste, J.C.; Merkus, P.J.F.M. Adverse Health Effects of Prenatal and Postnatal Tobacco Smoke Exposure on Children. Arch. Dis. Child. 2003, 88, 1086–1090. [CrossRef] [PubMed]

61. Wen, X.; Shenassa, E.D.; Paradis, A.D. Maternal Smoking, Breastfeeding, and Risk of Childhood Overweight: Findings from a National Cohort. Matern. Child Health J. 2013, 17, 746–755. [CrossRef]

62. González-Romero, E.; Martínez-Valiente, C.; García-Ruiz, C.; Vázquez-Manrique, R.P.; Cervera, J.; Sanjuan-Pla, A. CRISPR to Fix Bad Blood: A New Tool in Basic and Clinical Hematology. Haematologica 2019, 104, 881–893. [CrossRef]

63. Nidhi, S.; Anand, U.; Oleksak, P.; Tripathi, P.; Lal, J.A.; Thomas, G.; Kuca, K.; Tripathi, V. Novel CRISPR–Cas Systems: An Updated Review of the Current Achievements, Applications, and Future Research Perspectives. Int. J. Mol. Sci. 2021, 22, 3327. [CrossRef]

64. Buenrostro, J.D.; Wu, B.; Chang, H.Y.; Greenleaf, W.J. ATAC-seq: A Method for Assaying Chromatin Accessibility Genome-Wide. Curr. Protoc. Mol. Biol. 2015, 109, 21–29. [CrossRef]

65. Buenrostro, J.D.; Giresi, P.G.; Zaba, L.C.; Chang, H.Y.; Greenleaf,W.J. Transposition of Native Chromatin for Fast and Sensitive Epigenomic Profiling of Open Chromatin, DNA-Binding Proteins and Nucleosome Position. Nat. Methods 2013, 10, 1213–1218.[CrossRef]

66. Merad, M.; Manz, M.G.; Karsunky, H.; Wagers, A.; Peters, W.; Charo, I.; Weissman, I.L.; Cyster, J.G.; Engleman, E.G. Langerhans Cells Renew in the Skin throughout Life under Steady-State Conditions. Nat. Immunol. 2002, 3, 1135–1141. [CrossRef] [PubMed]

67. Leung, G.A.; Cool, T.; Valencia, C.H.; Worthington, A.; Beaudin, A.E.; Forsberg, E.C. The Lymphoid-Associated Interleukin 7 Receptor (IL7R) Regulates Tissue-Resident Macrophage Development. Development 2019, 146, dev176180. [CrossRef] [PubMed]

68. Cool, T.; Worthington, A.; Poscablo, D.; Hussaini, A.; Forsberg, E.C. Interleukin 7 Receptor Is Required for Myeloid Cell Homeostasis and Reconstitution by Hematopoietic Stem Cells. Exp. Hematol. 2020, 90, 39–45.e3. [CrossRef] [PubMed]

69. Worthington, A.; Cool, T.; Poscablo, D.; Hussaini, A.; Beaudin, A.E.; Forsberg, E.C. IL7R, but not Flk2/Flt3, is required for hematopoietic stem cell reconstitution of tissue-resident lymphoid cells. Development 2022, in press.

Chapter 4.

In Utero Nicotine Exposure Leads to Persistent Changes in Hematopoietic Function and Maintenance

Abstract

Tobacco use during pregnancy has many deleterious health consequences on not only the smoking mother, but on the unborn fetus. Children of smoking mothers are known to have increased susceptibility to respiratory diseases later in life. The mechanisms driving this increased susceptibility are not clearly understood. One potential source of disease susceptibility is an altered immune system, which is derived from Hematopoietic Stem and Progenitor Cells (HSPCs). Here, we report that nicotine, one of the main toxic compounds found in traditional and new tobacco products, has a deleterious effect on hematopoietic output and function. In utero nicotine exposure results in permanent changes within the HSPC compartment thus leading to inadequate immune responses to pathogens later in life.

Introduction

An emerging market of products that have become a focal point of research efforts is electronic cigarettes. Albeit advertised as a "safer" alternative to traditional cigarettes, these products contain many toxic compounds including nicotine, which is known for its addictive properties. According to the National Institute of Health (NIH), in 2021, 4.6% mothers in the United States smoked during pregnancy. Although this percentage

has declined since 2016, is it still a considerable amount given smoking during pregnancy is an established risk factor for adverse outcomes and severe health issues for the children[1–4]. Children of smoking mothers are known to have increased susceptibility to many diseases, especially diseases of the airways and lungs, including asthma, chronic obstructive pulmonary disease, and increased respiratory infections later in life[5]. However, what causes this increased disease susceptibility is poorly understood; the cellular and molecular mechanisms of altered health outcomes in children of smoking mothers remain not well investigated. It has been hypothesized that perinatal exposure to environmental toxins, such as nicotine, affects immune cell establishment and function leading to long lasting consequences. Nicotine is nicotinic receptor agonist and its binding triggers cellular responses such as proliferation, apoptosis, and differentiation. Additionally, nicotine is known to cause inflammation[6,7] which can lead to permanent alterations in fetal immunity and later in life[8,9].

The immune system is established through developmental immune layering, a complex orchestration of waves of unique hematopoietic stem and progenitor cells (HSPCs) that give rise to developmentally distinct subsets of immune cells[10]. This process comprises non-self-renewing progenitors that generate long-lived self-renewing mature cells, such as tissue-resident cells. The extent to which these fetal-derived immune cells persist and contribute to adult immunity, as well as whether these cells or their progenitor source may alter disease susceptibility for life, remains unclear. Additionally, there are self-renewing progenitors, such as traditional HSCs, that give

rise to non-self-renewing progeny. Several perinatally-established subsets of white blood cells (WBCs), including tissue-resident macrophages and innate-like lymphoid cells, have been implicated as modulators of inflammation across tissues. Therefore, they present interesting points of interrogation for the link between early life environmental exposures and elevated inflammation. In utero exposure to pathogens and toxicants coincides with developmental waves that generate long-lasting immune cells, which is one potential mechanism of altered life-long immunity in the children of smoking mothers.

Here, we implemented an *in vivo* exposure model to investigate how perinatal nicotine exposure (PNE) alters hematopoietic establishment and life-long function in the offspring. PNE causes a persistent decrease in HSPCs and alters the establishment of fetally-derived non-traditional immune cells in the lungs of mice. Additionally, PNE led to persistent altered hematopoietic function in a secondary insult model. Together, these experiments demonstrate that *in utero* nicotine exposure has deleterious consequences on hematopoietic establishment and function for life.

Results

Perinatal nicotine exposure alters seeding of HSCs by affecting the fetal liver niche

To determine how PNE affects hematopoiesis, we administered pregnant dams nicotine (100ug/ml[11]) in sucrose solution *ad libitum* via drinking water for the entirety of the gestation and nursing period (Figure 1A). Then, we analyzed the offspring at postnatal

day 0 (P0) to determine whether PNE nicotine exposure had any effects on the number of HSCs in the two major hematopoietic compartments at this timepoint, the liver and the bone marrow. We observed a decrease in the total number of cells in the liver (Supplementary Figure 1B), but more importantly the number of HSCs was significantly decreased in the liver of nicotine-exposed P0 pups compared to control pups (Figure 1B, Supplementary Figure 1A) suggesting either HSC exhaustion or niche-induced migration outside of the liver. Meanwhile, the number of HSCs seeded in the bone marrow was significantly increased in nicotine-exposed pups compared to controls (Figure 1C) but this increase in cell number did not fully account for the decreased HSC number in the liver of these pups as the total HSC number in the P0 pups was still significantly reduced in the nicotine group (Supplementary Figure 1C). Moreover, the cell cycle profile of liver HSCs (Figure 1D) and BM HSCs (Supplementary Figure 1D) remained unaltered excluding HSC exhaustion at this time point. We also did not detect any expression of the nicotinic receptor α7 (nAChRα7), which was previously reported to be expressed on hematopoietic cells[12], in HSCs from either control or nicotine-exposed P0 pups but detected expression in whole liver tissue from P0 pups both from control and nicotine-exposed (Supplementary Figure 1E), suggesting that nicotine might interact with the niche instead of directly affecting HSCs. Thus, we investigated whether PNE affected the liver microenvironment by collecting serum from the liver of these P0 pups and measuring an array of cytokines and chemokines secreted within the liver niche by a multiplex ELISA (Figure 1E). These data were normalized to the total protein concentration of each liver

(Supplementary Figure 1F). While the levels of some pro-inflammatory cytokines such as IL-1β, IL-6, and IFNβ remained surprisingly unaffected (Figure 1H), other molecules previously shown to be affected by nicotine or cigarette smoke followed similar patterns in this screen, such as TIMP-1[13,14], TNFα[15,16], and MCP-1[17] being significantly lower (Figure 1F), and MIG (CXCL9)[18] being significantly higher in nicotine-exposed pups compared to controls (Figure 1G). These changes in cytokine expression suggest that PNE can shape the fetal liver niche by remodeling the extracellular matrix[19], altering the localization, proliferation, and maturation of endothelial cells and other hematopoietic cells, and can also alter HSC migration and retention in the fetal liver[20]. This data suggests that nicotine-induced changes in the post-natal liver microenvironment can alter the HSC pool potentially leading to permanent alterations of the hematopoietic system.

Perinatal nicotine exposure permanently reduces numbers of HSPCs in the bone marrow

To determine if changes within the HSC compartment of nicotine exposed P0 pups (Figure 1) persisted during later time points, we further analyzed the offspring from the same PNE set up at post-natal day 14 (P14) and at 8-12 weeks (adulthood) (Figure 2A). We analyzed the bone marrow as it is the main hematopoietic organ at these time points. First, we observed no differences between the weight of control and nicotine-exposed P14 pups (Figure 2B), suggesting that the offspring were feeding and developing properly. Interestingly, at P14, the number of bone marrow HSCs (Figure 2C) remained

significantly lower in the nicotine-exposed pups and this decrease in cell number was reflected in other hematopoietic progenitor populations, namely multipotent progenitors (MPPs; Figure 2D) and myeloid progenitors (MyPros; Figure 2E), which can be phenotypically subdivided into common myeloid progenitors (CMPs), granulocyte-monocyte progenitors (GMPs), and megakaryocytic-erythroid progenitors (MEPs) (Supplementary Figure 2B-D). This was not due to an overall decrease in cellularity in the bone marrow of nicotine-exposed pups (Supplementary Figure 2A) and, similar to the P0 time point, we did not observe any changes in cycling of HSCs at P14 (Figure 2F). Then, we analyzed the bone marrow composition of adult offspring that had been exposed to nicotine *in utero*. Interestingly, we observed that at this time point there were no differences in the number of HSCs between control and nicotine-exposed mice (Figure 2G). However, similar to the P14 timepoint, the number of MPPs (Figure 2H) and MyPros (Figure 2I), primarily GMPs and MEPs (Supplementary Figure 2E-G), remained significantly lower in nicotine-exposed mice. A similar effect was previously observed upon chronic inhalation of E-cigarette smoke in mice[21]. These phenotypes were not concordant to what we observed when adult (8-12 weeks) mice were administered nicotine (100ug/ml[11]) in sucrose solution *ad libitum* via drinking water for ~8 weeks (Supplementary Figure 2H). As previously reported by others[12,22], we observed a significant increase in the number of HSCs in the bone marrow of nicotine-treated mice (Supplementary Figure 2J) along with a significant increase in white blood cell (WBC) counts (Supplementary Figure 2M). Meanwhile, MPPs and MyPros remained unaffected by nicotine treatment (Supplementary Figure 2K-L).

Taken together this data suggests that the developmental age during which mice are exposed to nicotine differentially affects hematopoiesis.

Perinatal nicotine exposure does not affect mature cell numbers in the peripheral blood

To determine if the changes observed within the bone marrow HSPC compartment of P14 and 8-12 weeks old adult offspring that had been exposed to nicotine *in utero* (Figure 2) was reflected in the composition of more "traditional" mature populations, we analyzed the peripheral blood of these mice (Figure 3). Interestingly, although PNE lead to altered bone marrow HSPC numbers, we observed no differences in cell number of GMs (Figure 3A), B cells (Figure 3B), T cell (Figure 3C), RBCs (Figure 3D), and platelets (Figure 3E) of P14 pups. Similarly, we observed no differences in cell numbers in the peripheral blood of adult offspring of nicotine-exposed mothers (Figure 3F-J). Potentially, decreased numbers within the hematopoietic stem and progenitor compartments in the bone marrow of nicotine-exposed offspring result from enhanced differentiation to sustain mature blood cell number and function in the peripheral blood.

PNE leads to persistent decrease in non-traditional immune cell numbers in the lungs of exposed mice

As smoking during pregnancy has been associated with higher susceptibility in the offspring for respiratory diseases, we wanted to determine if PNE resulted in persistent changes in establishment of non-traditional, or fetally-derived, immune cell populations. Thus, we analyzed the lungs of pups born from nicotine-exposed mothers

(Figure 4). By examining the lungs, we were able to simultaneously compare traditional and non-traditional immune cell populations. Surprisingly, although we observed a transient trend towards a burst in the generation of T cells in P14 animals (Figure 3B), we observed no differences in cell numbers of CD4+ T cells (Figure 4F) and CD8+ T cells (Figure 4G). However, while the number of adult-derived TCRβ T cells (Figure 4H) was unaltered, the lungs of PNE adult offspring had significantly fewer TCRγδ T cells (Figure 4I), a subset of T cells that are considered fetally derived. These data suggests that *in utero* nicotine exposure primarily affects the establishment of non-traditional immune cell types which are fetally derived and persist throughout life without contributions from adult HSCs.

PNE exacerbates immune response with secondary insult

Having demonstrated that PNE transiently altered the number of phenotypic HSCs (Figure 1-2**)**, we wanted to determine how adult mice that had been perinatally exposed to nicotine would respond to a secondary insult model. To test this, we infected the PNE adult offspring exposed with a single high dose of lipopolysaccharide (LPS) and analyzed their bone marrow and blood compartments 16 hours after injection (Figure 5A). The expected bone marrow HSPC composition of these PNE adult offspring was shown in Figure 2G-I. Generally, the peripheral blood is composed of ~75% B and T cells and ~25% GMs (Supplementary Figure 3A) but upon LPS exposed, there is a significantly increased proportion of the GM pool, making up most of the nucleated cells in the blood (Figure 5B). Here, we observed a significant increase in the

proportion of GMs in the peripheral blood of mice that were exposed to both nicotine perinatally and LPS in adulthood, compare to mice that were only exposed to LPS in adulthood (Figure 5B). As expected, we observed a significant expansion of the bone HSC pool and a significant depletion of MyPros in response to LPS (Supplementary Figure 3B-D). These responses to LPS seem to be independent of previous nicotine exposure. In fact, there were no differences in the response to LPS between the control mice exposed to LPS only and PNE mice exposed to LPS for HSCs (Figure 5B), MPPs (Figure 5C), and MyPros (Figure 5D). Taken together, these data indicate that perinatal nicotine exposure slightly exacerbates emergency myelopoiesis in response to LPS but does not cause any major alteration within the HSPC compartment. Finally, we also transplanted 1 million whole bone marrow cells from control, nicotine-exposed, LPS only and nicotine +LPS mice into sub-lethally irradiated mice to further determine any effects on the functionality of HSCs. We observed reduced chimerism over time in all groups except for the control group (where the donor was unexposed, untreated cells) (Figure 5F). Most of the mice from the nicotine only, LPS only, and nicotine +LPS groups did not sustain donor chimerism long-term (Figure 5F-G) suggesting that both PNE and LPS led to reduced engraftment and repopulation potential of HSCs.

Discussion

The prevalence of smoking during pregnancy in the United States is a significant concern, with approximately 5% of mothers engaging in this behavior[1-4]. Studying the specific risks associated with perinatal nicotine exposure is necessary in addressing

potential life-long health implications for the offspring. While the impact of inflammatory stimuli on adult hematopoietic stem cells is well-documented (Essers 2009, Pietras 2014, Haas 2015), our understanding of the effects of *in utero* exposure to toxic compounds on the establishment of the hematopoietic and immune system in mice remains limited.

To shed light on this, our investigation strategically focused on isolating the effects of nicotine alone, distinct from the diverse toxicants present in tobacco products. We observed a significant decrease in neonatal hematopoietic stem cells (HSCs) in PNE offspring, likely due to alterations in the hematopoietic niche leading to decreased HSC homing in the neonatal liver and/or increased mobilization. Although this HSC deficit normalized by adulthood, a persistent reduction in hematopoietic progenitors was observed, underscoring the enduring impact of perinatal nicotine exposure.

Interestingly, despite these changes, mature cell production in the peripheral blood of adult PNE offspring exhibited no significant alterations. This underscores the critical role of hematopoietic progenitors in maintaining proper hematopoietic functions, even when mature cell levels appear unchanged.

Motivated by these findings, we hypothesized that mice exposed to nicotine in utero would exhibit an aberrant response to infection in adulthood. However, when subjected to a high-dose lipopolysaccharide (LPS) treatment, the immune response in these mice, while increased, did not reach the anticipated magnitude. This discrepancy may stem from the inherently robust reaction that healthy mice exhibit to LPS, characterized by acute and systemic immune activation. This observation suggests that the impact of *in*

utero nicotine exposure might be underscored by the already pronounced reactivity to immune stimuli. Our data prompts further exploration into the nuanced ways perinatal nicotine exposure may shape immune responses later in life.

Having observed a notable impact on the establishment of immune cells in the lungs of mice exposed to nicotine *in utero*, particularly in the context of non-traditional fetally-derived immune cells, we decided to investigate the potential ramifications during a local inflammatory challenge induced by influenza, leading to a viral respiratory tract infection. Given the previously established link between cigarette smoking and increased susceptibility to respiratory infections in humans (citation). we hypothesize that adult mice with a history of *in utero* nicotine exposure will exhibit an exaggerated response to influenza virus resulting in increased disease severity and adverse outcomes.

Understanding the mechanisms behind the transient HSC deficit, as well as exploring the clinical implications of persistent changes in hematopoietic progenitors and mature cell function, provides valuable insights into the lifelong impact of perinatal nicotine exposure.

Methods

Mice

All animals were housed and bred in the AALAC accredited vivarium at UC Santa Cruz and group housed in ventilated cages on a standard 12:12 light cycle. All procedures were approved by the UCSC or the UC Merced Institutional Animal Care

and Use (IACUC) committees. WT C57Bl/6 mice were used for controls and for all expression experiments. Male and female mice were used equally and without sex discrimination for all experiments. Mice were fed normal chow diet and given nicotine solution (100µg/ml nicotine and 5% sucrose, diluted in water[11]) *ad libitum*. Mice were sacrificed at post-natal day 0 (P0), post-natal day 14 (P14), or adulthood (8-12 weeks of age). Recipients for transplantation assays were adult mice (8-12 weeks of age) irradiated at 500rads prior to transplantation of whole bone marrow cells from donor mice. For LPS exposure, adult mice (8-12 weeks) were administered a single intraperitoneal injection of 35µg of LPS. They were sacrificed for analysis ~16 hours post injection.

Tissue and cell isolation

Mice were sacrificed by CO2 inhalation. Neonatal livers were harvested and homogenized using mortar and pestle before filtering through a 70µm filter. Lungs were harvested and treated with 1X PBS (+/+) with 2% fetal bovine serum (WVR) and 2mg/ml Collagenase IV (Gibco) and 100U/ml DNaseI (Sigma)for 1 hour at 37C. Following incubation, tissue was passed through a 16g needle followed by 9g needle (approximately 10 times each) and then filtered through a 70µm filter. For all BM HSPC analysis, both long bones (tibia and femur) were pulled, crushed in 1X PBS supplemented with 5 mM EDTA with 2% fetal bovine serumserum, and single cell suspensions were filtered through a 70µm filter. Peripheral blood was analyzed by tail

bleeds for transplantation experiments and taken from the femoral artery at sacrifice for terminal analysis.

Cytokine analysis

Livers were extracted from P0 pups, weighed, and then homogenized in 200µl of PBS without calcium and magnesium to collect serum. After a 10-minute centrifugation at room temperature, 180µl of supernatant were transferred to a new tube, incubated at room temperature for 30 minutes (to allow clotting), centrifuged, and finally 75µl of the supernatant was sent to Eve's Technologies for "Mouse Cytokine/Chemokine 44-Plex Discovery Assay Array". Concentrations of these cytokines/chemokines in the liver serum was normalized to total protein concentrations.

Flow cytometry

Single cell suspensions were then stained with monoclonal anti-mouse antibodies on ice in the dark for 20 minutes and acquired using a FACSAria or an LSRII flow cytometer (BD Biosciences, San Jose, CA) at the University of California-Santa Cruz, as described previously[23–31]. Cell populations were defined by the following cell surface markers: P0 HSC (Live, CD3-CD4-CD5-CD8-B220-Gr1-Ter119-cKit+Sca1+Flk2-SLAM+); P14 and adult HSCs (Live, CD3-CD4-CD5-CD8-B220-Gr1-Mac1-Ter119-cKit+Sca1+Flk2-SLAM+); MPP (Live, CD3-CD4-CD5-CD8-B220-Gr1-Mac1-Ter119-cKit+Sca1+Flk2+SLAM-); MyPro (Live, CD3-CD4-CD5-CD8-B220-Gr1-Mac1-Ter119-cKit+Sca1-); CMP (Live, CD3-CD4-CD5-CD8-B220-

Gr1-Mac1-Ter119-cKit+Sca1-FCgRmidCD34+); GMP (Live, CD3-CD4-CD5-CD8-B220-Gr1-Mac1-Ter119-cKit+Sca1-FCgR+CD34+); MEP (Live, CD3-CD4-CD5-CD8-B220-Gr1-Mac1-Ter119-cKit+Sca1-FCgR-CD34-); GM (Live, Ter119-CD61-B220-CD3-Mac1+Gr1+), B cells (Live, Ter119-CD61- Mac1-Gr1-B220+CD3-), T cells (Live, Ter119-CD61-Mac1-Gr1-B220-CD3+), RBC (Live, CD61-B220-CD3-Ter119+),platelets (Live, CD61+B220-CD3-Ter119-); Data was analyzed with FlowJo.

Cell cycle analysis

Single cell suspension from P0 neonatal liver and P14 BM were first stained with lineage markers (Ter119, Gr1, B220, CD3, CD4, CD5, CD8) and HSPC markers (cKit, Sca1, SLAM, Flk2), then fixed, permeabilized with 4% PFA, treated with RNAase A (ThermoFisher), and stained with DAPI for cell cycle analysis by flow cytometry.

qPCR of nAChRa7

For whole tissue samples, total RNA was isolated, crushed brain and liver with a Direct-zol RNA MiniPrep kit (Zymo Research). For sorted cells, RNA was isolated from twenty thousand purified fetal liver HSCs using Trizol (Life Technologies) and a DNase treatment step. Complementary DNA (cDNA) was synthesized using the High Capacity cDNA Reverse Transcription Kit (Thermo Fisher). Quantitative PCR was performed using a Viia 7 Real-Time PCR (Applied Biosystems). Fold expression relative to the reference gene (GAPDH) was calculated using the comparative CT

method (ΔΔCT) and the values were normalized to the positive control (brain tissue). The primers used included: GAPDH - Forward: 5'-TGTGTCCGTCGTGGATCTGA-3'; GAPDH - Reverse: 5'-CCTGCTTCACCACCTTCTTGA-3'; nAChRa7 - Forward: 5'-TTGTGCTGCGATATCACCAC-3'; nAChRa7 - Reverse: 5'TTCATGCGCAGAAACCATGC-3'.

Transplantation assays

Transplantation assays were performed as previously described[24,24,27–32]. $1x10^6$ whole bone marrow cells from control, PNE only, LPS only, and PNE +LPS mice were transplanted into sub-lethally irradiated (500rads) mice. Retro-orbital transplantations were performed under isoflurane-induced short-term general anesthesia. Recipient mice were bled at 4, 8, 12 and 16-weeks post-transplantation via the tail vein and peripheral blood was analyzed for donor chimerism by means of fluorescence profiles and antibodies to lineage markers.

Quantification and statistical analysis

Unpaired two-tailed Student's t-tests and one-way ANOVAs adjusted for multiple comparisons

with Tukey or Dunnett's post-hoc tests were used to assess statistical significance for comparisons of different groups, as appropriate. The sample size (n), number of independent experiments (N), and p values are provided for each experiment in the

respective figure legend. All data are shown as mean ±S.E.M unless states otherwise. Outlier analysis tests were performed and data points were removed subsequently as appropriate.

Acknowledgments

This work was supported by Tobacco Disease Research Program (TRDRP) predoctoral fellowships to T.C., A.R.y.B, and A.K.W; a UCSC Dissertation Year Fellowship to A.R.y.B; a Howard Hughes Medical Institute (HHMI) and an American Heart Association (AHA) predoctoral fellowships to DMP; NIDDK and NIA awards (R01DK100917 and R01AG062879) to E.C.F; a CIRM Facilities awards CL1-00506 and FA1-00617-1 (RRIDs SCR_021149, SCR_021353 and SCR_021135) to University of California Santa Cruz (UCSC).

Figures

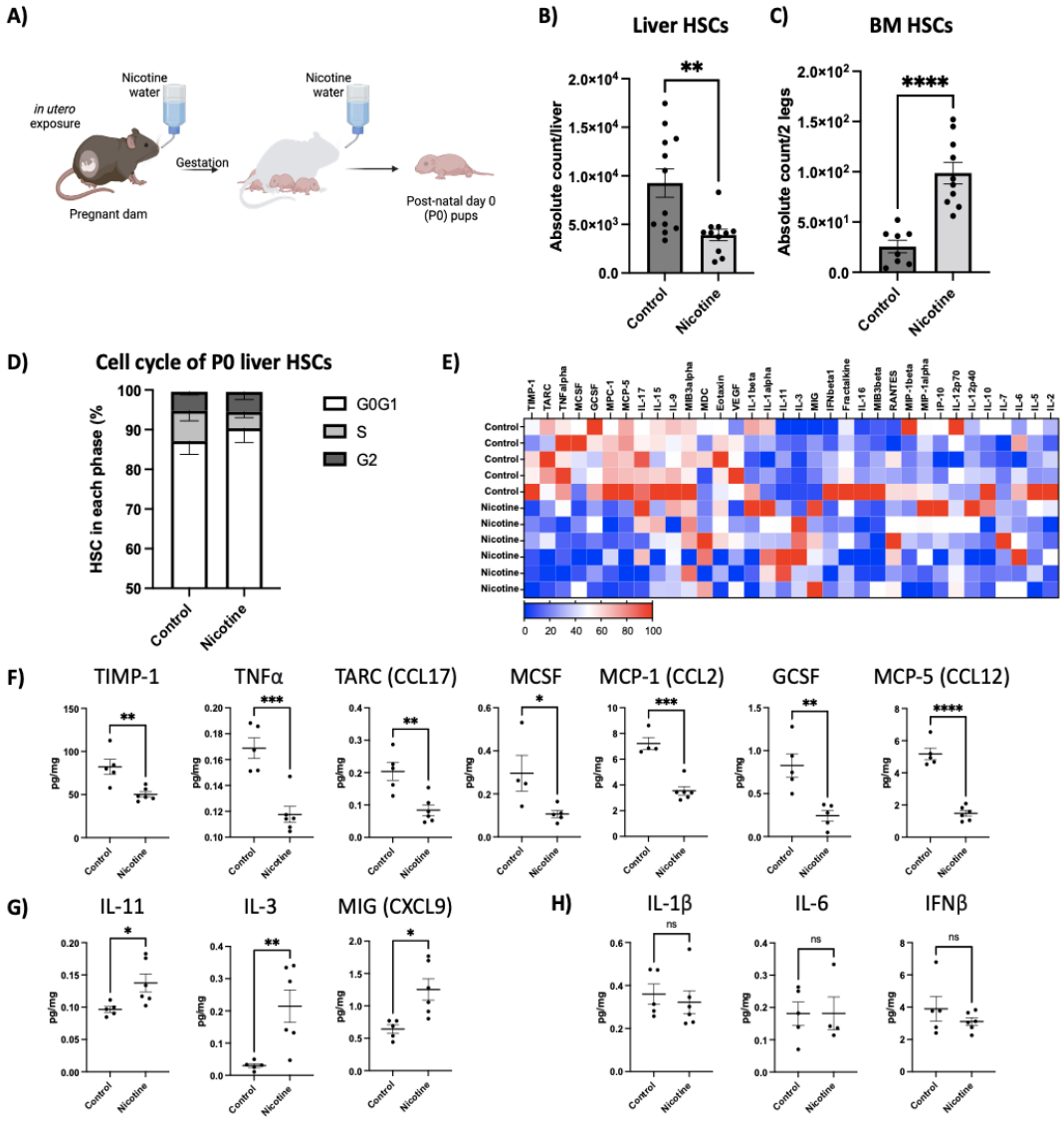

Figure 4.1. Perinatal nicotine exposure alters HSC number and liver niche in newborn pups

A) Experimental set up of PNE. B) Absolute cell counts of liver HSCs from control (dark gray bars, n=13) or nicotine-exposed (light gray bars, n=12) post-natal day 0 (P0) pups; **P<0.01 (Student's t-test); N=3 independent experiments. C) Absolute cell counts of bone marrow (BM) HSCs from control (n=9) or nicotine-exposed (n=10) P0 pups. ****P<0.001 (Student's t-test); N=3 independent experiments. D) Cell cycle status of liver HSCs from control (n=6) or nicotine-exposed (n=6) P0 pups; N=2 independent experiments. E) Heat-map representation of concentration for 35

cytokines/chemokines arrayed in liver serum from control (n=5) or nicotine-exposed (n=6) P0 pups. Concentrations were scaled and normalized within groups for each cytokine (shown as blue=low and red=high); the actual concentrations are shown in F-H. Concentrations of cytokines/chemokines that were significantly lower (F), higher (G), or unchanged (H) in liver serum from nicotine-exposed pups compared to control. NS, not significant; *P<0.05, **P<0.01, ***P<0.005 (Student's t-test). All errors bars represent SEM; each dot represents an individual animal.

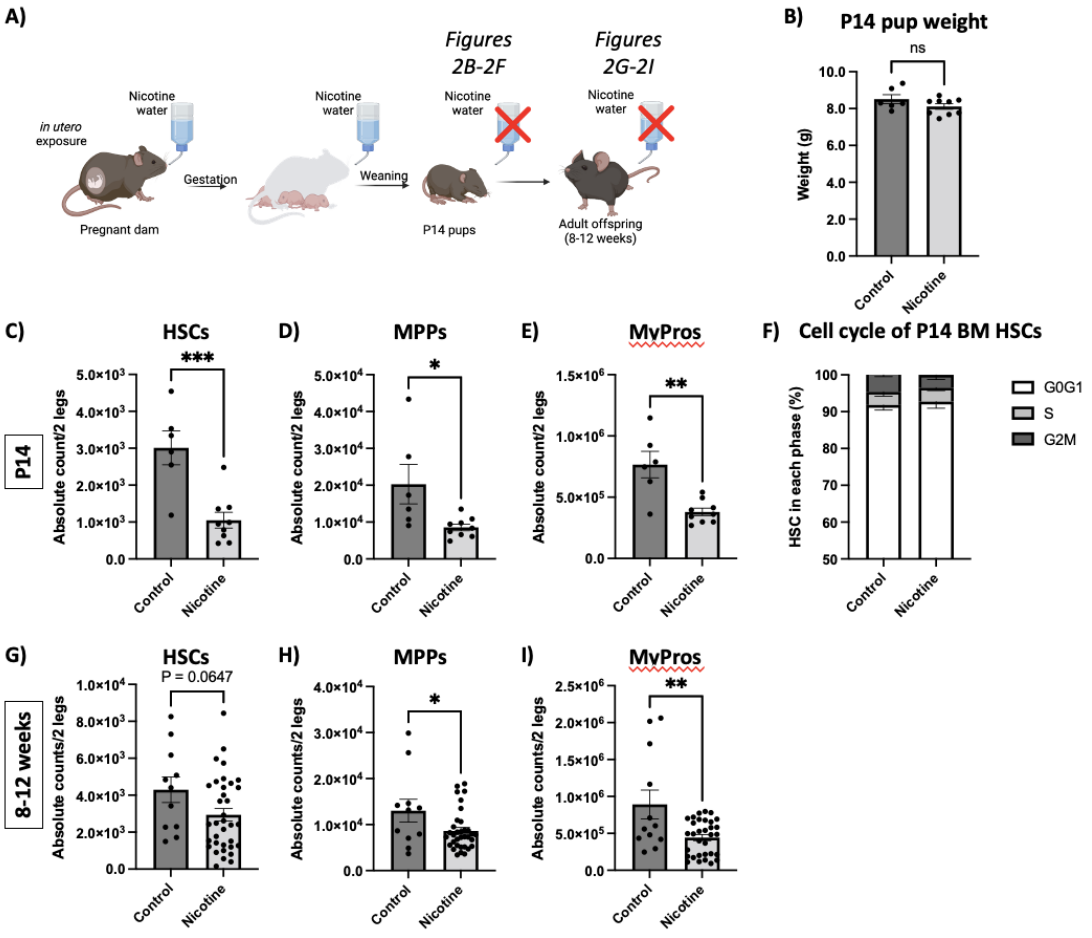

Figure 4.2. Perinatal nicotine exposure permanently reduced BM HSC numbers.

A) Experimental set up of PNE. B) Body weight of P14 pups from control (n=6) and nicotine-exposed groups (n=9); N=2 independent experiments. Absolute cell counts of BM HSCs (C), MPPs (D), and MyPros (E) from the same mice as (B). *P<0.05, **P<0.01, ***P<0.005 (Student's t-test). F) Cell cycle status of P14 BM HSCs from control (n=6) or nicotine-exposed (n=6) P14 pups; N=2 independent experiments. Absolute cell counts of BM HSCs (C), MPPs (D), and MyPros (E) from from control (n=12) or nicotine-exposed (n=35) adult offspring; N=6 independent experiments. *P<0.05, **P<0.01 (Student's t-test). All errors bars represent SEM; each dot represents an individual animal.

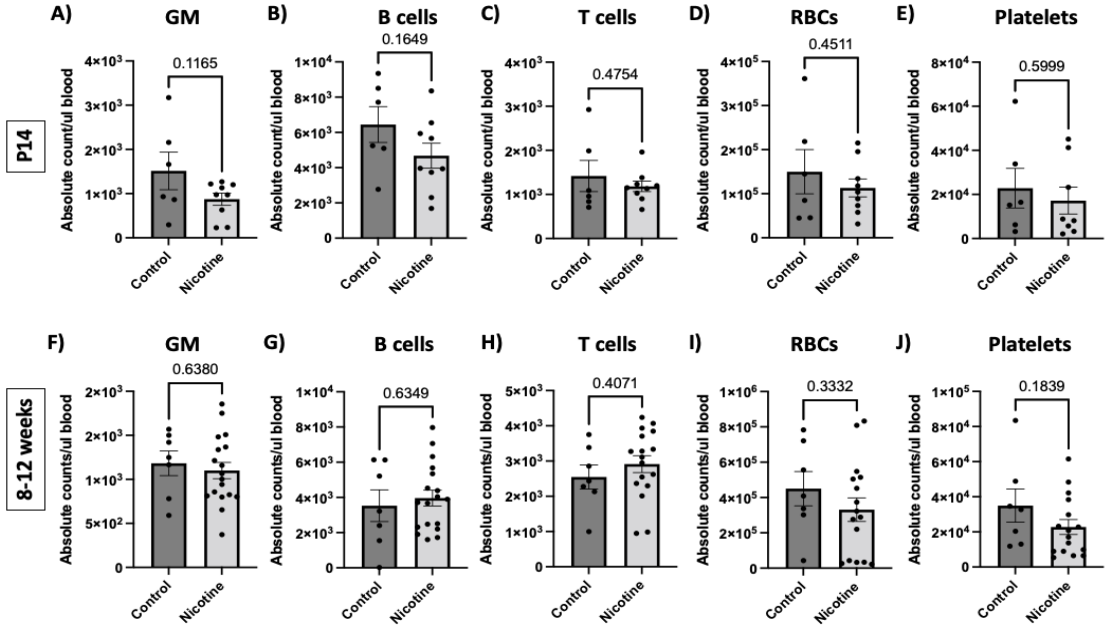

Figure 4.3. Perinatal nicotine exposure does not affect traditional mature cell production.

A-E) Quantification of absolute cell count per microliter of "traditional" mature cells in the peripheral blood of P14 pups from control (n=6) and nicotine-exposed groups (n=9); N=2 independent experiments. Absolute cell counts of GMs (A), B cells (B), T cells (C), RBCs (D), and platelets (E). F-J) Quantification of total numbers per microliter of "traditional" mature cells in the peripheral blood of adult offspring from control (n=7) and nicotine-exposed groups (n=18); N=5 independent experiments. Absolute cell counts of GMs (F), B cells (G), T cells (H), RBCs (I), and platelets (J). All errors bars represent SEM; each dot represents an individual animal.

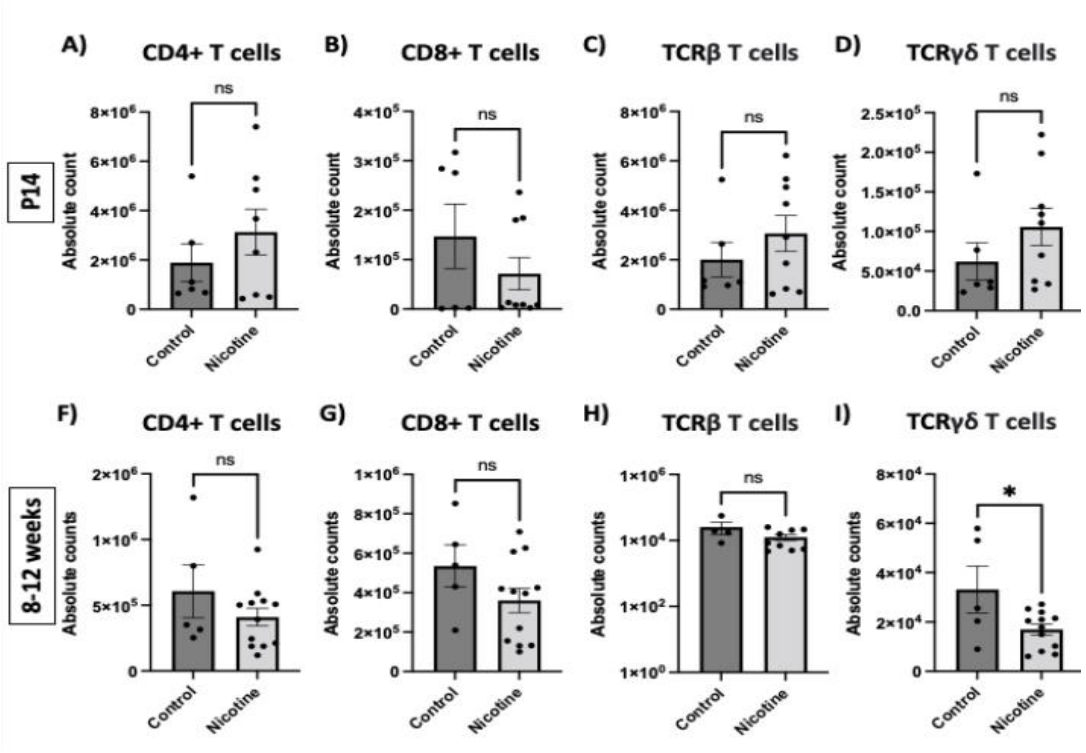

Figure 4.4. Perinatal nicotine exposure results in decreased non-traditional immune cells in the lungs.

A-E) Quantification of total numbers of "traditional" and "non-traditional" mature immune cells in the lungs of P14 pups from control (n=6) and nicotine-exposed groups (n=9); N=2 independent experiments. Absolute cell counts of CD3+ CD4+ T cells (A), CD3+ CD8+ T cells (B), TCRγδ T cells (C), and TCRβ (D). F-J) Quantification of total numbers of "traditional" and "non-traditional" mature immune cells in the lungs of of adult offspring from control (n=5) and nicotine-exposed groups (n=12); N=2 independent experiments. *P<0.05 0.01 (Student's t-test). All errors bars represent SEM; each dot represents an individual animal.

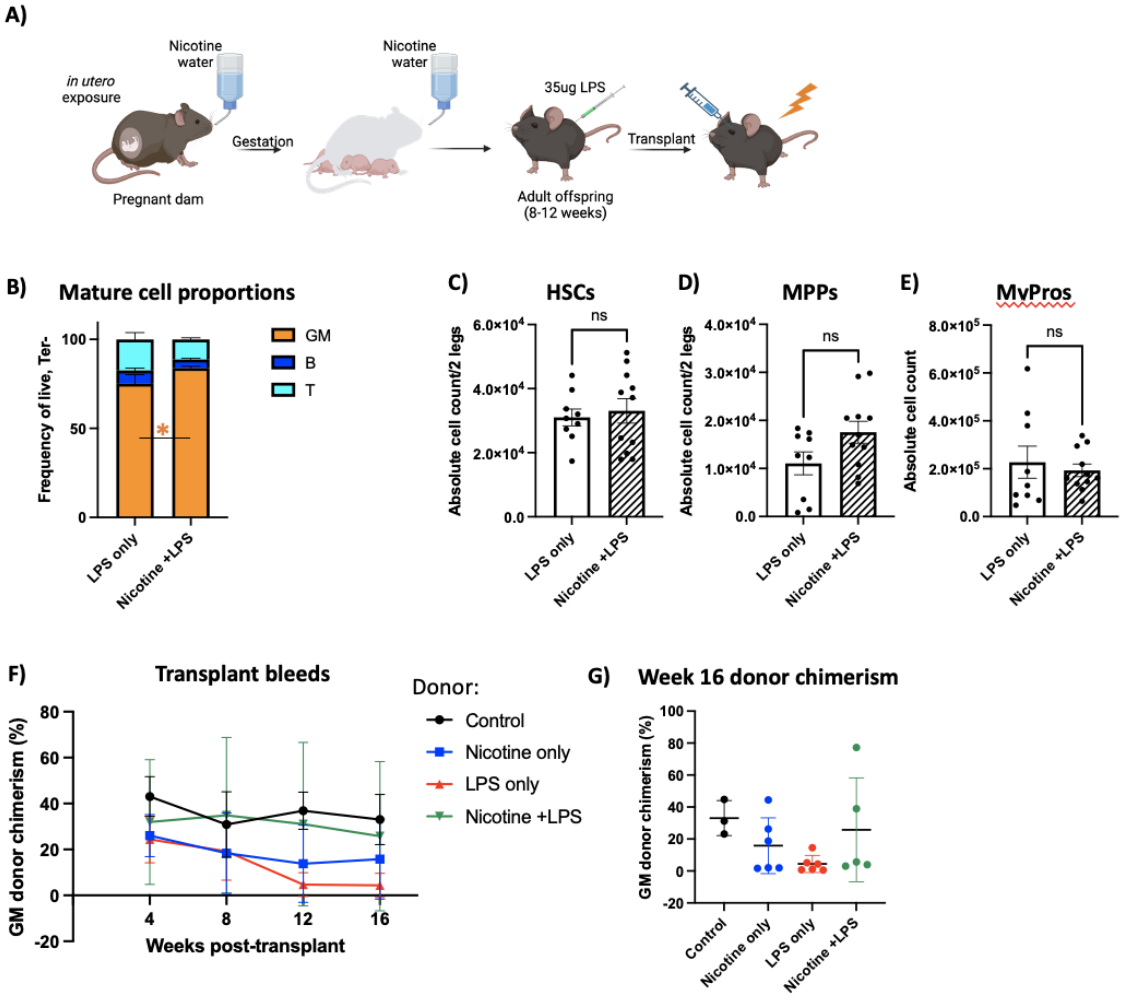

Figure 4.5. Perinatal nicotine exposure exacerbates emergency myelopoiesis in response to LPS.

A) Experimental set up of LPS treatment. B) Proportion of GM, B, and T cells in the peripheral blood of LPS only (n=10) and PNE +LPS (n=12) groups; N=3 independent experiments. *P<0.05 (Student's t-test). Absolute cell counts of BM HSCs (C), MPPs (D), and MyPros (E) from LPS only (n=9) and nicotine +LPS (n=11) groups; N=3 independent experiments. All errors bars represent SEM; each dot represents an individual animal. F) GM donor chimerism over 16 weeks post transplantation of 1 million whole bone marrow cells from control (n=3), nicotine only (n=6), LPS only (n=6), and nicotine +LPS (n=5) mice. Errors bars represent SD. G) GM donor chimerism at week 16 post transplantation showing individual mice from Figure 5F. Errors bars represent SD; each dot represents an individual animal.

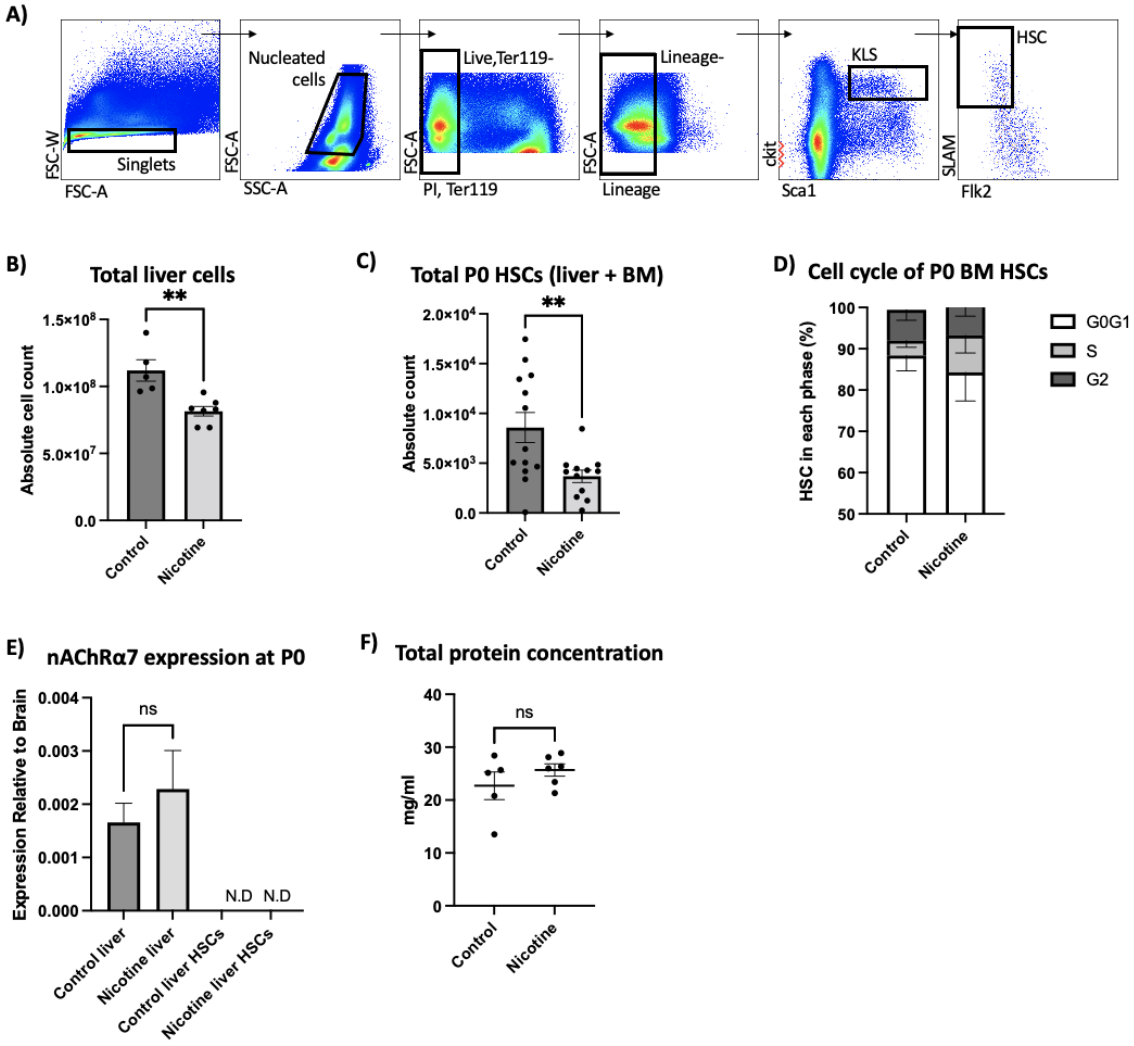

Figure 4.6. Supplementary Figure 1.

A) Liver/BM HSC gating strategy used for Figure 1. Lineage stain includes: B220, CD3, CD4, CD5, CD8. B) Cell count by hemocytometer of control (n=5) and nicotine-exposed (n=7) P0 mice. **P<0.01, ***P<0.005 (Student's t-test); N=2 independent experiments. C) Total P0 HSC cell number from adding P0 liver and BM HSCs from Figure 1B-C. D) Cell cycle status of liver HSCs from control (n=6) or nicotine-exposed (n=6) P0 pups; N=2 independent experiments. E) qPCR of nAChRα7 from liver tissue or sorted liver HSCs from control and nicotine-exposed P0 pups. Expression levels were normalized to a positive control for nAChRα7 expression, whole brain homogenate. N.D., not detected. F) Total protein concentration (mg/ml) from liver serum from Figure 1E-H. All errors bars represent SEM; each dot represents an individual animal.

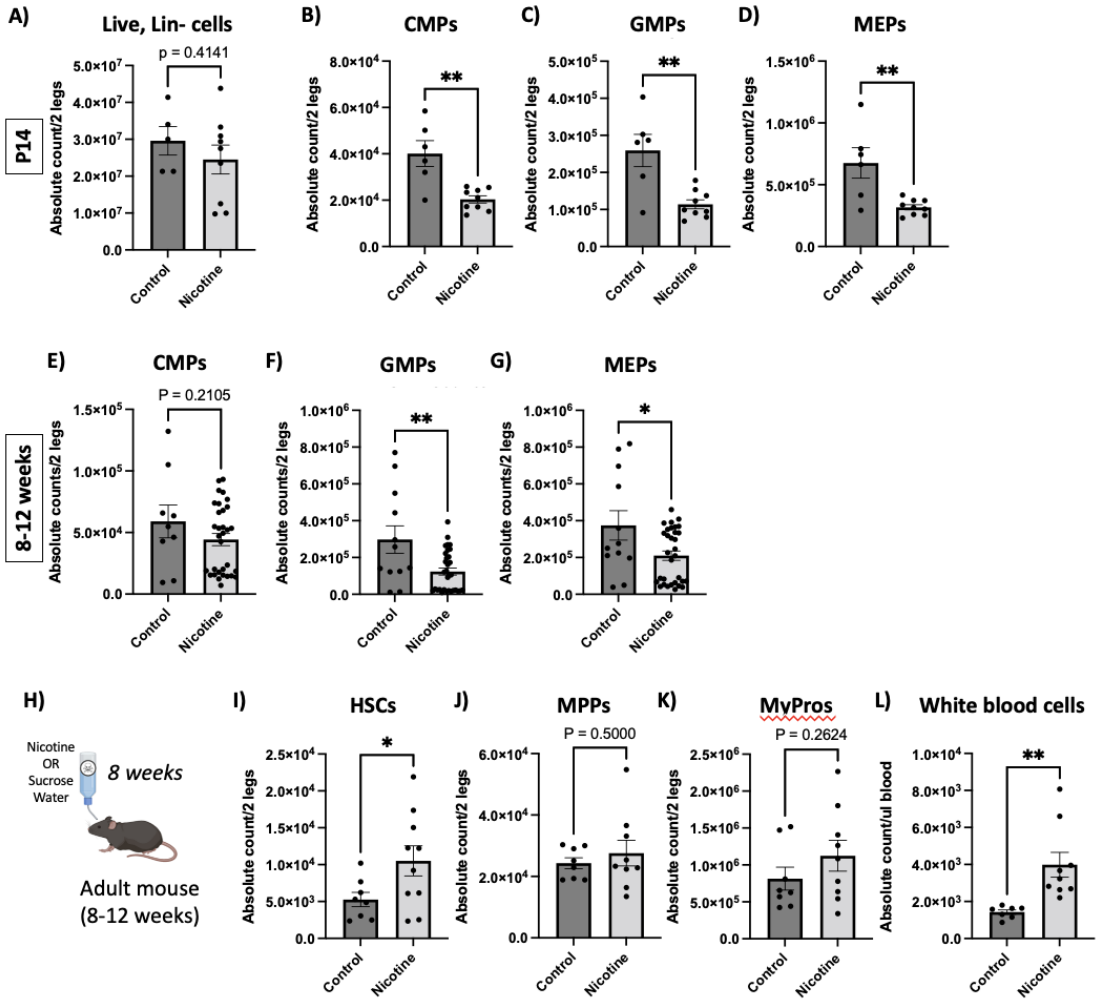

Figure 4.7. Supplementary Figure 2.

A) Absolute cell count of live, lineage negative cells in the bone marrow of control and nicotine-exposed P14 mice from Figure 2B-E. Absolute cell counts of CMPs (B), GMPs (C), and MEPs (D) within the MyPro cell fraction of control and nicotine-exposed P14 mice shown in Figure 2E. **P<0.01 (Student's t-test). Absolute cell counts of CMPs (E), GMPs (F), and MEPs (G) within the MyPro cell fraction of control and nicotine-exposed adult offspring shown in Figure 2I. **P<0.01 (Student's t-test). H) Experimental set up of adult nicotine exposure. Absolute cell counts of bone marrow HSCs (I), MPPs (J), MyPros (K), and peripheral blood white blood cells (L) from control (n=8) and nicotine-exposed (n=10) adult mice; N=2 independent experiments. *P<0.05, **P<0.01 (Student's t-test). All errors bars represent SEM; each dot represents an individual animal.

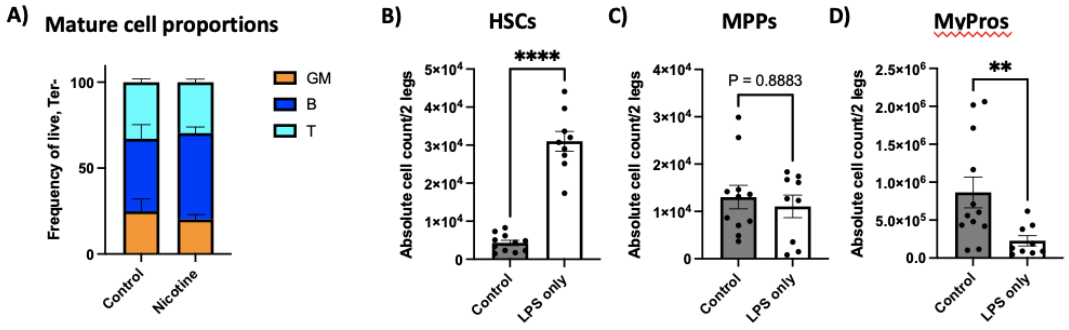

Figure 4.8. Supplementary Figure 3.

A) Proportion of GM, B, and T cells in the peripheral blood of adult offspring from control (n=7) and nicotine-exposed (n=11) groups; N=3 independent experiments. B) Absolute cell counts of BM HSCs (B), MPPs (C), and MyPros (D) from control (n=11) and LPS only (n=12) groups. **P<0.01, ****P<0.001 (Student's t-test). Control mice are the same as Figure 2-4 and LPS mice are the same as Figure 5. All errors bars represent SEM; each dot represents an individual animal.

References

1. Dietz, P. M. *et al.* Infant morbidity and mortality attributable to prenatal smoking in the U.S. *Am J Prev Med* **39**, 45–52 (2010).
2. Avşar, T. S., McLeod, H. & Jackson, L. Health outcomes of smoking during pregnancy and the postpartum period: an umbrella review. *BMC Pregnancy Childbirth* **21**, 254 (2021).
3. Quelhas, D. *et al.* The association between active tobacco use during pregnancy and growth outcomes of children under five years of age: a systematic review and meta-analysis. *BMC Public Health* **18**, 1372 (2018).
4. Cool, T., Baena, A. R. & Forsberg, E. C. Clearing the Haze: How Does Nicotine Affect Hematopoiesis before and after Birth? *Cancers* **14**, (2022).
5. Pattenden, S. *et al.* Parental smoking and children's respiratory health: Independent effects of prenatal and postnatal exposure. *Tobacco Control* **15**, 294–301 (2006).
6. Gracia, M. C. Exposure to nicotine is probably a major cause of inflammatory diseases among non-smokers. *Medical hypotheses* **65**, 253–258 (2005).
7. Mohsenzadeh, Y., Rahmani, A., Cheraghi, J., Pyrani, M. & Asadollahi, K. Prenatal exposure to nicotine in pregnant rat increased inflammatory marker in Newborn Rat. *Mediators of Inflammation* **2014**, (2014).
8. Apostol, A. C., Jensen, K. D. C. & Beaudin, A. E. Training the Fetal Immune System Through Maternal Inflammation—A Layered Hygiene Hypothesis. *Front. Immunol.* **11**, 123 (2020).

9. López, D. A. *et al.* Both maternal IFNγ exposure and acute prenatal infection with Toxoplasma gondii activate fetal hematopoietic stem cells. *EMBO J* **42**, e112693 (2023).
10. Cool, T. & Forsberg, E. C. Chasing Mavericks: The quest for defining developmental waves of hematopoiesis. *Current Topics in Developmental Biology* **132**, 1–29 (2019).
11. Maier, C. R. *et al.* Nicotine Does Not Enhance Tumorigenesis in Mutant *K* - *Ras* – Driven Mouse Models of Lung Cancer. *Cancer Prevention Research* **4**, 1743–1751 (2011).
12. Chang, E. *et al.* Cholinergic activation of hematopoietic stem cells: role in tobacco-related disease? *Vasc Med* **15**, 375–385 (2010).
13. Katono, T. *et al.* Nicotine Treatment Induces Expression of Matrix Metalloproteinases in Human Osteoblastic Saos-2 Cells. *ABBS* **38**, 874–882 (2006).
14. Watson, A. M., Benton, A. S., Rose, M. C. & Freishtat, R. J. Cigarette smoke alters tissue inhibitor of metalloproteinase 1 and matrix metalloproteinase 9 levels in the basolateral secretions of human asthmatic bronchial epithelium in vitro. *J Investig Med* **58**, 725–729 (2010).
15. Li, Q., Zhou, X.-D., Kolosov, V. P. & Perelman, J. M. Nicotine reduces TNF-α expression through a α7 nAChR/MyD88/NF-κB pathway in HBE16 airway epithelial cells. *Cell Physiol Biochem* **27**, 605–612 (2011).

16. Kizildag, S. *et al.* Nicotine lowers TNF-α, IL-1b secretion and leukocyte accumulation via nAChR in rat stomach. *Toxin Reviews* **40**, 17–24 (2021).
17. Valdez-Miramontes, C. E. *et al.* Nicotine modulates molecules of the innate immune response in epithelial cells and macrophages during infection with M. tuberculosis. *Clin Exp Immunol* **199**, 230–243 (2020).
18. Wang, H. *et al.* Effects of Smoking on Inflammatory-Related Cytokine Levels in Human Serum. *Molecules* **27**, 3715 (2022).
19. Arpino, V., Brock, M. & Gill, S. E. The role of TIMPs in regulation of extracellular matrix proteolysis. *Matrix Biology* **44–46**, 247–254 (2015).
20. Konno, K., Sasaki, T., Kulkeaw, K. & Sugiyama, D. Paracrine CCL17 and CCL22 signaling regulates hematopoietic stem/progenitor cell migration and retention in mouse fetal liver. *Biochemical and Biophysical Research Communications* **527**, 730–736 (2020).
21. Ramanathan, G. *et al.* E-Cigarette Exposure Decreases Bone Marrow Hematopoietic Progenitor Cells. *Cancers* **12**, 2292 (2020).
22. Zalokar, J. B., Richard, J. L. & Claude, J. R. Leukocyte Count, Smoking, and Myocardial Infarction. *N Engl J Med* **304**, 465–468 (1981).
23. Beaudin, A. E. *et al.* A transient developmental hematopoietic stem cell gives rise to innate-like B and T cells. *Cell Stem Cell* **19**, 768–783 (2016).
24. Beaudin, A. E., Boyer, S. W. & Forsberg, E. C. Flk2/Flt3 promotes both myeloid and lymphoid development by expanding non-self-renewing multipotent hematopoietic progenitor cells. *Exp Hematol* **42**, 218-229.e4 (2014).

25. Boyer, S. W., Schroeder, A. V., Smith-Berdan, S. & Forsberg, E. C. All hematopoietic cells develop from hematopoietic stem cells through Flk2/Flt3-positive progenitor cells. *Cell stem cell* **9**, 64 (2011).
26. Rajendiran, S., Boyer, S. W. & Forsberg, E. C. A quantitative hematopoietic stem cell reconstitution protocol: Accounting for recipient variability, tissue distribution and cell half-lives. *Stem Cell Res* **50**, 102145 (2020).
27. Smith-Berdan, S., Nguyen, A., Hong, M. A. & Forsberg, E. C. ROBO4-mediated vascular integrity regulates the directionality of hematopoietic stem cell trafficking. *Stem Cell Reports* **4**, 255–268 (2015).
28. Rodriguez Y Baena, A. *et al.* New transgenic mouse models enabling pan-hematopoietic or selective hematopoietic stem cell depletion in vivo. *Sci Rep* **12**, 3156 (2022).
29. Cool, T., Worthington, A., Poscablo, D., Hussaini, A. & Forsberg, E. C. Interleukin 7 receptor is required for myeloid cell homeostasis and reconstitution by hematopoietic stem cells. *Experimental Hematology* **90**, 39-45.e3 (2020).
30. Worthington, A. K. *et al.* IL7Rα, but not Flk2, is required for hematopoietic stem cell reconstitution of tissue-resident lymphoid cells. *Development* **149**, dev200139 (2022).
31. Poscablo, D. M., Worthington, A. K., Smith-Berdan, S. & Forsberg, E. C. Megakaryocyte progenitor cell function is enhanced upon aging despite the functional decline of aged hematopoietic stem cells. *Stem Cell Reports* **16**, 1598–1613 (2021).

32. Boyer, S. W. *et al.* Clonal and Quantitative In Vivo Assessment of Hematopoietic Stem Cell Differentiation Reveals Strong Erythroid Potential of Multipotent Cells. *Stem Cell Reports* **12**, 801–815 (2019).

PART III

Chapter 5.

From hematopoietic stem cells to platelets: unifying differentiation pathways identified by lineage tracing mouse models.

Abstract

Platelets are the terminal progeny of megakaryocytes, produced in the bone marrow, and play critical roles in blood homeostasis, clotting, and wound healing. Traditionally, megakaryocytes and platelets are thought to arise from multipotent hematopoietic stem cells (HSCs) via multiple, successive, lineage-restricting differentiation steps. However, this view has recently been challenged by studies suggesting that 1) some HSC clones are biased and/or restricted to the platelet lineage, 2) not all platelet generation follows the "canonical" megakaryocytic differentiation path of hematopoiesis, and 3) platelet output is the default program of steady-state hematopoiesis. Here, we investigate 1) the evidence on the route(s) of platelet formation by lineage tracing studies, 2) the involvement of various progenitor cell populations in this process, and 3) we highlight the challenges that will need to be overcome to determine the role and kinetics of these alternate pathways.

Highlights

- Lineage tracing reveals many potential avenues for platelet production during steady-state hematopoiesis
- HSC heterogeneity is partially due to platelet-biased/primed clones

- Platelet-biased HSCs manifest, at steady-state, as ensuring continuous platelet production
- Platelet generation may bypass traditional progenitors to allow for constant platelet production
- There remains a need for specific lineage tracing tools for interrogation of megakaryopoiesis

Introduction

The product of the megakaryocytic lineage are platelets, a blood component absolutely required for life[1,2]. Platelets (thrombocytes) are short-lived, small, anucleate cell fragments that arise via budding and/or fragmentation of their parent cell, the large polyploid megakaryocyte. Primarily involved in hemostasis[1,3], platelets also exhibit other functions related to immunity and cell communication depending on their local microenvironment (reviewed here[3]). The clinical relevance of platelets cannot be understated[4-6] and as such, understanding the developmental pathway(s) leading to their formation may reveal therapeutic targets to prevent and/or correct adverse thrombotic events, such as venous thrombosis, thrombocytopenia, thrombocytosis, and ischemic stroke (reviewed here[7-11]).

The mammalian adult bone marrow (BM) is host to the formation, maturation, and residence of megakaryocytes[2]. In classical models of hematopoiesis[12,13] (Figure 1), platelets have long been described as arising via the successively lineage-restricting differentiation of hematopoietic stem cells (HSCs), which reside at the apex of the

hematopoietic hierarchy. HSCs differentiate into multipotent progenitor cells (MPPs), which no longer self-renew yet maintain multipotency[14,15]. Further developmental progression through the oligopotent common myeloid progenitor (CMP)[16] occurs prior to the transition to the bipotent megakaryocyte-erythroid progenitor (MEP) before commitment to a unilineage megakaryocyte progenitor (MkP)[17-19]. After this stage, several maturation steps occur where the developing megakaryocyte undergoes molecular and cellular changes, including increasing in size and ploidy, before forming proplatelet extensions from which platelets bud off into blood circulation[1,3]. Platelet generation (megakaryopoiesis) is thought to largely parallel erythropoiesis (red blood cell/erythrocyte formation) due to this well-accepted model that positions both lineages immediately downstream of the bipotent MEP, necessitating shared progenitor populations for much of their differentiation[17,20]. However, as with other hematopoietic lineages, this traditionally accepted view of megakaryocytic specification is being contested[21], both at steady-state and under stress, highlighting the need to specifically and accurately trace the cellular origin(s) of platelets *in situ*, undisturbed, and at the single-cell level.

One powerful approach for studying platelet generation is lineage tracing, which is used to recreate partial or complete cellular lineage trees. First pioneered by Charles O. Whitman in 1905[22], the earliest instances of lineage tracing involved microinjection of dyes into cells and tracking their progeny[23,24]. Over the past century, this technique has adopted newer and more powerful technologies driven by the development of chimeric mice[25], genetically driven fluorescent reporter-based systems[26-28], cellular/DNA

barcoding[29-31], CRISPR/Cas9 scarring[32-39], identification and tracking of naturally occurring somatic mutations[40-49], and complex combinatorial approaches integrating two or more of these systems[50-54]. Importantly, most modern approaches make use of a permanent mark in a parental cell (such as HSCs) that is inherited by all daughter cells and their progeny. Lineage tracing has been widely applied and incredibly impactful to understanding HSCs and hematopoiesis[55], including seminal studies[56-64] that revealed the functional and differentiation cornerstones of HSCs that informed early iterations of the classical hematopoietic hierarchy[16,65]. Although outside the scope of this review, we acknowledge that recent lineage tracing data has refined how the field views HSC differentiation and hematopoiesis across multiple lineages. However, even though lineage tracing has markedly increased in resolution, sensitivity, and applicability, significant challenges remain when interrogating specific cell types, including those of the megakaryocytic lineage.

Many of the classical hematopoietic differentiation steps in platelet formation have been inferred via transplantation, perturbation and subsequent observation, and/or *in vitro* differentiation studies. However, it is important to recognize that these methods, including transplantation, are likely to reflect stress and/or high demand physiological states. That said, given the clinical and life-saving significance of transplantation, understanding platelet development beyond steady-state could offer important insights for clinical applications. Thus, even though these types of studies have elucidated much of our current knowledge, the most direct evidence for the developmental path of steady-state platelet formation would come from undisturbed *in situ* lineage tracing.

There have been numerous studies of lineage tracing from HSCs, but few have assessed the megakaryocytic/platelet lineage largely due to platelets lacking expression of the pan-hematopoietic marker CD45 and, being devoid of a nucleus, cannot be alternatively tracked via genetic barcoding or scarring. These limitations substantially reduce the number of tools available to lineage trace platelets. Additionally, among the few lineage tracing studies that have directly assessed platelets, only a small number have investigated the intermediate progenitors between HSCs and platelets in the BM. Here, we specifically review lineage tracing data that seeks to understand the cellular origins and progenitors of platelets in adult murine BM at steady-state, including recent data suggesting alternative routes of generation, and highlight the successes and challenges inherent to these models. We conclude by discussing the current feasibility of megakaryocytic-specific lineage tracing.

Are HSCs the source of platelets, and do HSCs possess a platelet lineage bias?

In the adult mouse, transplantation studies of labeled HSCs, including quantitative analysis by our group[20], have revealed that platelets (and all other blood lineages) are effectively generated following HSC engraftment, indicating their hematopoietic (and HSC) origin. Additionally, recent evidence suggests that a subset of HSCs exist along a continuum of platelet-bias, lineage priming, and/or restriction[66-68], similar to data suggesting heterogeneous HSC clonality and unilineage restriction of other cell lineages[15,69-75]. In this section, we explore key lineage tracing studies that allow direct observation of the platelet lineage.

Using a von Willebrand Factor (vWF)-GFP reporter mouse, Sanjuan-Pla et al. found that a subset of HSCs was labeled with GFP *in situ*[66], a surprising finding as vWF was previously reported to only be expressed in mature megakaryocytes, platelets, and endothelial cells. Functional analysis by transplantation of vWF+ (GFP+) and vWF- (GFP-) HSCs revealed that the vWF+ compartment produced more platelets and fewer lymphocytes than the vWF- fraction. Importantly, even though a bias was observed, both HSC subsets maintained multipotency. Additionally, vWF+ HSCs could give rise to both vWF+ and vWF- HSCs following transplantation, but wWF- HSCs never gave rise to their vWF+ counterparts, potentially indicating that vWF+ HSCs represent a cell state slightly further up the hierarchy (within the phenotypic HSC pool). Similarly, a follow up study driven by Carrelha et al. refined this notion using a dual-color GATA-1-GFP and vWF-Tomato (Tom) lineage tracing model that allowed specific assessment of platelet (and other blood cell) reconstitution[67]. Single vWF+ HSCs were transplanted into more than 1000 recipient mice and the resulting lineage contribution was measured. Building on the original results obtained by Sanjuan-Pla, this study found that ~11-12% of vWF+ HSCs exclusively reconstituted platelets, and no other lineage. Additionally, the data demonstrated a non-random lineage hierarchy of HSC clonal reconstitution capacity where transplanted vWF+ HSCs preferentially established platelet, then platelet-erythroid, then platelet-erythroid-myeloid, and finally platelet-erythroid-myeloid-lymphoid lineages. The finding that platelet generation from HSCs had the fastest kinetics was also observed by others[76,77] and may indicate a physiological mechanism for continual replenishment of this short lived, critical blood

component. Importantly, secondary transplantation of platelet-restricted HSCs by Carrelha et al. revealed maintenance of the platelet-bias by some HSC clones, whereas others underwent multilineage reconstitution as previously observed by others[15,66]. These studies allowed for the identification of two HSC subsets newly defined by vWF expression, indicate that platelet generation was a shared feature of all reconstituted mice, and argue for the existence of megakaryocytic lineage bias in the phenotypic vWF+ HSC pool. The authors also argue against the notion of a unilineage megakaryocyte progenitor contaminating the vWF+ HSC pool as, upon isolation from recipient mice, vWF+ Lin-Sca-1+cKit+ (LSK) cells showed robust multilineage capacity *in vitro*, indicating, when combined with the secondary transplants, that the vWF+ HSCs are *bona fide* HSCs. However, one caveat to these elegant lineage-tracing studies is the use of transplantation to test the functional output of the labeled HSCs; it is possible that the observed results (summarized in Figure 2A) are more a measure of functional capacity upon stress rather than *in situ*, steady-state output.

To that point, a recent *in situ* lineage tracing study by Rodriguez-Fraticelli et al. concluded that, at steady-state, over 30% of megakaryocytes can be directly derived from long-term (LT)-HSCs without contributions to other hematopoietic lineages[78], potentially indicating HSC lineage bias or restrictin. This position is largely shared by Morcos et al using a different model[77]. Rodriguez-Fraticelli et al utilized the doxycycline-inducible Sleeping Beauty transposon system and did not extensively evaluate many other intermediate progenitor cell types, obfuscating the differentiation path each HSC clone utilized. Further, upon transplantation of labeled LT-HSCs,

multilineage reconstitution was observed, highlighting that most platelet-biased LT-HSC clones retain full multilineage capacity and that transplantation can result in discordant results compared to *in situ* analysis[78]. Such differences within a study, or between studies, and the conclusions drawn, may also be attributed to the type of transplant (single cell vs. bulk) and the type of label utilized (individual clones labeled differently vs. a subset of HSCs containing the same label). Additionally, confirming previous reports[15,66,79,80], Rodriguez-Fraticelli's study demonstrates that a subset of the total LT-HSC pool exhibited a megakaryocytic transcriptomic profile but maintained multilineage reconstitution upon transplantation *in situ*, further reinforcing the hypothesis of bias over lineage restriction.

Given the relatively short-term (up to 8 weeks post label induction) tracing of the above studies, *in situ* evaluation over longer periods of time may refine the observation of potential platelet-bias and the kinetics of lineage output. One such study used two independent HSC inducible lineage tracing models, Krt18-CreER/YFP and Fgd5-CreER/Tom, and chased mice for one year post-label induction by tamoxifen administration[81]. Similar to the previous studies[66,67,76,77], they found that platelets showed the highest labeling efficiency (other than HSCs) early on, indicating a potential preference for and rapid kinetics of this lineage. Over time, all other lineages exhibited increasing, yet varying, levels of labeling. These findings were largely recapitulated by Morcos et al., who utilized a related Fgd5/zsGreen-CreERT2/RFP model with up to 92 weeks of chase post-tamoxifen label induction[77]. Another study, also taking advantage of the Fgd5-CreER/Tom model, induced labeling and chased for

up to 83 weeks[76]. In contrast to others, they observed initial labeling among HSCs and early progenitor cells. However, by 4 weeks-post label induction, platelets were the only mature cell type to express the induced label. Thus, it appears that HSCs, or at least a subset of HSCs sensitive to label induction due to Fgd5 expression, exhibit faster reconstitution of the platelet/myeloid lineage rather than lymphoid, and that platelets are robustly and continuously replenished by HSCs (summarized in Figure 2B).

Similar arguments for an HSC continuum of platelet-bias, lineage priming, and/or restriction in humans has been made, yet lack as much direct lineage tracing evidence as demonstrated in mice. Taking advantage of whole genome sequencing and clonal mutation analysis in humans as a method of retrospective lineage tracing, Osorio et al. concluded that there is platelet lineage bias in humans[82]. In this system, clonal somatic mutations were used to reconstruct lineage relationships, with lineages sharing similar mutational patters assumed to be more related than lineages with a low level of mutational overlap. They reasoned that the unique mutational identity of megakaryocytes (which was different from all other blood cell lineages) indicated an earlier divergence of the megakaryocyte lineage compared to all other myeloid/erythroid and lymphoid lineages, potentially indicating that a subset of HSCs primarily contributes to megakaryopoiesis in humans at steady-state.

The above findings, combined with the striking phenotypic and molecular similarities between HSCs and MkPs (reviewed here[83]), further reinforce the proposed paradigm shift in understanding megakaryopoiesis (Figure 2). The observed priming of HSCs may also contribute during perturbed hematopoiesis, such as under inflammatory

stress. Indeed, a fraction of phenotypic LT-HSCs, termed "stem-like MkPs," express the classical megakaryocyte lineage marker CD41 and megakaryocyte-lineage mRNA transcripts, including CD42b and vWF[79]. However, translation of these transcripts is suppressed until activation, commonly via inflammation. Transplantation of LT-HSCs fractionated by CD41 expression confirmed multilineage output, except by those with the highest levels of CD41, which were only obtainable post-inflammatory insult[79]. The inflammation-induced CD41^{hi} [LT-HSC] subpopulation exclusively, but transiently, produced platelets upon transplantation, possibly indicating a loss of true HSC function even though the LT-HSC phenotype was maintained. The finding that a subpopulation of vWF+ LT-HSCs is biased to the platelet lineage was supported by *in situ* lineage tracing that suggests steady-state platelet production is not exclusive to the CD41+ LT-HSC fraction, as shown by Rodriguez-Fraticelli et al[78]. Thus, these stem-like MkPs could represent steady-state platelet-biased HSCs that rapidly lose HSC function and gain platelet restriction upon exposure to inflammation and/or an independent progenitor population found within the phenotypic HSC pool that is held in reserve and primed for emergency use for specific inflammatory states[79,84]. Collectively, HSCs contribute to megakaryopoiesis and possess physiological and stress-induced bias, likely to preserve blood levels of the critical-for-life platelet.

Does megakaryopoiesis transition through MPPs?

Using dual-color Flk2(Flt3)-Cre mT/mG (termed FlkSwitch) lineage tracing mice[85-92], our group was able to ascertain if hematopoietic lineages progress through the non-

self-renewing, multipotent MPPs (defined by Flk2 expression)[85,90]. As Flk2 is expressed during the transition from HSC to MPP and detected as early as the short term (ST)-HSC state, Cre recombinase leads to a permanent "switch" from Tom to GFP expression and all progeny of MPPs must therefore also express GFP. Thus, any progenitor cell, intermediate transitory cell state, or terminally differentiated cell that transitions through a Flk2+ stage at any point during their differentiation path will irreversibly express GFP. Using this model, we found a high proportion of cells expressing GFP among MPPs [all MPP subsets] and equivalent proportions of GFP-expressing cells among the downstream CMPs, MEPs, MkPs, and platelets (similar to all other progenitors and mature cells). This *in situ* model demonstrates that, regardless of any HSC-bias/restriction to the platelet lineage, adult steady-state megakaryopoiesis transitions through a Flk2+ stage during its developmental trajectory. Importantly, when MPPs or other progenitor populations (including CMPs, GMPs, and MEPs) were isolated and transplanted, the cellular output of each compartment was consistent with our lineage tracing data; MPPs maintained the ability to produce all mature cell types including platelets while losing self-renewal, and more committed progenitors transiently produced their classically expected terminal progeny[20]. Transplantation of single or limiting numbers of MPPs (and HSCs) also demonstrated multilineage capacity and the expected cellular intermediates for each major blood lineage.

Indeed, other lineage tracing studies also support megakaryopoiesis transitioning through an MPP stage. In vWF+ HSCs, even those that are platelet-restricted, label is robustly detected in the MPP2 (LSK Flk2-CD150+CD48+) compartment, a

subpopulation contained within the MPP pool proposed to enrich for platelet production[67]. Similarly, other HSC-labeling lineage tracing models enrich for subsequent label in MPP2 cells[76,81,93] and, compared to other MPP subpopulations, MPP2s were found to contain megakaryocytic-specific clones[78] and transcriptionally cluster with more lineage committed megakaryocyte/erythroid progenitors[76]. These findings are supported by another study that argues for functional megakaryocyte lineage bias in the MPP2 population[94]. Thus, although not always assessed, platelet generation appears to [require] transition through an MPP cell state.

Are CMPs and/or MEPs intermediates in platelet generation?

Classically, the oligopotent progenitor of the myeloid lineage, the CMP, is downstream of MPPs (Figure 1). Further bifurcation via differentiation of this progenitor pool gives rise to the GMP and MEP progenitor populations, the latter of which generates MkPs and erythroid progenitors, the proposed unipotent precursors of platelets and erythrocytes, respectively. However, given the evidence discussed above, is there a role for CMPs and/or MEPs in platelet generation?

The FlkSwitch lineage tracing mouse model our group utilizes[85-92] uniformly labels Flk2- CMPs and MEPs with GFP, indicating transition through a Flk2+ stage, consistent with them serving as developmental intermediates of platelets. Additionally, transplanted CMPs (and MEPs) transiently produced platelets[20]. Using the inducible HSC-selective Pdzklip1-CreER/Tom lineage tracing mouse model, Upadhaya et al. found that, one week post-label induction, Lin-cKit+Sca1-CD150-CD41- myeloid

progenitors (containing phenotypic CMPs) were label-negative, whereas MPP2 and MkP populations contained label-positive cells[93]. However, when the inducible HSC labeling Krt18-CreER/YFP or Fgd5-CreER/Tom models were used, different results were observed[81]. In these models, one week-post induction, HSCs and HPC2s (similar to MPP2) harbored label-containing cells whereas there was nearly no label found in downstream progenitors or platelets. By four weeks post-label induction, platelets, and most other progenitors, showed varying frequencies of label positive cells, obfuscating the route(s) of platelet generation at this time point. Säwen et al, also using the Fgd5-CreER/Tom model, obtained similar results in the first four weeks post-labeling[76]. However, they did conclude that at earlier time points, MkPs acquire label with faster kinetics than any other CMP/MEP progenitor. Together, these studies may indicate that at least partial replenishment of platelets could bypass CMPs (and MEPs) or indicate fast differentiation kinetics not suitable for labeling by these models. However, this data does not discount platelets arising via a megakaryopoiesis consisting of multiple intermediate progenitors.

A bipotent MEP has been described in the mouse[16,95], but does lineage tracing implicate its involvement in megakaryopoiesis? When our group transplanted MEPs, platelet and erythrocyte production was detected in recipient mice[20]. Carrelha et al., using their dual-color GATA-1-GFP/vWF-Tom lineage tracing post-transplant of vWF+ HSCs model, identified that some, but not all, mice that exhibited platelet-restricted output also contained labeled MEPs[67]. However, the frequency of label-positive MEPs was low, so it is possible that the contribution by MEPs is underestimated in this system.

Additionally, inducible HSC lineage tracing conducted by Upadhaya et al. showed that, early on (when HSC, MPP2, and MkP exhibited labeling but CMPs did not), there was no or minimal labeling among MEPs[93]. Similarly, the Krt18-CreER/YFP and Fgd5-CreER/Tom HSC lineage tracing models employed by Chapple et al. also found enriched early labeling in HSCs, HPC2s, and platelets with minimal labeling among MEPs (and CMPs)[81]. The *in situ* Sleeping Beauty lineage tracing model Rodriguez-Fraticelli et al. employed also did not label any MEPs, and attributed that to the possibility that the MEP stage is too transient to be detected[78]. If so, labeling of MEPs may be less robust than other progenitor cell states and reflect an important caveat of these lineage tracing studies. It is worth noting that significant heterogeneity among phenotypic human MEPs has been identified[96], and there is likely similar heterogeneity in mice. Thus, it is possible that phenotypic analyses routinely performed do not accurately capture and/or delineate between myeloerythroid progenitors in murine BM. Collectively, this data sets suggest that at least a fraction of platelet generation may bypass CMP/MEP intermediates, but does not rule out the possibility of multiple routes of production with different output kinetics.

Can platelets arise directly from HSCs by "skipping" intermediate cell states?

One hypothesis to arise out of some of the models generated from the studies discussed above[66,67,76-79,81,93] is the possibility of a shortcut/bypass mechanism whereby megakaryocytic-restricted HSCs directly give rise to MkPs/platelets without progressing through MPPs or other classical intermediate cell states. The evidence for

this is largely the result of the rate at which labeled cells accumulate in any given cellular compartment post-HSC labeling. Many of the studies highlighted above specifically indicate that platelets accumulate a higher proportion of labeled cells far faster than any other cell type, including their own progenitors (i.e. CMP, MEP, MkP), seemingly indicating a direct LT-HSC>platelet pathway. Morcos et al. even suggested that approximately 50% of steady-state platelet generation is derived via such a pathway whereas the remaining proportion is derived via the classically viewed hematopoietic hierarchy[77]. However, and of fundamental importance, our FlkSwitch lineage tracing model[85-92] directly contradicts a direct LT-HSC>MkP/platelet (i.e. MPP "bypass") pathway under true steady-state in young adult mice as 1) all platelets have excised the Tomato reporter (indicating transition through a Flk2+/MPP stage downstream of the LT-HSC) and 2) label switching is abundantly detected as early as the ST-HSC stage. Thus, if LT-HSCs bypass all other progenitors for direct platelet production, retention of the Tomato label in platelets would be present at a greater frequency than what is measured among MPPs, which we did not observe.

One possible way to reconcile these data is a strong effect of HSC clonal restriction paired with accelerated kinetics, where certain HSC clones preferentially only give rise to platelets with such accelerated kinetics that label retention among intermediate progenitors is too transient to measure in inducible lineage tracing models. Another consideration is the time it takes to transition between cell states, if clonal expansion occurs, and if labeled cells are exhausted from a cellular pool upon differentiation. That is, if labeled progenitors differentiate without clonally expanding (or all clonally

expanded, labeled cells differentiate), then low level labeling within a compartment may be misinterpreted. A comprehensive assessment of every hematopoietic stem and progenitor cell at multiple successive time points would need to be conducted to measure the kinetics of labeled progenitors. Further, given that one megakaryocyte is predicted to give rise to thousands of platelets[97], then low level labeling of upstream progenitors does not necessarily preclude a high proportion of labeling among terminally differentiated platelets, especially given that platelets generated prior to label induction turn over quickly. A final possible, yet unlikely, scenario is that certain HSC clones transiently activate Flk2 gene expression so quickly that cell surface protein is undetected (i.e. maintaining a LT-HSC phenotype as Flk2-) yet allowing excision of the Tomato gene in our FlkSwitch mice. The resulting progeny would be GFP+ and prevent direct determination for the existence of a LT-HSC>platelet pathway. Moreover, this scenario would be irreconcilable with platelets, erythrocytes, and granulocyte/macrophages always showing similar proportions of labeling in our model, thus suggesting they all share the same progenitor. Clearly, additional work will be required to interpret these results and to gain better understanding of all platelet production paths at steady-state.

Are MkPs unilineage platelet progenitors?

Since their initial characterization in 2003[17], and refinement in 2007[19], MkPs have largely been thought to be the unilineage progenitor immediately preceding megakaryocyte maturation as *in vitro* experiments in those studies concluded.

Additionally, to our knowledge, no *in situ* lineage tracing directly targeting the MkP cell state has been performed. However, we recently conducted transplantations of MkPs and tracked blood cell output in recipient mice[18]. Interestingly, in addition to transient platelet generation, a small burst of erythroid (and nominal GM) cell reconstitution was observed (Figure 2A). Even in the context of transplantation, these new data, in combination with the studies discussed throughout, highlights the need for additional *in situ* analysis of all stages of megakaryopoiesis and continued refinement of progenitor cells. To that point, Säwen et al. compared the equilibrium ratios of MkP labeling to that of platelets and found that, in the Fgd5-CreER/Tom model, MkPs appear to be an obligatory step preceding platelet generation[76]. However, the phenotypic and functional heterogeneity of the MkP compartment has yet to be fully elucidated and might reveal additional plasticity given our MkP transplant data[18].

Is megakaryocyte-specific lineage tracing possible?

We recognize that megakaryocytic lineage tracing using a lineage-specific gene and a Cre-based system can be challenging due to the established phenotypic and molecular similarity between HSCs and MkPs[83]. However, there are a few tools that have demonstrated potential success. The most commonly employed megakaryocyte lineage system is Pf4(CXCL4)-Cre, initially described by Tiedt et al.[98] and most commonly used for megakaryopoiesis-selective genetic deletion. This model was quickly adapted to fluorescent reporter lineage tracing studies[80]. However, the first example of this found that Pf4-Cre expression was not restricted to the megakaryocyte lineage, but also

labeled BM HSCs and their progeny between ~40-60%. This "non-specificity" could, potentially, strengthen the evidence for megakaryocyte lineage priming in HSCs. In this study, Pf4-Cre activity was found in ~40% of phenotypic LT-HSCs, and varying levels in the Lin-cKit+Sca1+ and Lin-cKit+Sca1- compartments, broadly comprising HSCs/MPPs and CMPs/GMPs/MEPs/MkPs, respectively. Label was also detected in a large frequency in lymphoid, granulocyte, erythroid, monocyte, and osteoclast cell types. This could be indicative of two potential conclusions: 1) some LT-HSCs express megakaryocytic lineage genes, potentially due to lineage priming or as a megakaryocyte-biased subpopulation, but clearly still maintain multilineage differentiation potential or 2) the Pf4-Cre system is not megakaryocyte-lineage specific, and results generated using that model should be carefully considered for off-target labeling. Importantly, these two conclusions are not mutually exclusive. In contrast, others have found that the Pf4-Cre system is largely selective for the megakaryocyte lineage with little expression in other lineages, although non-megakaryocyte lineage labeling increased slightly during inflammation[99]. Together, these contradicting data indicate that the Pf4-Cre model may be useful for megakaryocyte lineage tracing but could potentially be hindered by suboptimal specificity.

Another study that leveraged Pf4-Cre, in addition to several other fluorescent reporter lines, identified the lung as a major source of platelet production[100]. They reported that the lung contains hematopoietic progenitors, including HSCs, their direct progeny, and MkPs, and harbors relatively immature megakaryocytes that directly produce platelets

in the lung space. However, it remains unknown if the hematopoietic hierarchy explored in the BM, particularly the classical platelet lineage and possible alternative routes discussed here, remain the same in other tissues. Future lineage tracing studies could leverage platelet production in non-BM tissues to gain a clearer understanding of megakaryopoiesis. As a recent example, myeloid progenitors, including MEPs, have been detected in the murine brain which contain the capacity to undergo megakaryopoiesis[101].

Recently, an alternative system to Pf4-Cre has been developed, the Gp1ba(CD42ba)-Cre mouse line[102]. As summarized in a recent review[103], the Gp1ba-Cre model has been characterized as acting later (primarily at the megakaryocyte) during megakaryopoiesis than Pf4-Cre, but may be more selective for the megakaryocytic lineage. It is therefore conceivable that a potential combination of Gp1ba and Pf4 (i.e. dual reporter) could be used for lineage tracing of late megakaryocyte development, maturation, and platelet generation. And, if Pf4 is found to truly be expressed in HSCs, may provide a unique system in which specific megakaryopoiesis cellular intermediates and events can be interrogated.

Can discordant lineage tracing outcomes be unified?

In this review, we have highlighted the major lineage tracing findings for platelet differentiation. Further, we underscored the conclusions drawn based on the employment of either transplantation-based or *in situ*-based lineage tracing experimental design and explored the discordant results. However, is it possible to

unify observations from both methods into an updated model of steady-state platelet generation? Given the critical need for platelets to sustain life of an organism, it is not surprising that multiple redundancies and/or competencies may exist to ensure constant platelet production. This may help explain why some classically defined progenitor populations may be dispensable under some conditions and why at least a few HSC clones are primed for the megakaryocytic lineage. Further, a recent study sought to re-evaluate some of the lineage tracing models reviewed here to determine if diverse *in situ* HSC labeling strategies could be unified[104]. It was suggested that the seemingly discordant results obtained from different models (specifically Fgd5-CreER[76,81] and Krt18-CreER[81]) can actually be integrated mathematically, at least with respect to labeling kinetics of LT-HSCs, ST-HSCs, and MPPs, as each strategy marks HSCs with slightly different properties. They further conclude that this reconciliation highlights the heterogeneity of HSCs and reinforces the importance of diverse experimental approaches and careful interpretation. It should, therefore, be possible to extrapolate this mathematical reinterpretation to evaluate the platelet lineage across multiple studies to potentially unify the diverse findings of *in situ* lineage tracing.

Given the interpretations of the data reviewed herein, we propose an updated model of megakaryopoiesis (Figure 3). The heterogenous HSC comportment presents vWF^{hi} (and/or CD41^{hi})[66,67,78,79] LT-HSCs residing at the apex of our proposed hierarchy. Immediately downstream are vWF- LT-HSCs that-give rise to a heterogenous MPPs pool. The majority of lineage tracing studies identified the MPP2 (HPC2) subset as the likely primary MPP intermediate involved in platelet generation[67,76,81,93], yet others

may contribute as well. MPPs may then transition through the classical hierarchy of CMP>MEP>MkP, or bypass CMPs and/or MEPs altogether. Specifically, MPP2 cells may comprise the subset of MPPs that directly differentiate into MkPs. Convergence upon an MkP does appear to be an obligatory step in platelet generation. Differentiation of platelets may occur in a biased manner or operate in conjunction with the classical view of hematopoiesis. This updated view of megakaryopoiesis unifies the available lineage tracing data, yet requires additional experimental investigation of *in situ* stem and progenitor cell fate choice to verify.

Conclusions, outlook, and open questions

Clearly, recent advances in lineage tracing have expanded the traditional view of megakaryopoiesis. However, even though multiple parallel routes of platelet generation are not necessarily mutually exclusive, future endeavors will be required to confirm pathway(s), their importance and prevalence, and if they are altered or induced outside of steady-state megakaryopoiesis. This includes obtaining a better understanding of platelet generation path(s) during ontogeny and aging, following bleeding or hemorrhaging, in response to injury and infection, and in disorders such as autoimmunity, immune thrombocytopenia, and cancer.

Multiple challenges remain for elucidation of the megakaryocytic lineage, including ensuring that labeling is robust enough to be detected in both progenitors and platelets, inducing highly selective megakaryocytic labeling, and addressing clonality of HSCs, MkPs, and any intermediate progenitors. These experimental challenges extend beyond

model organisms, as the inability to retrospectively lineage trace human platelets via somatic mutations limits the opportunity to investigate platelet generation pathway(s) in humans. Improved understanding of megakaryopoiesis has tremendous therapeutic potential, as differentiation of induced pluripotent stem cells (iPSCs) into platelets would offer significant clinical relief and are a major ongoing research avenue. Further, lineage tracing in any hematopoietic compartment, including megakaryocytic, could benefit from a host of improvements that include refining the markers and strategies employed for HSC and progenitor cell identification and isolation, discriminating between a lineage-committed cell, one that is lineage primed, and/or between multipotent cells located in an environment that is permissive to a single lineage[105], improvement and development of *in situ* models, lineage tracing technologies[106], and enhanced graphical representations[107].

We have previously proposed that erythrocyte and/or platelet generation may be the default fate of HSCs and hematopoiesis[20]. Indeed, the lineage tracing studies reviewed herein support the hypothesis of alternative, co-existing, continuous pathways supporting the critical-for-life generation of megakaryocytes and platelets. Thus, HSCs may primarily function to support blood integrity and oxygen transport via platelet and erythrocyte generation at the expense of immune cell replenishment[20,108].

Acknowledgments

This work was supported by a NIH NIGMS IRACDA Postdoctoral Training Grant (K12GM139185) to B.A.M., a Tobacco-Related Disease Research Program (TRDRP)

Predoctoral Fellowship (T31DT1690) to A.R.y.B., and a NIH NIA Award (R01AG062879) to E.C.F.

Author Contributions

B.A.M., A.R.y.B., and E.C.F. wrote the paper.

Figures

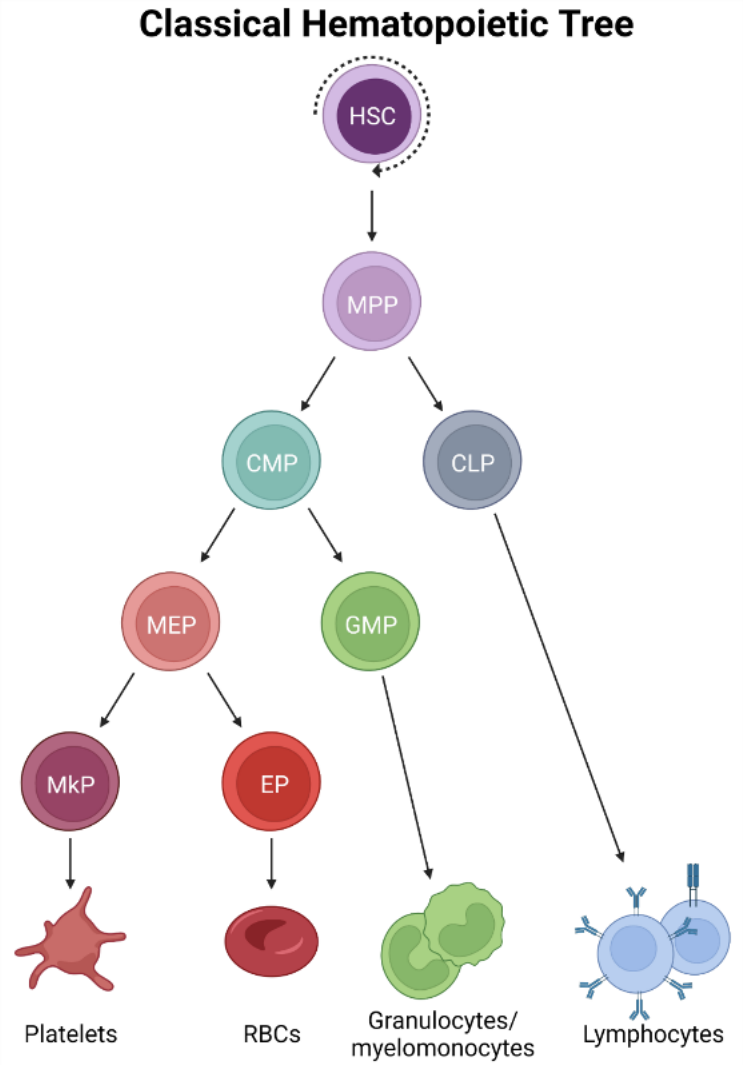

Figure 5.1. Classical Hematopoietic Tree.

Self-renewing, multipotent HSCs reside at the apex of the hematopoietic hierarchy. Differentiation into MPPs results in loss of self-renewal, with retention of multipotency. Successive differentiation stages leads to increased lineage-restriction. Classically, platelets arise by differentiation of MPPs into CMPs, MEPs, and MkPs, which mature into megakaryocytes that ultimately generate platelets.

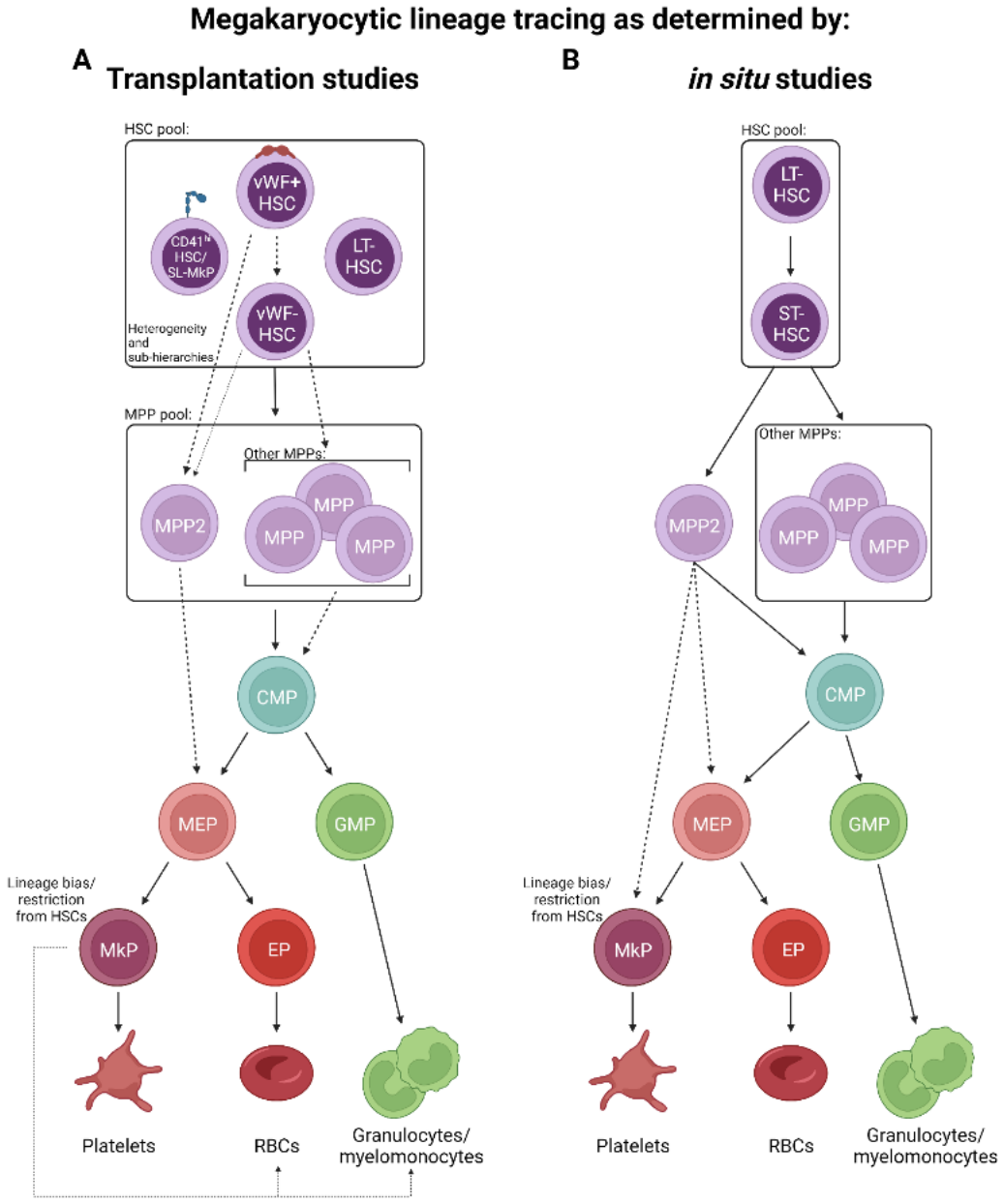

Figure 5.2. Routes of platelet generation revealed by lineage tracing.

Two major lineage tracing methods have been employed to interrogate the route(s) of platelet specification. **(A)** Single and bulk cell transplantation and **(B)** *in situ* labeling have uncovered multiple possible paths of megakaryopoiesis involving differential use of progenitor cell states. Solid lines indicate "classical" paths whereas dashed lines represent new and/or expanded differentiation steps elucidated by the studies discussed here.

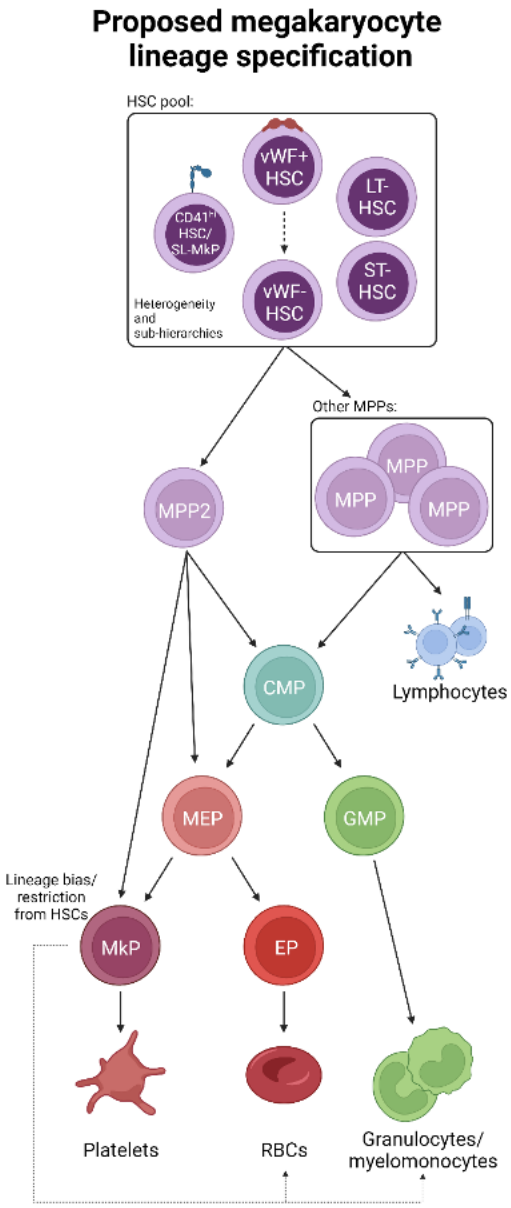

Figure 5.3. Proposed unification of platelet generation from HSCs.

Combining the available lineage tracing data, we propose an expanded and unified view of megakaryopoiesis. The phenotypic HSC pool is comprised of heterogeneous populations that are ordered into various sub-hierarchies that may possess varying degrees of lineage bias and/or restriction. HSCs then transition to MPPs, including MPP2 which may be the primary MPP subset involved in platelet formation. The "classical" CMP>MEP>MkP differentiation may then occur, or specific progenitor cell states may be bypassed. All possible pathways converge upon the MkP, which

possesses minor plasticity to contribute minimally to erythroid and/or other myeloid cell output.

References

1 Guo, T. *et al.* Megakaryopoiesis and platelet production: insight into hematopoietic stem cell proliferation and differentiation. *Stem Cell Investig* **2**, 3, doi:10.3978/j.issn.2306-9759.2015.02.01 (2015).

2 Machlus, K. R. & Italiano, J. E., Jr. The incredible journey: From megakaryocyte development to platelet formation. *J Cell Biol* **201**, 785-796, doi:10.1083/jcb.201304054 (2013).

3 Holinstat, M. Normal platelet function. *Cancer Metastasis Rev* **36**, 195-198, doi:10.1007/s10555-017-9677-x (2017).

4 Poscablo, D. M. & Forsberg, E. C. The Clot Thickens: Recent Clues on Hematopoietic Stem Cell Contribution to Age-Related Platelet Biology Open New Questions. *Adv Geriatr Med Res* **3**, doi:10.20900/agmr20210019 (2021).

5 Thompson, C. B. & Jakubowski, J. A. The pathophysiology and clinical relevance of platelet heterogeneity. *Blood* **72**, 1-8 (1988).

6 van der Meijden, P. E. J. & Heemskerk, J. W. M. Platelet biology and functions: new concepts and clinical perspectives. *Nat Rev Cardiol* **16**, 166-179, doi:10.1038/s41569-018-0110-0 (2019).

7 Feske, S. K. Ischemic Stroke. *Am J Med* **134**, 1457-1464, doi:10.1016/j.amjmed.2021.07.027 (2021).

8 Lee, E. J. & Lee, A. I. Thrombocytopenia. *Prim Care* **43**, 543-557, doi:10.1016/j.pop.2016.07.008 (2016).

9 Olaf, M. & Cooney, R. Deep Venous Thrombosis. *Emerg Med Clin North Am* **35**, 743-770, doi:10.1016/j.emc.2017.06.003 (2017).

10 Schafer, A. I. Thrombocytosis. *N Engl J Med* **350**, 1211-1219, doi:10.1056/NEJMra035363 (2004).

11 Wolberg, A. S. *et al.* Venous thrombosis. *Nat Rev Dis Primers* **1**, 15006, doi:10.1038/nrdp.2015.6 (2015).

12 Pang, L., Weiss, M. J. & Poncz, M. Megakaryocyte biology and related disorders. *J Clin Invest* **115**, 3332-3338, doi:10.1172/JCI26720 (2005).

13 Wen, Q., Goldenson, B. & Crispino, J. D. Normal and malignant megakaryopoiesis. *Expert Rev Mol Med* **13**, e32, doi:10.1017/S1462399411002043 (2011).

14 Cheng, H., Zheng, Z. & Cheng, T. New paradigms on hematopoietic stem cell differentiation. *Protein Cell* **11**, 34-44, doi:10.1007/s13238-019-0633-0 (2020).

15 Yamamoto, R. *et al.* Clonal analysis unveils self-renewing lineage-restricted progenitors generated directly from hematopoietic stem cells. *Cell* **154**, 1112-1126, doi:10.1016/j.cell.2013.08.007 (2013).

16 Akashi, K., Traver, D., Miyamoto, T. & Weissman, I. L. A clonogenic common myeloid progenitor that gives rise to all myeloid lineages. *Nature* **404**, 193-197, doi:10.1038/35004599 (2000).

17 Nakorn, T. N., Miyamoto, T. & Weissman, I. L. Characterization of mouse clonogenic megakaryocyte progenitors. *Proc Natl Acad Sci U S A* **100**, 205-210, doi:10.1073/pnas.262655099 (2003).

18 Poscablo, D. M., Worthington, A. K., Smith-Berdan, S. & Forsberg, E. C. Megakaryocyte progenitor cell function is enhanced upon aging despite the functional decline of aged hematopoietic stem cells. *Stem Cell Reports* **16**, 1598-1613, doi:10.1016/j.stemcr.2021.04.016 (2021).

19 Pronk, C. J. *et al.* Elucidation of the phenotypic, functional, and molecular topography of a myeloerythroid progenitor cell hierarchy. *Cell Stem Cell* **1**, 428-442, doi:10.1016/j.stem.2007.07.005 (2007).

20 Boyer, S. W. *et al.* Clonal and Quantitative In Vivo Assessment of Hematopoietic Stem Cell Differentiation Reveals Strong Erythroid Potential of Multipotent Cells. *Stem Cell Reports* **12**, 801-815, doi:10.1016/j.stemcr.2019.02.007 (2019).

21 Noetzli, L. J., French, S. L. & Machlus, K. R. New Insights Into the Differentiation of Megakaryocytes From Hematopoietic Progenitors. *Arterioscler Thromb Vasc Biol* **39**, 1288-1300, doi:10.1161/ATVBAHA.119.312129 (2019).

22 Conklin, E. G. *The organization and cell-lineage of the ascidian egg*. ([Academy of Natural Sciences], 1905).

23 Thomas, P. Q., Brown, A. & Beddington, R. S. Hex: a homeobox gene revealing peri-implantation asymmetry in the mouse embryo and an early transient marker of endothelial cell precursors. *Development* **125**, 85-94 (1998).

24 Kit, S., Beck, C., Graham, O. L. & Gross, A. Effect of 5-bromodeoxyuridine on deoxyribonucleic acid-thymine synthesis and cell metabolism of lymphatic tissues and tumors. *Cancer Res* **18**, 598-602 (1958).

25 Mintz, B. Genetic Mosaicism in Adult Mice of Quadriparental Lineage. *Science* **148**, 1232-1233, doi:10.1126/science.148.3674.1232 (1965).

26 Livet, J. *et al.* Transgenic strategies for combinatorial expression of fluorescent proteins in the nervous system. *Nature* **450**, 56-62, doi:10.1038/nature06293 (2007).

27 Weissman, T. A. & Pan, Y. A. Brainbow: new resources and emerging biological applications for multicolor genetic labeling and analysis. *Genetics* **199**, 293-306, doi:10.1534/genetics.114.172510 (2015).

28 Pei, W. *et al.* Polylox barcoding reveals haematopoietic stem cell fates realized in vivo. *Nature* **548**, 456-460, doi:10.1038/nature23653 (2017).

29 Kebschull, J. M. & Zador, A. M. Cellular barcoding: lineage tracing, screening and beyond. *Nat Methods* **15**, 871-879, doi:10.1038/s41592-018-0185-x (2018).

30 Schepers, K. *et al.* Dissecting T cell lineage relationships by cellular barcoding. *J Exp Med* **205**, 2309-2318, doi:10.1084/jem.20072462 (2008).

31 Doetsch, F., Caille, I., Lim, D. A., Garcia-Verdugo, J. M. & Alvarez-Buylla, A. Subventricular zone astrocytes are neural stem cells in the adult mammalian brain. *Cell* **97**, 703-716, doi:10.1016/s0092-8674(00)80783-7 (1999).

32 Junker, J. P. *et al.* Massively parallel clonal analysis using CRISPR/Cas9 induced genetic scars. *bioRxiv*, 056499, doi:10.1101/056499 (2017).

33 Kalhor, R. *et al.* Developmental barcoding of whole mouse via homing CRISPR. *Science* **361**, doi:10.1126/science.aat9804 (2018).

34 Kalhor, R., Mali, P. & Church, G. M. Rapidly evolving homing CRISPR barcodes. *Nat Methods* **14**, 195-200, doi:10.1038/nmeth.4108 (2017).

35 McKenna, A. *et al.* Whole-organism lineage tracing by combinatorial and cumulative genome editing. *Science* **353**, aaf7907, doi:10.1126/science.aaf7907 (2016).

36 Perli, S. D., Cui, C. H. & Lu, T. K. Continuous genetic recording with self-targeting CRISPR-Cas in human cells. *Science* **353**, doi:10.1126/science.aag0511 (2016).

37 Spanjaard, B. *et al.* Simultaneous lineage tracing and cell-type identification using CRISPR-Cas9-induced genetic scars. *Nat Biotechnol* **36**, 469-473, doi:10.1038/nbt.4124 (2018).

38 Alemany, A., Florescu, M., Baron, C. S., Peterson-Maduro, J. & van Oudenaarden, A. Whole-organism clone tracing using single-cell sequencing. *Nature* **556**, 108-112, doi:10.1038/nature25969 (2018).

39 Frieda, K. L. *et al.* Synthetic recording and in situ readout of lineage information in single cells. *Nature* **541**, 107-111, doi:10.1038/nature20777 (2017).

40 Dou, Y., Gold, H. D., Luquette, L. J. & Park, P. J. Detecting Somatic Mutations in Normal Cells. *Trends Genet* **34**, 545-557, doi:10.1016/j.tig.2018.04.003 (2018).

41 Casasent, A. K. *et al.* Multiclonal Invasion in Breast Tumors Identified by Topographic Single Cell Sequencing. *Cell* **172**, 205-217 e212, doi:10.1016/j.cell.2017.12.007 (2018).

42 Frumkin, D., Wasserstrom, A., Kaplan, S., Feige, U. & Shapiro, E. Genomic variability within an organism exposes its cell lineage tree. *PLoS Comput Biol* **1**, e50, doi:10.1371/journal.pcbi.0010050 (2005).

43 Reizel, Y. *et al.* Colon stem cell and crypt dynamics exposed by cell lineage reconstruction. *PLoS Genet* **7**, e1002192, doi:10.1371/journal.pgen.1002192 (2011).

44 Reizel, Y. *et al.* Cell lineage analysis of the mammalian female germline. *PLoS Genet* **8**, e1002477, doi:10.1371/journal.pgen.1002477 (2012).

45 Salipante, S. J. & Horwitz, M. S. Phylogenetic fate mapping. *Proc Natl Acad Sci U S A* **103**, 5448-5453, doi:10.1073/pnas.0601265103 (2006).

46 Evrony, G. D. *et al.* Single-neuron sequencing analysis of L1 retrotransposition and somatic mutation in the human brain. *Cell* **151**, 483-496, doi:10.1016/j.cell.2012.09.035 (2012).

47 Blokzijl, F. *et al.* Tissue-specific mutation accumulation in human adult stem cells during life. *Nature* **538**, 260-264, doi:10.1038/nature19768 (2016).

48 Lee-Six, H. *et al.* Population dynamics of normal human blood inferred from somatic mutations. *Nature* **561**, 473-478, doi:10.1038/s41586-018-0497-0 (2018).

49 Ju, Y. S. *et al.* Somatic mutations reveal asymmetric cellular dynamics in the early human embryo. *Nature* **543**, 714-718, doi:10.1038/nature21703 (2017).

50 Pontes-Quero, S. *et al.* Dual ifgMosaic: A Versatile Method for Multispectral and Combinatorial Mosaic Gene-Function Analysis. *Cell* **170**, 800-814 e818, doi:10.1016/j.cell.2017.07.031 (2017).

51 Moor, A. E. & Itzkovitz, S. Spatial transcriptomics: paving the way for tissue-level systems biology. *Curr Opin Biotechnol* **46**, 126-133, doi:10.1016/j.copbio.2017.02.004 (2017).

52 Wu, S. S., Lee, J. H. & Koo, B. K. Lineage Tracing: Computational Reconstruction Goes Beyond the Limit of Imaging. *Mol Cells* **42**, 104-112, doi:10.14348/molcells.2019.0006 (2019).

53 Fletcher, R. B., Das, D. & Ngai, J. Creating Lineage Trajectory Maps Via Integration of Single-Cell RNA-Sequencing and Lineage Tracing: Integrating transgenic lineage tracing and single-cell RNA-sequencing is a robust approach for mapping developmental lineage trajectories and cell fate changes. *Bioessays* **40**, e1800056, doi:10.1002/bies.201800056 (2018).

54 McKenna, A. & Gagnon, J. A. Recording development with single cell dynamic lineage tracing. *Development* **146**, doi:10.1242/dev.169730 (2019).

55 Zhang, Y., Gao, S., Xia, J. & Liu, F. Hematopoietic Hierarchy - An Updated Roadmap. *Trends Cell Biol* **28**, 976-986, doi:10.1016/j.tcb.2018.06.001 (2018).

56 Till, J. E. & Mc, C. E. A direct measurement of the radiation sensitivity of normal mouse bone marrow cells. *Radiat Res* **14**, 213-222 (1961).

57 Becker, A. J., Mc, C. E. & Till, J. E. Cytological demonstration of the clonal nature of spleen colonies derived from transplanted mouse marrow cells. *Nature* **197**, 452-454, doi:10.1038/197452a0 (1963).

58 Wu, A. M., Till, J. E., Siminovitch, L. & McCulloch, E. A. A cytological study of the capacity for differentiation of normal hemopoietic colony-forming cells. *J Cell Physiol* **69**, 177-184, doi:10.1002/jcp.1040690208 (1967).

59 Abramson, S., Miller, R. G. & Phillips, R. A. The identification in adult bone marrow of pluripotent and restricted stem cells of the myeloid and lymphoid systems. *J Exp Med* **145**, 1567-1579, doi:10.1084/jem.145.6.1567 (1977).

60 Dick, J. E., Magli, M. C., Huszar, D., Phillips, R. A. & Bernstein, A. Introduction of a selectable gene into primitive stem cells capable of long-term reconstitution of the hemopoietic system of W/Wv mice. *Cell* **42**, 71-79, doi:https://doi.org/10.1016/S0092-8674(85)80102-1 (1985).

61 Keller, G., Paige, C., Gilboa, E. & Wagner, E. F. Expression of a foreign gene in myeloid and lymphoid cells derived from multipotent haematopoietic precursors. *Nature* **318**, 149-154, doi:10.1038/318149a0 (1985).

62 Lemischka, I. R., Raulet, D. H. & Mulligan, R. C. Developmental potential and dynamic behavior of hematopoietic stem cells. *Cell* **45**, 917-927, doi:https://doi.org/10.1016/0092-8674(86)90566-0 (1986).

63 Muller-Sieburg, C. E., Whitlock, C. A. & Weissman, I. L. Isolation of two early B lymphocyte progenitors from mouse marrow: a committed pre-pre-B cell and a clonogenic Thy-1-lo hematopoietic stem cell. *Cell* **44**, 653-662, doi:10.1016/0092-8674(86)90274-6 (1986).

64 Spangrude, G. J., Heimfeld, S. & Weissman, I. L. Purification and characterization of mouse hematopoietic stem cells. *Science* **241**, 58-62, doi:10.1126/science.2898810 (1988).

65 Reya, T., Morrison, S. J., Clarke, M. F. & Weissman, I. L. Stem cells, cancer, and cancer stem cells. *Nature* **414**, 105-111, doi:10.1038/35102167 (2001).

66 Sanjuan-Pla, A. *et al.* Platelet-biased stem cells reside at the apex of the haematopoietic stem-cell hierarchy. *Nature* **502**, 232-236, doi:10.1038/nature12495 (2013).

67 Carrelha, J. *et al.* Hierarchically related lineage-restricted fates of multipotent haematopoietic stem cells. *Nature* **554**, 106-111, doi:10.1038/nature25455 (2018).

68 Shin, J. Y., Hu, W., Naramura, M. & Park, C. Y. High c-Kit expression identifies hematopoietic stem cells with impaired self-renewal and megakaryocytic bias. *J Exp Med* **211**, 217-231, doi:10.1084/jem.20131128 (2014).

69 Challen, G. A., Boles, N. C., Chambers, S. M. & Goodell, M. A. Distinct hematopoietic stem cell subtypes are differentially regulated by TGF-beta1. *Cell Stem Cell* **6**, 265-278, doi:10.1016/j.stem.2010.02.002 (2010).

70 Benz, C. *et al.* Hematopoietic stem cell subtypes expand differentially during development and display distinct lymphopoietic programs. *Cell Stem Cell* **10**, 273-283, doi:10.1016/j.stem.2012.02.007 (2012).

71 Morita, Y., Ema, H. & Nakauchi, H. Heterogeneity and hierarchy within the most primitive hematopoietic stem cell compartment. *J Exp Med* **207**, 1173-1182, doi:10.1084/jem.20091318 (2010).

72 Dykstra, B. *et al.* Long-term propagation of distinct hematopoietic differentiation programs in vivo. *Cell Stem Cell* **1**, 218-229, doi:10.1016/j.stem.2007.05.015 (2007).

73 Muller-Sieburg, C. E., Cho, R. H., Karlsson, L., Huang, J. F. & Sieburg, H. B. Myeloid-biased hematopoietic stem cells have extensive self-renewal capacity but generate diminished lymphoid progeny with impaired IL-7 responsiveness. *Blood* **103**, 4111-4118, doi:10.1182/blood-2003-10-3448 (2004).

74 Lee, J. *et al.* Lineage specification of human dendritic cells is marked by IRF8 expression in hematopoietic stem cells and multipotent progenitors. *Nat Immunol* **18**, 877-888, doi:10.1038/ni.3789 (2017).

75 Jacobsen, S. E. W. & Nerlov, C. Haematopoiesis in the era of advanced single-cell technologies. *Nat Cell Biol* **21**, 2-8, doi:10.1038/s41556-018-0227-8 (2019).

76 Säwen, P. *et al.* Murine HSCs contribute actively to native hematopoiesis but with reduced differentiation capacity upon aging. *Elife* **7**, doi:10.7554/eLife.41258 (2018).

77 Morcos, M. N. F. *et al.* Fate mapping of hematopoietic stem cells reveals two pathways of native thrombopoiesis. *Nat Commun* **13**, 4504, doi:10.1038/s41467-022-31914-z (2022).

78 Rodriguez-Fraticelli, A. E. *et al.* Clonal analysis of lineage fate in native haematopoiesis. *Nature* **553**, 212-216, doi:10.1038/nature25168 (2018).

79 Haas, S. *et al.* Inflammation-Induced Emergency Megakaryopoiesis Driven by Hematopoietic Stem Cell-like Megakaryocyte Progenitors. *Cell Stem Cell* **17**, 422-434, doi:10.1016/j.stem.2015.07.007 (2015).

80 Calaminus, S. D. *et al.* Lineage tracing of Pf4-Cre marks hematopoietic stem cells and their progeny. *PLoS One* **7**, e51361, doi:10.1371/journal.pone.0051361 (2012).

81 Chapple, R. H. *et al.* Lineage tracing of murine adult hematopoietic stem cells reveals active contribution to steady-state hematopoiesis. *Blood Adv* **2**, 1220-1228, doi:10.1182/bloodadvances.2018016295 (2018).

82 Osorio, F. G. *et al.* Somatic Mutations Reveal Lineage Relationships and Age-Related Mutagenesis in Human Hematopoiesis. *Cell Rep* **25**, 2308-2316 e2304, doi:10.1016/j.celrep.2018.11.014 (2018).

83 Yang, J., Zhao, S. & Ma, D. Biological Characteristics and Regulation of Early Megakaryocytopoiesis. *Stem Cell Rev Rep* **15**, 652-663, doi:10.1007/s12015-019-09905-3 (2019).

84 Chavez, J. S. *et al.* PU.1 Expression Defines Distinct Functional Activities in the Phenotypic HSC Compartment of a Murine Inflammatory Stress Model. *Cells* **11**, doi:10.3390/cells11040680 (2022).

85 Boyer, S. W., Schroeder, A. V., Smith-Berdan, S. & Forsberg, E. C. All hematopoietic cells develop from hematopoietic stem cells through Flk2/Flt3-positive progenitor cells. *Cell Stem Cell* **9**, 64-73, doi:10.1016/j.stem.2011.04.021 (2011).

86 Hoeffel, G. *et al.* C-Myb(+) erythro-myeloid progenitor-derived fetal monocytes give rise to adult tissue-resident macrophages. *Immunity* **42**, 665-678, doi:10.1016/j.immuni.2015.03.011 (2015).

87 Epelman, S. *et al.* Embryonic and adult-derived resident cardiac macrophages are maintained through distinct mechanisms at steady state and during inflammation. *Immunity* **40**, 91-104, doi:10.1016/j.immuni.2013.11.019 (2014).

88 Cool, T., Worthington, A., Poscablo, D., Hussaini, A. & Forsberg, E. C. Interleukin 7 receptor is required for myeloid cell homeostasis and reconstitution by hematopoietic stem cells. *Exp Hematol* **90**, 39-45 e33, doi:10.1016/j.exphem.2020.09.001 (2020).

89 Leung, G. A. *et al.* The lymphoid-associated interleukin 7 receptor (IL7R) regulates tissue-resident macrophage development. *Development* **146**, doi:10.1242/dev.176180 (2019).

90 Boyer, S. W., Beaudin, A. E. & Forsberg, E. C. Mapping differentiation pathways from hematopoietic stem cells using Flk2/Flt3 lineage tracing. *Cell Cycle* **11**, 3180-3188, doi:10.4161/cc.21279 (2012).

91 Beaudin, A. E. *et al.* A Transient Developmental Hematopoietic Stem Cell Gives Rise to Innate-like B and T Cells. *Cell Stem Cell* **19**, 768-783, doi:10.1016/j.stem.2016.08.013 (2016).

92 Hashimoto, D. *et al.* Tissue-resident macrophages self-maintain locally throughout adult life with minimal contribution from circulating monocytes. *Immunity* **38**, 792-804, doi:10.1016/j.immuni.2013.04.004 (2013).

93 Upadhaya, S. *et al.* Kinetics of adult hematopoietic stem cell differentiation in vivo. *J Exp Med* **215**, 2815-2832, doi:10.1084/jem.20180136 (2018).

94 Pietras, E. M. *et al.* Functionally Distinct Subsets of Lineage-Biased Multipotent Progenitors Control Blood Production in Normal and Regenerative Conditions. *Cell Stem Cell* **17**, 35-46, doi:10.1016/j.stem.2015.05.003 (2015).

95 Vannucchi, A. M. *et al.* Identification and characterization of a bipotent (erythroid and megakaryocytic) cell precursor from the spleen of phenylhydrazine-treated mice. *Blood* **95**, 2559-2568, doi:10.1182/blood.V95.8.2559 (2000).

96 Psaila, B. *et al.* Single-cell profiling of human megakaryocyte-erythroid progenitors identifies distinct megakaryocyte and erythroid differentiation pathways. *Genome Biol* **17**, 83, doi:10.1186/s13059-016-0939-7 (2016).

97 Patel, S. R., Hartwig, J. H. & Italiano, J. E., Jr. The biogenesis of platelets from megakaryocyte proplatelets. *J Clin Invest* **115**, 3348-3354, doi:10.1172/JCI26891 (2005).

98 Tiedt, R., Schomber, T., Hao-Shen, H. & Skoda, R. C. Pf4-Cre transgenic mice allow the generation of lineage-restricted gene knockouts for studying megakaryocyte and platelet function in vivo. *Blood* **109**, 1503-1506, doi:10.1182/blood-2006-04-020362 (2007).

99 Pertuy, F. *et al.* Broader expression of the mouse platelet factor 4-cre transgene beyond the megakaryocyte lineage. *J Thromb Haemost* **13**, 115-125, doi:10.1111/jth.12784 (2015).

100 Lefrancais, E. *et al.* The lung is a site of platelet biogenesis and a reservoir for haematopoietic progenitors. *Nature* **544**, 105-109, doi:10.1038/nature21706 (2017).

101 Koeniger, T. *et al.* Bone marrow-derived myeloid progenitors in the leptomeninges of adult mice. *Stem Cells* **39**, 227-239, doi:10.1002/stem.3311 (2021).

102 Nagy, Z. *et al.* The Gp1ba-Cre transgenic mouse: a new model to delineate platelet and leukocyte functions. *Blood* **133**, 331-343, doi:10.1182/blood-2018-09-877787 (2019).

103 Gollomp, K. & Poncz, M. Gp1ba-Cre or Pf4-Cre: pick your poison. *Blood* **133**, 287-288, doi:10.1182/blood-2018-11-887513 (2019).

104 Takahashi, M. *et al.* Reconciling Flux Experiments for Quantitative Modeling of Normal and Malignant Hematopoietic Stem/Progenitor Dynamics. *Stem Cell Reports* **16**, 741-753, doi:10.1016/j.stemcr.2021.02.020 (2021).

105 Pinho, S. *et al.* Lineage-Biased Hematopoietic Stem Cells Are Regulated by Distinct Niches. *Dev Cell* **44**, 634-641 e634, doi:10.1016/j.devcel.2018.01.016 (2018).

106 Carrelha, J. *et al.* Single-cell lineage tracing approaches in hematology research: technical considerations. *Exp Hematol* **89**, 26-36, doi:10.1016/j.exphem.2020.07.007 (2020).

107 Laurenti, E. & Gottgens, B. From haematopoietic stem cells to complex differentiation landscapes. *Nature* **553**, 418-426, doi:10.1038/nature25022 (2018).

108 McRae, H. M., Voss, A. K. & Thomas, T. Are transplantable stem cells required for adult hematopoiesis? *Exp Hematol* **75**, 1-10, doi:10.1016/j.exphem.2019.05.007 (2019).

Chapter 6.

Dynamics of Chromatin Accessibility during Hematopoietic Stem Cell Differentiation into Progressively Lineage-Committed Progeny

The text of this chapter includes a reprint of the following previously published paper: Martin EW, Rodriguez Y Baena A, Reggiardo RE, Worthington AK, Mattingly CS, Poscablo DM, Krietsch J, McManus MT, Carpenter S, Kim DH, Forsberg EC. Dynamics of Chromatin Accessibility During Hematopoietic Stem Cell Differentiation Into Progressively Lineage-Committed Progeny. Stem Cells. 2023 May 15;41(5):520-539. doi: 10.1093/stmcls/sxad022. PMID: 36945732; PMCID: PMC10183972.

Summary

Epigenetic mechanisms regulate the multilineage differentiation capacity of hematopoietic stem cells (HSCs) into a variety of blood and immune cells. Mapping the chromatin dynamics of functionally defined cell populations will shed mechanistic insight on two major, unanswered questions in stem cell biology: how does epigenetic identity contribute to a cell type's lineage potential, and how do cascades of chromatin remodeling dictate ensuing fate decisions? Our recent work revealed evidence of multilineage gene priming in HSCs, where open *cis*-regulatory elements (CREs) exclusively shared between HSCs and unipotent lineage cells were enriched for DNA binding motifs of known lineage-specific transcription factors. Oligopotent progenitor populations operating between the HSCs and unipotent cells play essential roles in effecting hematopoietic homeostasis. To test the hypothesis that selective HSC-primed

lineage-specific CREs remain accessible throughout differentiation, we used ATAC-seq to map the temporal dynamics of chromatin remodeling during progenitor differentiation. We observed epigenetic-driven clustering of oligopotent and unipotent progenitors into distinct erythromyeloid and lymphoid branches, with multipotent HSCs and MPPs associating with the erythromyeloid lineage. We mapped the dynamics of lineage-primed CREs throughout hematopoiesis and identified both unique and shared CREs as potential lineage reinforcement mechanisms at fate branch points. Additionally, quantification of genome-wide peak count and size revealed overall greater chromatin accessibility in HSCs, allowing us to identify HSC-unique peaks as putative regulators of self-renewal and multilineage potential. Finally, CRISPRi-mediated targeting of ATACseq- identified putative CREs in HSCs allowed us to demonstrate the functional role of selective CREs in lineage-specific gene expression. These findings provide insight into the regulation of stem cell multipotency and lineage commitment throughout hematopoiesis and serve as a resource to test functional drivers of hematopoietic lineage fate.

Highlights:

- HSCs displayed higher chromatin accessibility than any progeny population
- Epigenetic branchpoints were evident between CMPs and CLPs and between MkPs and EPs
- Lineage priming was selectively maintained throughout differentiation

- HSC-unique accessible chromatin regions were highly enriched for regulatory elements of erythrocyte differentiation
- CRISPRi-mediated targeting of primary HSCs identified functionally significant CREs

Introduction

Hematopoiesis is the process by which multipotent hematopoietic stem cells (HSCs) undergo orchestrated epigenetic and transcriptional changes to produce increasingly lineage-restricted progenitors. According to classical models of hematopoiesis, progressively restricting cell fate decisions allow the differentiation of HSCs into multipotent progenitors (MPPs), which further differentiate into common lymphoid progenitors (CLPs) and common myeloid progenitors (CMPs) (Boyer et al., 2011; Orkin and Zon, 2008; Pronk et al., 2007). Lymphopoiesis further results in unipotent progenitors, ProB and ProT, of B and T cells respectively. In myelopoiesis, granulocyte-macrophage progenitors (GMPs) generate primarily mature granulocytes and macrophages (GMs), while megakaryocytic-erythroid progenitors (MEPs), megakaryocyte progenitors (MkPs) and erythroid progenitors (EPs) produce primarily platelets and red cells (Krause, 2002; Orkin and Zon, 2008; Seita and Weissman, 2010; Boyer et al., 2019). Though it is clear that hematopoiesis is incredibly dynamic with variable flux within and between cell populations, this well characterized mammalian hematopoietic system serves as a superb model for the analysis of factors responsible for the development of functionally distinct progenitors and mature cell populations from stem cells. Lineage-specific cell fate decisions are regulated through epigenetic remodeling of cis-regulatory elements (CREs), including promoters and enhancer regions. While proximal promoter sequences can suffice to assemble the Pol II transcriptional machinery, non-promoter CREs are often necessary to confer cell type-specific transcriptional regulation. These enhancer regions can be located far upstream

or downstream of the target promoter and serve as sequence-specific binding sites for lineage-determining transcription factors (TFs) that regulate the expression of genes specifying cell identity (Surani et al., 2007; Whyte et al., 2013). While TFs are important contributors to cellular lineage specification and progressive lineage restriction, accessibility of enhancers to TFs is fundamental for spatiotemporal gene regulation during stem cell differentiation (Creyghton et al., 2010; Heintzman et al., 2009; Koch et al., 2007; Rada-Iglesias et al., 2011; Visel et al., 2009).

In hematopoietic progenitors, there is evidence that multilineage priming of CREs precedes commitment to the different cell lineages (Hu et al., 1997). “Priming”, here defined as chromatin accessibility of a putative CRE despite lack of expression of its presumed target gene, likely contributes to stem and progenitor lineage potential. As differentiation of HSCs proceeds, genes involved in the target lineage are progressively upregulated in progenitor populations while genes involved in non-target lineages are repressed (Chambers et al., 2007; Forsberg et al., 2005; Phillips et al., 2000; Terskikh et al., 2003), suggesting an essential role of epigenetic regulation in cell fate decisions. In our previous work, we showed evidence of multilineage priming in HSCs, where HSCs had increased global chromatin accessibility compared to their progeny (Ugarte et al., 2015) and where open CREs exclusively shared between HSCs and unipotent lineage cells were enriched for DNA binding motifs for known lineage-specific TFs (Martin et al., 2021). These data led us to hypothesize that HSC-primed lineage-specific CREs remain accessible throughout differentiation into that specific lineage. Since CREs are often devoid of nucleosomes to allow TF binding (Gross and

Garrard, 1988; Heintzman et al., 2007), we performed the Assay for Transposase Accessible Chromatin by high throughput sequencing (ATAC-seq) (Buenrostro et al., 2015, 2013) of seven, functionally well-characterized hematopoietic progenitor cell types (Boyer et al., 2019; Poscablo et al., 2021) to understand CRE priming across hematopoiesis. Importantly, cell fate decisions, as well as lineage-selective expansion and apoptosis, appear to occur primarily in progenitor cell populations (Rodriguez-Fraticelli et al., 2018; Mohrin et al., 2010; Boyer et al., 2011; 2019)**.** In this study, in-depth ATAC-seq investigation and comparative analysis of HSCs and 12 progeny populations of the five main hematopoietic cell lineages revealed potential multipotency, lineage-driving and/or lineage-reinforcing regulatory elements and their corresponding transcription factors that orchestrate differentiation through epigenetic remodeling. As proof-of-concept, we used CRISPRi-mediated silencing of CREs in primary HSCs isolated from a new transgenic CRISPRi mouse model to functionally link distal and proximal putative CREs to target genes.

Results

HSCs had greater global chromatin accessibility compared to hematopoietic progenitor cell types

To determine the dynamics of genome accessibility of multipotent and increasingly lineage-restricted hematopoietic progenitors, we purified 7 primary hematopoietic progenitor cell types **(**Figure 1A**)** by fluorescent-activated cell sorting (FACS) and performed ATAC-seq. After careful quality control of individual and replicate samples

(see below), we tested the hypothesis that multipotency is correlated with overall chromatin openness (Gaspar-Maia et al., 2011; Martin et al., 2021; Ugarte et al., 2015). We reasoned that multipotent cell populations would have the highest level of accessibility relative to oligopotent cells, and that unipotent progenitors would have the least. Thus, we ranked the relative overall accessibility of the hematopoietic progenitors relative to HSCs from our previous report (Martin et al., 2021). We first combined the peak lists from each replicate (n=2) using the Irreproducible Discovery Rate (IDR) (Li et al., 2011) for each cell type to quantify the number of peaks. HSCs had the highest number of peaks, followed by MPPs **(**Figure 1B, Table 1**)**. We also quantified global accessibility by calculating the cumulative normalized average signal over the master peak-list for each cell type by generating histograms using HOMER (Heinz et al., 2010). HSCs had by far the largest peak signal of any progenitor cell type, while all the progenitors had a similar average signal **(Figure 1C).** Although these two measurements are not completely independent, HSCs displayed both the highest number of peaks **(**Figure 1B**)** and the cumulative greatest peak signal **(**Figure 1C**)**. Overall, these results are consistent with epigenetic stem cell priming and our previous reports (Martin et al., 2021; Ugarte et al., 2015) where HSCs have the greatest chromatin accessibility compared to their progeny and differentiated cells.

Chromatin accessibility of cell type-specific genes correlated with known expression patterns in hematopoietic cells

We began the search for lineage-specific regulatory elements by using the Gene Expression Commons (GEXC) expression database (Seita et al., 2012) to generate lists of genes that were expressed specifically in each progenitor cell type (examples shown in Figure 1D). In parallel, we filtered the ATAC-seq peak lists of each progenitor cell type (HSC, MPP, CMP, GMP, MEP, CLP, ProB, ProT) against each other to generate unique peak-lists for each cell type. We then intersected the unique peak lists with the uniquely expressed genes for each progenitor. For populations that had more than ten unique promoter peaks (HSCs, MEPs, ProBs, ProTs) we used HOMER (Heinz et al., 2010) to calculate the normalized average signal centered at the promoter for peaks that overlapped with expressed genes (Figure 1E). We observed cell type-specific read-count accumulation for each progenitor cell with minimal signal from other cell types, indicating that our strategy indeed resolved lineage-specific accessibility.

Lymphoid commitment displayed more extensive chromatin remodeling compared to myelopoiesis

Next, we sought to pinpoint epigenetic changes at a main branchpoint in hematopoiesis, where the multipotent stem and progenitor cells differentiate into either erythromyeloid- or lymphoid- committed CMPs or CLPs, respectively (Seita and Weissman, 2010). We compared the peaks gained and lost between multipotent HSCs and MPPs (combined as “KLS” peaks) and CMPs or CLPs (Figure 2A). First, we

determined the number of peaks either CMPs or CLPs gained or lost from KLS. The CMP and CLP peaks were filtered against each other to focus only on peaks that were uniquely altered in either cell type. At a global level, CLPs had a higher number of peaks altered from KLS cells compared to CMPs with a significant difference in the distribution of peaks gained/lost between the two cell types (Figure 2B**).** When categorizing peaks into promoter vs non-promoter, we observed more promoter peaks altered in CLPs than CMPs (Figure 2C), whereas similar numbers of non-promoter peaks were altered in both progenitors (Figure 2D). We annotated the peaks that were gained and lost using Genomic Regions Enrichment of Annotations Tool (GREAT) (McLean et al., 2010; Tanigawa et al., 2022) and reported the top 4 biological process Gene Ontology (GO) terms enriched, along with example genes in each GO term. We also performed motif enrichment by HOMER (Heinz et al., 2010) (Figure 2E-H). The peaks gained in CMPs included "Negative Regulation of B-cell Activation", and the annotated genes of all four GO terms have known roles in myeloid differentiation, such as *Prdm1* (Chang et al., 2000) and *Btk* (Schmidt et al., 2004). Gata1/2 motifs were among the highest enriched sequences (Figure 2E). The CLP peaks gained were enriched for GO terms that pertained mainly to immune response and immunity, with genes *Ikzf1, Il6,* and *Jun* present within the top 4 GO terms, and were notably enriched with IRF8 and SpiB motifs (Figure 2F). Peaks lost from KLS to CMPs were related to immune system activation and proliferation (Figure 2G), with known immune development genes such as *CD180, Ikzf1, and Gata3*. In addition, there were enriched motifs from ETS/ERG transcription factors as well as SpiB, a known factor in immune

development (Figure 2G). In CLPs, peaks lost from KLS were enriched for GO terms related to the immune response, including genes expressed by innate immune cells that have known roles in complement activation (e.g. *CD55* (Fang et al., 2011)), antigen presentation (e.g. *Nod2, Lamp1* (Cooney et al., 2010)), and activation of innate immune system pathways (e.g. *Fcgr3, Ifng* (Hazenbos et al., 1998; Ivashkiv, 2018)) (Figure 2H). CLPs also lost peaks lined to *CD44*, *Gata2*, and *Gata3,* genes which all have known roles in HSC maintenance, engraftment, and self-renewal (Cao et al., 2016; Frelin et al., 2013; Rodrigues et al., 2012; Yoshida and Georgopoulos, 2013). The CLP-lost peaks were enriched in motifs for erythromyeloid specific Gata factors as well as CTCF motifs (Figure 2H). These analyses suggest that at the first branchpoint, both myeloid and lymphoid differentiation require a combination of silencing of both HSC maintenance and alternative lineage genes, and *de novo* activation of lineage drivers for the induced fate. Quantitatively, lymphoid differentiation appears to require more chromatin remodeling than myeloid differentiation, particularly in promoter regions.

Differential chromatin dynamics at the megakaryocyte-erythroid fate branch

Using a similar strategy, we investigated epigenetic changes at another branchpoint in the hematopoietic hierarchy where MEPs differentiate in either MkPs or EPs (Figure 3A). We identified peaks gained or lost between bipotent MEPs and unipotent MkPs or EPs, and then filtered them against each other to specifically focus on uniquely altered peaks upon fate determination (Figure 3B). Interestingly, of the ~18,000 peaks altered, the distribution of peaks uniquely gained or lost from MEPs was opposite for

MkPs and EPs: ~77% of peaks altered in MkPs were gained peaks, while a similar proportion (~61%) of peaks altered in EPs were lost (Figure 3C). Of these, the large majority were non-promoter peaks (Figure 3D-E). The gained and lost peaks were annotated using GREAT, for which we report the top 4 enriched GO Terms for "Mouse Phenotype" (Figure 3F-G, Supplementary Figure 1) and motif enrichment (Figure H-I, Supplementary Figure 1). The mutation/deletion of genes associated with the MkP-specific gained peaks led to phenotypes characterized under abnormal or decreased inflammation, as with multiple genes within these categories having known roles in megakaryopoiesis and platelet function/physiology (Figure 3F). The mutation/deletion of genes associated with the EP-specific gained peaks led to phenotypes characterized under erythroid lineage, function, and morphology, with example genes including *Gata1* and *Slc4a1* (Figure 3G). MkP (Figure 3H) or EP (Figure 3I) gained peaks were enriched for motifs of transcription factors known to be involved in the respective lineage. As examples of putative megakaryopoiesis-promoting CREs, we identified two MkP-specific peaks gained from MEPs in the gene *Alox5ap* (Figure 3J). The promoter peak along with the enhancer just downstream of the promoter were called only in MkPs, while the second putative enhancer was called in both MEPs and MkPs, indicating possible priming in MEPs from this site. No peaks were called for this gene in EPs. The enhancer-gene map from ENCODE 3 showed interaction between the promoter of *Alox5ap* and two putative enhancer regions (as shown by the interaction lines below the signal track). Concordant with its chromatin accessibility, *Alox5ap* is highly expressed in MkPs but not MEPs or EPs (Figure 3K).

Mapping of chromatin accessibility throughout hematopoiesis identified distinct erythromyeloid and lymphoid clusters

To test our hypothesis that CREs primed in HSCs maintained accessibility throughout hematopoiesis, we needed to determine the dynamics of genome accessibility and further characterize lineage selective CREs throughout the whole continuum of hematopoiesis. To do so, we combined the ATAC-seq data from the 7 progenitors cell types with our previously reported HSCs and 5 unilineage cell types (Martin et al., 2021) (Figure 1A). A master peak-list of 92,842 peaks was produced by combining and filtering the peaks from 2 biological replicates for each of the 13 cell types using chromVAR (Martin et al., 2021; Schep et al., 2017) **(**Table 1**)**. Principal Component Analysis (PCA) of the peak profiles of our 13 populations revealed a high concordance of replicates, as well as a distinct bifurcation of erythromyeloid and lymphoid populations, with the multipotent HSCs and MPPs landing within the erythromyeloid fraction **(**Figure 4A**)**. CMPs, MEPs, EPs, and MkPs all clustered together high on PC2, while CLPs, ProBs, and B cells clustered together, with ProTs and T cells grouped on the same PC1 scale but with higher PC2. HSCs and MPPs, together with GMPs and GMs, fell between the main myeloid and lymphoid groups. As a complement to PCA analysis, we performed Uniform Manifold Approximation and Projection (UMAP) using components derived from PCA of normalized ATAC-seq peak counts **(**Figure 4B**)**. We observed a similar bifurcation between erythromyeloid and lymphoid cell types with the multipotent HSCs and MPPs falling within the erythromyeloid quadrant.

Additionally, we performed hierarchical clustering using the chromVAR output which similarly grouped the 13 populations into two distinct clusters, one erythromyeloid and one lymphoid **(**Figure 4C**)**. All biological replicates clustered directly next to each other, except for the two HSC samples which were separated by MPPs and GMPs. We ruled out batch-effects as closely associated samples were processed independently; the separation of the HSC replicates may instead reflect the presence of primed CREs of all lineages (Martin et al., 2021; also see below). In all three clustering analyses, the multipotent HSCs and MPPs associated near each other and within the erythromyeloid cluster, indicating a similar accessibility profile of these cell types. Overall, clustering analysis confirmed a high degree of reproducibility. Regardless of the method used, we observed distinct clustering based on similar accessibility profiles of lymphoid cell types, erythromyeloid cell types, multipotent HSCs and MPPs, and of unipotent/mature cells with their presumed immediate upstream progenitor. The bifurcation of lymphoid and erythromyeloid lineages observed in the PCA **(**Figure 4A**)**, UMAP **(**Figure 4B**)** and hierarchical clustering **(**Figure 4C**)** is consistent with the myeloid/lymphoid separation found in models of classical hematopoiesis, and with analyses independent of the purity of multi- and oligo-potent progenitor cells (Martin et al., 2021). Of note, the observed similarity between HSCs/MPPs and erythromyeloid cells provides a potential epigenetic basis for the previously reported erythroid functional bias, where HSCs and MPPs predominantly produce red blood cells over all other cell types (Boyer et al., 2019).

Visualization and comparison of ATAC-seq data generated in this study correlated with known expression patterns at two well characterized loci.

To determine whether our mapping could detect known CREs, we visualized our ATAC-seq data across two well-characterized loci: the mouse b-globin cluster **(**Figure 5A) and the mouse *Rag* locus (Figure 5B/C**)**. At the b-globin cluster (chr7: 103,792,027-103,879,340; mm10), we observed expected EP-selective accessibility of the HS3 site in the locus control region (LCR) and *b-minor (bmin)* promoter (Li et al., 2002; Palstra et al., 2008) (Figure 5A). At the 3' end of this gene we observed a B-lineage-selective peak. Further investigation revealed that the peak contains Pax5 binding motifs. It is possible that this site serves as a binding site for Pax5-mediated repression of globin gene expression in lymphoid cells (Linderson et al., 2004). Alternatively, the site could be a distal CRE for a gene regulating lymphoid development (Nutt et al., 2001). We observed erythroid-lineage specific accessibility (HSCs, MEPs, and EPs) of the *b-major (ßmaj*) promoter as well as DNase I hypersensitive sites (HS1,2,4,6) of the LCR that are known to regulate erythroid-specific expression of the genes in this locus. This observation could indicate a "permissive" chromatin state in these erythroid-competent progenitor cells (HSCs, CMPs, MEPs, and EPs). Unexpectedly, we observed robust HS2 accessibility in GMPs, MkPs, and ProT cells, which are not currently known to have any erythroid cell potential. As expected, we did not observe any accessibility at the fetal-specific *epsilon Y globin (Ey), b-h1 (ßh1), b-h2 (ßh2)* genes, or HS5, and no accessibility was observed at any of these sites in GMs, CLPs, ProBs, and ProTs. Taken together, we observed

expected accessibility in the *b*-globin locus in progenitors that give rise to cells that express *b*-globin genes, and little to no accessibility in progenitors that do not give rise to cells that express *b*-globin genes.

Similar specificity was observed for the *Rag* gene locus (chr2: 101,542,312-101,656,796; mm10) which consists of four CREs (Ep, D3, Erag, ASE) and the gene bodies for *Rag1* and *Rag2*. Both *Rag1* and *Rag2* have lymphoid-specific gene expression patterns (Figure 5B**)**, and we observed lymphoid-specific accessibility of both *Rag1* and *Rag2* promoters (Figure 5C). The progenitor- and myeloid-selective peak in the *Rag2* locus corresponds to the promoter for the *Iftap* gene that is expressed selectively by those cell types from the opposite strand of the *Rag* genes (Laszkiewicz et al., 2012) (Figure 5C). The CREs Ep and Erag, which have been characterized to be enhancers in B cell lines (Hsu et al., 2003; Wei et al., 2002), exhibited CLP and B-cell specific (ProBs and B cells) accessibility. D3 has been characterized to act as a lymphoid specific enhancer (Kuo and Schlissel, 2009; Wei et al., 2002) and was accessible in all lymphoid cell types, while the previously characterized anti-silencing element (ASE), important for T cell differentiation (Yannoutsos et al., 2004; Yu et al., 1999), was only accessible in ProTs (Figure 5C). In conclusion, our data demonstrated cell type-specific accessibility for multiple progenitors and recapitulated the dynamics of regulatory element priming throughout differentiation at two well characterized erythroid and lymphoid loci, suggesting that our dataset is sufficiently robust and accurate to also reveal novel CREs that can be functionally tested using the CRISPRi strategies described below.

A subset of lineage-specific CREs were primed in HSCs as well as in select progenitors

Previously, we reported evidence of multilineage priming in HSCs of CREs specific for each unipotent lineage (Martin et al., 2021). We hypothesized that lineage-primed CREs are maintained throughout differentiation. To test this, we first compared the average cumulative accessibility of the lineage-specific peaks (Supplemental Tables 1-5) primed in HSCs to all 13 cell types (Figure 6A). As expected, we observed strong signals from HSCs and the corresponding unipotent progenitor cell type for each lineage-specific primed peak list. MPPs had a discernable peak in four out of the five primed peak lists, with a less distinct signal in EP-primed peaks. Notably, each unilineage region displayed accessibility signal in the presumed immediate upstream progenitor (MEPs in EP-primed peaks; GMPs in GM-primed peaks; ProB in B-cell peaks; and ProTs in T-primed peaks), except for MkPs, which lacked MEP signal and instead had notable accessibility in MPPs and CMPs. These observations revealed that lineage priming of a sizeable proportion of CREs persists throughout differentiation for every lineage.

To assess the distribution of the primed peaks in each progenitor population, we performed a *bedtools* intersect of the lineage-specific peaks primed in HSCs and determined the number of overlapping peaks with each progenitor. Interestingly, all progenitors from every lineage contained peaks from all 5 primed peak lists (Figure 6B, Supplemental Tables 1-5). The distribution of primed peaks of all five lineages was

about equally distributed at ~20% each in HSCs, with similar distribution in MPPs, and CLPs (Chi-square > 0.01). Clear lineage bias was evident in other populations: erythromyeloid progenitors (CMPs, MEPs) were significantly enriched for EP- and MkP-primed peaks, GMPs were enriched for GM-primed elements, while the unipotent lymphoid progenitors (ProBs and ProTs) were significantly enriched with peaks from their immediate downstream progeny (B and T cells).

To accomplish direct longitudinal analysis of priming through multiple differentiation stages, we intersected the 5 HSC-primed peak lists with every assumed intermediate progenitor between HSCs and the unipotent lineage (i.e for HSC/EP shared peaks, we intersected MPPs, CMPs, and MEPs with the shared peak list, as those populations are in the HSC-to-EP lineage as shown in Figure 1A). From those intersections, we identified and quantified the number of peaks that maintained accessibility throughout differentiation for each lineage and reported each peak as a heatmap throughout the expected differentiation trajectory (Figure 6C, Supplemental Table 6). Surprisingly, even though ubiquitously primed CREs were detected for every lineage, this was far from the norm, as no lineage had more than 25% of the HSC-primed peaks maintain openness throughout differentiation. About 10% of the persistently primed peaks were promoters, with the B cell lineage specific *BAFF-R* and T cell specific *CD28* as examples that have known functional roles in those cell types (Dodson et al., 2009; Shulga-Morskaya et al., 2004). Next, we examined two example CREs that were primed throughout differentiation for the GM (Figure 6D) and T cell (Figure 6E) lineages. The GM specific *Fcnb* gene is expressed only in GMPs and GMs,

while the putative CRE associated to *Fcnb* was accessible in HSCs, MPPs, CMPs, GMPs, and GMs (Figure 6D). The T cell specific *Wnt8b* is only expressed in T cells, while its putative CRE is accessible in HSCs, MPPs, CLPs, ProTs, and T cells. (Figure 6E). These findings support that lineage priming observed in HSCs is maintained throughout differentiation for certain CREs. Unexpectedly, most of the peaks primed in HSCs did not exhibit persistent priming in every intermediate progenitor. These observations, combined with the bias in signal and peak counts in progenitors could suggest preferred lineages at specific branchpoints. For example, EP-primed peaks had a high average signal and made up most of the overlapping peaks in MEPs which could suggest that MEPs are biased towards EPs over MkPs, or reinforce fate decisions initiated in upstream progenitors.

HSC-unique peaks indicated an erythropoiesis-primed chromatin state

Because HSCs are the only cell type in the hematopoietic tree that is capable of long-term reconstitution, we reasoned that HSC-unique peaks would be enriched in elements that promote self-renewal and/or engraftment. To test this, we identified and examined HSC-unique peaks **(**Figure 7A**)**. We found 3,026 HSC-unique peaks, 92.7% of which classified as non-promoter **(**Figure 7B**)**. To identify transcription factor motifs enriched within the HSC-unique peaks, we performed *de novo* motif finding and enrichment using the HOMER package and reported the top 10 results sorted by p-value (Figure 7C). ELF3 (E74 Like ETS Transcription Factor 3) was the top ranked motif, followed by CTCFL. There were 3 instances of CTCF-like motifs in the top 10 *de novo* motifs,

while single instances of NF-E2, RUNX, HIC1, Gata6, Foxo1, and IRF4 rounded out the enriched motifs. Next, we annotated the CREs to nearby genes using GREAT. The top GO term was *definitive erythrocyte differentiation* (Figure 7D), *comprised of 14 peaks linked to 4 genes: Ncor1, Tgfbr3, Zfpm1,* and *Smarca4.* All four genes have known roles in hematopoiesis, with knock-out studies presenting severe defects in erythropoiesis, or the entire hematopoietic compartment (Bultman et al., 2005; Chi et al., 2003; Jepsen et al., 2000; Stenvers et al., 2003; Tsang et al., 1998), consistent with important roles in HSCs. We then visualized the ATAC accessibility of three example peaks enriched in the *definitive erythrocyte differentiation* GO term, along with their respective linked motif enrichment (Figure 7E-G**)**. The CRE linked to *Ncor1* contained the NF-E2 and Foxo1 motif (Figure 7E). The CRE linked to *Zfpm1* contained the motif for ELF3 (Figure 7F), while the CRE linked to *Tgfbr3* contained CTCFL and Foxo1 motifs (Figure 7G). Taken together, the unique HSC peaks are enriched for elements that prime erythroid cell fate in HSCs, such as NF-E2 binding sites and the 14 peaks that are linked to *Ncor1, Tgfbr3, Zfpm1,* and *Smarca4, all of which have known roles in erythropoiesis.*

CRISPRi-mediated targeting functionally linked CREs to gene expression

An immediate extension of the chromatin accessibility mapping accomplished in this study is to determine the functional role of putative CREs. Linking regulatory elements to the expression of specific genes is essential for understanding epigenetic regulation of fate decisions, but has proven persistently challenging, in particular in the context of

native chromatin structure of primary, multipotent cells. To begin to tackle this, we employed a new genetic mouse model that ubiquitously express the dCas9-KRAB repressor protein from the safe harbor H11 locus (CRISPRi mouse) (Figure 7H). We isolated hematopoietic stem and progenitor cells (HSPCs) from these CRISPRi mice and first, as proof-of-concept, transduced them with lentivirus expressing a single guide RNA (sgRNA) targeting the promoter of the cell surface protein CD81 (Oguri et al., 2020). HSPCs were cultured under non-differentiation conditions for 2 days, then analyzed for CD81 cell-surface expression by flow cytometry. We observed significant reduction in CD81 expression in HSPCs transduced with CD81 sgRNA compared to a scrambled control sgRNA (Figure 7I), thereby demonstrating efficient and selective gene silencing in HSPCs.

Next, we tested whether CRISPRi targeting initiated in HSCs is maintained upon differentiation into mature cells, and if silencing of putative distal CREs, like promoter-proximal CREs, can repress gene expression. We designed two sgRNAs for both the promoter and a putative CRE of the myeloid-associated cell surface proteins CD115 and CD11b, based on their ATAC peak profiles (Figure 7J) and cloned the top two sgRNAs for each putative CRE into a dual-guide lentiviral vector (Replogle et al., 2020). HSCs from CRISPRi mice were isolated, transduced with the dual-guide lentivirus, and then cultured in a myeloid differentiation media for 5 days before surface expression of CD115 and CD11b was quantified via flow cytometry. As expected, the vast majority of cells infected with scrambled control sgRNAs expressed CD115 (Figure 7K) or CD11b (Figure 7L). We observed a significant reduction in the

frequency of CD115+ cells when HSCs were transduced with sgRNAs targeting either the promoter or putative CRE targeting guides (Figure 7K). Interestingly, we only observed a significant decrease in the frequency of CD11b+ cells with sgRNAs targeting the CD11b promoter, but not the putative CD11b CRE (Figure 7L). These data establish the new CRISPRi mice as a powerful tool for identifying functional CREs based on ATAC-seq peaks. Specifically, we showed that CRISPRi-mediated targeting initiated in HSCs led to selective gene repression upon differentiation into myeloid cells, and that the accessible sequence in the CD115 locus is essential for its expression, whereas targeting of the putative CD11b CRE does not significantly alter CD11b expression under these conditions.

Discussion

Global chromatin accessibility throughout hematopoiesis is highly dynamic

Here, we mapped accessible loci in seven hematopoietic progenitor cell types with distinct functional capacities. Integration of these new data with HSCs and mature progeny revealed epigenetic-based cell clustering into erythromyeloid and lymphoid branches (Figure 4) and robust identification of known regulatory elements (Figure 5). Consistent with previous evidence by us and others that stem cells have relatively decondensed chromatin structure (Lara-Astiaso et al., 2014; Martin et al., 2021; Ugarte et al., 2015; Wang et al., 2015)**,** we found that both the ATAC peak number and cumulative signal was greatest for HSCs (Figure 1). This study advances previous reports by pinpointing the location both of all putative CREs genome-wide in each

population, as well as HSC-specific putative CREs (Figure 7) and those associated with the major erythromyeloid/lymphoid branchpoints (Figures 2 and 3). Importantly, only a subset of HSC peaks remained accessible throughout differentiation, substantially focusing the search for sequences serving as lineage priming elements (Figure 6). Likewise, our CRISPRi experiments demonstrated selective functionality of putative distal CREs in regulating gene expression (Figure 7). Although the models of hematopoiesis and phenotypes of progenitors are constantly reshaped and refined (Challen et al., 2021; Laurenti and Göttgens, 2018), our maps and strategies derived from pre-defined cell types at known branchpoints will serve as valuable resources to identify, characterize, and functionally interrogate *cis* regulatory elements and their roles in gene regulation, stem cell self-renewal, and fate decisions.

Defining differential chromatin accessibility at major lineage branchpoints

Functional studies have suggested that differential epigenetic priming may be evident at major branchpoints (Boyer et al., 2019; Rodriguez-Fraticelli et al., 2018). Indeed, we identified thousands of differential CREs at both the CMP/CLP and MkP/EP branchpoints. We found that HSC/MPP-descendant CLPs had a greater proportion of lost peaks compared to CMPs (Figure 2). Interestingly, though most of the peaks altered were classified as non-promoter, the differential was mainly driven by promoter peak changes, possibly indicating that multipotency priming, but not implementation of non-lymphoid programs, may remain present in CLPs. Emergence of CMPs was associated with significantly less promoter remodeling, loss of accessibility of lymphoid lineage

drivers, and gain of accessibility at negative regulators of lymphoid differentiation (Figures 2C, E and G**).** Further down the erythromyeloid trajectory, MkPs gained significantly more peaks from MEPs compared to EPs, with gained peaks in MkPs and EPs linked to genes important for megakaryopoiesis and erythropoiesis, respectively (Figure 3). In contrast to the CMP/CLP branchpoint, divergence of MkPs versus EPs occurred primarily at non-promoter peaks. Interestingly, specification of both CMPs (compared to CLPs) and EPs (compared to MkPs) entailed significantly reduced proportions of "peaks lost", indicating that relatively larger fractions of CREs were already accessible in their respective progenitor (MPPs and MEPs). This is consistent with strong erythroid priming in HSCs (also see below) and the predominant erythroid cell production observed in quantitative functional assays (Boyer et al 2019). Collectively, the differential priming throughout differentiation uncovered here and previously (Heuston et al., 2018; Martin et al., 2021) is now available for functional testing by CRISPRi or analogous strategies to determine the CREs and chromatin remodeling events required for balanced hematopoiesis.

Lineage priming was selectively maintained throughout differentiation

Our previous study identified CREs that were exclusively shared between unipotent lineage cells and HSCs (Martin et al., 2021). Here, we found that a limited subset of those primed CREs maintained accessibility throughout differentiation in intermediate progenitors (Figure 6). Lineage priming was also detected at the b-globin locus, where the strongest enhancer, HS2, was primed in HSCs and MPPs, with additional

accessibility of HS1 and HS4 in CMPs, and then also HS3 and HS6 in MEPs and EPs **(**Figure 5**).** The global enrichment of peaks within the intermediate progenitors reflected the distinct bifurcation found in hematopoiesis, with erythromyeloid-primed peaks enriched in erythromyeloid progenitors and lymphoid-primed peaks enriched in lymphoid progenitors. Surprisingly, CLPs did not significantly deviate from the distribution of peaks in HSCs and MPPs (Figure 6B), potentially indicating "inherited" priming that is not implemented *in vivo* (Schlenner et al., 2010) but can be reignited in vitro (Karsunky et al., 2003). We also tracked the accessibility of the primed peaks throughout differentiation and found that the majority of peaks do not maintain accessibility in every intermediate progenitor throughout differentiation (Figure 6C,D). Collectively, these findings provide insight into the dynamics of CRE accessibility throughout differentiation and support a model where lineage priming in HSCs guides lineage competence during differentiation, while the gain and loss of accessibility at certain intermediate progenitors could regulate or reinforce differentiation in specific lineages.

HSC-unique peaks were highly enriched for CREs that drive erythroid differentiation

While HSCs are capable of producing all blood cell lineages, several studies have suggested lineage-specific priming within HSCs (Boyer et al., 2019; Carrelha et al., 2018; Ema et al., 2014; Yamamoto et al., 2013, 2018). From these studies we hypothesized that CREs within HSCs would uncover drivers of erythro- and/or megakaryopoiesis. Our GREAT analysis of HSC-unique peaks revealed "definitive

erythrocyte differentiation" as the top GO-Biological Process hit (Figure 7D), and we observed HSC-specific accessibility in the CREs linked to genes that have known roles in erythropoiesis (Figure 7E-G). Furthermore, we observed *de novo* enrichment of transcription factor motifs in the HSC-unique peaks that are known to be key regulators of hematopoiesis, such as NF-E2 and Runx (Gasiorek et al., 2012; Shivdasani and Orkin, 1995; Willcockson et al., 2019). This suggests that establishment of developmental competence for erythropoiesis in HSCs may occur primarily in CREs that are uniquely accessible in HSCs.

In summary, we present evidence that multilineage priming is present in HSCs and selectively maintained, or repressed, throughout differentiation. In addition, the observation that HSCs harbor the most ATAC-seq peaks of all hematopoietic cell types (Figure 1) is consistent with previous findings that linked multipotency with global epigenetic regulation and the presence of poised loci that are distal to promoters in stem cells (Lara-Astiaso et al., 2014; Ugarte et al., 2015; Wang et al., 2015). We also found that accessibility, especially of distal CREs, is highly dynamic, and that some, but not all, serve as functional CREs (Figure 7I-L). Our results provide insight to how lineage fate is reinforced at branchpoints through the collective action of specific transcription factors at these CREs. Future investigations using CRISPR-based technologies paired with *in vivo* methods (Rodriguez y Baena et al., 2021; Worthington and Forsberg, 2022, Figure 7I-L) will allow us to determine which of these CREs are a consequence of differentiation and which elements drive differentiation into specific fates.

Experimental Procedures

Mice and Cells

All experiments were performed using 8- to 12-week-old C57BL/6 wild-type mice in accordance with UCSC IACUC guidelines. Hematopoietic stem, progenitor and mature cells were isolated from BM of murine femurs, tibias, hips, and sternums as previously described (Boyer et al., 2011; Poscablo et al., 2021; Rodriguez y Baena et al., 2022; Worthington et al., 2022). Stem and progenitor cell fractions were enriched using cKit-coupled magnetic beads (Miltenyi). Cells were stained with unconjugated lineage rat antibodies (CD3, CD4, CD5, CD8, B220, Gr1, Mac1, and Ter119) followed by goat-α-rat PE-Cy5 (Invitrogen). Stem and progenitor cells were isolated using fluorescently labeled or biotinylated antibodies for the following antigens: cKit (2B8, Biolegend), Sca1 (D7, Biolegend), Slamf1 (CD150) (TC15-12F12.2, Biolegend), CD34 (RAM34, ebiosciences), FcγrII (93, Biolegend), and Il7rα (A7R34, Biolegend). Cells were sorted by Fluorescence-Activated Cell Sorting (FACS) with a target of 50,000 cells per cell type using a FACS Aria II (BD Bioscience). HSCs were defined as $cKit^+$ Lin^- $Sca1^+$ $Flk2^-$ and $Slamf1^+$; MPPs as $cKit^+Lin^-Sca1^+$ $Flk2^+$ $Slamf1^-$ cells. CMPs were defined as $cKit^+Lin^-Sca1^-$ $CD34^{mid}$ $Fc\gamma rII^{mid}$; GMPs as $cKit^+Lin^-Sca1^-$ $CD34^{mid}$ $Fc\gamma rII^{high}$, MEPs as $cKit^+Lin^-Sca1^-$ $CD34^{low}$ $Fc\gamma rII^{low}$. CLPs were isolated by lineage depleting BM cells through staining of unconjugated lineage rat antibodies (CD3, CD4, CD5, CD8, B220, Gr1, Mac1, and Ter119) followed by sheep-α-rat Dynabeads (Life Technologies) and separation via EasySep magnet (Stem Cell Technologies). CLPs were isolated by Lin^- $Flk2^+$ $Il7r\alpha^+$ $cKit^{mid}$ $Sca1^{mid}$. Lineage restricted hematopoietic progenitor and mature

cells were isolated by the following markers: EPs, Lin(CD3, CD4, CD5, CD8, B220, Gr1, and Mac1)$^{-}$CD71^{+}Ter119$^{+/-}$; GMs, Lin(CD3, CD4, CD5, CD8, B220, and Ter119)$^{-}$Gr1^{+}Mac1^{+} ("GM" cells were positive for both Gr1 and Mac1); T-progenitors (ProT), Lin(CD5, B220, Gr1, Mac1, and Ter119)$^{-}$CD3^{+}CD25^{+}; T cells, Lin(CD5, B220, Gr1, Mac1, and Ter119)$^{-}$CD25^{-}CD3^{+}CD4$^{+/-}$CD8$^{+/-}$; B-progenitors (ProB), Lin(CD3, CD4, CD8, Gr1, Mac1, and Ter119)$^{-}$CD43^{+}B220^{+}; B cells, Lin(CD3, CD4, CD8, Gr1, Mac1, and Ter119)$^{-}$CD43^{-}B220^{+}.

CRISPRi mice were generated by site-specific integration of CAG promoter-driven sequences for nuclease-deficient Cas9 protein (dCas9) fused to a zinc-finger protein 10 (ZNF10) Krüppel-Associated Box (KRAB) domain. The expression cassette was inserted into the H11 safe harbor locus of C57BL/6J mice using a site-specific integrase-mediated method (Tasic et al., 2011). The resulting CRISPRi mouse is similar to a previously generated CRISPRi mouse (Oguri et al., 2020), but lacks the mCherry and Puro resistance genes.

ATAC-seq

ATAC-seq was performed as previously described (Buenrostro et al., 2013). Briefly, cells were collected after sorting into microcentrifuge tubes, and centrifuged at 500xg for 5 minutes at 4˚C to pellet the cells. The supernatant was aspirated, and the cells were washed with ice-cold 1xDPBS. Cells were centrifuged and the supernatant was discarded. Cells were immediately resuspended in ice-cold lysis buffer (10 mM Tris-

HCl, pH 7.4, 10 mM NaCl, 3 mM MgCl2 and 0.1% IGEPAL CA-630) and centrifuged at 500xg for 10 minutes. The supernatant was aspirated, and pellets were resuspended in transposase reaction mix (25µL 2xTD Buffer, 2.5µL transposase (Illumina), and 22.5µL nuclease free water). The transposition reaction was carried out at 37˚C for 30 minutes at 600rpm in a shaking thermomixer (Eppendorf). Immediately after completion of the transposition reaction, the samples were purified using the MinElute Reaction Clean up kit (Qiagen) and eluted into 10 µL of EB. Samples were stored at -20˚C until PCR amplification step. PCR amplification was performed as previously described (Buenrostro et al., 2013) using custom Nextera primers. After initial amplification (5 cycles), a portion of the samples were run on qPCR (ViiA7 Applied Biosystems) to determine the additional number of cycles needed for each library (typically 5-8 cycles). The libraries were purified using the MinElute Reaction Clean up kit (Qiagen), eluted into 20 µL EB and then size selected using AmpureXP (Beckman-Coulter) beads at a ratio of 1.8:1 beads/sample, and eluted into 40µL of nuclease-free water. Library size distribution was determined by Bioanalyzer (Agilent) capillary electrophoresis and library concentration was determined by Qubit 3 (Life Technologies). Quality of libraries were checked by shallow sequencing (1 million raw reads) on a Miseq (Illumina) at 75 x 75 paired-end sequencing. Those libraries that appeared to have size distributions similar to previous reports were pooled together and deep sequenced on a HiSeq2500 (Illumina) at 100 x 100 reads at the Vincent J. Coates Genomics Sequencing Laboratory at UC Berkeley.

Data processing

Demultiplexed sequencing data was processed using the ENCODE ATAC-seq pipeline version 1.1.6 and 1.4.2 (https://github.com/ENCODE-DCC/atac-seq-pipeline) using the mm10 assembly and the default parameters. In version 1.4.2 changed: atac.multimapping=0, atac.smooth_win=150, atac.enable_idr=true, atac.idr_thresh=0.1 to be consistent with the mapping/peak calling performed with previous versions.

Peak filtering and hierarchical clustering was performed using the chromVAR package (https://github.com/GreenleafLab/chromVAR). First, the optimal peak-list from the IDR output for each cell type was concatenated and sorted, then used as the peak input for chromVAR. The blacklist filtered bam files for each replicate (n=2 for each cell type) was used as input along with the sorted peak file. The fragment counts in each peak for each replicate and GC bias was calculated, and then the peaks were filtered using filterPeaks function with the default parameters and nonoverlapping=TRUE. The master peak-list was extracted at this point, which contained 92,842 peaks, and used throughout the study. The deviations were calculated using every peak, and the tSNE and correlation functions were also performed using the deviations output and the default parameters.

Normalized chromVAR counts were log+1 scaled, centered, and filtered to peaks that had above-median coefficient of variance. These filtered counts were use in principal component analysis (PCA) with the R package *prcomp*. Following this, the resulting

components were used to calculate UMAP dimensions using the R package *uwot*. The component values were plotted using the R package *ggplot2*.

We noted that although showing strong similarity by PCA (Figure 4A) and designating to the same main cluster by hierarchical clustering (Figure 4C), the two HSC samples were the only replicate pair not localized immediately adjacent to each other. Analysis of additional HSC ATAC-seq samples did not resolve the hierarchical clustering in a meaningful way, as the results were similar with regards to intermixing within other cell types and failed to pinpoint one of the original HSC samples as an outlier.

Annotation of peaks, generation of histogram plot, merging of peaks, and motif enrichment was performed by HOMER (http://homer.ucsd.edu/homer/). Peaks were annotated using the annotatePeaks.pl function with the mm10 assembly and default parameters. Histogram was created by first shifting the bam files using DeepTools alignmentSieve.py with the flag –ATACshift. Next, tag directories were made using the Tn5 shifted bam files using HOMER makeTagDirectory. The histogram was made using the annotatePeaks.pl function with the default settings and the flags: -size -500,500 and -hist 5. Peak lists were compared using the mergePeaks.pl function with default settings and the flags -d given, -venn, and for the unique peak lists -prefix. Motif enrichment was performed using the findMotifsGenome.pl package with default parameters using the flag -size given.

The GREAT tool (http://great.stanford.edu/public/html/) was used to annotate non-promoter peaks to target genes. The peak lists were reduced to BED4 files from the HOMER annotations output and used as input. The whole mm10 genome was used as

the background regions, and the association rule settings were set as Basal plus extension, proximal window 2kb upstream, 1kb downstream, plus distal up to 1Mb and included curated regulatory domains. All genome track visualizations were made using the UCSC genome browser. Statistical analysis was performed using GraphPad Prism 9. Graphs were made in either Microsoft Excel or GraphPad Prism 9. Annotations to figures was performed using Adobe Illustrator CC and Adobe Photoshop CC.

CRISPRi experiments

Single guide RNA (sgRNA) sequence targeting CD81 was from (Oguri et al., 2020). Dual targeting sgRNAs for promoter regions were non-overlapping guide sequences from previously published libraries (Horlbeck et al., 2016). The dual sgRNAs for candidate CREs were designed by generating a 200bp window centered on the peak summit and inputting those coordinates into the CRISPOR tool (Concordet and Haeussler, 2018; Haeussler et al., 2016). The top two non-overlapping guides were selected and cloned into pJR85 (Addgene plasmid #140095) (Replogle et al., 2020). psPAX2 (Addgene plasmid #12260) and pMD2.G (Addgene plasmid # 12259) were combined with pJR85 and transfected into 293T cells by Lipofectamine 2000. 72 hours after transfection, the supernatant was collected, 0.45 µ filtered, and concentrated by PEG precipitation. Concentrated lentivirus was resuspended in a minimal volume of Optimem.

HSPCs (Lin-, cKit+, Sca+ BM cells) or HSCs (Lin-, cKit+, Sca+, SLAM mid-hi, Flk2-) from CRISPRi mice were FACS isolated and plated at 6,000 cells/well (CD81) or 200 cells/well (CD11b/CD115) in either HSC minimal media (IMDM; TPO 50 ng/mL; SCF 50 ng/mL; Polybrene 5 ug/mL) or HSC maintenance media (IMDM; 20% FBS; TPO 50ng/mL; SCF 50 ng/mL; IL-6 20ng/mL; IL-3 10 ng/mL, IL-11 20 ng/mL, Primocin, Non-Essential Amino Acids) . After 24 hours in culture, lentivirus containing sgRNAs was added to each well and spinoculated for 1 hour, 400xg at 32˚C. 24 hours later, virus was washed out and the media was changed into HSC minimal media (CD81) or to a myeloid differentiation media (CD11b/CD115) (Forsberg et al., 2006) and cells were allowed to expand in culture for 2 days (CD81) or 5 days (CD11b/CD11b) before analysis by flow cytometry.

List of sgRNAs used:

CD81 Promoter	ATGAGACGTAGGGTAGAGAA
CD115 Promoter 1	GAGCGTGAGCCGATGCAGGT
CD115 Promoter 2	GCCGATGCAGGTTGGAGAGT
CD11b Promoter 1	GCTTCTGGTCACAGGTATGT
CD11b Promoter 2	GGTAGGTGGGGAGAGATCAA
CD115 Enhancer 1	GTGAGAGCCCAAGTGTCGAA
CD115 Enhancer 2	CAATGTGTTTCCGCCCACAC
CD11b Enhancer 1	AGTTGTCTATATCCGCTGTG

CD11b Enhancer 2	GGTCTGAATCACTAAAGATA
Scrambled Control (for CD81 expts.)	GTCCATACGCATAATCACCG
Scrambled Control 1 (for CD115/CD11b expts.)	CTGTGCAATCCGCATGATAT
Scrambled Control 2 (for CD115/CD11b expts.)	ATCTGGCACCTCACCCACGT

Data availability

The datasets generated in the current study are available in the Gene Expression Omnibus (GEO), accession number GSE184851, reviewer token **mpinagaaxxoffyt**. The exclusively primed peaks are provided as Supplemental Tables 1-6. Previously published datasets are available at GSE162949. Signal tracks and called peaks for all 13 cell types are available as a custom session on the UCSC genome browser at: https://genome.ucsc.edu/s/ewmartin/atac_bw_mean_allpeaks

Acknowledgements

We thank Bari Nazario and the IBSC flow cytometry core (RRID:SCR_021149) for assistance and support; Sol Katzman for bioinformatic assistance; Joseph Replogle, Angela Pogson and Jonathan Weissman for CRISPRi vectors and advice, and Forsberg lab members for comments on the manuscript. This work was supported by NIH/NHLBI (R01HL115158), NIDDK (R01DK100917) and NIA (R01AG062879) awards to E.C.F.; by NIH/NHLBI fellowship (F31HL144115) to E.W.M.; by CIRM

SCILL grant TB1-01195 to E.W.M. via San Jose State University; by CIRM Training grant TG2-01157 to J.K.; by a UCSC Genomic Sciences Graduate Training Program from NIH/NHGRI (NIH T32 HG008345) and an F99 (5F99DK131504-02) to R.E.R., by a Tobacco-Related Disease Research Program (TRDRP) predoctoral award to A.R.y.B. (T31DT1690); by an NIH T32 Training Grant (T32GM8646), a TRDRP predoctoral award (T30DT0878) and NHLBI F31 predoctoral award (F31HL151199) to A.K.W., by an NIH IMSD Training Grant (R25GM058903), an American Heart Association Predoctoral Fellowship Award, and Howard Hughes Medical Institute Gilliam fellowships to D.M.P.; by the Baskin School of Engineering and the Ken and Glory Levy Fund for RNA Biology to D.H.K., and by CIRM Shared Stem Cell Facilities (CL1-00506) and CIRM Major Facilities (FA1-00617-1) awards to the University of California, Santa Cruz.

Figures

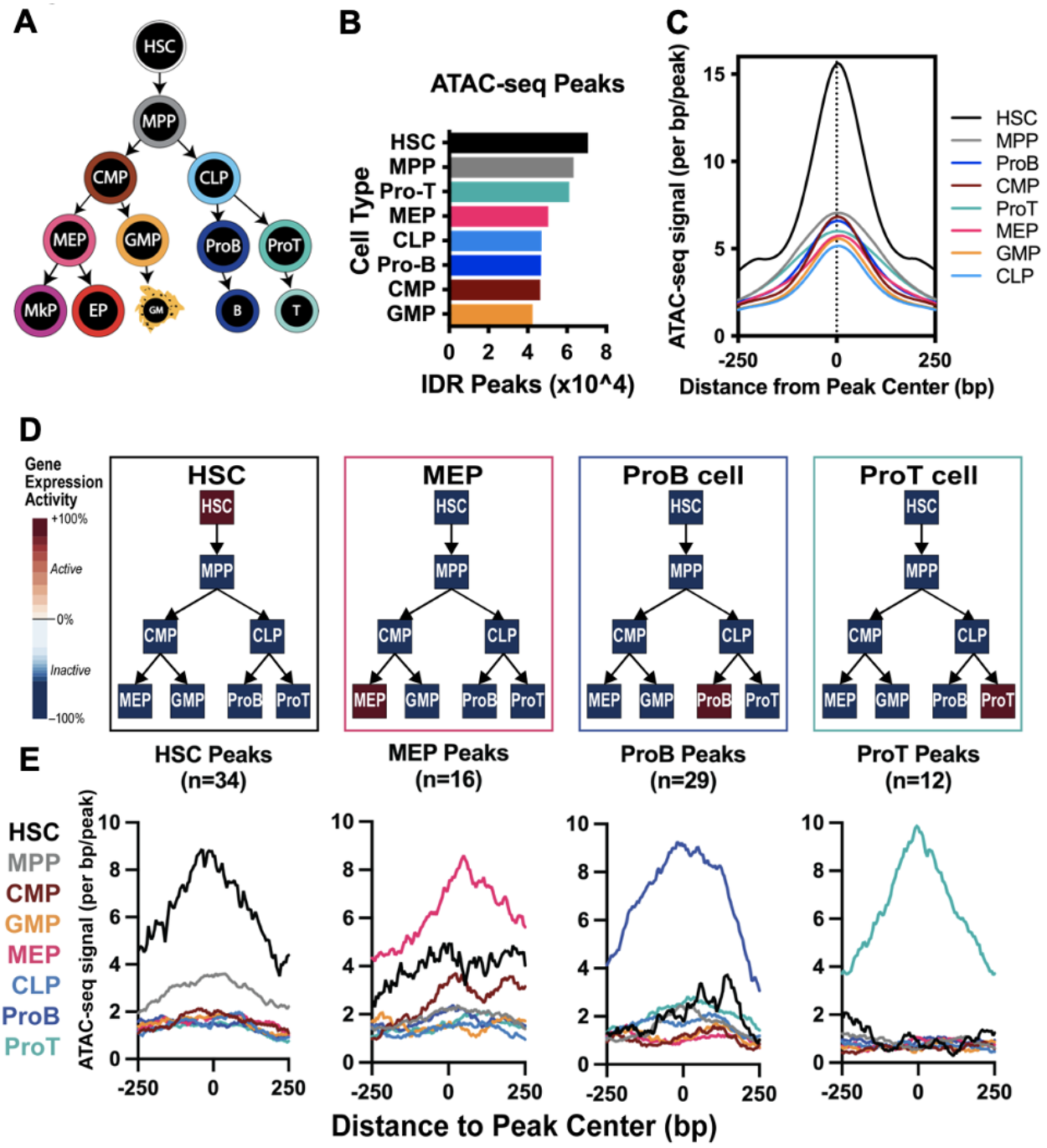

Figure 6.1 ATAC-seq analysis of hematopoietic progenitor cell populations revealed progressive and lineage-specific chromatin condensation.

A) Schematic diagram of the hematopoietic cells analyzed in this study. Thirteen cell populations were investigated: multipotent HSCs (Hematopoietic Stem Cells) and MPPs (Multipotent Progenitors); lineage-restricted/oligopotent CMPs (Common Myeloid Progenitors), CLPs (Common Lymphoid Progenitors), GMPs (Granulocyte Macrophage Progenitors), MEPs (Megakaryocyte Erythrocyte Progenitors); unilineage MkPs (Megakaryocyte Progenitors), EPs (Erythroid Progenitors), ProBs (B cell Progenitors), ProTs (T cell Progenitors), and mature GMs (Granulocyte/Macrophages), B cells, and T cells. ATAC-seq profiles for HSCs and unilineage MkPs, EPs, GMs, B and T cells were reported previously (Martin et al., 2021); data were integrated in selective analyses of the new data for intermediate progenitors for a comprehensive perspective of hematopoiesis.
B) HSCs had the highest number of peaks of all hematopoietic progenitor cell types. The total number of Irreproducible Discovery Rate (IDR) peaks per cell type are displayed. HSCs had the highest number of peaks, followed by MPPs and then lineage-committed progenitors.
C) HSCs had the highest average signal across all peaks. Average cumulative signal across the peak-list for each population was determined by the -hist function of HOMER annotatePeaks.pl. Multipotent HSCs and MPPs had the highest average peak signal, whereas lineage-restricted progenitors had overall lower signal.
D) Lineage-specific gene expression patterns used to find examples of genes selectively expressed within each indicated cell type. The level of expression (red=high; blue=low/not expressed) was obtained from the Gene Expression Commons (GEXC) database.
E) Promoter accessibility correlated with cell type-specific gene expression in the corresponding progenitor cell types. Plots depict HOMER histograms of the average cumulative signal across the cell type-specific promoters for HSCs (34 peaks), MEPs (16 peaks), ProBs (29 peaks), and ProTs (12 peaks). MPPs, CMPs, GMPs, and CLPs were not displayed as each of these populations had fewer than 10 promoter peaks of uniquely expressed gene

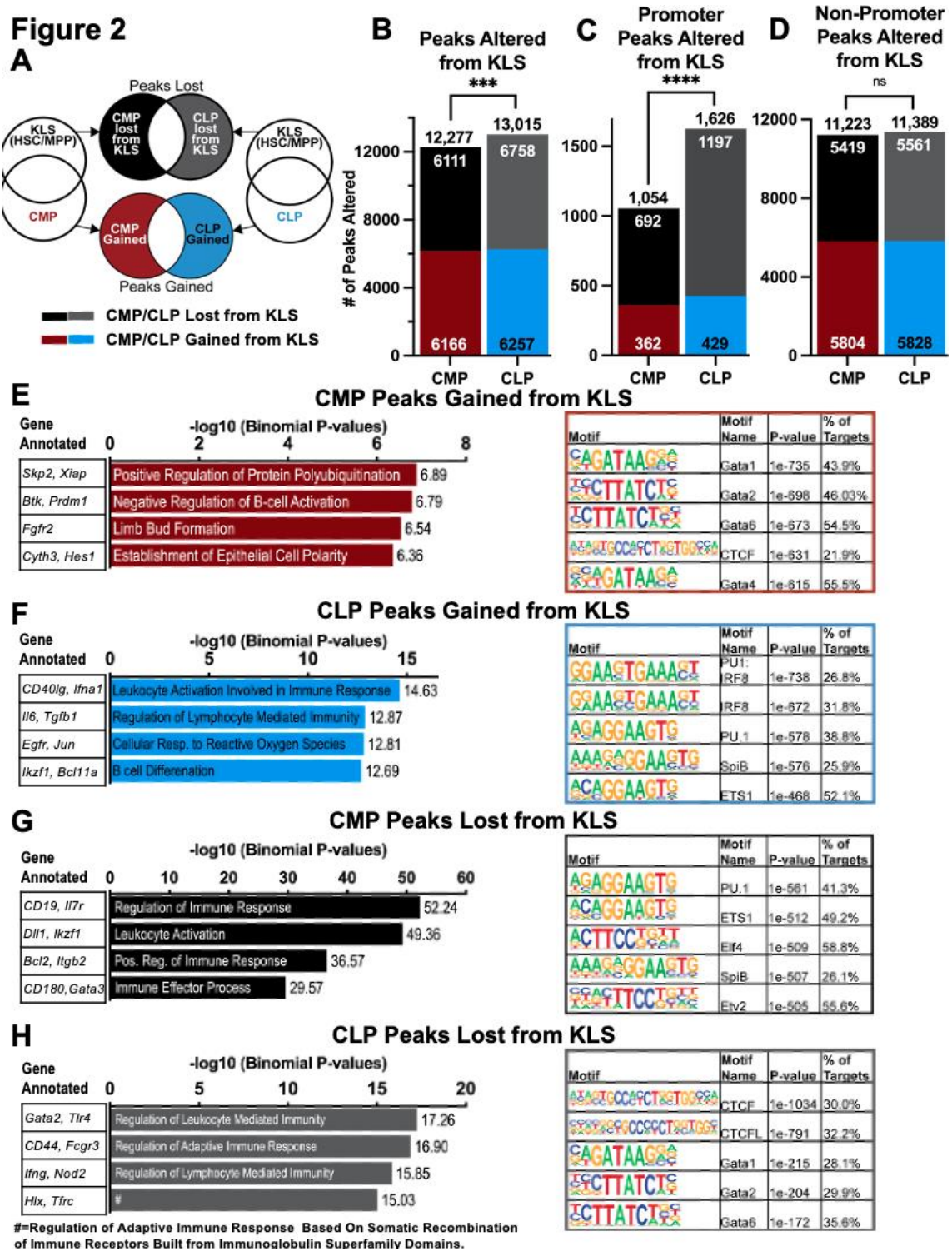

Figure 6.2 Comparisons of peak dynamics as multipotent HSCs and MPPs differentiate into CMPs or CLPs revealed quantitatively differential gain and loss of accessibility.

A) Schematic of the comparisons made between multipotent HSCs and MPPs (ckit+Lin-Sca1+; KLS) to lymphoid- or erythromyeloid-committed CLPs or CMPs. First, the peaks from HSCs and MPPs were combined using *bedtools merge* and then compared to CLPs or CMPs. The altered peak lists from the CMP and CLP comparisons were then intersected against each other to generate CMP- or CLP-specific peaks that were either gained or lost from KLS.
B-D) CLPs had more peak alterations than CMPs. The number of peaks gained and lost in each cell type are displayed. Compared to CMPs, CLPs had more total number of peaks gained/lost **(B)**, promoter peaks altered **(C)**, and similar numbers of non-promoter peaks altered **(D)**. The distribution of peaks between CMPs and CLPs was significant by Chi-square for the total number of peaks **(B)** (*** $p < 0.001$) and promoter peaks **(C)** (**** $p < 0.0001$); and not significant for non-promoter peaks **(D)** ($p = 0.42$).
E-H) Cis-regulatory element analysis, GO term enrichment, and motif enrichment of the peaks that were altered between KLS and CLPs or CMPs, along with example target genes from each GO term. Briefly, each list of altered peaks was submitted to GREAT using the basal extension function with a parameter of 2kb upstream, 1kb downstream, and up to 1Mb extension. Example genes were extracted from the region-target association table for each GO term. The top 5 enriched known motifs from HOMER and corresponding transcription factors were also reported.
E) GREAT analysis of CMP-gained peaks contained the GO term "Negative Regulation of B cell Activation", and were enriched for motifs of Gata transcription factors. **F)** Peaks gained by CLPs were primarily enriched in immune cell activation GO terms, with "Leukocyte Activation Involved in Immune Response" as the top hit. Peaks were enriched for motifs of ETS factor ETS1, as well as known lymphoid drivers IRF8 and SpiB. **G)** CMP peaks that were lost from KLS cells all relate to immune cell processes, and were enriched with motifs for ETS factors and SpiB, similar to the peaks gained by CLPs. **H)** CLP peaks lost from KLS contained GO terms that were immune related, such as "Regulation of Leukocyte Mediated Immunity" with *Gata2* and *Tlr4* as example genes. The peaks were enriched for Gata and CTCF/CTCFL transcription factor motifs. # the full title of this GO term is "Regulation of Adaptive Immune Response Based On Somatic Recombination of Immune Receptors Built from Immunoglobulin Superfamily Domains".

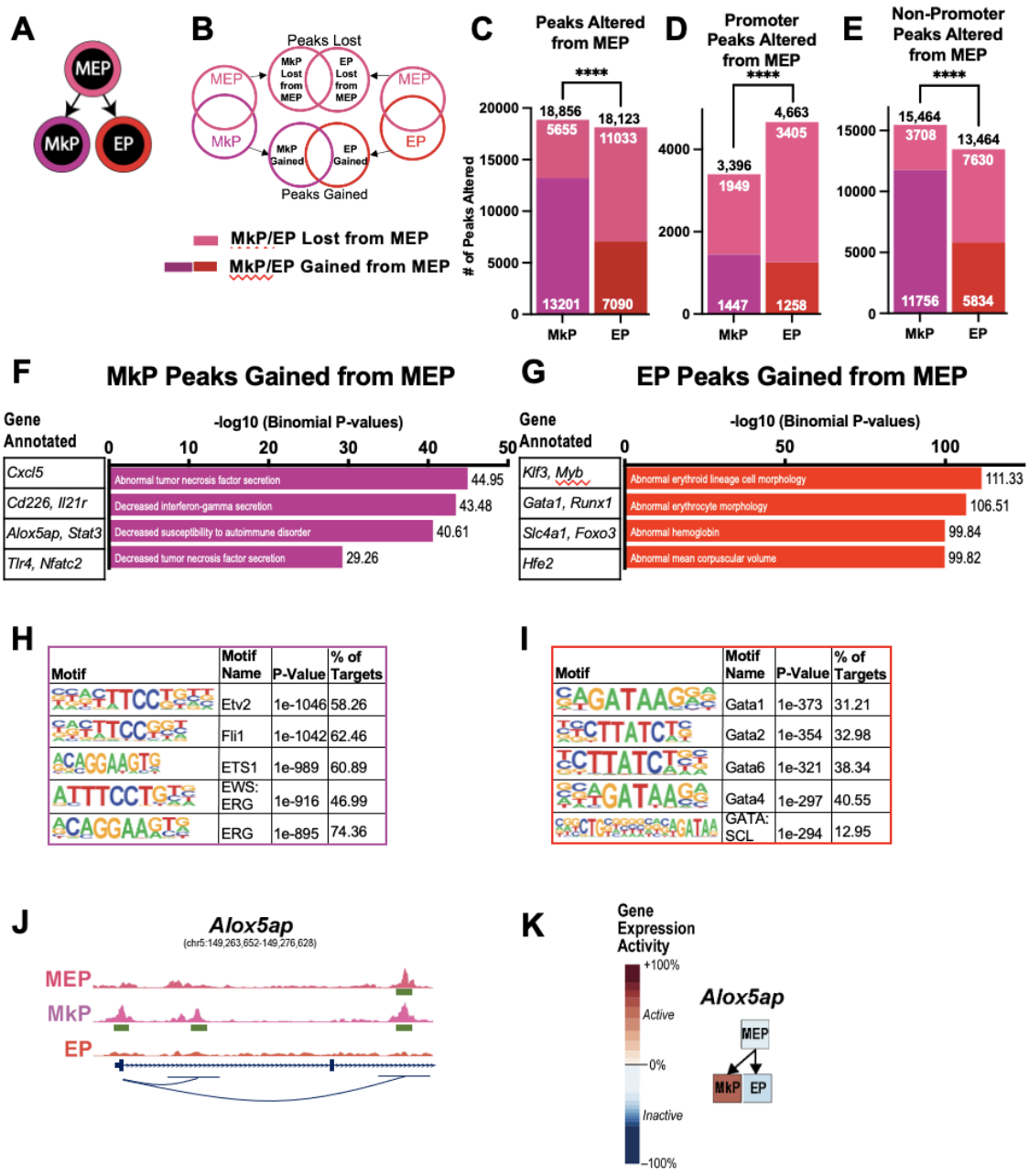

Figure 6.3. Comparison of peak dynamics as MEPs differentiate into MkPs or EPs revealed more gain of chromatin accessibility in MkPs and more loss in EPs.

A) Schematic of the differentiation branch analyzed for this figure, where MEPs differentiate into either MkPs or EPs.
B) Schematic of the comparisons made between MEPs and MkPs or EPs, similar to Figure 2A. The peak profile of MEPs was compared to MkPs and EPs to assess which peaks were uniquely altered (gained or lost from MEPs) by MkPs or EPs during differentiation.

C-E) MkPs and EPs had a similar number of peaks altered. The number of peaks gained (purple for MkPs and red for EPs) and lost (pink) in each cell type are also displayed. **D)** Compared to EP, MkPs had a lower number of promoter peaks altered with a greater percentage of promoter peaks gained and **(E)** a greater number of non-promoter peaks gained. The distribution of peaks between MkPs and EPs was significantly different by Chi-square for **(C-E)** (**** $p < 0.0001$).
(F-G) The lists of peaks gained from MEPs for each cell type were submitted to GREAT for functional annotation. The top 4 over-represented categories in Mouse Phenotype are reported, containing information about genotype-phenotype associations. Examples genes with known roles in MkPs (and/or platelets/megakaryopoiesis) or EPs (and/or red blood cells/erythropoiesis) were extracted from the term's genomic region-gene association tables. **(F)** The MkP gained peaks were enriched for genes whose alterations generate phenotypes related to inflammation. **(G)** The EP gained peaks were enriched for genes whose alterations generate phenotypes related erythroid cell lineage, function, and morphology.
(H-I) Motif enrichment analysis by HOMER was performed on the lists of peaks gained from MEPs for each cell type and the top 5 transcription factor motifs were reported. **(H)** Peaks gained in MkPs were enriched for transcription factors known to be key players in the megakaryocytic lineage, such as Fli-1 and Erg. **(I)** Peaks gained in EPs were enriched for transcription factors required for erythropoiesis, including various Gata family members.
(J-K) Example gene extracted from the lists of gained peaks in MkPs: Alox5ap. **(J)** ATAC-seq signal tracks for MEPs, MkPs, and EPs at the Alox5ap locus (12,000 bps shown). Peaks highlighted by green boxes represent called peaks by IDR at the promoter and putative enhancers for Alox5ap. **(K)** GEXC expression data reported high expression of Alox5ap in MkPs but not in MEPs or EPs.

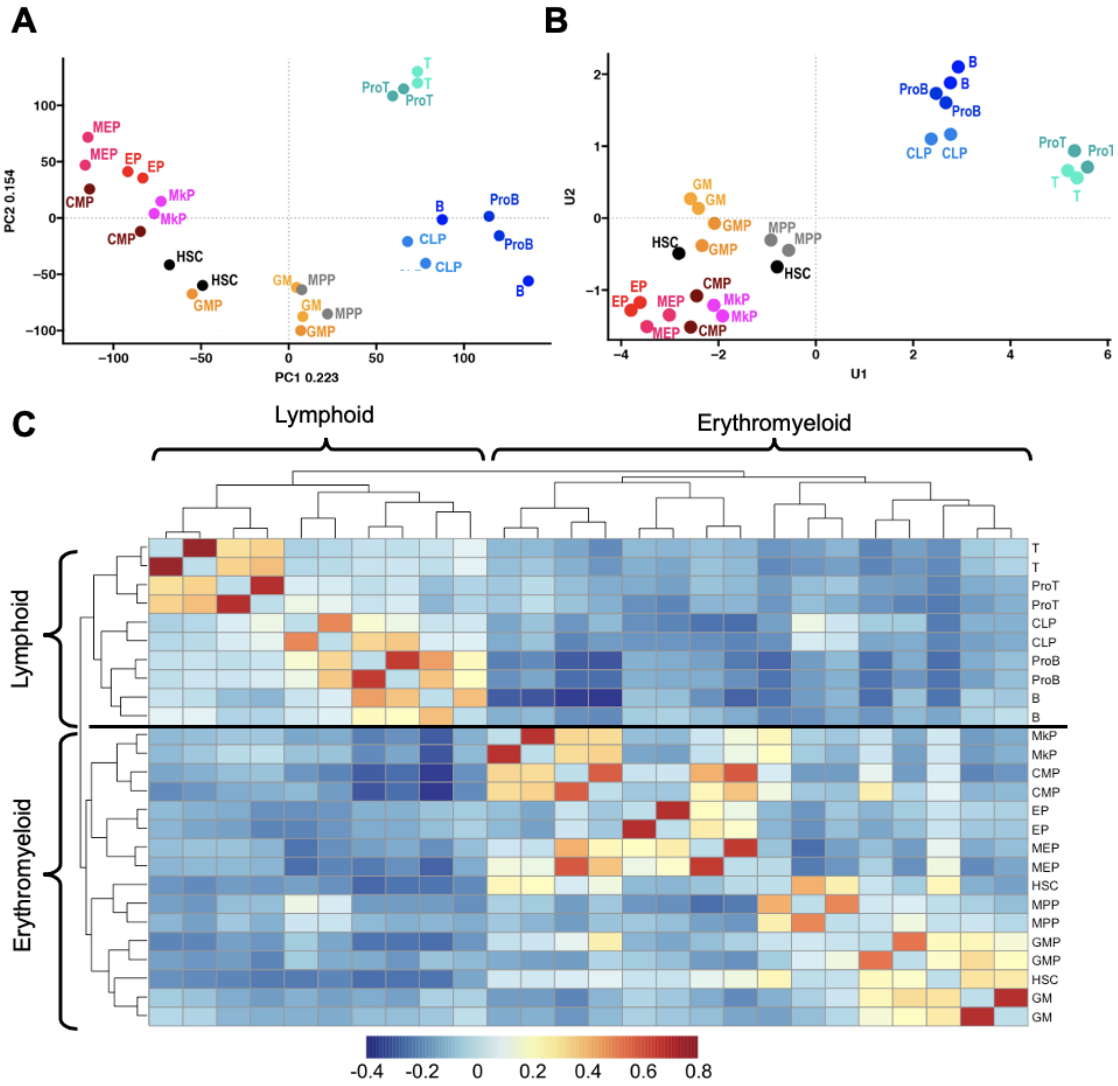

Figure 6.4 ATAC-seq maps of hematopoietic cell populations revealed distinct erythromyeloid and lymphoid clusters.

A) Principal Component Analysis (PCA) of chromVAR-normalized ATAC-seq peak counts revealed high concordance of replicates, and distinct erythromyeloid and lymphoid quadrants. Percent of total variance explained by each component are displayed on respective axes.
B) Uniform Manifold Approximation and Projection (UMAP) using components derived from PCA generated distinct erythromyeloid and lymphoid clusters with the multipotent HSCs and MPPs associated with the erythromyeloid quadrant, similar to the PCA.
C) Hierarchical clustering of all 13 cell types revealed high concordance of replicates and distinct clusters consistent with classical models of hematopoiesis (Figure 1A). Two primary associations were revealed: one erythromyeloid cluster and one lymphoid

cluster. Multipotent HSCs and MPPs were designated to the erythromyeloid cluster. Additionally, there were four distinct sub-clusters: MkPs with CMPs; MEPs with EPs; ProBs with B cells and CLPs; and ProTs with T cells.

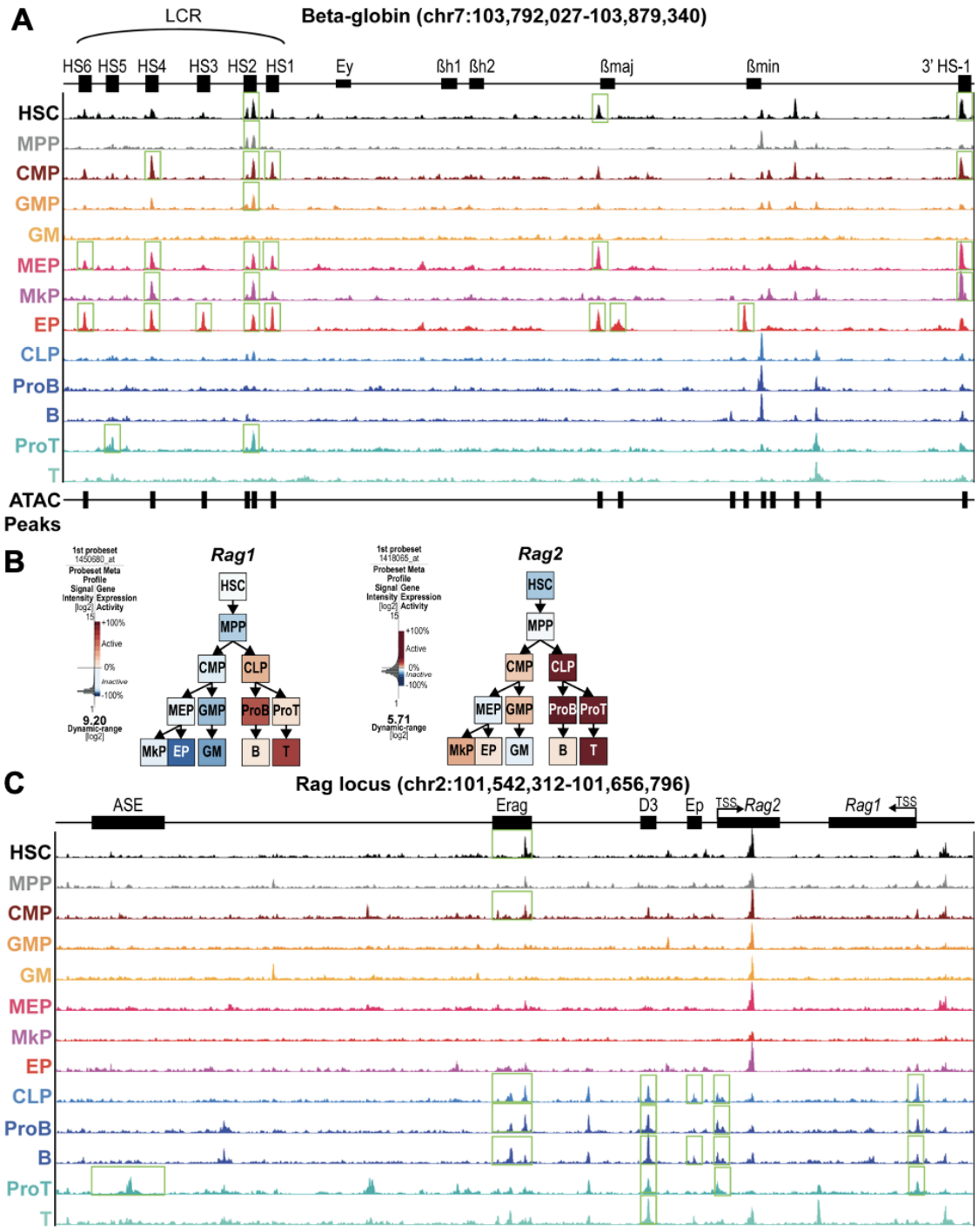

Figure 6.5 Accessibility correlated with known regulatory elements of well-characterized cell type-specific genes.

A) Chromatin accessibility of the b-globin locus revealed expression-selective patterns at known *cis*-regulatory elements (CREs). ATAC-seq signal tracks at the b-globin cluster (chr7: 103,792,027-103,879,340; mm10) of the thirteen cell types are shown.

Peaks highlighted by green boxes represent called peaks by Irreproducible Discovery Rate (IDR) at known CREs for each cell type.
B) Lymphoid-selective expression of *Rag1* and *Rag2*. GEXC expression data reported expression of *Recombination activating gene 1 (Rag1*) and *Recombination activating gene 2 (Rag2*) in CLPs, ProBs, ProTs, B, and T cells. *Rag2* expression in non-lymphoid cell types (CMPs, GMPs, MkPs, and EPs) is due to the *Iftap* promoter on the opposite strand of the *Rag* genes in the second intron of *Rag2* (Laszkiewicz et al., 2012).
C) Lymphoid-selective accessibility of the *Rag* locus. ATAC-seq signal tracks of the thirteen cell types in this study at the lymphoid-selective *Rag* gene locus (chr2: 101,542,312-101,656,796; mm10). The *Rag* gene locus consists of four previously characterized CREs (Ep, D3, Erag, ASE) and the gene bodies for *Rag1* and *Rag2*. The promoter for both *Rag1* and *Rag2* had accessibility only in lymphoid cell types (CLPs, ProBs, B cells, ProTs, and T cells). The lymphoid specific D3 CRE had expected lymphoid-only accessibility, and the B cell specific CREs Ep and Erag had accessibility only in CLPs, ProBs, and B cells. The T cell development specific anti-silencing element (ASE) only exhibited accessibility in ProT cells.

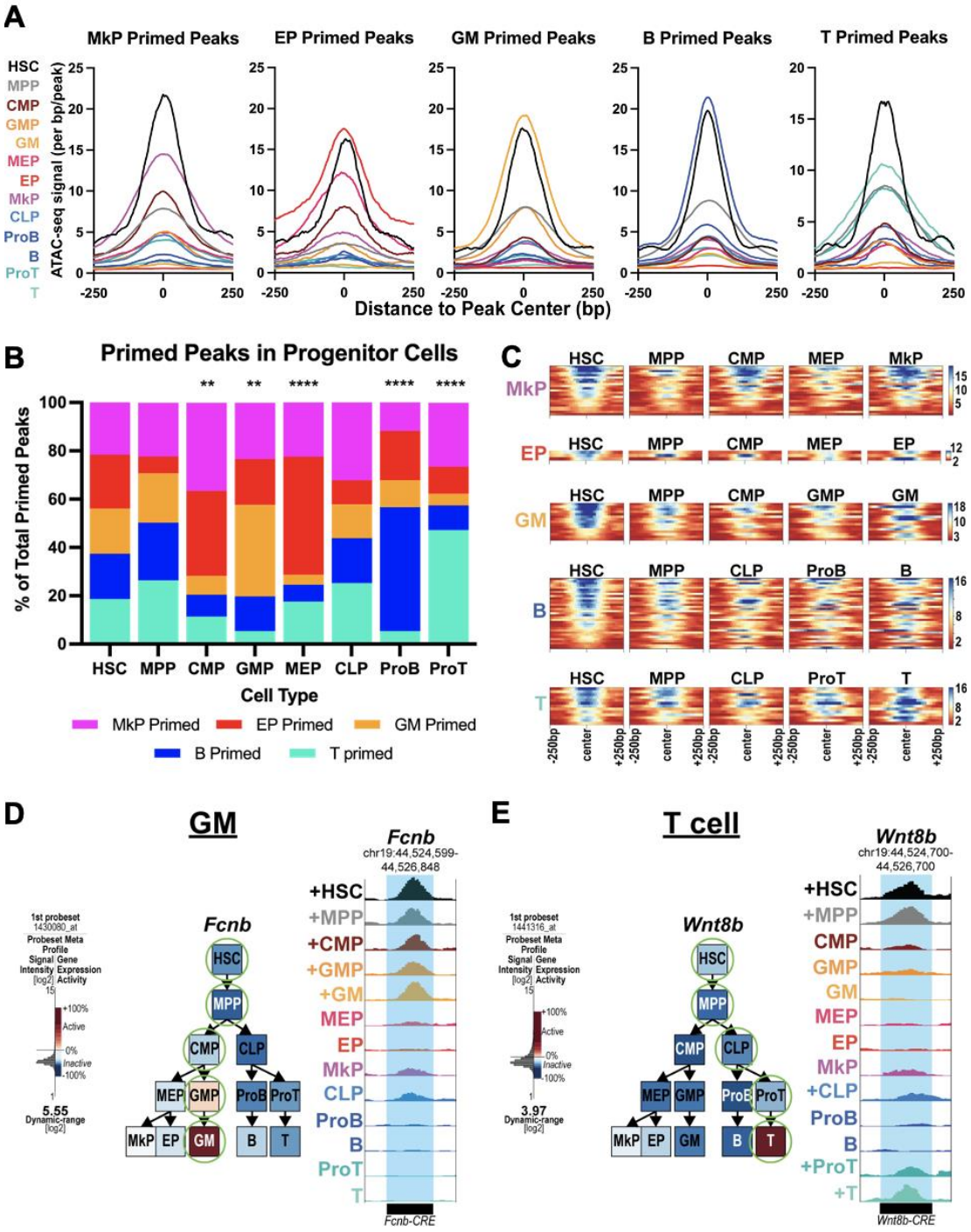

Figure 6.6. CREs of lineage-specific genes primed in HSCs also displayed accessibility in progenitors.

A) Lineage-specific peaks primed in HSCs also displayed selective enrichment in intermediate progenitors. HOMER histograms of the average cumulative accessibility

in each of the 13 cell types in each lineage-primed peak-list. MkP lineage peaks that were primed in HSCs were also enriched in MPPs and CMPs, but less so in GMPs, CLPs, ProB, and ProTs; EP peaks were selectively enriched in MEPs and CMPs; GM peaks were enriched primarily in MPPs and GMPs; B cell peaks were enriched in ProBs and MPPs, and T cell peaks were enriched in ProTs and MPPs.

B) Peak distribution analysis revealed lineage skewing within progenitors. The distribution of lineage-primed peaks was displayed for each progenitor cell type. All progenitors contained lineage-primed peaks representing unique peaks of each of the five lineages, but at different proportions. HSCs had an almost equal distribution of peaks from all five lineages that did not deviate from an expected equal distribution (Chi-square, $p = 0.97$). MPPs and CLPs had similar peak distributions and were not significantly different when compared pairwise to HSCs (Chi-square, $p \geq 0.01$). In contrast, pairwise comparison of the distribution of peaks between HSCs and progenitors revealed significant differences in CMPs, GMPs, MEPs, ProBs, and ProTs by Chi-square. CMPs had a relative expansion primarily of erythromyeloid (MkP, EP) peaks; GMPs had primarily GM-unique peaks; MEPs were enriched for EP-unique peaks; whereas ProBs had more B cell peaks, and ProTs had mainly T cell peaks. ** $p < 0.01$, **** $p < 0.0001$.

C) Heatmaps of primed peaks that maintain accessibility throughout the expected differentiation trajectory for each lineage. Each line is one peak, with accessibility indicated in blue centered around the peak +/-250 bp. Less than 30% of the primed peaks for each lineage followed the expected trajectory by maintaining accessibility throughout differentiation. 17% of MkP peaks, 11% of EP peaks, 13% of GM peaks, 12% of B cell peaks, and 26% of T cell peaks maintained priming throughout differentiation.

D) A *cis* regulatory element (CRE) predicted by GREAT to be associated with *Fcnb* maintained accessibility ("priming") throughout differentiation into GMs. GEXC reported expression of *Fcnb* selectively in GMPs and GMs. Green circles indicate which cell type contained a called peak. Genome track snapshot of the *cis* regulatory element of *Fcnb* reported accessibility in HSCs, MPPs, CMPs, GMPs, and GMs. A "+" sign designated which cell type contained a called peak.

E) A CRE predicted by GREAT to be associated with *Wnt8b* maintained accessibility throughout differentiation into T cells. GEXC reported expression of *Wnt8b* selectively in T cells only. Green circles indicate which cell type contained a called peak. Genome track snapshot of the *cis* regulatory element of *Wnt8b* reported accessibility in HSCs, MPPs, CLPs, ProTs, and T cells. A "+" sign designated which cell type contained a called peak.

Figure 7

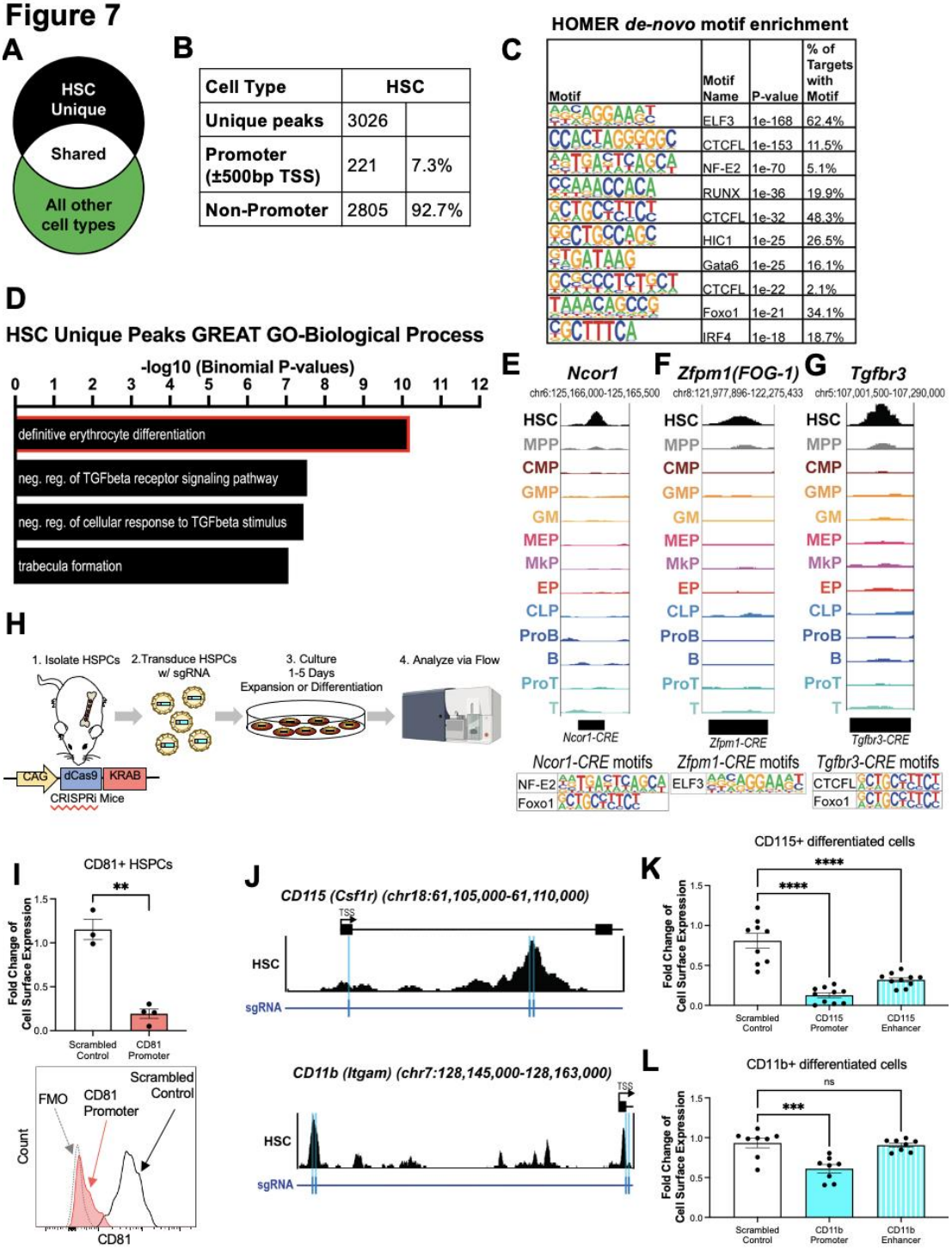

Figure 6.7. HSC-unique *cis* regulatory elements are primarily enriched for transcription factors that drive erythropoiesis

A) The HSC-unique peak-list was generated by filtering HSC peaks against the peak lists of the other 12 hematopoietic cell types.

B) HSC-unique peaks are primarily non-promoter peaks. Table of the composition of the HSC-unique peaks and percentage of non-promoter and promoter peaks.
C) *De novo m*otif enrichment of HSC-unique peaks revealed binding sites for known hematopoietic regulators. ELF3, CTCFL, NF-E2, and Runx motifs were the top 5 enriched *de novo* motifs.
D) "Definitive erythroid differentiation" was the top enriched GO term from GREAT annotation and analysis of the unique HSC peaks. The resulting graphs are GO Biological Process terms and the -log10 p-value for the top four terms.
E-G) Three examples of putative CREs for target genes that were enriched in "definitive erythrocyte differentiation" and displayed unique HSC accessibility. **E)** A putative CRE for *Ncor1* was unique to HSCs and contained motifs that closely match NF-E2 and Foxo1 binding sites. **F)** A putative *Zfpm1* CRE contained the binding motif that closely matches ELF3. **G)** A putative *Tgfbr3* CRE contained DNA motifs that closely matched CTCFL and Foxo1 binding sites.
H) Experimental setup using a CRISPRi model to functionally test putative CREs identified in this study.
I) CD81 expression was significantly reduced in HSPCs when CRISPRi HSPCs were transduced with lentivirus targeting the CD81 promoter. The fold change in the frequency of CD81+ cells of transduced cells compared to untransduced cells is represented in the bar graph and the representative histogram of CD81 expression in HSPCs transduced with CD81 promoter targeting sgRNA (red) compared to HSPCs transduced with a non-targeting scrambled sgRNA (blue) and CD81 FMO (grey dotted line).
J) ATAC-seq accessibility profiles of the CD115 (top) and CD11b (bottom) loci. The location of the single guide RNAs (sgRNA) designed to target the promoter or a putative CRE of each gene are denoted by blue bars below the respective locus.
K) CD115 expression was significantly reduced in differentiated cells when CRISPRi HSCs were transduced with lentivirus targeting either the CD115 promoter or enhancer. The fold change in the frequency of CD115+ cells of transduced cells compared to untransduced cells is represented in the bar graph.
L) CD11b expression was significantly reduced in differentiated cells when CRISPRi HSCs were transduced with lentivirus targeting only the CD11b promoter, but not the enhancer. The fold change in the frequency of CD11b+ cells of transduced cells compared to untransduced cells is represented in the bar graph.

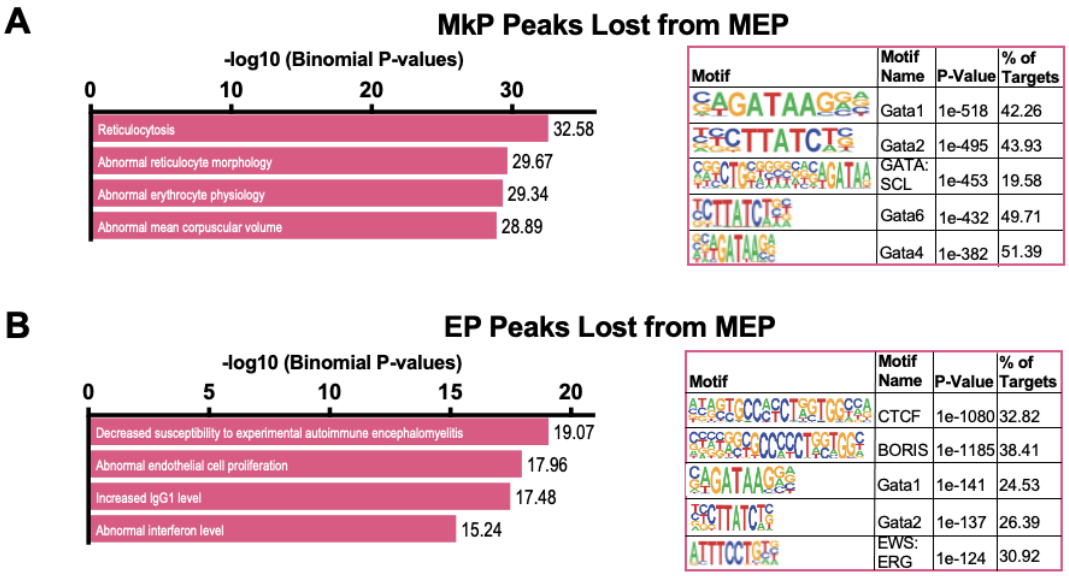

Figure 6.8. Supplemental Figure 1: Comparison of peaks lost as MEPs differentiate into MkPs or EPs revealed a shutting down of erythropoiesis as megakaryopoiesis progresses.

A-B) The lists of peaks lost from MEPs for each cell type were submitted to GREAT for functional annotation. The top 4 over-represented categories in Mouse Phenotype are reported, containing information about genotype-phenotype associations. In addition, motif enrichment analysis by HOMER was performed on the lists of peaks lost from MEPs for each cell type and the top 5 transcription factor motifs were reported. (**A**) The MkP lost peaks were enriched for genes whose alterations generate phenotypes related to erythropoiesis. The MkP peaks lost were enriched for transcription factor motifs important in erythropoiesis, such as Gata1 and Gata:SCL. (**B**) The EP lost peaks were enriched for genes whose alterations generate phenotypes related to immune modulation and cell proliferation. The EP peaks were enriched for transcription factor motifs important in chromatin remodeling and hematopoiesis.

Table 1: Peak counts and peak distribution relative to protein-coding gene promoters in each cell type.

Cell Type	ATAC peaks	Promoter Peaks (±500bp of TSS)	Sum of all non-promoter peaks	non-promoter peaks		
				coding (exons+TTS+TSS)	Introns	Intergenic
Master Peak-list	92,842	12,702	80,140	5,543	38,090	36,507
HSC	70,731	27,973	42,758	4,166	18,931	19,661
MPP	63,349	23,415	39,934	3,685	17,872	18,377
CLP	47,054	21,467	25,587	2,126	11,414	12,047
CMP	46,431	21,648	24,783	1,951	10,701	12,131
GMP	42,447	20,823	21,624	1,939	9,317	10,368
GM	30,529	15,559	14,970	1,440	6,697	6,833
MEP	50,483	26,064	24,419	2,281	10,803	11,335
EP	38,007	23,243	14,764	2,014	7,040	5,710
MkP	47,363	23,998	23,365	2,013	10,036	11,316
ProB	46,790	24,837	21,953	2,003	9,355	10,595
B	70,358	24,596	45,762	4,461	21,210	20,091
ProT	61,141	27,073	34,068	2,796	14,950	16,322
T	51,832	25,103	26,729	2,016	11,929	12,784

Table 6.1. Peak counts and peak distribution relative to protein-coding gene promoters in each cell type

References

Boyer, S.W., Schroeder, A. V., Smith-Berdan, S., and Forsberg, E.C. (2011). All Hematopoietic Cells Develop from Hematopoietic Stem Cells through Flk2/Flt3-Positive Progenitor Cells. Cell Stem Cell *9*, 64–73.

Boyer, S.W., Rajendiran, S., Beaudin, A.E., Smith-berdan, S., Muthuswamy, P.K., Perez-Cunningham, J., Martin, E.W., Cheung, C., Tsang, H., Landon, M., et al. (2019). Clonal and Quantitative In Vivo Assessment of Hematopoietic Stem Cell Differentiation Reveals Strong Erythroid Potential of Multipotent Cells. Stem Cell Reports *12*, 801–815.

Buenrostro, J., Wu, B., Chang, H., and Greenleaf, W. (2015). ATAC-seq: A Method for Assaying Chromatin Accessibility Genome-Wide. Curr. Protoc. Mol. Biol. *109*, 21.29.1-21.29.9.

Buenrostro, J.D., Giresi, P.G., Zaba, L.C., Chang, H.Y., and Greenleaf, W.J. (2013). Transposition of native chromatin for fast and sensitive epigenomic profiling of open chromatin, DNA-binding proteins and nucleosome position. Nat Meth *10*, 1213–1218.

Bultman, S.J., Gebuhr, T.C., and Magnuson, T. (2005). A Brg1 mutation that uncouples ATPase activity from chromatin remodeling reveals an essential role for SWI/SNF-related complexes in β-globin expression and erythroid development. Genes Dev. *19*, 2849–2861.

Cao, H., Heazlewood, S.Y., Williams, B., Cardozo, D., Nigro, J., Oteiza, A., and Nilsson, S.K. (2016). The role of CD44 in fetal and adult hematopoietic stem cell regulation. Haematologica *101*, 26–37.

Carrelha, J., Meng, Y., Kettyle, L.M., Luis, T.C., Norfo, R., Alcolea, V., Boukarabila, H., Grasso, F., Gambardella, A., Grover, A., et al. (2018). Hierarchically related lineage-restricted fates of multipotent haematopoietic stem cells. Nature *554*, 106–111.

Challen, G.A., Pietras, E.M., Wallscheid, N.C., and Signer, R.A.J. (2021). Simplified murine multipotent progenitor isolation scheme: Establishing a consensus approach for multipotent progenitor identification. Exp. Hematol. *104*, 55–63.

Chambers, S.M., Boles, N.C., Lin, K.Y.K., Tierney, M.P., Bowman, T. V., Bradfute, S.B., Chen, A.J., Merchant, A.A., Sirin, O., Weksberg, D.C., et al. (2007). Hematopoietic Fingerprints: An Expression Database of Stem Cells and Their Progeny. Cell Stem Cell *1*, 578–591.

Chang, D.H., Angelin-Duclos, C., and Calame, K. (2000). BLIMP-1: trigger for differentiation of myeloid lineage. Nat. Immunol. *1*, 169–176.

Chi, T.H., Wan, M., Lee, P.P., Akashi, K., Metzger, D., Chambon, P., Wilson, C.B., and Crabtree, G.R. (2003). Sequential Roles of Brg, the ATPase Subunit of BAF Chromatin Remodeling Complexes, in Thymocyte Development. Immunity *19*, 169–182.

Concordet, J.-P., and Haeussler, M. (2018). CRISPOR: intuitive guide selection for

CRISPR/Cas9 genome editing experiments and screens. Nucleic Acids Res. *46*, W242–W245.

Cooney, R., Baker, J., Brain, O., Danis, B., Pichulik, T., Allan, P., Ferguson, D.J.P., Campbell, B.J., Jewell, D., and Simmons, A. (2010). NOD2 stimulation induces autophagy in dendritic cells influencing bacterial handling and antigen presentation. Nat. Med. *16*, 90–97.

Creyghton, M.P., Cheng, A.W., Welstead, G.G., Kooistra, T., Carey, B.W., Steine, E.J., Hanna, J., Lodato, M.A., Frampton, G.M., Sharp, P.A., et al. (2010). Histone H3K27ac separates active from poised enhancers and predicts developmental state. Proc. Natl. Acad. Sci. 201016071.

Dodson, L.F., Boomer, J.S., Deppong, C.M., Shah, D.D., Sim, J., Bricker, T.L., Russell, J.H., and Green, J.M. (2009). Targeted Knock-In Mice Expressing Mutations of CD28 Reveal an Essential Pathway for Costimulation. Mol. Cell. Biol. *29*, 3710–3721.

Ema, H., Morita, Y., and Suda, T. (2014). Heterogeneity and hierarchy of hematopoietic stem cells. Exp. Hematol. *42*, 74-82.e2.

Fang, C., Miwa, T., and Song, W.-C. (2011). Decay-accelerating factor regulates T-cell immunity in the context of inflammation by influencing costimulatory molecule expression on antigen-presenting cells. Blood *118*, 1008–1014.

Forsberg, E.C., Prohaska, S.S., Katzman, S., Heffner, G.C., Stuart, J.M., and

Weissman, I.L. (2005). Differential expression of novel potential regulators in hematopoietic stem cells. PLoS Genet. *1*, e28.

Forsberg, E.C., Serwold, T., Kogan, S., Weissman, I.L., and Passegué, E. (2006). New Evidence Supporting Megakaryocyte-Erythrocyte Potential of Flk2/Flt3+ Multipotent Hematopoietic Progenitors. Cell *126*, 415–426.

Frelin, C., Herrington, R., Janmohamed, S., Barbara, M., Tran, G., Paige, C.J., Benveniste, P., Zuñiga-Pflücker, J.-C., Souabni, A., Busslinger, M., et al. (2013). GATA-3 regulates the self-renewal of long-term hematopoietic stem cells. Nat. Immunol. *14*, 1037–1044.

Gasiorek, J.J., Nouhi, Z., and Blank, V. (2012). Abnormal differentiation of erythroid precursors in p45 NF-E2−/− mice. Exp. Hematol. *40*, 393–400.

Gaspar-Maia, A., Alajem, A., Meshorer, E., and Ramalho-Santos, M. (2011). Open chromatin in pluripotency and reprogramming. Nat. Rev. Mol. Cell Biol. *12*, 36–47.

Gross, D.S., and Garrard, W.T. (1988). Nuclease hypersensitive sites in chromatin. Annu. Rev. Biochem. *57*, 159–197.

Haeussler, M., Schönig, K., Eckert, H., Eschstruth, A., Mianné, J., Renaud, J.-B.B., Schneider-Maunoury, S., Shkumatava, A., Teboul, L., Kent, J., et al. (2016). Evaluation of off-target and on-target scoring algorithms and integration into the guide RNA selection tool CRISPOR. Genome Biol. *17*, 148.

Hazenbos, W.L., Heijnen, I.A., Meyer, D., Hofhuis, F.M., Renardel de Lavalette, C.R., Schmidt, R.E., Capel, P.J., van de Winkel, J.G., Gessner, J.E., van den Berg, T.K., et al. (1998). Murine IgG1 complexes trigger immune effector functions predominantly via Fc gamma RIII (CD16). J. Immunol. *161*, 3026–3032.

Heintzman, N.D., Stuart, R.K., Hon, G., Fu, Y., Ching, C.W., Hawkins, R.D., Barrera, L.O., Van Calcar, S., Qu, C., Ching, K.A., et al. (2007). Distinct and predictive chromatin signatures of transcriptional promoters and enhancers in the human genome. Nat. Genet. *39*, 311–318.

Heintzman, N.D., Hon, G.C., Hawkins, R.D., Kheradpour, P., Stark, A., Harp, L.F., Ye, Z., Lee, L.K., Stuart, R.K., Ching, C.W., et al. (2009). Histone modifications at human enhancers reflect global cell-type-specific gene expression. Nature *459*, 108–112.

Heinz, S., Benner, C., Spann, N., Bertolino, E., Lin, Y.C., Laslo, P., Cheng, J.X., Murre, C., Singh, H., and Glass, C.K. (2010). Simple Combinations of Lineage-Determining Transcription Factors Prime cis-Regulatory Elements Required for Macrophage and B Cell Identities. Mol. Cell *38*, 576–589.

Heuston, E.F., Keller, C.A., Lichtenberg, J., Giardine, B., Anderson, S.M., Hardison, R.C., and Bodine, D.M. (2018). Establishment of regulatory elements during erythro-megakaryopoiesis identifies hematopoietic lineage-commitment points. Epigenetics and Chromatin *11*, 1–18.

Horlbeck, M.A., Gilbert, L.A., Villalta, J.E., Adamson, B., Pak, R.A., Chen, Y., Fields, A.P., Park, C.Y., Corn, J.E., Kampmann, M., et al. (2016). Compact and highly active next-generation libraries for CRISPR-mediated gene repression and activation. Elife *5*, 1–20.

Hsu, L.-Y., Lauring, J., Liang, H.-E., Greenbaum, S., Cado, D., Zhuang, Y., and Schlissel, M.S. (2003). A Conserved Transcriptional Enhancer Regulates RAG Gene Expression in Developing B Cells. Immunity *19*, 105–117.

Hu, M., Krause, D., Greaves, M., Sharkis, S., Dexter, M., Heyworth, C., and Enver, T. (1997). Multilineage gene expression precedes commitment in the hemopoietic system. Genes Dev. *11*, 774–785.

Ivashkiv, L.B. (2018). IFNγ: signalling, epigenetics and roles in immunity, metabolism, disease and cancer immunotherapy. Nat. Rev. Immunol. *18*, 545–558.

Jepsen, K., Hermanson, O., Onami, T.M., Gleiberman, A.S., Lunyak, V., McEvilly, R.J., Kurokawa, R., Kumar, V., Liu, F., Seto, E., et al. (2000). Combinatorial Roles of the Nuclear Receptor Corepressor in Transcription and Development. Cell *102*, 753–763.

Karsunky, H., Merad, M., Cozzio, A., Weissman, I.L., and Manz, M.G. (2003). Flt3 Ligand Regulates Dendritic Cell Development from Flt3+ Lymphoid and Myeloid-committed Progenitors to Flt3+ Dendritic Cells In Vivo . J. Exp. Med. *198*, 305–313.

Koch, C.M., Andrews, R.M., Flicek, P., Dillon, S.C., Karaöz, U., Clelland, G.K.,

Wilcox, S., Beare, D.M., Fowler, J.C., Couttet, P., et al. (2007). The landscape of histone modifications across 1% of the human genome in five human cell lines. Genome Res. *17*, 691–707.

Krause, D.S. (2002). Plasticity of marrow-derived stem cells. Gene Ther *9*.

Kuo, T.C., and Schlissel, M.S. (2009). Mechanisms controlling expression of the RAG locus during lymphocyte development. Curr. Opin. Immunol. *21*, 173–178.

Lara-Astiaso, D., Weiner, A., Lorenzo-Vivas, E., Zaretsky, I., Jaitin, D.A., David, E., Keren-Shaul, H., Mildner, A., Winter, D., Jung, S., et al. (2014). Chromatin state dynamics during blood formation. Science *55*, 1–10.

Laszkiewicz, A., Sniezewski, L., Kasztura, M., Bzdzion, L., Cebrat, M., and Kisielow, P. (2012). Bidirectional Activity of the NWC Promoter Is Responsible for RAG-2 Transcription in Non-Lymphoid Cells. PLoS One *7*, e44807.

Laurenti, E., and Göttgens, B. (2018). From haematopoietic stem cells to complex differentiation landscapes. Nature *553*, 418–426.

Li, Q., Peterson, K.R., Fang, X., and Stamatoyannopoulos, G. (2002). Locus control regions. Blood *100*, 3077–3086.

Li, Q., Brown, J.B., Huang, H., and Bickel, P.J. (2011). Measuring reproducibility of high-throughput experiments. Ann. Appl. Stat. *5*, 1752–1779.

Martin, E.W., Krietsch, J., Reggiardo, R.E., Sousae, R., Kim, D.H., and Forsberg, E.C.

(2021). Chromatin accessibility maps provide evidence of multilineage gene priming in hematopoietic stem cells. Epigenetics and Chromatin *14*, 1–15.

McLean, C.Y., Bristor, D., Hiller, M., Clarke, S.L., Schaar, B.T., Lowe, C.B., Wenger, A.M., and Bejerano, G. (2010). GREAT improves functional interpretation of cis-regulatory regions. Nat. Biotechnol. *28*, 495–501.

Nutt, S.L., Eberhard, D., Horcher, M., Rolink, A.G., and Busslinger, M. (2001). Pax5 Determines the Identity of B Cells from the Beginning to the End of B-lymphopoiesis. Int. Rev. Immunol. *20*, 65–82.

Oguri, Y., Shinoda, K., Kim, H., Alba, D.L., Bolus, W.R., Wang, Q., Brown, Z., Pradhan, R.N., Tajima, K., Yoneshiro, T., et al. (2020). CD81 Controls Beige Fat Progenitor Cell Growth and Energy Balance via FAK Signaling. Cell *182*, 563-577.e20.

Orkin, S.H., and Zon, L.I. (2008). Hematopoiesis: An Evolving Paradigm for Stem Cell Biology. Cell *132*, 631–644.

Palstra, R., de Laat, W., and Grosveld, F.B.T.-A. in G. (2008). Chapter 4 β-Globin Regulation and Long-Range Interactions. In Long-Range Control of Gene Expression, (Academic Press), pp. 107–142.

Phillips, R., Ernst, R.E., Brian, B., Natalia, I., Mahan, M.A., Deanehan, J.K., Moore, K.A., Christian, O.G., and Lemischka, I.R. (2000). The Genetic Program of Hematopoietic Stem Cells. Science (80). *288*, 1635–1640.

Poscablo, D.M., Worthington, A.K., Smith-Berdan, S., and Forsberg, E.C. (2021).

Megakaryocyte progenitor cell function is enhanced upon aging despite the functional decline of aged hematopoietic stem cells. Stem Cell Reports *16*, 1598–1613.

Pronk, C.J.H., Rossi, D.J., Månsson, R., Attema, J.L., Norddahl, G.L., Chan, C.K.F., Sigvardsson, M., Weissman, I.L., and Bryder, D. (2007). Elucidation of the Phenotypic, Functional, and Molecular Topography of a Myeloerythroid Progenitor Cell Hierarchy. Cell Stem Cell *1*, 428–442.

Rada-Iglesias, A., Bajpai, R., Swigut, T., Brugmann, S.A., Flynn, R.A., and Wysocka, J. (2011). A unique chromatin signature uncovers early developmental enhancers in humans. Nature *470*, 279–283.

Replogle, J.M., Norman, T.M., Xu, A., Hussmann, J.A., Chen, J., Cogan, J.Z., Meer, E.J., Terry, J.M., Riordan, D.P., Srinivas, N., et al. (2020). Combinatorial single-cell CRISPR screens by direct guide RNA capture and targeted sequencing. Nat. Biotechnol.

Rodrigues, N.P., Tipping, A.J., Wang, Z., and Enver, T. (2012). GATA-2 mediated regulation of normal hematopoietic stem/progenitor cell function, myelodysplasia and myeloid leukemia. Int. J. Biochem. Cell Biol. *44*, 457–460.

Rodriguez-Fraticelli, A.E., Wolock, S.L., Weinreb, C.S., Panero, R., Patel, S.H., Jankovic, M., Sun, J., Calogero, R.A., Klein, A.M., and Camargo, F.D. (2018). Clonal analysis of lineage fate in native haematopoiesis. Nature *553*, 212–216.

Rodriguez y Baena, A., Manso, B.A., and Forsberg, E.C. (2021). CFU-S assay: a

historical single-cell assay that offers modern insight into clonal hematopoiesis. Exp. Hematol. *104*, 1–8.

Rodriguez y Baena, A., Rajendiran, S., Manso, B.A., Krietsch, J., Boyer, S.W., Kirschmann, J., and Forsberg, E.C. (2022). New transgenic mouse models enabling pan-hematopoietic or selective hematopoietic stem cell depletion in vivo. Sci. Rep. *12*, 3156.

Schep, A.N., Wu, B., Buenrostro, J.D., and Greenleaf, W.J. (2017). ChromVAR: Inferring transcription-factor-associated accessibility from single-cell epigenomic data. Nat. Methods *14*, 975–978.

Schlenner, S.M., Madan, V., Busch, K., Tietz, A., Läufle, C., Costa, C., Blum, C., Fehling, H.J., and Rodewald, H.-R. (2010). Fate Mapping Reveals Separate Origins of T Cells and Myeloid Lineages in the Thymus. Immunity *32*, 426–436.

Schmidt, U., van den Akker, E., Parren-van Amelsvoort, M., Litos, G., de Bruijn, M., Gutiérrez, L., Hendriks, R.W., Ellmeier, W., Löwenberg, B., Beug, H., et al. (2004). Btk is required for an efficient response to erythropoietin and for SCF-controlled protection against TRAIL in erythroid progenitors. J. Exp. Med. *199*, 785–795.

Seita, J., and Weissman, I.L. (2010). Hematopoietic stem cell: self-renewal versus differentiation. WIREs Syst. Biol. Med. *2*, 640–653.

Seita, J., Sahoo, D., Rossi, D.J., Bhattacharya, D., Serwold, T., Inlay, M.A., Ehrlich, L.I.R., Fathman, J.W., Dill, D.L., and Weissman, I.L. (2012). Gene expression

commons: An open platform for absolute gene expression profiling. PLoS One *7*, 1–11.

Shivdasani, R.A., and Orkin, S.H. (1995). Erythropoiesis and globin gene expression in mice lacking the transcription factor NF-E2. Proc. Natl. Acad. Sci. *92*, 8690 LP – 8694.

Shulga-Morskaya, S., Dobles, M., Walsh, M.E., Ng, L.G., MacKay, F., Rao, S.P., Kalled, S.L., and Scott, M.L. (2004). B Cell-Activating Factor Belonging to the TNF Family Acts through Separate Receptors to Support B Cell Survival and T Cell-Independent Antibody Formation. J. Immunol. *173*, 2331 LP – 2341.

Stenvers, K.L., Tursky, M.L., Harder, K.W., Kountouri, N., Amatayakul-Chantler, S., Grail, D., Small, C., Weinberg, R.A., Sizeland, A.M., and Zhu, H.-J. (2003). Heart and Liver Defects and Reduced Transforming Growth Factor β2 Sensitivity in Transforming Growth Factor β Type III Receptor-Deficient Embryos. Mol. Cell. Biol. *23*, 4371 LP – 4385.

Surani, M.A., Hayashi, K., and Hajkova, P. (2007). Genetic and Epigenetic Regulators of Pluripotency. Cell *128*, 747–762.

Tanigawa, Y., Dyer, E.S., and Bejerano, G. (2022). WhichTF is functionally important in your open chromatin data? PLOS Comput. Biol. *18*, e1010378.

Tasic, B., Hippenmeyer, S., Wang, C., Gamboa, M., Zong, H., Chen-Tsai, Y., and Luo, L. (2011). Site-specific integrase-mediated transgenesis in mice via pronuclear

injection. Proc. Natl. Acad. Sci. *108*, 7902–7907.

Terskikh, A. V, Miyamoto, T., Chang, C., Diatchenko, L., and Weissman, I.L. (2003). Gene expression analysis of purified hematopoietic stem cells and committed progenitors. Blood *102*, 94–101.

Tsang, A.P., Fujiwara, Y., Hom, D.B., and Orkin, S.H. (1998). Failure of megakaryopoiesis and arrested erythropoiesis in mice lacking the GATA-1 transcriptional cofactor FOG. Genes Dev. *12*, 1176–1188.

Ugarte, F., Sousae, R., Cinquin, B., Martin, E.W., Krietsch, J., Sanchez, G., Inman, M., Tsang, H., Warr, M., Passegué, E., et al. (2015). Progressive Chromatin Condensation and H3K9 Methylation Regulate the Differentiation of Embryonic and Hematopoietic Stem Cells. Stem Cell Reports *5*, 728–740.

Visel, A., Blow, M.J., Li, Z., Zhang, T., Akiyama, J. a, Holt, A., Plajzer-Frick, I., Shoukry, M., Wright, C., Chen, F., et al. (2009). ChIP-seq accurately predicts tissue-specific activity of enhancers. Nature *457*, 854–858.

Wang, A., Yue, F., Li, Y., Xie, R., Harper, T., Patel, N.A., Muth, K., Palmer, J., Qiu, Y., Wang, J., et al. (2015). Epigenetic priming of enhancers predicts developmental competence of hESC-derived endodermal lineage intermediates. Cell Stem Cell *16*, 386–399.

Wei, X.-C., Kishi, H., Jin, Z.-X., Zhao, W.-P., Kondo, S., Matsuda, T., Saito, S., and Muraguchi, A. (2002). Characterization of Chromatin Structure and Enhancer

Elements for Murine Recombination Activating Gene-2. J. Immunol. *169*, 873 LP – 881.

Whyte, W.A., Orlando, D.A., Hnisz, D., Abraham, B.J., Lin, C.Y., Kagey, M.H., Rahl, P.B., Lee, T.I., and Young, R.A. (2013). Master Transcription Factors and Mediator Establish Super-Enhancers at Key Cell Identity Genes. Cell *153*, 307–319.

Willcockson, M.A., Taylor, S.J., Ghosh, S., Healton, S.E., Wheat, J.C., Wilson, T.J., Steidl, U., and Skoultchi, A.I. (2019). Runx1 promotes murine erythroid progenitor proliferation and inhibits differentiation by preventing Pu.1 downregulation. Proc. Natl. Acad. Sci. *116*, 17841 LP – 17847.

Worthington, A.K., and Forsberg, E.C. (2022). A CRISPR view of hematopoietic stem cells: Moving innovative bioengineering into the clinic. Am. J. Hematol. *97*, 1226–1235.

Worthington, A.K., Cool, T., Poscablo, D.M., Hussaini, A., Beaudin, A.E., and Forsberg, E.C. (2022). IL7Rα, but not Flk2, is required for hematopoietic stem cell reconstitution of tissue-resident lymphoid cells. Development *149*, dev200139.

Yamamoto, R., Morita, Y., Ooehara, J., Hamanaka, S., Onodera, M., Rudolph, K.L., Ema, H., and Nakauchi, H. (2013). Clonal Analysis Unveils Self-Renewing Lineage-Restricted Progenitors Generated Directly from Hematopoietic Stem Cells. Cell *154*, 1112–1126.

Yamamoto, R., Wilkinson, A.C., Ooehara, J., Lan, X., Lai, C.-Y., Nakauchi, Y.,

Pritchard, J.K., and Nakauchi, H. (2018). Large-Scale Clonal Analysis Resolves Aging of the Mouse Hematopoietic Stem Cell Compartment. Cell Stem Cell *22*, 600-607.e4.

Yannoutsos, N., Barreto, V., Misulovin, Z., Gazumyan, A., Yu, W., Rajewsky, N., Peixoto, B.R., Eisenreich, T., and Nussenzweig, M.C. (2004). A cis element in the recombination activating gene locus regulates gene expression by counteracting a distant silencer. Nat. Immunol. *5*, 443–450.

Yoshida, T., and Georgopoulos, K. (2013). GATA-3 controls self-renewal in stressed HSCs. Nat. Immunol. *14*, 1032–1033.

Yu, W., Misulovin, Z., Suh, H., Hardy, R.R., Jankovic, M., Yannoutsos, N., and Nussenzweig, M.C. (1999). Coordinate Regulation of RAG1 and RAG2 by Cell Type-Specific DNA Elements 5' of RAG2. Science (80-.). *285*, 1080–1084.

Chapter 7.

Nupr1 as a regulator of aging hematopoiesis and megakaryopoiesis

Abstract

Hematopoietic stem cells (HSCs) are multipotent stem cells that self-renew and differentiate into all blood cell types. Aging of HSCs is accompanied by myeloid lineage bias and decreased reconstitution potential. However, the molecular mechanisms of aging hematopoiesis remain unclear, thus limiting the identification of promising rejuvenation interventions. To reveal potential regulators of aging HSCs, significant effort was placed on identifying gene expression changes between young and aged HSCs, revealing that alternative splicing may contributes to this process. To this end, we performed differential isoform usage analysis of highly purified HSCs from these two age groups, and we uncovered an increase in expression of protein-coding isoforms in aged HSCs comparted to their young counterparts. Following this analysis, we focused on the Nuclear protein 1 (*Nupr1*) gene, previously demonstrated to be robustly upregulated in aged HSCs. Interestingly, we demonstrate that *Nupr1* is also significantly upregulated in an age-specific megakaryocyte progenitor (MkP) population derived by direct differentiation from aged HSCs. Thus, we hypothesized that *Nupr1* is a regulator of aging hematopoiesis potentially resulting in age-specific megakaryopoiesis. We are testing this hypothesis by performing CRISPR-mediated knockout of Nupr1 in aged HSCs and assessing differentiation, self-renewal, and engraftment potential upon transplantation. These experiments will reveal the role of Nupr1 in defining the defects of aged HSCs and highlight potential avenues for rejuvenation of aged HSCs.

Introduction

Aging, an inevitable biological process, impacts all physiological system, exerting significant effects on hematopoiesis, the continuous replenishment of all blood and immune cells by hematopoietic stem cells (HSCs). The aging hematopoietic system undergoes a myriad of changes, resulting in a decline in the regenerative capacity and functionality of HSCs. Aged HSCs exhibit skewed lineage differentiation towards myelopoiesis(Morrison et al. 1996; Rossi et al. 2005), DNA damage accumulation, reduced clonal diversity with an increase in myeloid- and platelet-biased clones(Beerman et al. 2010; Challen et al. 2010; Cho, Sieburg, and Muller-Sieburg 2008), and decreased reconstitution ability upon transplantation(Dykstra et al. 2007; Poscablo et al. 2021), among other phenotypes.

Recently, we made a novel discovery that aged HSCs differentiate directly into an additional population of megakaryocyte progenitors (MkP), the unipotent progenitors of platelets (Poscablo et al, submitted). This age-specific pathway leads to production of age-specific MkPs that are more responsive to stress conditions and produce hyperactive platelets, increasing the risk for thrombotic diseases. Understanding the molecular mechanisms underpinning these age-specific alterations in hematopoiesis is imperative for the development of strategies to mitigate age-associated hematopoietic decline. Thus, the identification of targetable candidates assumes paramount significance. Through targeted interventions, it may be possible to modulate key players and signaling cascades that govern aging hematopoiesis,

ultimately offering avenues for the development of innovative therapies to enhance blood cell production and immune competence in the elderly.

This study focuses on understanding the changes in the epigenetic and transcriptional landscape HSCs and MkPs throughout the aging process. The primary objective is to identify potential candidates that may play a crucial role in triggering and sustaining the age-specific platelet differentiation pathway.

Results and Discussion

An age-specific platelet differentiation pathways in aged mice

In previous studies, we demonstrated that all hematopoietic cells undergo differentiation through a Flk2+ MPP stage. In adult mice, the FlkSwitch mouse model, utilizing a dual-color reporter system, illustrated that all progenitor and mature cells downstream of MPPs are nearly 100% GFP+ after Flk2 expression triggers the irreversible excision of the Tomato (Tom) transgene, resulting in permanent GFP expression (Boyer et al 2011; **Figure 1A**). In adult FlkSwitch mice, the differentiation of HSCs into platelets occurs through intermediate progenitors, including MPPs, CMPs, and MEPs, ultimately leading to the generation of GFP+ MkPs (canonical MkPs, cMkPs), the unipotent progenitors of platelets.

Recently, using the FlkSwitch mouse model, we made a novel discovery regarding an age-specific platelet differentiation pathway (Poscablo et al, submitted). In older mice (20-24 months), an additional platelet differentiation pathway emerges, bypassing intermediate progenitors and giving rise to Tom+ MkPs (non-canonical

MkPs, ncMkPs) and Tom+ platelets (**Figure 1B**). Consequently, young mice exhibit GFP+ cMkPs, while aged mice present both GFP+ cMkPs and Tom+ ncMkPs. Data from our recently submitted manuscript (Poscablo et al) reveal that aged ncMkPs possess unique properties compared to both young and aged cMkPs. Upon transplantation, aged ncMkPs exhibit a greater ability to reconstitute platelets compared to both cMkP populations. Similarly, in vitro studies demonstrate that aged ncMkPs have greater proliferation potential than young or aged cMkPs. These findings highlight the functional differences between aged ncMkPs and co-existing aged cMkPs, as well as young cMkPs. This project is dedicated to unraveling the mechanisms underlying this age-specific differentiation pathway."

ATACseq profiling of young and aged HSCs and MkPs

The ability of a stem cell to differentiate into specific lineages is regulated by epigenetic remodeling at cis-regulatory regions, including promoter and enhancer regions, at the stem cell level. This phenomenon, known as epigenetic priming, involves making regulatory regions accessible in stem cells before the transcription of lineage-specific genes upon differentiation (Heintzman et al. 2009; Hu et al. 1997; Koch et al. 2007; Rada-Iglesias et al. 2011; Visel et al. 2009, 2009).

Recently, we conducted bulk ATACseq analysis on adult hematopoietic stem cells (HSCs), multipotent progenitors (MPPs), myeloid (CMP, MEP, GMP) and lymphoid (CLP, ProB, and ProT) progenitors, as well as unipotent/mature lineages (MkPs, EPs, GMs, Bs, and Ts) to investigate lineage priming in hematopoiesis (E. W.

Martin et al. 2021; Martin et al. 2023). Comparative analysis of chromatin accessibility between HSCs and the five unipotent/mature lineages revealed multi-lineage epigenetic priming in adult HSCs (E. W. Martin et al. 2021). Furthermore, we demonstrated that priming of lineage-specific cis-regulatory regions is maintained across different progenitor stages (Martin et al. 2023). For instance, MkP-lineage specific cis-regulatory elements maintain accessibility throughout differentiation from HSCs, through MPPs, CMPs, and MEPs, until MkPs where their associated genes are expressed.

With aging, HSCs gain the ability to differentiate into age-specific non-canonical MkPs (ncMkPs). Given our understanding that changes in lineage fate decisions depend on priming, we hypothesize that aged HSCs acquire epigenetic priming for age-specific MkP differentiation. To address this hypothesis and identify candidate regulatory elements responsible for the age-specific differentiation of ncMkPs, we isolated five populations of interest - young HSCs, young cMkPs, aged HSCs, aged cMkPs, aged ncMkPs - using fluorescence-activated cell sorting (FACS) and performed bulk ATACseq analysis (**Figure 1C**). Hierarchical clustering using the ChromVAR output (**Figure 2A**) and principal component analysis (PCA) (**Figure 2B**) of the ATACseq profiles showed clear clustering between replicates as well as a distinct separation between HSCs and MkPs. Moreover, aged ncMkPs appeared to be epigenetically more similar to HSCs, possibly explained by their direct differentiation from HSC

Differential accessibility analysis comparing aged ncMkPs to young cMkPs, as well as aged ncMkPs to aged cMkPs, revealed potential regulatory regions uniquely more accessible in aged ncMkPs. Specifically, 3,032 peaks were more accessible in aged ncMkPs compared to young cMkPs, and 3,091 peaks were more accessible in young cMkPs compared to aged ncMkPs (**Figure 2C**). Meanwhile, 552 peaks were more accessible in aged ncMkPs compared to aged cMkPs, while 212 peaks were more accessible in aged cMkPs compared to aged ncMkPs (**Figure 2D**). Overall, fewer differentially accessible peaks were observed between aged cMkPs and aged ncMkPs, potentially due to their coexistence in the same aged mouse environment, leading to similar changes in chromatin accessibility across cell types.

Notably, the promoter of the Nupr1 gene (chr7: 126,622,511-123,626,569) exhibited significant accessibility in aged ncMkPs compared to both cMkP populations, as indicated by the uploaded ATACseq signal tracks on the UCSC Genome Browser (**Figure 2E**). To explore whether Nupr1 could be a potential candidate for epigenetic priming for the age-specific MkP pathway in aged HSCs, we uploaded signal tracks for young and aged HSCs in the same UCSC Genome Browser session. As shown in Figure 2E, the Nupr1 promoter was more accessible in aged HSCs compared to young HSCs, fitting the parameters for a potential regulator of the age-specific pathway.

Nupr1 as a potential regulator of aging HSCs

Nupr1, also known as p8/Com1, is a small, intrinsically disordered protein encoded by the Nupr1 gene. Originally discovered in acute-phase pancreatitis (Mallo et al. 1997), Nupr1 has since been extensively studied in various cancers (T. Martin et al. 2021). Functioning as a stress-response gene, Nupr1, under stressful conditions, acts as a transcriptional regulator influencing the expression of genes associated with cell survival, proliferation, autophagy, and apoptosis (Chen et al. 2016; De Conti et al. 2017; Grasso et al. 2015; Wang et al. 2020). Despite its well-documented role in cancer, the involvement of Nupr1 in hematopoiesis remains poorly understood.

Our collaborators conducted a comprehensive meta-analysis and re-analysis of 12 published studies that sequenced young and aged HSCs. Focusing on differentially expressed genes consistently observed across multiple studies, they identified an "aging signature" (**Figure 3A**). Notably, Nupr1 emerged as one of the top consistently deregulated genes, showing upregulation in aged HSCs compared to young HSCs in 11 out of 12 studies (Svendsen et al. 2021; **Figure 3B**). Supporting these findings, our own unpublished single-cell (sc)RNAseq data of hematopoietic stem and progenitor cells (HSPCs) demonstrated a significant upregulation of Nupr1 in aged HSCs compared to their younger counterparts (**Figure 3C**). Additionally, re-analysis of a recently published HSC scRNAseq dataset (Hérault et al. 2021) (**Figure 3D**) revealed that while only a few HSCs expressed Nupr1 in young mice, more than 90% of HSCs exhibited upregulated Nupr1 in aged mic

Despite multiple studies indicating a significant upregulation of Nupr1 in aged HSCs, its specific role in aging hematopoiesis remains unexplored. This project aims to delve into the functional implications of Nupr1 in the context of aging HSCs, shedding light on its potential regulatory role in the aging hematopoietic process

Nupr1 as a potential regulator of age-specific ncMkP differentiation.

A meta-analysis and a re-analysis of 12 published studies that sequenced (using different platforms) young and aged HSCs came up with a "aging signature", made up of 142 genes from the meta-analysis and 220 genes from the reanalysis (**Figure 3A**). Nupr1 was one of the most most consistently deregulated genes with 11 out of 12 studies showing upregulation with aging in HSCs(Flohr Svendsen et al. 2021) (**Figure 3B**). Our unpublished single cell RNAseq data from hematopoietic stem and progenitors for young and aged mice showed significantly higher expression of Nupr1 in aged HSCs compared to young HSC (**Figure 3C**). Similarly, re-analysis of single cell RNAseq data from published data for HSCs (Hérault et al. 2021) showed Nupr1 was expressed by a small percentage of HSCs in the young mice but upregulated at the population level in the aged mice.

Recently, a single-cell RNAseq study by Rodriguez-Fraticelli et al 2020 showed that Nupr1 is expressed specifically in a subset of adult HSCs that are more primitive, or at the top of the HSC hierarchy, here referred to as "low output". These are HSCs that are more likely to self-renew than differentiate. Moreover, Nupr1 is upregulated in HSCs that are biased towards differentiation into

megakaryocytes/platelets instead of other lineages (namely RBC, GM, B, and T) (Rodriguez-Fraticelli et al. 2020). Thus, we sought to investigate whether the increased Nupr1 expression in aged HSC could be responsible for age-specific ncMkP differentiation.

Our single cell RNAseq data of hematopoietic stem and progenitor cells not only showed that Nupr1 to be significantly upregulated in aged HSCs compared to young (**Figure 3C**), but also showed Nupr1 to significantly upregulated in aged ncMkPs compared to both young cMkP and aged cMkPs (**Figure 4A**). To determine the potential regulators of this age-specific MkP differentiation pathway, we further analyzed previously published bulk RNAseq data from young cMkPs, aged cMkPs, and aged ncMkPs (Poscablo et al. 2021) (**Figure 4B**). Pairwise differential expression analysis of these three MkP populations revealed Nupr1 to be one of the most highly expressed genes in aged ncMkPs compared to both young and aged cMkPs (**Figure 1B**).

<u>Aged HSCs and aged ncMkPs express the protein coding isoform of Nupr1.</u>

Recently, an additional non-coding isoform of Nupr1 (Nupr1-202) has been identified alongside the coding isoform (Nupr1-201) (Figure 5A). However, the functional implications of the non-coding isoform have not been reported. Intriguingly, upon reanalysis of epigenetic sequencing data (Sun et al. 2014) from young and aged HSCs at alternative transcription start sites (aTSS), an increase in chromatin modifications marking active gene transcription was observed, suggesting increased

usage of alternative TSS in aged HSCs compared to young HSCs (**Supplementary Figure 1**).

Further examination of published bulk RNAseq data(Sun et al. 2014) from young and aged HSCs revealed that the substantial upregulation of Nupr1 expression in aged HSCs compared to young HSCs (**Figure 5B**) is primarily attributed to the increased expression of the Nupr1-201 isoform (coding) of Nupr1 (**Figure 5C**). In contrast, the minimal Nupr1 expression observed in young HSCs (**Figure 5B**) is due to the comparable usage of both isoforms. This indicates an isoform usage switch in aging HSCs and underscores the potential significance of the Nupr1 protein in aging hematopoiesis.

Given the identification of Nupr1 as a potential candidate regulator of age-specific MkP differentiation, we aimed to determine which isoforms are expressed in MkPs. We designed primers to amplify cDNA, resulting in differently sized amplification products based on the isoform expressed. Consistent with isoform analysis for HSCs shown in Figure 5C, aged HSCs exhibited high expression of the coding isoform of Nupr1 with undetectable expression of the non-coding isoform by this method (**Figure 5D**). A parallel pattern was observed in aged ncMkPs, demonstrating elevated expression of the coding Nupr1 isoform and minimal expression of the non-coding isoform. In alignment with the data for young HSCs shown in Figure 5C, both isoforms were similarly expressed in both young and aged cMkPs as determined by real-time PCR (**Figure 5D**).

Inhibition of Nupr1 expression leads to halted MkP differentiation.

To functionally assess the role of Nupr1 in aging hematopoiesis and megakaryopoiesis, we employed a CRISPRi mouse line (E. W. Martin et al. 2021) with a catalytically inactive Cas9 (deadCas9 or dCas9), fused to a repressive KRAB domain, under a CAG promoter for ubiquitous CRISPRi machinery expression (**Figure 6A**). Lentiviral transduction of sequence-specific gRNAs (sgRNAs) can direct the dCas9-KRAB to a specific locus, inducing transcription repression through chromatin condensation at the targeted locus. Thus, we designed two sgRNAs targeting the promoter of Nupr1 (**Figure 6B**).

In an in vitro experiment, aged HSCs from CRISPRi mice were transduced with lentivirus containing gRNAs targeting Nupr1 (**Figure 6C**). Successful transduction resulted in BFP expression, and after a few days in culture, transduced cells were analyzed by flow cytometry. We observed a decrease in the percentage of BFP+ MkPs compared to BFP+ HSCs (**Figure 6D**), indicating that Nupr1 inhibition led to reduced differentiation of HSCs into MkPs. Moreover, an increase in the number of HSCs with silenced Nupr1 compared to the control was observed (**Figure 6D**), suggesting a block in differentiation and a potential increase in self-renewal.

While in vitro assays provide valuable insights, they may not fully replicate physiological conditions. Ongoing experiments aim at in vivo interrogation of the role of Nupr1 in aged HSCs (**Figure 6E**). We transplanted aged HSCs transduced with Nupr1-targeting sgRNAs into irradiated recipient mice. At 16 weeks post-transplant, analysis of the blood and bone marrow will determine the reconstitution ability of

Nupr1-silenced aged HSCs. We hypothesize that Nupr1 inhibition will reverse the age-specific phenotype, restoring hematopoiesis to a young-like state. Conversely, Nupr1 overexpression in HSCs from young mice transplanted into irradiated recipients is hypothesized to activate the age-specific pathway, replicating an aged-like phenotype.

Methods

Mice and Cells

All experiments were performed using young (8-12 weeks) or aged (20-24 months) 8- to 12-week-old C57BL/6 wild-type or CRISPRi(Martin et al. 2023) mice in accordance with UCSC IACUC guidelines. Hematopoietic stem, progenitor and mature cells were isolated from BM of murine femurs, tibias, and hips as previously described (Boyer et al. 2011; Poscablo et al. 2021; Rodriguez y Baena et al. 2022). Stem and progenitor cell fractions were enriched using cKit-coupled magnetic beads (Miltenyi). Cells for ATACseq were isolated by fluorescent activated cell sorting (FACS) using the following markers: HSC (Lin-, c-kit+, Sca-1+, SLAM mid-high, Flk2+) and MkP (Lin-, c-kit+, Sca-1-, SLAM+,CD41+). Lineage stain included the following antibodies: CD3, CD4, CD5, CD8, B220, Gr1, Mac1, and Ter119.

ATAC-seq

ATAC-seq was performed as previously described (Buenrostro et al. 2013; E. W. Martin et al. 2021; Martin et al. 2023). Briefly, cells were collected after sorting into microcentrifuge tubes, and centrifuged at 500xg for 5 minutes at 4˚C to pellet the cells. The supernatant was aspirated, and the cells were washed with ice-cold 1xDPBS. Cells were centrifuged and the supernatant was discarded. Cells were immediately resuspended in ice-cold lysis buffer (10 mM Tris-HCl, pH 7.4, 10 mM NaCl, 3 mM MgCl2 and 0.1% IGEPAL CA-630) and centrifuged at 500xg for 10 minutes. The supernatant was aspirated, and pellets were resuspended in transposase reaction mix

(25µL 2xTD Buffer, 2.5µL transposase (Illumina), and 22.5µL nuclease free water). The transposition reaction was carried out at 37˚C for 30 minutes at 600rpm in a shaking thermomixer (Eppendorf). Immediately after completion of the transposition reaction, the samples were purified using the MinElute Reaction Clean up kit (Qiagen) and eluted into 10 µL of EB. Samples were stored at -20˚C until PCR amplification step. PCR amplification was performed as previously described (Buenrostro et al. 2013) using custom Nextera primers. After initial amplification (5 cycles), a portion of the samples were run on qPCR (ViiA7 Applied Biosystems) to determine the additional number of cycles needed for each library (typically 5-8 cycles). The libraries were purified using the MinElute Reaction Clean up kit (Qiagen), eluted into 20 µL EB and then size selected using AmpureXP (Beckman-Coulter) beads at a ratio of 1.8:1 beads/sample, and eluted into 40µL of nuclease-free water. Library size distribution was determined by Bioanalyzer (Agilent) capillary electrophoresis and library concentration was determined by Qubit 3 (Life Technologies). Quality of libraries were checked by shallow sequencing (1 million raw reads) on a Miseq (Illumina) at 75 x 75 paired-end sequencing. Those libraries that appeared to have size distributions similar to previous reports were pooled together and deep sequenced on a HiSeq2500 (Illumina) at 100 x 100 reads at the Vincent J. Coates Genomics Sequencing Laboratory at UC Berkeley.

Data processing

Demultiplexed sequencing data was processed using the ENCODE ATAC-seq pipeline version 1.1.6 and 1.4.2 (https://github.com/ENCODE-DCC/atac-seq-pipeline) using the mm10 assembly and the default parameters. In version 1.4.2 changed: atac.multimapping=0, atac.smooth_win=150, atac.enable_idr=true, atac.idr_thresh=0.1 to be consistent with the mapping/peak calling performed with previous versions.

Peak filtering and hierarchical clustering was performed using the chromVAR package (https://github.com/GreenleafLab/chromVAR). First, the optimal peak-list from the IDR output for each cell type was concatenated and sorted, then used as the peak input for chromVAR. The blacklist filtered bam files for each replicate (n=2 for each cell type) was used as input along with the sorted peak file. The fragment counts in each peak for each replicate and GC bias was calculated, and then the peaks were filtered using filterPeaks function with the default parameters and nonoverlapping=TRUE.

Normalized chromVAR counts were log+1 scaled, centered, and filtered to peaks that had above-median coefficient of variance. These filtered counts were use in principal component analysis (PCA) with the R package *prcomp*.

Differential accessibility analysis was performed using csaw workflow for ATACseq differential accessibility analysis in R (https://github.com/reskejak/ATAC-seq/blob/master/csaw_workflow.R) using MAC2 narrowpeaks as input for loess based normalization. Output was plotted as volcano plots using GraphPad Prism.

Annotation of peaks was performed by HOMER (http://homer.ucsd.edu/homer/). Peaks were annotated using the annotatePeaks.pl function with the mm10 assembly and default parameters.

All genome track visualizations were made using the UCSC genome browser.

Published data

ATACseq, RNAseq, and ChIPseq data sets from published studies were re-analyzed for this study(Hérault et al. 2021; E. W. Martin et al. 2021; Poscablo et al. 2021; Sun et al. 2014).

CRISPRi experiments

Single guide RNA (sgRNA) sequence targeting the Nupr1 promoter was designed using the CRISPR10K(Concordet and Haeussler 2018; Haeussler et al. 2016) on the UCSC Genome Browser. The non-overlapping guides were selected and cloned into pJR85 (Addgene plasmid #140095)(Replogle et al. 2022). psPAX2 (Addgene plasmid #12260) and pMD2.G (Addgene plasmid # 12259) were combined with pJR85 and transfected into 293T cells by Lipofectamine 2000. 72 hours after transfection, the supernatant was collected, 0.45 μ filtered, and concentrated by PEG precipitation. Concentrated lentivirus was resuspended in a minimal volume. Lentivirus was tittered by transducing HEK293T cells and determining MOI after 3 days from transduction.

HSCs (Lin-, c-kit+, Sca1+, SLAMmid-hi, Flk2-) from aged CRISPRi mice were isolated by FACS and plated at 200-500 cells/well in either HSC maintenance media

(Ham's F12; 1X Pen/Strep; 1X Glutamax; 10mM HEPES; 1mg/ml PVA; 1X ITSX; 100ng/ml TPO; 10ng/ml SCF)(Wilkinson et al. 2019) or HSC to MkP differentiation media (IMDM; 20% FBS; TPO 50ng/mL; SCF 50 ng/mL; IL-6 20ng/mL; IL-3 10 ng/mL, IL-11 20 ng/mL, Primocin, Non-Essential Amino Acids). After 24 hours in culture, lentivirus containing sgRNAs was added to each well and spinoculated for 1 hour, 400xg at 32˚C. 24 hours later, virus was washed out and the media was replaced. Cells were analyzed at day 7 by flow cytometry.

List of sgRNAs used:

Nupr1 Promoter guide 1	GGTCTCCTCCCTAAACCACG
Nupr1 Promoter guide 2	GGAGGCGAGAGCTTTCCACG
Scrambled Control guide 1	GGGAACCACATGGAATTCGA
Scrambled Control guide 2	GAGGTTACCCACCCAGCGGT

RNA isolation, cDNA synthesis, and real-time PCR for Nupr1 isoforms

RNA was isolated, using Trizol (T9424; Ambion) according to manufacturer's instructions, from sorted HSCs, MPPs, cMkPs, and ncMkPs from young and aged mice. RNA was reverse transcribed using the High Capacity cDNA Reverse Transcription Kit. cDNA was used as input for PCR using the following thermocycle parameters: 98°C for 3 min, followed by 35X cycles of 98°C for 15, 60°C for 15 sec, and 72°C for 15 sec, followed by 72C for 1 min. Oligos used in qPCR analysis were designed using Primer3 Input version 0.4.0. Primers used were: Gapdh Forward 5-

TGTGTCCGTCGTGGATCTGA-3; Gapdh Reverse 5-CCTGCTTCACCACCTTCTTGA-3, Nupr1 Forward 5-ggcaagactttggagagagc-3; Nupr1 Revers 5-gcagcagcttctctcttggt-3. Samples were run in a 150ml 2% agarose gel with 6ul EtBr and a 50bp ladder was used.

Figures

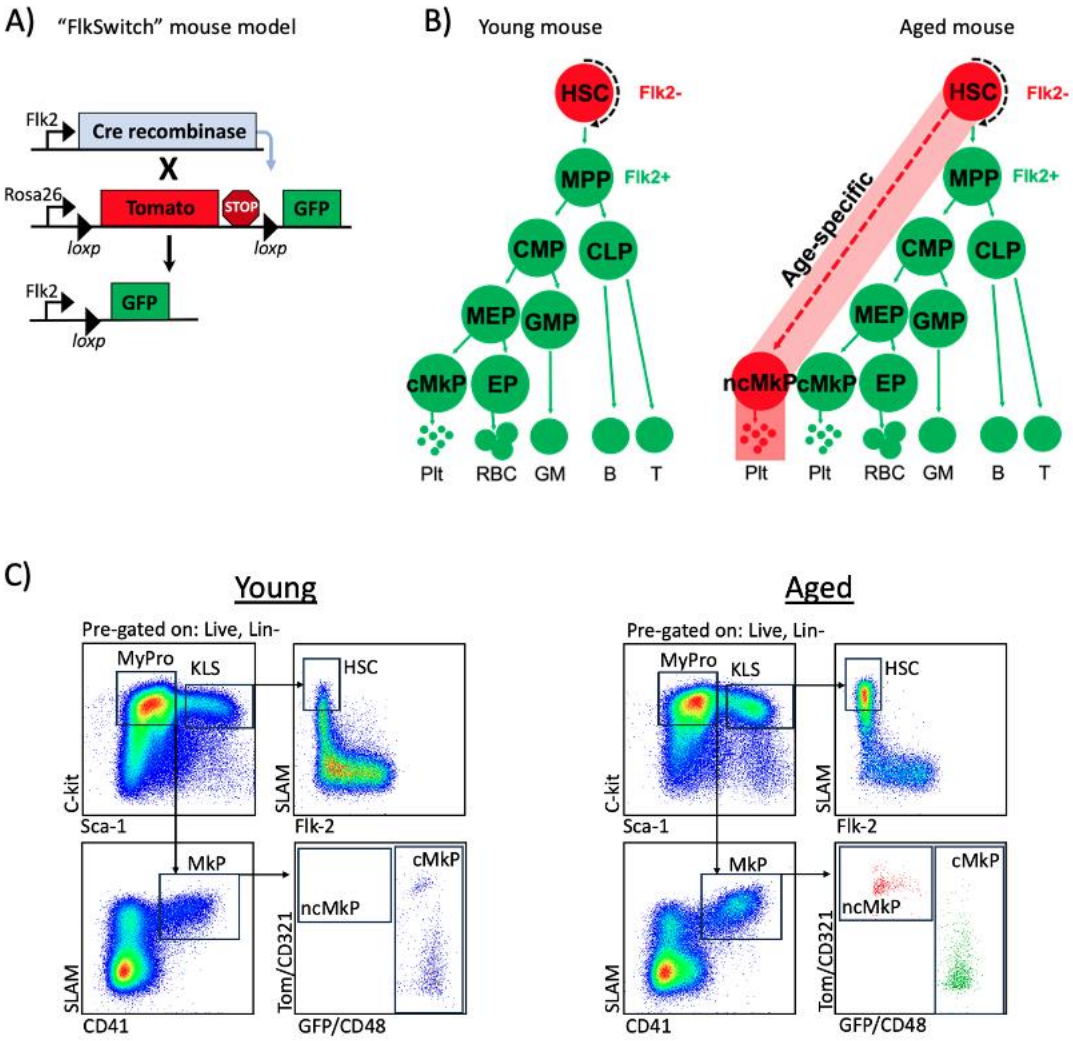

Figure 7.1. An age-specific MkP differentiation pathway was identified in aged FlkSwitch mice.

A) Schematic representation of the genetic reporters of the FlkSwitch lineage tracing mouse model.
B) Model hematopoietic tree in young (left) and aged (right) FlkSwitch mice, highlighting the canonical (green) and non-canonical, age-specific (red) megakaryopoiesis pathways.
C) Representative flow cytometry plots of the gating strategy used to phenotype and isolate HSCs, cMkPs, and ncMkPs from young and aged mice.

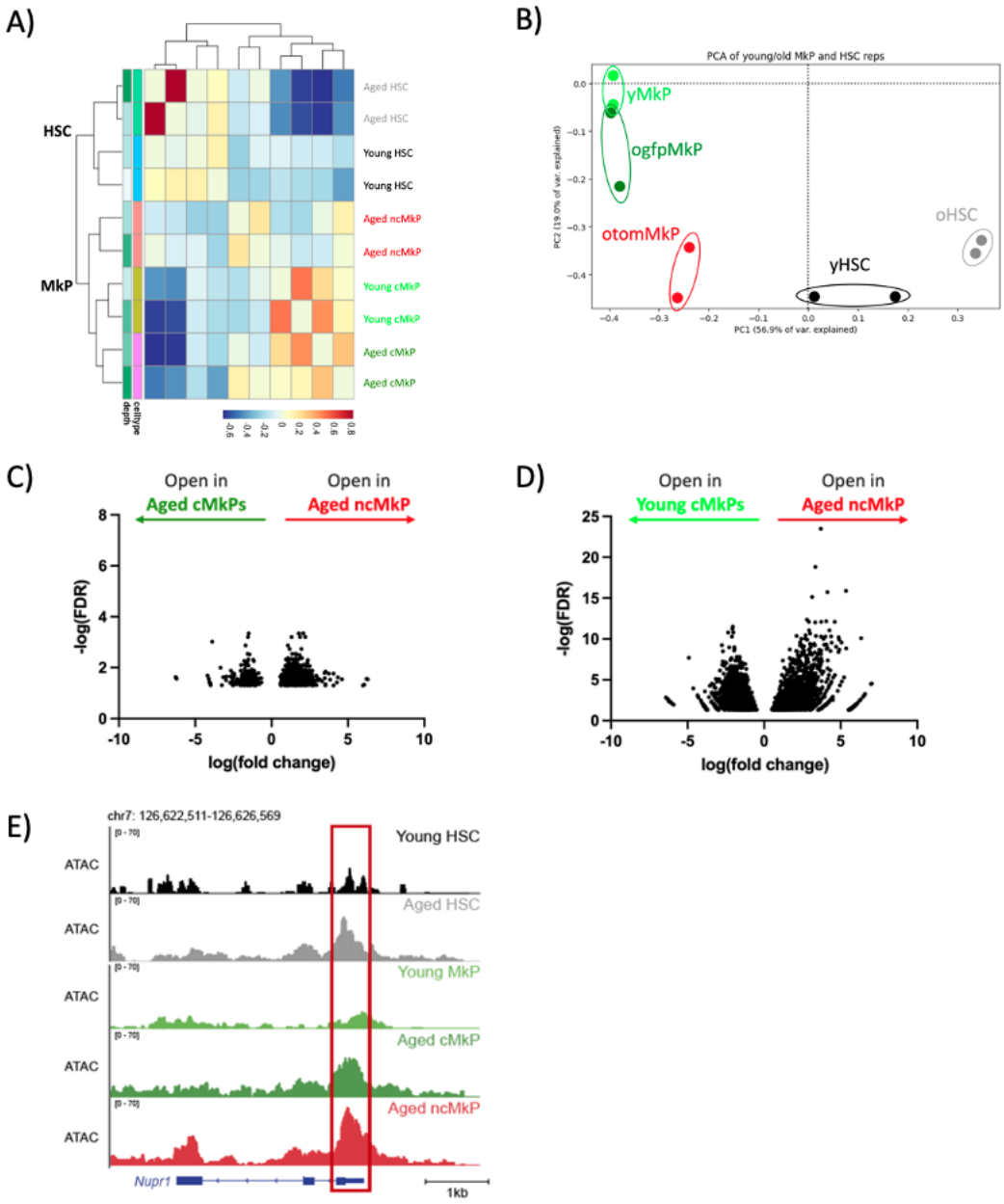

Figure 7.2. ATACseq profiling of young and aged HSCs and MkPs

A) Hierarchical clustering of young and aged HSCs and MkPs revealed high concordance of replicates, and distinct clusters between HSCs and MkPs, with aged ncMkPs clustering more closely to HSCs.
B) Principal Component Analysis (PCA) of ChromVAR-normalized ATAC-seq peak counts revealed high concordance of replicates, and distinct separation between HSCs and MkPs.
C) Differential accessibility analysis between aged cMkPs and aged ncMkPs.
D) Differential accessibility analysis between young cMkPs and aged ncMkPs.

E) UCSC Genome snapshot at the Nupr1 locus showing uploaded ATACseq tracks for young HSCs, aged HSCs, young cMkPs, aged cMkPs, and aged ncMkPs. Red box highlights the peaks present at the Nupr1 promoter.

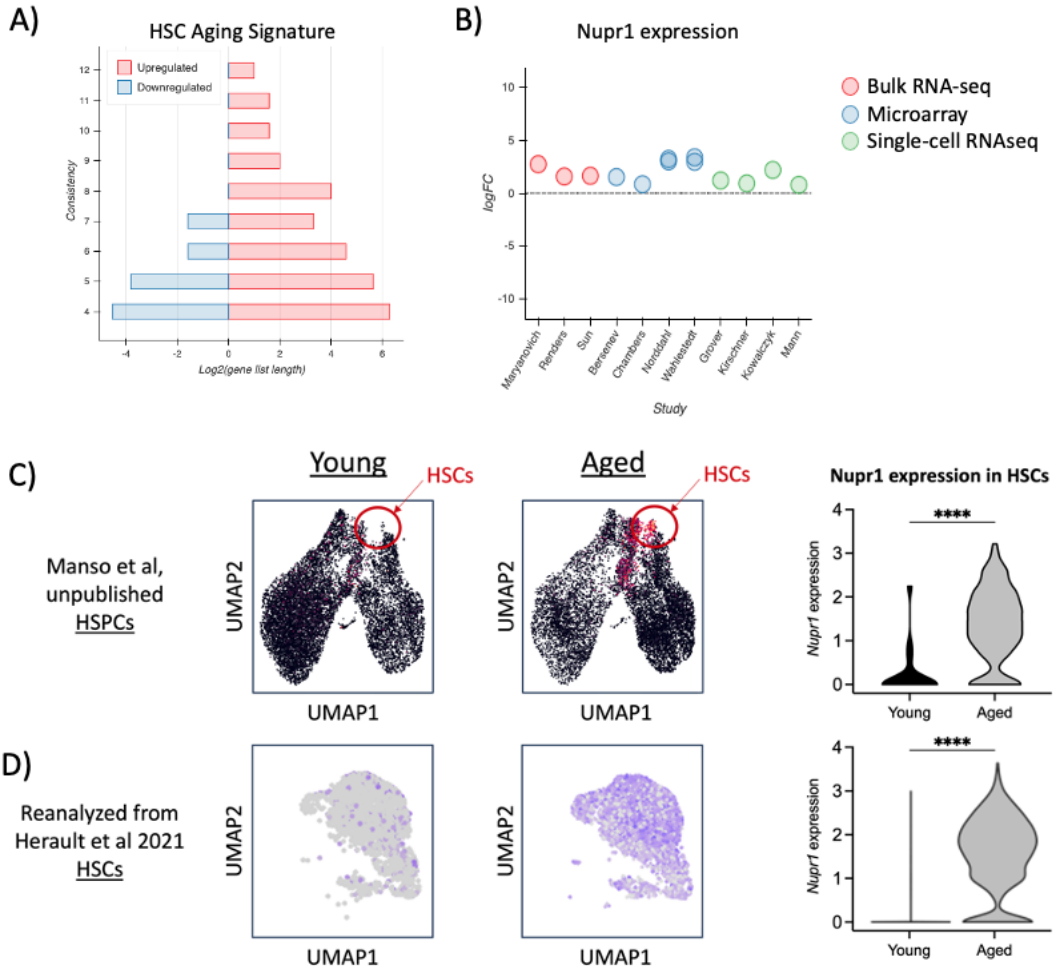

Figure 7.3. Nupr1 is one of the most consistently upregulated genes in aged HSCs compared to young HSCs.

A) HSC aging signature from Svendsen et al 2021: x-axis represents number of genes and y-axis represents number of studies in which specific genes are either upregulated or downregulated
B) Summary plot showing Nupr1 expression in aged HSCs compared to young HSCs for each of the published studies represented in the x-axis. Each dot represents a different study and the color of the dots shows the type of sequencing performed.
C) Uniform Manifold Approximation and Projection (UMAP) of hematopoietic stem and progenitor cells (HSPCs: Lin-, ckit+, Sca+/-) from young (left) and aged (right) mice. Circled cluster was annotated as HSCs based on published HSC signatures. Nupr1 expression in young and aged HSCs is shown in the violin plot. **** p-value <0.001 (Student's t-test).

D) UMAP of HSCs from the re-analysis of scRNAseq from Herault et al 2021. Nupr1 expression in young (left) and aged (right) HSCs is shown in the violin plot. **** p-value <0.001 (Student's t-test).

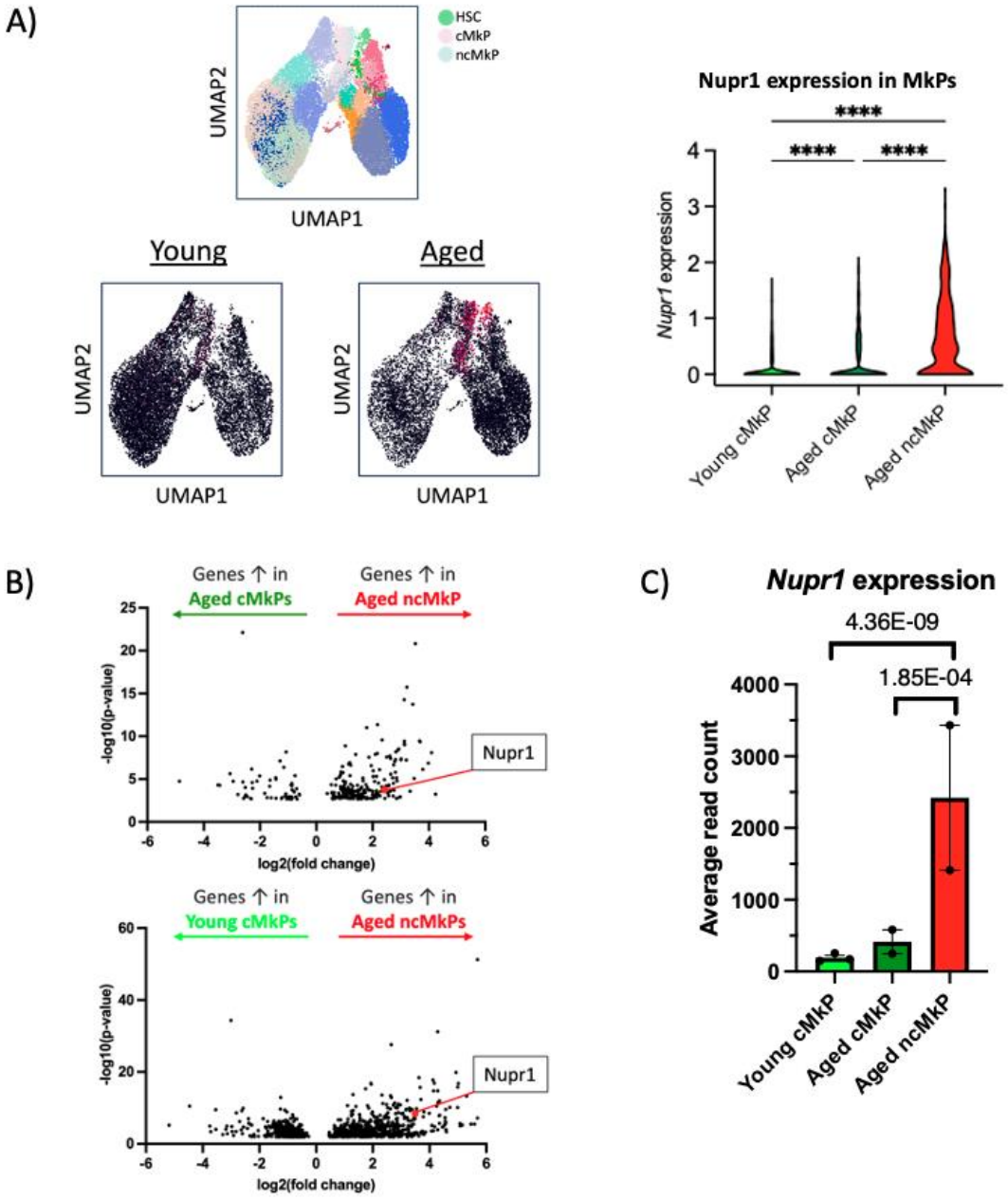

Figure 7.4. Nupr1 is significantly upregulated in aged ncMkPs compared to young and aged cMkPs.

A) UMAP of hematopoietic stem and progenitor cells (HSPCs: Lin-, ckit+, Sca+/-) from young and aged mice combined. Each color represents a cluster (HSCs in green, cMkPs in pink, ncMkP in blue). The bottom UMAPs are divided into young (left) and aged (right) cells and show expression levels of Nupr1 in red. Nupr1 expression in young and aged HSCs is shown in the violin plot. **** p-value <0.001 (ANOVA).

B) Differential expression analysis between aged cMkPs and aged ncMkPs (top) and between young cMkPs and aged ncMkPs (bottom).
C) Nupr1 expression from bulk RNAseq analysis of young cMkP, aged cMkPs, and aged ncMkPs. P values from DESeq2 pairwise comparisons.

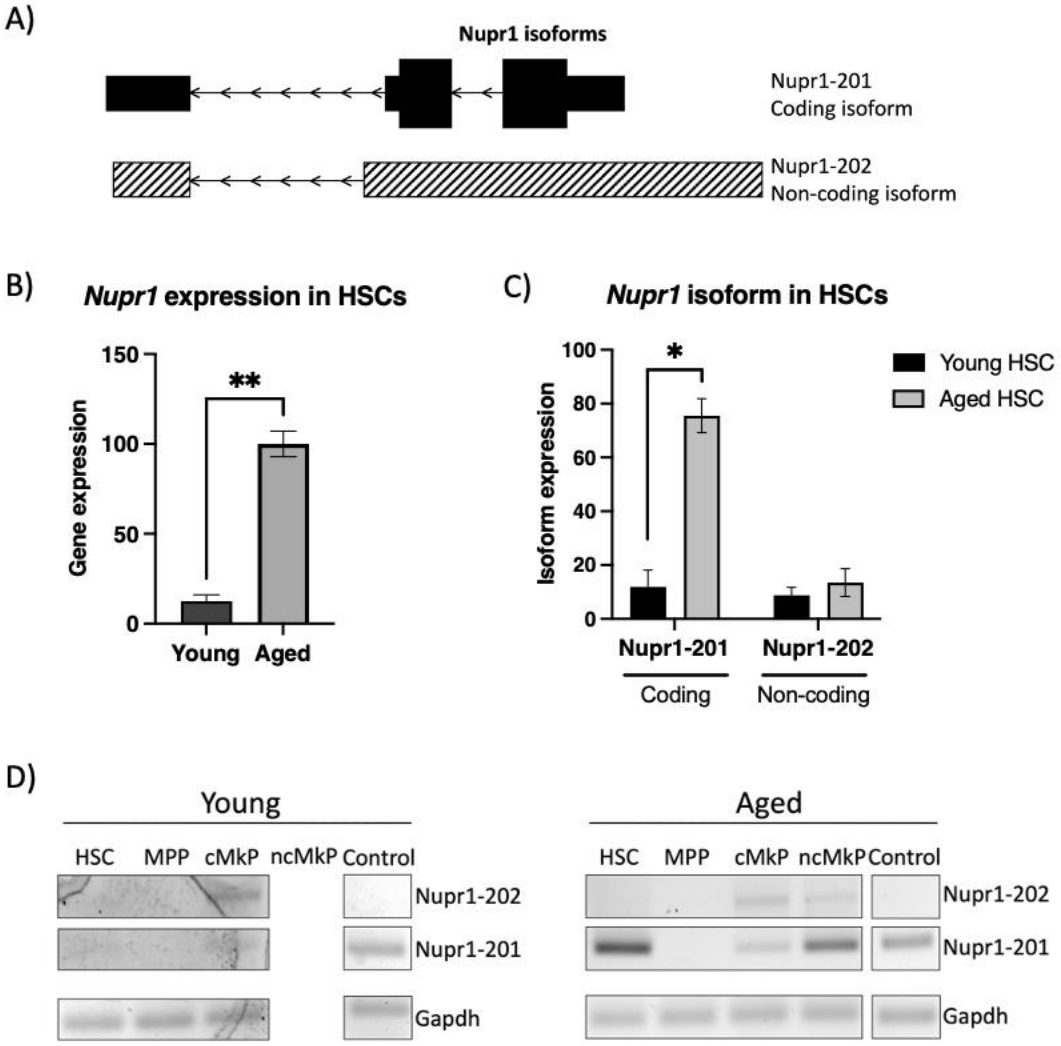

Figure 7.5. Aging is accompanied by a switch from non-coding to coding Nupr1 isoforms in HSCs and MkPs.

A) Schematic of the 2 main Nupr1 isoforms: Nupr1-201 (coding) and Nupr1-202 (non-coding)
B) Nupr1 gene expression from re-analysis of Sun et al 2014 bulk RNAseq data. ** p-value <0.01 (Student's t-test)
C) Nupr1 gene expression based on isoform expression. * <0.05 (Student's t-test)
D) RT-PCR for GAPDH, Nupr1-201, Nupr1-202 in young and aged HSCs, MPPs, cMkPs, ncMkPs, and bone marrow derived macrophages (BMDMs; control). Expected band sizes: 77bps (*Gapdh*); 187bps (*Nupr1-201, coding*); 455bps (*Nupr1-202, non-coding*). Ladder used was 50bp; 2% agarose gel with EtBr.

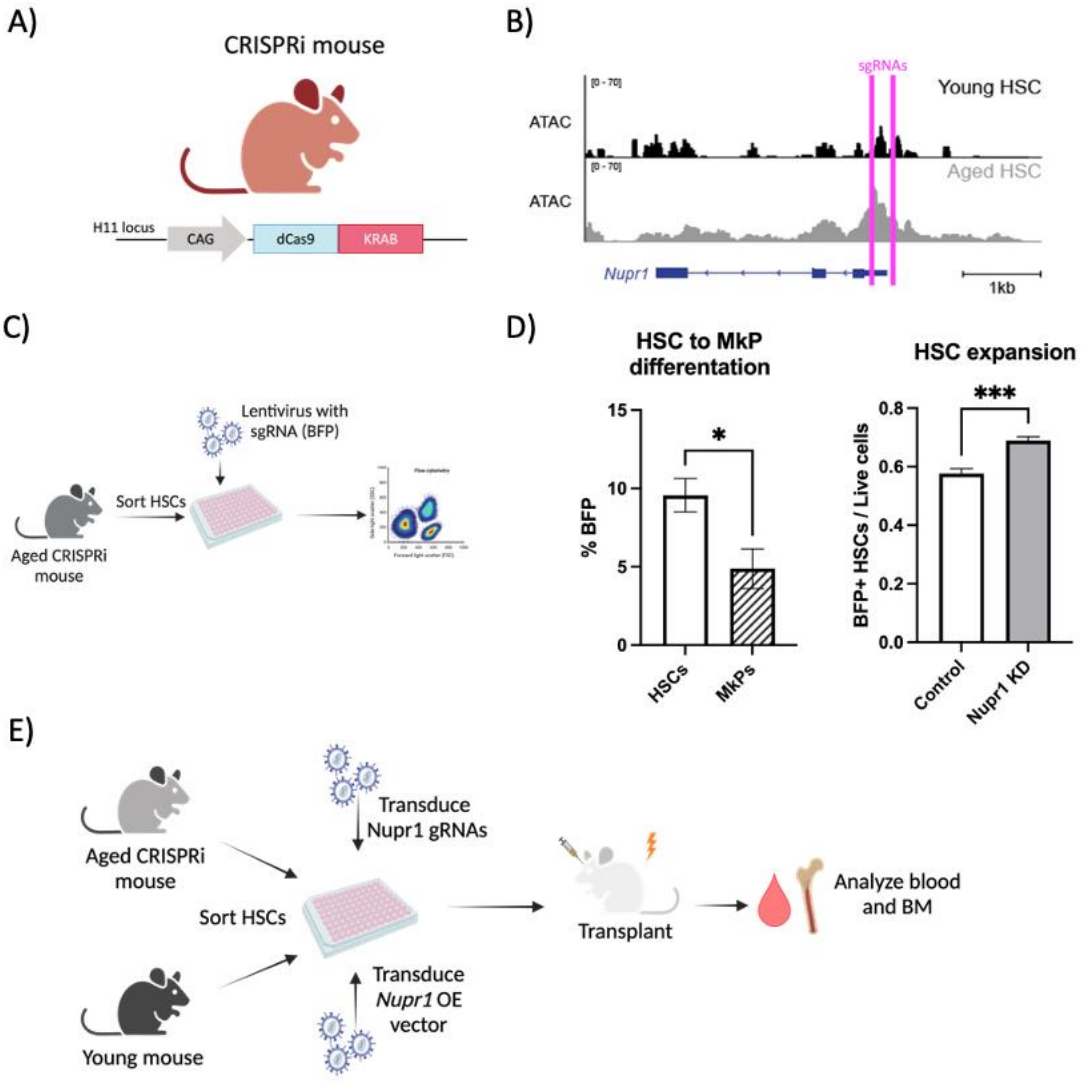

Figure 7.6. CRISPRi silencing of Nupr1 leads to decreased MkP differentiation from aged HSCs.

A) Schematic of CRISPRi mouse model: dCas-KRAB in a safe harbor locus (H11) locus in the mouse genome, under a ubiquitous promoter [CAG (CMV early enhancer/chicken β actin)]
B) UCSC Genome snapshot at the Nupr1 locus showing uploaded ATACseq tracks for young HSC and aged HSCs. The pink boxes show the location targeted by the two Nupr1-targeting sgRNAs
C) Schematic of experimental design to investigate the role of Nupr1 in vitro.
D) Percent BFP+ (transduced) HSCs and MkPs (left) and number of HSCs over live cells for each condition. * p-value <0.05, *** <0.001 (Student's t-test).
E) Schematic of ongoing in vivo transplantation experiments to investigate the role of Nupr1 in aging.

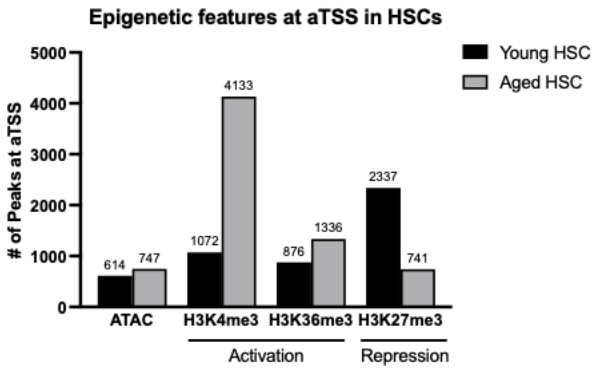

Figure 7.7. Supplementary Figure 1. Re-analysis of young and aged HSC ATACseq and ChIPseq data from Sun et al 2014.

References

Beerman, Isabel, Deepta Bhattacharya, Sasan Zandi, Mikael Sigvardsson, Irving L. Weissman, David Bryder, and Derrick J. Rossi. 2010. "Functionally Distinct Hematopoietic Stem Cells Modulate Hematopoietic Lineage Potential during Aging by a Mechanism of Clonal Expansion." *Proceedings of the National Academy of Sciences* 107(12):5465–70. doi: 10.1073/pnas.1000834107.

Boyer, Scott W., Aaron V. Schroeder, Stephanie Smith-Berdan, and E. Camilla Forsberg. 2011. "All Hematopoietic Cells Develop from Hematopoietic Stem Cells through Flk2/Flt3-Positive Progenitor Cells." *Cell Stem Cell* 9(1):64–73. doi: 10.1016/j.stem.2011.04.021.

Buenrostro, Jason D., Paul G. Giresi, Lisa C. Zaba, Howard Y. Chang, and William J. Greenleaf. 2013. "Transposition of Native Chromatin for Fast and Sensitive Epigenomic Profiling of Open Chromatin, DNA-Binding Proteins and Nucleosome Position." *Nat Meth* 10(12):1213–18. doi: 10.1038/nmeth.2688.

Challen, Grant A., Nathan C. Boles, Stuart M. Chambers, and Margaret A. Goodell. 2010. "Distinct Hematopoietic Stem Cell Subtypes Are Differentially Regulated by TGF-B1." *Cell Stem Cell* 6(3):265–78. doi: 10.1016/j.stem.2010.02.002.

Chen, Danqi, Thomas Kluz, Lei Fang, Xiaoru Zhang, Hong Sun, Chunyuan Jin, and Max Costa. 2016. "Hexavalent Chromium (Cr(VI)) Down-Regulates Acetylation of Histone H4 at Lysine 16 through Induction of Stressor Protein Nupr1" edited by W.-G. Zhu. *PLOS ONE* 11(6):e0157317. doi: 10.1371/journal.pone.0157317.

Cho, Rebecca H., Hans B. Sieburg, and Christa E. Muller-Sieburg. 2008. “A New Mechanism for the Aging of Hematopoietic Stem Cells: Aging Changes the Clonal Composition of the Stem Cell Compartment but Not Individual Stem Cells.” *Blood* 111(12):5553–61. doi: 10.1182/blood-2007-11-123547.

Concordet, Jean-Paul, and Maximilian Haeussler. 2018. “CRISPOR: Intuitive Guide Selection for CRISPR/Cas9 Genome Editing Experiments and Screens.” *Nucleic Acids Research* 46(W1):W242–45. doi: 10.1093/nar/gky354.

De Conti, Aline, Kostiantyn Dreval, Volodymyr Tryndyak, Orish E. Orisakwe, Sharon A. Ross, Frederick A. Beland, and Igor P. Pogribny. 2017. “Inhibition of the Cell Death Pathway in Nonalcoholic Steatohepatitis (NASH)-Related Hepatocarcinogenesis Is Associated with Histone H4 Lysine 16 Deacetylation.” *Molecular Cancer Research* 15(9):1163–72. doi: 10.1158/1541-7786.MCR-17-0109.

Dykstra, Brad, David Kent, Michelle Bowie, Lindsay McCaffrey, Melisa Hamilton, Kristin Lyons, Shang-Jung Lee, Ryan Brinkman, and Connie Eaves. 2007. “Long-Term Propagation of Distinct Hematopoietic Differentiation Programs in Vivo.” *Cell Stem Cell* 1(2):218–29. doi: 10.1016/j.stem.2007.05.015.

Flohr Svendsen, Arthur, Daozheng Yang, KyungMok Kim, Seka Lazare, Natalia Skinder, Erik Zwart, Anna Mura-Meszaros, Albertina Ausema, Björn von Eyss, Gerald de Haan, and Leonid Bystrykh. 2021. “A Comprehensive Transcriptome Signature of Murine Hematopoietic Stem Cell Aging.” *Blood* 138(6):439–51. doi: 10.1182/blood.2020009729.

Grasso, Daniel, Jennifer Bintz, Gwen Lomberk, Maria Ines Molejon, Celine Loncle, Maria Noé Garcia, Maria Belen Lopez, Raul Urrutia, and Juan L. Iovanna. 2015. "Pivotal Role of the Chromatin Protein Nupr1 in Kras-Induced Senescence and Transformation." *Scientific Reports* 5:17549. doi: 10.1038/srep17549.

Haeussler, Maximilian, Kai Schönig, Hélène Eckert, Alexis Eschstruth, Joffrey Mianné, Jean-Baptiste Baptiste Renaud, Sylvie Schneider-Maunoury, Alena Shkumatava, Lydia Teboul, Jim Kent, Jean-Stephane Stephane Joly, and Jean-Paul Paul Concordet. 2016. "Evaluation of Off-Target and on-Target Scoring Algorithms and Integration into the Guide RNA Selection Tool CRISPOR." *Genome Biology* 17(1):148. doi: 10.1186/s13059-016-1012-2.

Heintzman, Nathaniel D., Gary C. Hon, R. David Hawkins, Pouya Kheradpour, Alexander Stark, Lindsey F. Harp, Zhen Ye, Leonard K. Lee, Rhona K. Stuart, Christina W. Ching, Keith A. Ching, Jessica E. Antosiewicz-Bourget, Hui Liu, Xinmin Zhang, Roland D. Green, Victor V. Lobanenkov, Ron Stewart, James A. Thomson, Gregory E. Crawford, Manolis Kellis, and Bing Ren. 2009. "Histone Modifications at Human Enhancers Reflect Global Cell-Type-Specific Gene Expression." *Nature* 459(7243):108–12. doi: 10.1038/nature07829.

Hérault, Léonard, Mathilde Poplineau, Adrien Mazuel, Nadine Platet, Élisabeth Remy, and Estelle Duprez. 2021. "Single-Cell RNA-Seq Reveals a Concomitant Delay in Differentiation and Cell Cycle of Aged Hematopoietic Stem Cells." *BMC Biology* 19(1):19. doi: 10.1186/s12915-021-00955-z.

Hu, M., D. Krause, M. Greaves, S. Sharkis, M. Dexter, C. Heyworth, and T. Enver. 1997. “Multilineage Gene Expression Precedes Commitment in the Hemopoietic System.” *Genes & Development* 11(6):774–85. doi: 10.1101/gad.11.6.774.

Koch, Christoph M., Robert M. Andrews, Paul Flicek, Shane C. Dillon, Ulaş Karaöz, Gayle K. Clelland, Sarah Wilcox, David M. Beare, Joanna C. Fowler, Phillippe Couttet, Keith D. James, Gregory C. Lefebvre, Alexander W. Bruce, Oliver M. Dovey, Peter D. Ellis, Pawandeep Dhami, Cordelia F. Langford, Zhiping Weng, Ewan Birney, Nigel P. Carter, David Vetrie, and Ian Dunham. 2007. “The Landscape of Histone Modifications across 1% of the Human Genome in Five Human Cell Lines.” *Genome Research* 17(6):691–707. doi: 10.1101/gr.5704207.

Mallo, Gustavo Vidal, Fritz Fiedler, Ezequiel Luis Calvo, Emilia Mariana Ortiz, Sophie Vasseur, Volker Keim, Jean Morisset, and Juan Lucio Iovanna. 1997. “Cloning and Expression of the Rat P8 cDNA, a New Gene Activated in Pancreas during the Acute Phase of Pancreatitis, Pancreatic Development, and Regeneration, and Which Promotes Cellular Growth.” *Journal of Biological Chemistry* 272(51):32360–69. doi: 10.1074/jbc.272.51.32360.

Martin, Eric W., Jana Krietsch, Roman E. Reggiardo, Rebekah Sousae, Daniel H. Kim, and E. Camilla Forsberg. 2021. “Chromatin Accessibility Maps Provide Evidence of Multilineage Gene Priming in Hematopoietic Stem Cells.” *Epigenetics & Chromatin* 14(1):2. doi: 10.1186/s13072-020-00377-1.

Martin, Eric W., Alessandra Rodriguez Y Baena, Roman E. Reggiardo, Atesh K. Worthington, Connor S. Mattingly, Donna M. Poscablo, Jana Krietsch, Michael

T. McManus, Susan Carpenter, Daniel H. Kim, and E. Camilla Forsberg. 2023. "Dynamics of Chromatin Accessibility During Hematopoietic Stem Cell Differentiation Into Progressively Lineage-Committed Progeny." *Stem Cells (Dayton, Ohio)* 41(5):520–39. doi: 10.1093/stmcls/sxad022.

Martin, Tracey, Amber Li, Andrew Sanders, Lin Ye, Kathryn Frewer, Rachel Hargest, and Wen Jiang. 2021. "NUPR1 and Its Potential Role in Cancer and Pathological Conditions (Review)." *International Journal of Oncology* 58(5):21. doi: 10.3892/ijo.2021.5201.

Morrison, Sean J., Antoni M. Wandycz, Koichi Akashi, Amiela Globerson, and Irving L. Weissman. 1996. "The Aging of Hematopoietic Stem Cells." *Nature Medicine* 2(9):1011–16. doi: 10.1038/nm0996-1011.

Poscablo, Donna M., Atesh K. Worthington, Stephanie Smith-Berdan, and E. Camilla Forsberg. 2021. "Megakaryocyte Progenitor Cell Function Is Enhanced upon Aging despite the Functional Decline of Aged Hematopoietic Stem Cells." *Stem Cell Reports* 16(6):1598–1613. doi: 10.1016/j.stemcr.2021.04.016.

Rada-Iglesias, Alvaro, Ruchi Bajpai, Tomek Swigut, Samantha A. Brugmann, Ryan A. Flynn, and Joanna Wysocka. 2011. "A Unique Chromatin Signature Uncovers Early Developmental Enhancers in Humans." *Nature* 470(7333):279–83. doi: 10.1038/nature09692.

Replogle, Joseph M., Jessica L. Bonnar, Angela N. Pogson, Christina R. Liem, Nolan K. Maier, Yufang Ding, Baylee J. Russell, Xingren Wang, Kun Leng, Alina Guna, Thomas M. Norman, Ryan A. Pak, Daniel M. Ramos, Michael E. Ward,

Luke A. Gilbert, Martin Kampmann, Jonathan S. Weissman, and Marco Jost. 2022. “Maximizing CRISPRi Efficacy and Accessibility with Dual-sgRNA Libraries and Optimal Effectors.” *eLife* 11:e81856. doi: 10.7554/eLife.81856.

Rodriguez y Baena, Alessandra, Smrithi Rajendiran, Bryce A. Manso, Jana Krietsch, Scott W. Boyer, Jessica Kirschmann, and E. Camilla Forsberg. 2022. “New Transgenic Mouse Models Enabling Pan-Hematopoietic or Selective Hematopoietic Stem Cell Depletion in Vivo.” *Scientific Reports* 12(1):3156. doi: 10.1038/s41598-022-07041-6.

Rodriguez-Fraticelli, Alejo E., Caleb Weinreb, Shou-Wen Wang, Rosa P. Migueles, Maja Jankovic, Marc Usart, Allon M. Klein, Sally Lowell, and Fernando D. Camargo. 2020. “Single-Cell Lineage Tracing Unveils a Role for TCF15 in Haematopoiesis.” *Nature* 583(7817):585–89. doi: 10.1038/s41586-020-2503-6.

Rossi, Derrick J., David Bryder, Jacob M. Zahn, Henrik Ahlenius, Rebecca Sonu, Amy J. Wagers, and Irving L. Weissman. 2005. “Cell Intrinsic Alterations Underlie Hematopoietic Stem Cell Aging.” *Proceedings of the National Academy of Sciences* 102(26):9194–99. doi: 10.1073/pnas.0503280102.

Sun, Deqiang, Min Luo, Mira Jeong, Benjamin Rodriguez, Zheng Xia, Rebecca Hannah, Hui Wang, Thuc Le, Kym F. Faull, Rui Chen, Hongcang Gu, Christoph Bock, Alexander Meissner, Berthold Göttgens, Gretchen J. Darlington, Wei Li, and Margaret A. Goodell. 2014. “Epigenomic Profiling of Young and Aged HSCs Reveals Concerted Changes during Aging That Reinforce Self-Renewal.” *Cell Stem Cell* 14(5):673–88. doi: 10.1016/j.stem.2014.03.002.

Visel, Axel, Matthew J. Blow, Zirong Li, Tao Zhang, Jennifer A. Akiyama, Amy Holt, Ingrid Plajzer-Frick, Malak Shoukry, Crystal Wright, Feng Chen, Veena Afzal, Bing Ren, Edward M. Rubin, and Len A. Pennacchio. 2009. "ChIP-Seq Accurately Predicts Tissue-Specific Activity of Enhancers." *Nature* 457(7231):854–58. doi: 10.1038/nature07730.

Wang, Tongjie, Chengxiang Xia, Qitong Weng, Kaitao Wang, Yong Dong, Sha Hao, Fang Dong, Xiaofei Liu, Lijuan Liu, Yang Geng, Yuxian Guan, Juan Du, Tao Cheng, Hui Cheng, and Jinyong Wang. 2020. "Loss of Nupr1 Promotes Engraftment by Tuning the Quiescence Threshold of Hematopoietic Stem Cells via Regulation of the P53-Checkpoint Pathway." *Haematologica* 107(1):154–66. doi: 10.3324/haematol.2019.239186.

Wilkinson, Adam C., Reiko Ishida, Misako Kikuchi, Kazuhiro Sudo, Maiko Morita, Ralph Valentine Crisostomo, Ryo Yamamoto, Kyle M. Loh, Yukio Nakamura, Motoo Watanabe, Hiromitsu Nakauchi, and Satoshi Yamazaki. 2019. "Long-Term Ex Vivo Haematopoietic-Stem-Cell Expansion Allows Nonconditioned Transplantation." *Nature* 571(7763):117–21. doi: 10.1038/s41586-019-1244-x.